DIFFERENTIAL INVOLVEMENT OF GLUTAMATE RECEPTORS IN NEURONAL RESPONSES OF THE CEREBRAL CORTEX

MARIE POLLARD

Oriel College, Oxford

Thesis submitted for the degree of Doctor of Philosophy at the University of Oxford

Hilary Term, 2001

Éste libro está dedicado
con mi alma y esfuerzos
a mi mamá, Marisol y a mi
abuela, mamIsabel;
mis buenas compañeras
que estaran conmigo para la
eternidad.
Estoy tan agradecida.

ACKNOWLEDGEMENTS

The gratitude that I have towards my supervisor, Professor Peter Somogyi, extends beyond words to describe. He has been my guidance, support and courage through all circumstances further to his duty as a supervisor. I owe my scientific progress to him and will always remember his kind efforts. I am forever grateful.

I am also most grateful to my co-supervisor, Dr. Ole Paulsen, for his excellent scientific advice, teaching and encouragement throughout my D.Phil.

I especially thank Professor A. David Smith for attending to me as if I was his own student.

I am thankful to my college graduate tutor, Professor C. K. Prout, for his supportive and good-natured spirit. I thank Dr. Sean A. Eaton and Dr. Naoki Kogo for excellent in vivo and in vitro training, respectively.
I also thank Dr. Darrell Henze for specialised in vivo training and the inclusion of one of his recorded cells in the thesis.

I extend my warmest thanks to Mr J. David B. Roberts for being an excellent teacher and a great person all around. I am also grateful to Mr Philip Cobden, Dr. Laszlo Marton and Mr Paul Jays for their technical assistance.

I thank Dr. Yannis Dalezios and Dr. Francesco Ferraguti for those crucial tips that either make or break a project.
I also thank Professor J. Paul Bolam, not only for his kindness but for being such a reasonable human being.

I am equally thankful to all those others who have made an impact on my years here. You know who you are.

Finally, I cherish the love and patience that Jozsef has kept for me from many miles away.

DIFFERENTIAL INVOLVEMENT OF GLUTAMATE RECEPTORS IN NEURONAL RESPONSES OF THE CEREBRAL CORTEX

Marie Pollard
Oriel College, Oxford
Thesis submitted for the degree of Doctor of Philosophy at the University of Oxford
Hilary Term, 2001

ABSTRACT

I studied how glutamate receptor-mediated responses, spatial arrangements, intrinsic properties and molecular specificity of cells serve cortical functions. I tested whether two somatosensory submodalities in the primary somatosensory (SI) cortex can be distinguished by glutamate receptor involvement in vivo. Low-threshold responses evoked by innocuous stimuli had a short-duration and long-duration component. The short-duration responses were mostly mediated by AMPA/kainate receptors and the long-duration responses involved the additional recruitment of NMDA receptors. High-threshold responses evoked by noxious stimuli were unimodal and mediated by both AMPA/kainate and NMDA receptors throughout the entire response. During noxious stimulus trials, an increase in baseline activity in SI cortical cells was observed. I attribute the changes in baseline activity to cells in the medial thalamic nuclei, which project to the SI cortex and are involved in the affective-motivational aspects of nociceptive signalling.

To gain insight into the influence of synaptic organisation of a well-defined cortical area, I studied in vitro whether the intrinsic properties of two anatomically well-defined nonpyramidal cells in the hippocampus can provide clues into the modulation of neuronal signalling. During a depolarising current pulse, O-LM and O-Bi cells were distinguished by their accommodation of action potentials depending on the early or late part of the response. Also, during a hyperpolarising current pulse, O-LM cells displayed a prominent voltage 'sag' as compared to O-Bi cells. Both cell types contain somatostatin and I showed that O-LM cells express the metabotropic glutamate receptor type 1α. Although O-LM and O-Bi cells have a similar somatodendritic position their different axonal arbours imply that they are involved in the feedback modulation of the entorhinal and CA3 glutamatergic influences, respectively. I also found that contrary to previous reports not only somatostatin but also vasoactive intestinal polypeptide containing cells express mGluR1α, which might facilitate their oscillatory responses.

To relate the action potential discharge of specific cortical cell classes to behaviourally relevant network activity, I also sought to identify hippocampal cells following in vivo recording. Novel information was provided for both the temporal and anatomical properties of cells not recorded previously. In particular, a putative interneuron targeting nonpyramidal cell and backprojection cell was recorded in relation to theta field events. A novel nonpyramidal projection cell was recorded in relation to sharp wave field events. A remarkable specificity was found in the dendritic and axonal patterns of these cells.

The results show that distinct types of glutamate receptors are differentially involved in cortical function. The intrinsic properties and expression of mGluR1α in particular is highly specific in distinct nonpyramidal cell classes.

CONTENTS

CHAPTER 1: General Introduction

1.1 Glutamate Receptor Types

The advent of pharmacological tools such as selective agonists and antagonists acting at subgroups of glutamate receptors has led to advancements in elucidating the functional roles of glutamate receptors in different brain areas. Following the cloning of most of the receptors, in situ hybridisation and immunocytochemical techniques have helped to determine the distribution of receptors and together with the physiological findings the results often provided molecular explanations for complex physiological phenomena.

Glutamate receptors are currently divided into four groups based on sequence homology, pharmacology and where applicable, signal transduction pathways. These groups consist of the α-amino-3-hydroxy-5-methylisoxazole-4-propionic acid (AMPA) receptors, kainate receptors, N-methyl-D-aspartate (NMDA) receptors and the metabotropic glutamate receptors (mGluRs). The AMPA and kainate receptors are frequently grouped into the category of non-NMDA receptors because the selectivity of most antagonists has been tested against NMDA and AMPA/kainate agonist-evoked responses but not mGluR agonist-evoked responses. This is important in light of the fact that AMPA and kainate are also agonists, albeit very weak, at group I mGluRs (Houamed et al. 1991; Masu et al. 1991; Pin et al. 1992). In addition, selective antagonists at AMPA but not kainate receptors have only recently been produced. The AMPA, kainate and NMDA receptors are classified as ionotropic receptors because they are integral ligand-gated ion channels whilst mGluRs generally use second messenger systems to activate an ion channel complex away from the ligand binding site.

1.2 Molecular Classification

There are four AMPA receptor subunits (GluR1-4) that can form functional homomeric or heteromeric complexes in *Xenopus laevis* oocytes or transfected cells (Hollmann et al. 1989; Boulter et al. 1990; Keinanen et al. 1990; Nakanishi et al. 1990; Sakimura et al. 1990). The GluR2 subunit confers upon the AMPA receptor a characteristic linear or outward rectification as well as a block in Ca^{2+} and Mg^{2+} permeability (Boulter et al. 1990; Nakanishi et al. 1990; Verdoorn et al. 1991; Hollmann et al. 1991). Desensitisation of AMPA receptors may occur faster than NMDA receptors depending on the agonist involved and subunit composition (Burnashev et al. 1992). However, lectins decrease or prevent native AMPA receptor desensitisation (Mayer and Vyklicky 1989; Huettner 1990). Kainate-evoked currents of AMPA receptors are enhanced by a cyclic adenosine monophosphate (cAMP)-dependent protein kinase A (PKA) possibly via GluR1 and GluR3 co-expressed subunits (Liman et al. 1989; Keller et al. 1992).

Kainate receptors consist of low-affinity (GluR5-7) and high-affinity (KA1 and KA2) subunits to [^{3}H]kainate binding (Bettler et al. 1990; Egebjerg et al. 1991; Werner et al. 1991; Bettler et al. 1992; Morita et al. 1992; Sommer et al. 1992; Herb et al. 1992; Sakimura et al. 1992). The GluR5 and GluR6 subunits can form functional homomeric complexes and depending on their edited form can exhibit either linear or inward rectification (Egebjerg et al. 1991; Sommer et al. 1992; Dingledine et al. 1992; Morita et al. 1992; Egebjerg and Heinemann 1993). The GluR5 and GluR6 subunits can also form functional heteromeric complexes with KA2 (Lomeli et al. 1992) such that kainate ligand binding properties and activity of the AMPA agonist are altered in comparison to the homomeric assemblies (Herb et al. 1992). The homomeric receptor channel comprised of GluR6 subunits is permeable to Ca^{2+} (Egebjerg and Heinemann 1993) and can be modulated with phosphorylation by PKA (Raymond et al. 1993; Wang et al. 1993).

The NMDA receptors consist of an NMDAR1 subunit, which can be expressed as a functional homomeric receptor in vitro but co-assembles with either of the four other subunits (NMDAR2A-2D) into functional heteromeric complexes in vivo (Moriyoshi et al. 1991; Ikeda et al. 1992; Kutsuwada et al. 1992; Meguro et al. 1992). The NMDAR1 subunit alone accounts for the outward rectification due to the Mg^{2+} channel blocker (Moriyoshi et al. 1991; Nakanishi et al. 1992), modulation by Zn^{2+} (Hollmann et al. 1993), antagonist action of protons (Traynelis et al. 1995), the binding of the co-agonist glycine (Nakanishi et al. 1992), polyamine activation (Benveniste and Mayer 1993) and modulation by protein kinase C (PKC; Durand et al. 1992), although these effects are slightly different between different splice variants. The most notable change in forming heteromeric complexes is an increase in current amplitudes (Ikeda et al. 1992; Kutsuwada et al. 1992; Meguro et al. 1992). There are also some differences between the different co-assemblies such as the strength of Mg^{2+} block, rise time of currents, decay of currents and potentiation of responses by PKC activators.

Eight mGluRs have been isolated (Pin and Duvoisin 1995; Duvoisin et al. 1995) and subdivided into three groups on the basis of amino acid sequence, signal transduction pathways and pharmacology. Group I comprises mGluR1 and mGluR5, which are both linked to inositol phosphate/Ca^{2+} signal transduction usually via a Pertussis toxin (PTX)-insensitive Gq protein (Abe et al. 1992; Aramori and Nakanishi 1992). Additionally, mGluR1 is coupled to activation of cAMP signal transduction and arachidonic acid release from cultured striatal neurones via separate G proteins (Aramori and Nakanishi 1992). Response kinetics are different between mGluR1 splice variants, particularly mGluR1α shows shorter latency and duration of Ca^{2+} transients to agonist application (Pin et al. 1992). However, activation of mGluR5a, but not mGluR1α, induces Ca^{2+} oscillations in transfected cells (Kawabata et al. 1996). Based on similar pharmacology of responses, group I mGluRs may also be involved in arachidonic acid release via phospholipase A2 (PLA2) activation provided the cell is depolarised by AMPA or

veratridine, a Na^+ channel activator which increases intracellular Ca^{2+} (Dumuis et al. 1990). Group I mGluRs have also been noted to inhibit the voltage-dependent K^+-current I_M and the Ca^{2+}-activated K^+-current I_{AHP} in hippocampal neurones (Baskys et al. 1990; Charpak et al. 1990; Gerber et al. 1992). Potentiation of AMPA and NMDA evoked responses as well as inhibition of an NMDA-mediated Ca^{2+} increase and $GABA_A$ receptor-mediated currents have also been implicated for group I mGluRs in several brain areas and in oocytes (Aniksztejn et al. 1992; Bleakman et al. 1992; Courtney and Nicholls 1992; Glaum and Miller 1993; Harvey and Collingridge 1993). Group II mGluRs comprise mGluR2 and mGluR3 and group III mGluRs comprise mGluR4, mGluR6, mGluR7 and mGluR8. Both group II and III mGluRs were shown to be coupled to inhibition of forskolin stimulation of cAMP production via a PTX-sensitive G protein (Tanabe et al. 1992, 1993). In addition, mGluR6 is a likely candidate for activation of a cyclic guanosine monophosphate (cGMP)-phosphodiesterase cascade leading to closure of cGMP-gated channels in ON-bipolar cells of the retina (Nawy and Jahr 1990; Shiells and Falk 1990). All mGluR groups can inhibit L-type Ca^{2+}-channels (Chavis et al. 1994; Lester and Jahr 1990; Sayer et al. 1992) although group I mGluRs can activate these channels under particular conditions (Chavis et al. 1994). Moreover, group I and II mGluRs also inhibit N-type Ca^{2+}-channels (Swartz and Bean 1992; Swartz et al. 1993). Lastly, a phospholipase D-coupled mGluR has been reported but as yet unassigned to a particular group (Boss and Conn 1992).

1.3 Glutamate Receptor Involvement in Neuronal Systems

1.3.1 Sensory Relays

Within several different sensory-driven central nervous system (CNS) areas, non-NMDA and NMDA receptors appear to maintain general roles in mediating responses evoked by both natural and artificial stimuli. Non-NMDA receptors typically mediate the main relay (monosynaptic) responses whereas NMDA receptors predominantly mediate polysynaptic responses resulting from the additional recruitment of local circuit neuronal activation. These characteristics of ionotropic glutamate receptors have been observed throughout sensory-driven areas such as the dorsal and ventral horn of the spinal cord (Davies et al. 1981, 1984, 1986; Davies and Watkins 1983; Ziskind-Conhaim 1990; King et al. 1992; Pinco and Lev-Tov 1993); ventrobasal thalamus (Salt 1986, 1987; Salt and Eaton 1989, 1991); lateral geniculate nucleus (Sillito et al. 1990a, 1990b); geniculo-cortical pathway (Tsumoto et al. 1986; Hagihara et al. 1988; Shirokawa et al. 1989); visual cortex (Stern et al. 1992); motor cortex (Herrling et al 1990; Salt et al. 1995); auditory cortex (Cox et al. 1992) and somatosensory cortex (Agmon and O'Dowd 1992; Armstrong-James et al. 1993). Furthermore, NMDA receptors were found to be lacking at especially large active zones presumed to be thalamocortical synapses in the primary somatosensory (SI) cortex (Kharazia and Weinberg 1999). The predominant involvement of non-NMDA receptors in fast monosynaptic responses versus NMDA receptors in slower polysynaptic responses has been attributed to a sensory-discriminative role. For instance, in the rat somatosensory cortex, Armstrong-James et al. (1993) found that short-latency responses to innocuous stimulation of the centre receptive field of a recorded neurone were mediated primarily by non-NMDA receptors whereas NMDA receptors mostly mediated the longer latency responses to either stimulation of the centre or surround receptive field. They suggest that the NMDA receptor-mediated response results partly from intracortical synapses due to the

latency of the response. A more direct example of an intracortical origin for an NMDA receptor-mediated response was shown in the cat motor cortex. For instance, a predominantly NMDA receptor-mediated recurrent excitatory postsynaptic potential (EPSP) evoked by stimulation of the pyramidal tract was recorded in pyramidal tract neurones (Herrling et al. 1990; Salt et al. 1995). In support of a functional role of both non-NMDA and NMDA receptors in specific sensory-discriminative aspects of neuronal responses, it was shown that NMDA receptors were recruited for mediating geniculo-cortical responses after using visual stimuli, but not when using electrical stimulation of the pathway (Tsumoto et al. 1986; Hagihara et al. 1988; Shirokawa et al. 1989).

The use of intracellular recordings has unmasked a participation of NMDA receptors in mediating monosynaptic EPSPs evoked in some sensory-driven areas such as in motoneurones of the ventral horn (Ziskind-Conhaim 1990; King et al. 1992; Pinco and Lev-Tov 1993); and the ventrobasal thalamus (Salt and Eaton 1991). Moreover, depending on the sensory-submodality, NMDA receptors may play a prominent role in mediating responses in certain areas. For example, NMDA receptors along with group I mGluR receptors but not non-NMDA receptors were involved in mediating nociceptive responses of single ventrobasal neurones (Eaton and Salt 1990; Eaton et al. 1993; Salt and Eaton 1994). Also, in the spinal cord, NMDA receptors are more likely to be involved in mediating nociceptive responses evoked by stimuli that produce sensitisation (Dickenson and Sullivan 1990; Haley et al. 1990; Schaible et al. 1991). Therefore, it appears that NMDA receptors have a substantial contribution to sensory synaptic relay in the form of a longer latency and/or longer duration component of responses throughout the CNS.

However, some exceptions exist concerning the involvement of NMDA receptors in sensory-evoked transmission in some CNS areas. Purkinje cells of the adult rat cerebellum which possess few or no NMDA receptors have responses originating from climbing fibre and

parallel fibre synapses which are almost entirely mediated by non-NMDA receptors (Hirano and Hagiwara 1988; Garthwaite and Beaumont 1989; Konnerth et al. 1990).

Although numerous pharmacological studies have shown the involvement of mGluRs in synaptic transmission, a physiological role with respect to sensory-evoked responses has been less explored partly due to a previous lack of specific agonist and antagonists acting at either pre- or post-synaptic mGluRs. The existence of presynaptic mGluRs based on anatomical and physiological findings predicts a regulatory role for mGluRs in synaptic efficacy. Presynaptic effects, typically involving group II or III mGluR-mediated suppression of synaptic transmission have been observed e.g. in the spinal cord (Jane et al. 1994; King and Liu 1996); ventrobasal thalamus (Salt and Eaton 1994, 1995); visual cortex (Sladeczek et al. 1993) and somatosensory cortex (Taylor and Cahusac 1994). Postsynaptic excitatory effects evoked by group I mGluR agonists have also been observed in the spinal cord (Birse et al. 1993), including enhancing responses to ionotropic agonists (Cerne and Randic 1992; Ugolini et al. 1997) and in the somatosensory cortex (Taylor and Cahusac 1994).

The involvement of mGluRs in sensory-evoked responses was shown in ventrobasal neurones (Eaton et al. 1993; Salt and Eaton 1994). In these studies, group I mGluRs substantially contributed to mediating nociceptive responses evoked by a noxious thermal stimulus. In support of these findings, mGluR1α immunoreactivity was shown on dendrites of thalamic relay neurones (Martin et al. 1992). Evidence also exists for the involvement of mGluRs in mediating nociceptive responses in the spinal cord evoked by brief stimuli (Neugebauer et al. 1999) or mostly by sustained stimuli (Young et al. 1997) and during development of hyperalgesia (Fisher and Coderre 1998). In contrast to mGluR5, mGluR1 was shown to play a crucial role in mediating nociception in the spinal cord, particularly following sustained noxious input (Young et al. 1997, 1998). The similar role of NMDA receptors in mediating nociceptive responses in the spinal cord as well as their general involvement in longer

latency synaptic influences would imply that nociceptive responses are longer latency responses, especially in supraspinal structures where nociceptive transmission may be integrated. In addition to nociception, group I mGluRs have been shown to mediate a switch from burst to tonic activity of lateral geniculate nucleus cells resulting in a decrease of the detection of a visual stimulus (Godwin et al. 1996).

1.3.2 Synaptic Plasticity

The fact that NMDA receptors require sufficient depolarisation to relieve the channel block by Mg^{2+} and that mGluRs can exist presynaptically makes them probable candidates for coincident event detection between neurones, which is required for long-term changes in synaptic efficacy. Furthermore, the role of NMDA and mGluR receptors in Ca^{2+} conductances and intracellular cascades leading to protein synthesis, makes them prime candidates for involvement in maintained activity and plasticity. Interestingly, the increased expression of AMPA receptors in the late phase of long-term potentiation (LTP) has been shown to depend on transcription and PKA (Nayak et al. 1998).

The hippocampus has become the focus of research concerning synaptic plasticity due to its involvement in learning and memory. In the hippocampus, there are four well-studied excitatory synapses that can display LTP: i) the perforant path to granule cell synapse, ii) the CA3 Schaffer collateral/commissural fibre to CA1 pyramidal cell synapse iii) the CA3 associational/commissural fibre to CA3 pyramidal cell synapse iv) and the mossy fibre to CA3 pyramidal cell synapse. The first three synaptic relays typically share common receptor pharmacology for LTP. These synapses have been shown to rely on postsynaptic NMDA receptors for the induction of LTP (Collingridge et al. 1983; Urban et al. 1996; Debanne et al. 1998) by a mechanism involving increase in postsynaptic Ca^{2+} (Lynch et al. 1983). Although a presynaptic mechanism for the maintenance of LTP cannot be excluded at these synapses,

evidence for increased expression of postsynaptic AMPA receptors during LTP would add to support for a postsynaptic mechanism (Nicoll and Malenka 1999). Variable roles of mGluRs in LTP have been shown, yet more evidence exists for the involvement of mGluRs in the induction phase rather than the maintenance phase of LTP. Previous results showed that mGluRs were involved in the initial induction of LTP at synapses that have not previously undergone LTP (Bortolotto et al. 1994).

The mossy fibre to CA3 pyramidal cell synapse has been distinguished by displaying an NMDA receptor-independent LTP (Zalutsky and Nicoll 1990), which was shown to be induced by kainate (Bortolotto et al. 1999), opioids (Derrick et al. 1991) or increase in presynaptic Ca^{2+} concentration corresponding to an enhancement of neurotransmitter release (Regehr and Tank 1991). However, an NMDA receptor-independent LTP was also observed in the CA1 area and was induced by the involvement of group II and III mGluRs but not group I mGluRs (Grover and Yan 1999). Nevertheless, mGluRs (likely group I) have more often been shown to facilitate the induction and persistence of NMDA receptor-dependent LTP (Cohen et al. 1999; Raymond et al. 2000).

Homosynaptic long-term depression (LTD) arising from activated, as opposed to inactive synapses, also involves NMDA receptors for the induction phase (Dudek and Bear 1992; Mulkey and Malenka 1992) and increase in Ca^{2+} throughout. However, unlike LTP, voltage-dependent Ca^{2+} channels (VDCC) do not appear to be involved in homosynaptic LTD (Mulkey and Malenka 1992). Recently, group I and II mGluRs were also shown to be involved in the induction of LTD (Huang et al. 1999). There is also increasing evidence of LTD induction resulting from internalisation of AMPA receptors (Lusher et al. 1999; Luthi et al. 1999).

Neocortical areas also exhibit LTP and LTD similar to that observed in the hippocampus. In the neocortex of freely moving rats, LTP induced by high- or low-intensity extracellular stimulation was blocked by an NMDA receptor antagonist, which also unmasked a

depression of the population spike and polysynaptic components evoked by the same stimulation (Trepel and Racine 1998). Similarly, depression of spontaneous firing was also observed when nociceptive responses in the SI cortex of anaesthetised rats were blocked by an NMDA receptor antagonist (Pollard 2000). The unmasked depression observed following maintained responses across cortical areas suggests that NMDA receptors play a specific role in plasticity.

The NMDA receptor-independent LTP has been associated with a reduction in paired pulse facilitation during its induction. In the corticothalamic synapse, LTP is induced in a Ca^{2+}-dependent manner by a presynaptic action, perhaps via an mGluR, as activation of PKA induced a synaptic enhancement associated with a decrease in paired pulse facilitation (Castro-Alamancos and Calcagnotto 1999). There is also evidence for the facilitation of LTP induction through postsynaptic group I mGluRs in layer V neurones of the prelimbic cortex (Morris et al. 1999). In the rat prefrontal cortex, group I and II mGluRs were shown to be involved in the induction of LTD through a postsynaptic mechanism (Otani et al. 1999). However, in layer IV of the SI cortex, LTD was induced by activation of group II mGluRs via coincident presynaptic and postsynaptic activity excluding NMDA or AMPA receptors (Egger et al. 1999).

Plasticity also occurs in the CNS during development. Ocular dominance of neuronal responses, occurring in the visual cortex and visuo-motor areas, involves the enhancement of responses to stimulation from one eye at the expense of the other during a critical period of development. The involvement of NMDA receptors is evident and as in LTP and LTD, coincident detection between the presynaptic and postsynaptic cell appears to be required (Raushecker and Singer 1979, 1981). The mechanism of ocular dominance can be explained from data obtained in vitro, which would suggest that heterosynaptic LTD may be more readily induced when NMDA receptor conductances are strong enough to activate VDCC at inactive sites (Lynch et al. 1977; Abraham and Goddard 1983; Pockett et al. 1990). As detailed

previously (Artola and Singer 1993), the occurrence of LTP and LTD may be determined by intracellular Ca^{2+} concentrations. Presumably, heterosynaptic LTD would occur if the depolarisation due to the increase in intracellular Ca^{2+} reaches the threshold for LTD, but is below the threshold for LTP at inactive sites. In addition, a recent study showed that homosynaptic LTD occurred at visually deprived inputs as a result of spontaneous residual activity (Rittenhouse et al. 1999).

In the cerebellum, disruption of spinocerebellar afferent topography refinement occurred during antagonism of NMDA receptors (Tolbert et al. 1994). Similarly, disruption of topographic refinement has been shown to occur in the SI cortex when non-NMDA and NMDA receptors were antagonised during the critical period for barrel development (Fox et al. 1996). Somatotopic refinement involving sensory-evoked responses was also disrupted during NMDA receptor antagonism in the dorsal horn of the spinal cord (Lewin et al. 1994) and in the trigeminal and dorsal column pathways (Iwasato et al. 1997).

1.3.3 Rhythmic Activity

Rhythmic activity is a means by which neuronal elements can bind multiple inputs coherently and periodically to produce a composite effect. The generation of synchronous rhythmic activity during behaviourally relevant experiences is not entirely understood although inhibition and intrinsic membrane oscillations are key players. Clearly, the underlying circuitry involved in synchronous activity will determine the generating factors. Little is known about the involvement of specific glutamate receptors in rhythmic activity in vivo. However, in vitro experiments have shown similar roles to those described above for glutamate receptors in synaptic transmission activity with an involvement of different receptor kinetics and inhibitory influences.

Fast rhythmic activity consisting of 100-400 Hz or gamma frequency (20-80 Hz) was shown to be mediated or synchronised by AMPA/kainate receptors in the hippocampus (Taylor et al. 1995; Lamsa et al. 2000; Palva et al. 2000) and somatosensory cortex (Buhl et al. 1998; Fisahn and Buhl, 2000). Additionally, two studies have shown the involvement of AMPA/kainate receptors in 4-8 Hz and 1-5 Hz rhythmic activity near the trigeminal motor nucleus (Kogo et al. 1996) and layer II/III of the somatosensory cortex (Flint and Connors 1996) respectively.

In comparison to AMPA/kainate receptors, NMDA receptors have been shown to participate in slower rhythmic activity. In the presence of tetrodotoxin (TTX), NMDA application induced rhythmic low-frequency (0.09-1.45 Hz) voltage oscillations in spinal cord motoneurones (Hochman et al. 1994). In addition, long-duration slow rhythmic oscillations were shown to involve NMDA receptors in trigeminal motoneurones (Katakura and Chandler 1990). In retrohippocampal regions, NMDA receptors were involved in mediating a slow depolarising potential, which determined the period of superimposed gamma-frequency oscillations (Funahashi and Stewart 1998). Although the gamma-frequency activity could be abolished when the depolarising potential was blocked, GABAA receptors were necessary in phasing gamma-frequency activity, which has been shown to exist without the slow depolarisation (Traub et al. 1996a; Jefferys et al. 1996; Funahashi and Stewart 1998). In Mg^{2+}-free medium, NMDA receptor-dependent oscillations (1-4 Hz) were shown to occur in thalamocortical neurones (Leresche et al. 1991) and they similarly mediated oscillations (8-12 Hz) in layer V somatosensory cortex (Flint and Connors 1996). Intrinsically bursting neurones of layer V somatosensory cortex showed spontaneous oscillations (4-12 Hz) also in the absence of extracellular Mg^{2+} (Flint et al. 1997), presumably mediated by NMDA receptors (Traub et al. 1994). Although NMDA receptors may allow for synchronising neocortical oscillations occurring in Mg^{2+}-free medium, NMDA receptor expression does not change over the age-

dependent occurrence of these oscillations, which therefore might be generated as a result of the developing intrinsic membrane properties of intrinsically bursting neurones of layer V somatosensory cortex (Flint et al. 1997). Interestingly, neuronal modelling has predicted that NMDA receptors at recurrent synapses with slow desensitising kinetics (150 msec) are suited for recall of heteroassociative memories represented as a sequence of seven gamma-frequency (~40 Hz) cycles enveloped in theta-frequency (~6 Hz) oscillations (Jensen and Lisman 1996). Furthermore, based on neuronal modelling, NMDA receptors with faster kinetics (15-50 msec) found in neocortical areas were proposed to be involved in forming long-term memories from short-term memories by mediating single gamma-frequency cycles through other recurrent synapses (Jensen et al. 1996). Along this focus, there are studies that have shown NMDA receptor-mediated rhythmic bursts comprising of low-threshold Ca^{2+} spikes (Khateb et al. 1995) and Na^{+} spikes (Hu and Bourque 1992; Kim and Chandler 1995) in CNS neurones. Depending on the hyperpolarisation of the neurone, the intra-burst frequency of the Ca^{2+} spikes can occur within the gamma-frequency range (Khateb et al. 1995). Also, Ca^{2+} oscillations occurring via the L-type VDCCs in cortical neurones were shown to involve activation of NMDA receptors and consisted of brief action potential bursts on the rising phase (Robinson et al. 1993; Wang and Gruenstein 1997).

Second messenger systems linked to mGluRs could provide flexibility of neuronal signalling for example, via activation of membrane channels and/or intracellular Ca^{2+} stores. For instance, mGluRs were shown to be involved in inducing oscillatory activity, which could permit synchronisation between hippocampal CA3 neurones by AMPA/kainate receptor-mediated conductances (Taylor et al. 1995). Some nonpyramidal cells in the stratum oriens of the CA1 hippocampus were shown to exhibit group I and II mGluR-mediated Ca^{2+} oscillations involving VDCC and intracellular Ca^{2+} stores (Woodhall et al. 1999). In the immature neocortex, mGluR5-mediated Ca^{2+} neuronal oscillations have been proposed to play a role in the

regulation of gene expression and developmental events (Flint et al. 1999). In addition, there are presynaptic mGluR-induced oscillations in inmmature CA3 hippocampal neurones acting via Ca^{2+} release from intracellular stores (Aniksztejn et al. 1995). In support of the above, there is a high expression of mGluR7 at pyramidal cell terminals presynaptic to mGluR1α-expressing nonpyramidal cells in the hippocampus (Shigemoto et al. 1996). Also, recordings from nonpyramidal cells in stratum oriens of the CA1 hippocampus showed that miniature EPSCs were not increased in contrast to mGluR-activated EPSCs (McBain et al. 1994).

1.4 Aims

As specific roles for glutamate receptors throughout the CNS have emerged, it was the aim of this study to investigate the differential involvement of AMPA/kainate and NMDA receptors in neuronal responses evoked by two types of sensory stimuli in the SI cortex. However, the relevance of receptor-mediated responses depends upon the underlying circuitry involved. In order to gain insight into the organisation of cortical circuits, three anatomically identified subtypes of nonpyramidal cells in the CA1 region of the hippocampus were studied for their expression of mGluR1α receptors as well as their intrinsic membrane properties. The organisation of cortical circuits was studied in the hippocampus because it is the best-defined area of the cerebral cortex. Further to this, the hippocampus is considered to be a high-order associational cortical area providing a better understanding of the role of glutamate receptors in cortical areas influenced by behaviourally relevant experiences. As such, recordings of anatomically identified nonpyramidal cells in the CA1 region were also obtained during state-dependent synchronous activity.

CHAPTER 2: Ionotropic Glutamate Receptor-Mediated Responses in the Rat Primary Somatosensory Cortex Evoked by Noxious and Innocuous Cutaneous Stimulation In Vivo

2.1 Introduction

Glutamate receptors have been shown to be the key mediators of sensory-driven excitatory synaptic transmission (Salt and Herrling 1995). Considering the variety of somatosensory sensations and the variety of glutamate receptors that exist, it is of interest to establish whether different somatosensory stimuli can be distinguished on the basis of the involvement of glutamate receptor subtypes. The ionotropic glutamate receptors, AMPA/kainate and NMDA, have been shown to mediate responses evoked by innocuous cutaneous stimuli in somatosensory-driven areas of the brain (Salt 1986; Armstrong-James et al. 1993). These receptors also mediate responses evoked by noxious cutaneous stimuli. The relative contribution of the ionotropic glutamate receptors in nociceptive responses differs along the neuroaxis. In the spinal cord, there is evidence for the involvement of both NMDA (Dickenson and Sullivan 1990; Haley et al. 1990) and AMPA/kainate receptors (Cumberbatch et al. 1994). In the lateral thalamus, however, NMDA receptors have been shown to mediate nociceptive responses whereas AMPA/kainate receptors made little contribution (Eaton and Salt 1990).

The involvement of glutamate receptors in nociceptive responses in the primary somatosensory (SI) cortex has not been determined but several other physiological properties of SI nociceptive responses have been characterised. Neurones in the SI cortex that respond to noxious stimuli can be classified into two main types (Lamour et al. 1983) similar to the

spinal cord (Price and Dubner 1977) and thalamus (Guilbaud et al. 1980). Nociceptive specific (NS) neurones respond only to noxious stimuli whereas wide dynamic range (WDR) neurones respond to noxious as well as non-noxious stimuli. Both types of SI nociceptive neurones show graded responses in accordance with the degree of the noxious stimulus (Lamour et al. 1983; Kenshalo et al. 1988).

The aim of the present study was to determine which types of ionotropic glutamate receptors may be involved in mediating SI high-threshold (HT) responses evoked by noxious mechanical and thermal stimuli applied to the peripheral cutaneous receptive field. High-threshold responses were recorded from individual SI neurones in urethane anaesthetised rats in vivo. Anaesthesia was maintained at a level in which the rat showed a lack of hindpaw and corneal reflexes. The intensity of the noxious stimuli used in the present study was above that which has been reported to elicit a painful reaction and nociceptive responses in animal behavioral studies (Cahusac et al. 1990). These noxious stimuli were able to evoke similar response characteristics as nociceptive responses reported in the previous studies cited above. However, it was not possible to establish that the responses to noxious stimuli resulted from nociceptive perception rather than non-specific activation. Therefore, noxious stimulus-evoked responses in this study were referred to as HT responses instead of nociceptive responses. Low-threshold (LT) responses evoked by innocuous cutaneous stimuli were also examined to enable comparison of the involvement of ionotropic glutamate receptors in both HT and LT responses of individual neurones.

2.2 Materials and Methods

2.2.1 Animal Preparation

Male Wistar rats (200-500 g; Charles River, UK) were housed with 12 h to 12 h light/dark cycles and *ad libitum* food and water. These animal living conditions and the following procedures were in accordance with the approved Project Licence [The Animals (Scientific Procedure) Act, UK] and the "Principles of laboratory animal care" (NIH publication 86-23). Animals were given an inhalation anaesthetic of 5 % halothane in air followed by urethane (25 % w/v, 1.2 g kg^{-1}; Sigma-Aldrich Ltd., Dorset, England) injection intraperitoneally to maintain the animal anaesthetised for long periods. An additional 10 % of the original urethane dose was administered until the general anaesthetic effects of urethane resulted in a lack of hindpaw and corneal reflexes. After general anaesthesia was established, the neck and cranial areas were shaved for surgical procedures. Lignocaine (1 %) with adrenaline (1:200,000) was applied intradermally prior to incisions. Anaesthetic level was monitored throughout the entire experiment by periodically checking for hindpaw or corneal reflexes and observing any increases in heart rate which was continuously monitored. The precautions taken resulted in a stable heart rate throughout the entire experiment.

A tracheotomy was performed for the insertion of a cannula (nylon tubing, ID 1.50 mm) into the trachea as an external aid to clearing the airway. The animal was gently positioned in the stereotaxic frame with non-traumatic ear bars and an incisor bar so as to orient the head in a flat-skull position (Paxinos and Watson 1986). A thermostatically controlled heating pad (Harvard Apparatus Ltd., Kent, England) maintained the animal's temperature at 37°C. The animal was earthed with a silver wire inserted subcutaneously along the dorsal side of the

neck. Heart rate was monitored by two silver wires inserted subcutaneously through the dorsal side of the forelimb and hindlimb, ipsilateral to the recording site. A craniotomy was then performed and the dura removed to expose the SI cortex over the representation of the forepaw (1.5 to -1 mm AP, 3 to 4.5 mm ML) or hindpaw (0.5 to -2 mm AP, 2 to 3.5 mm ML), according to the atlas of Chapin and Lin (1984). Saline (150 mM NaCl) or mineral oil was applied in the craniotomy to avoid drying of the cortex. The electrode was placed over the appropriate region using a micromanipulator. After the experiment, the animal was killed with an intracardial overdose of urethane.

2.2.2 Recording and Iontophoresis

Multibarreled electrodes consisting of 7 barrels (~6 μm in total tip diameter) were made from borosilicate glass tubes with filament (1.5 mm O.D.) and used for extracellular single unit recording and iontophoresis. The middle barrel was filled with 4 M NaCl for extracellular single unit recordings. Each surrounding barrel was filled with a different solution: (RS)-α-amino-3-hydroxy-5-methyl-4-isoxazolepropionic acid (AMPA; 5 mM in 150 mM NaCl, pH 8), N-methyl-D-aspartic acid (NMDA; 50 mM in dH_2O, pH 8), 6-nitro-7-sulphamoylbenz[f]quinoxaline-2,3-dione (NBQX; 1 mM in 50 mM NaCl, pH 8), (RS)-3-(2-carboxypiperazin-4-yl)-propyl-1-phosphonic acid (CPP; 20 mM in 75 mM NaCl, pH 8) and 1 M NaCl (for automatic current balancing). All pH levels of drug solutions were adjusted with 1M NaOH. Iontophoresis of drugs was achieved using the Neurophore-BH2 Micro-Iontophoresis System (Medical Systems Corp., New York, USA) and all drugs were retained with positive current (16 to 23 nA). Retaining currents were empirically tested during experiments for values that did not allow the electrode to block and did not allow increased

activity of neurones via the individual agonists or inhibition of spontaneous activity via the individual antagonists. The average agonist and antagonist ejection values were -91 nA for AMPA, -104 nA for NMDA, -4 nA for CPP and -8 nA for NBQX (n=13 cells tested with both innocuous and noxious stimulation). The drugs AMPA, NMDA, NBQX and CPP were obtained from Tocris Cookson Ltd., Bristol, England. All neurones were recorded from a depth of 1300 to 1700 μm below the pial surface, where most neurones responding to noxious stimulation were encountered with our electrodes. Agonist and sensory stimuli were automatically timed using a programmable pulse generator (Master-8, A.M.P.I, Jerusalem, Israel). Extracellular signals were amplified (x10 Axoprobe-1A, Axon Instruments Inc., California, USA; x100 NeuroLog System, Digitimer Ltd., Hertfordshire, England), filtered (500 Hz to 2 kHz band width, NeuroLog) and action potentials detected by a window discriminator (NeuroLog System) were recorded as TTL pulses via a 1401plus CED interface (Cambridge Electronic Design Ltd., Cambridge, England) to a computer running Spike (courtesy of Dr. T. E. Salt) and Spike 2 (Cambridge Electronic Design Ltd.) software.

2.2.3 Sensory Stimulation

As the electrode was stepped down, a glass probe was lightly swept across or tapped manually on the animal's forepaw or hindpaw to confirm the region of recording and to determine the low-threshold receptive field. Some neurones were analyzed for low-threshold responses using a computer controlled jet of air, typically a train of ten air jets of 10 ms duration every 2 s. The noxious mechanical stimulus was a peripheral pinch (usually 5 s) of the forepaw or hindpaw. The paw at the level of the digits and palm/plantar was placed in the serrated forceps having a triangular contact area of 13 mm^2. The forceps was

pneumatically closed exerting a pressure of 183 g/mm^2 which was above the threshold of pain in behaving rats (Cahusac et al. 1990). The noxious thermal stimulus was applied by immersion (10-30 s) of the distal 3/4 of the tail into water at 52°C. The thermal stimulus of 52°C was above the noxious thermal threshold for SI nociceptive neurones (45-47°C) previously determined for awake and anaesthetised animals (Lamour et al. 1983; Kenshalo et al. 1988; Chudler et al. 1990). During noxious stimulus trials, a long interstimulus interval (5 min) was used to allow recovery of responses. Noxious mechanical stimulation was applied outside the low-threshold receptive field of the recorded neurone so as to avoid possible influences from innocuous stimulation. A response was considered to be high-threshold if it was not influenced by low-threshold stimulation, both by light brushing or applying an innocuous pressure with a glass probe outside the low-threshold receptive field of the recorded neurone.

2.2.4 Experimental Protocol

One neurone per animal was studied. Once a single neurone was isolated, controls with reproducible responses were established for agonist-evoked responses, and in some neurones, preceded by low-threshold sensory-evoked responses. Intervals following the end of a train of 10 air jet stimuli (10 ms every 2 s) and agonist ejection (10 s each) were 10 s and 50 s, respectively. An antagonist was then continuously ejected until it blocked the appropriate agonist-evoked response. All responses were allowed to recover before the second antagonist was ejected. Upon termination of the ejection of the antagonist, the period of response recovery ranged between 2 and 11 min. Noxious stimulus trials at 5 minute trial intervals were started one or two minutes afterwards. The antagonist was tested against the response

evoked by the noxious stimulus, using the same duration and current previously determined to antagonise selectively a particular agonist-evoked response. Upon termination of the antagonist ejection, the HT response was allowed to recover and in some cases, a second antagonist was tested similarly. The recovery period of the HT response after termination of the antagonist ejection ranged between 3 and 19 min.

2.2.5 Response Analysis

Peristimulus time histograms (PSTHs) representing the number of action potentials were created on-line using the Spike and Spike2 software. Cumulative PSTHs over all trials (including responses during antagonist ejection) for each recorded neurone were made to distinguish slow responses from the average baseline activity. Vertical cursors were positioned by eye, after the stimulus onset, at the beginning and end of the period where firing exceeded the baseline activity. Responses were measured as the number of spikes within the cursors exceeding the average baseline activity for each trial. Responses evoked by an air jet were summed over a train of 10 air jets in one trial. Inhibition was quantified as a negative response value (i.e. baseline activity exceeding the evoked response). The effects of each antagonist on the sensory responses are presented as the mean ± SEM for clarity of the response variability, although the data are not normally distributed. The Wilcoxon rank sum test was used as a paired nonparametric test for significance between two sets of similar data and is reported as two-tailed p values. Correlation coefficients (r) indicate whether distinct responses were correlated.

2.3 Results

2.3.1 Response Characteristics

Quantitative data were obtained for a total of 31 primary somatosensory neurones tested with noxious somatosensory stimuli. Additionally, LT responses were recorded from thirteen of these neurones to compare the receptors involved in mediating two sub-modality types.

Most single units encountered in one vertical penetration responded to an innocuous cutaneous stimulus. The LT receptive fields were small and located contralaterally in accordance with the SI low-threshold hindpaw or forepaw somatotopic region of recording. A short-latency component of the LT responses was detected in two or three 10 ms bins (n=11/13 and n=2/13, respectively) and had an average percent increase in response of 87 ± 13 % from baseline activity (n=13/13). The average firing rate of the short-latency response evoked in the first 10 ms bin and the baseline activity was 74 ± 11 spikes/s and 7 ± 2 spikes/s, respectively (n=13/13; Figure 2.1). The short-latency response was sometimes followed by an inhibition observed as an action potential rate below baseline activity (n=3/13) but more often by a lower frequency excitatory component lasting an average of 415 ± 92 ms (n=8/13; Figure 2.1).

Less than 10 % of neurones encountered responded to noxious stimuli. Some mechanical and thermal HT responses were weak, possibly due to an effect of anaesthesia. Mechanical or thermal HT responses could be evoked by applying the noxious stimulus outside the verified LT receptive field and this was always done to avoid any influence from LT responses. A light touch or light pressure applied with a glass probe outside of the LT

receptive field did not evoke a response, although a noxious stimulus did. The receptive fields pertaining to neurones evoked by noxious stimuli were often large, e.g. including the ipsilateral or contralateral limbs and ears, and sometimes the tail as well.

The duration of the mechanical HT responses evoked by a 5 s peripheral noxious pinch was analyzed for 10 of 13 neurones tested with noxious as well as non-noxious stimuli. The other three neurones were not included in the analysis of the response duration because they were tested with varying durations of noxious thermal stimuli. High-threshold responses decayed gradually upon termination of the 5 s noxious pinch and lasted on average for 15.1 ± 1.9 s (Figures 2.1 and 2.2) for 10 neurones. The increase in baseline activity made it difficult to evaluate the magnitude of mechanical (Figure 2.1) and thermal HT responses. Measured from the increased baseline activity, the average percent increase of peak mechanical and thermal HT responses was 56 ± 8 % (n=13/13).

Figure 2.1 Sensory-evoked responses and increase in baseline activity. Single-trial PSTHs represent action potential responses counted in 10 ms bins for responses evoked by a train of 10 air jets of 10 ms duration each **(A)** and responses evoked by a 5 s noxious pinch **(B and C)**. The bars above each PSTH correspond to the period of sensory stimulation. The short-latency component of the LT response occurs in the first two 10 ms bins after the air jet stimuli followed by a longer latency component (A). Baseline activity prior to the noxious stimulus (B) was similar to (A). Note the bin size for air jet-evoked responses is different so as to show both the short-latency and long-latency components (A). Noxious stimuli were repeated until trials were reproducible (C). Baseline activity increased after the first pinch, and in this case, the response also increased (C).

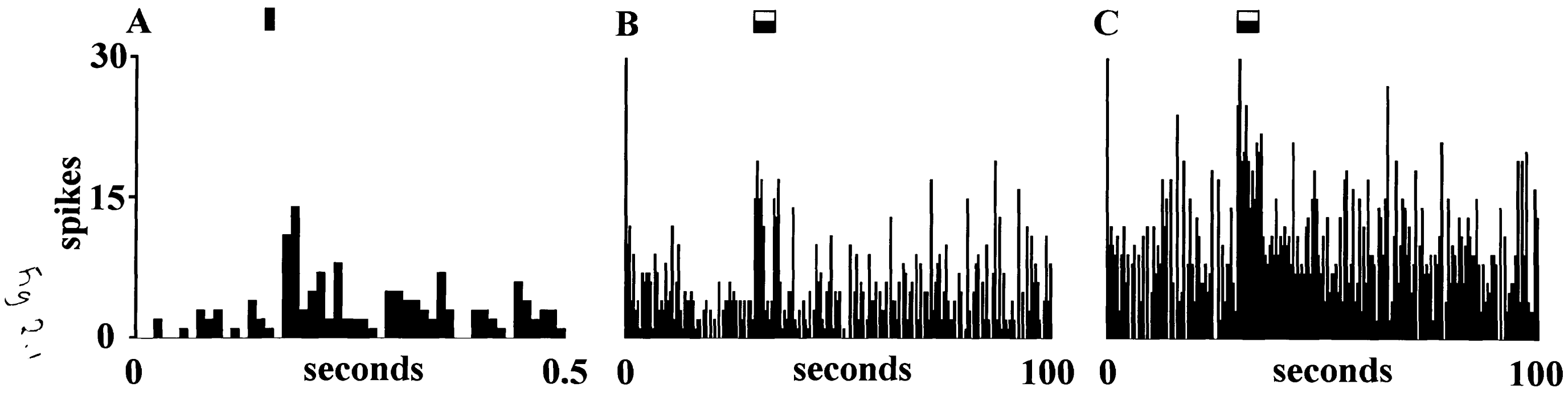

▮ 10 ms Air Jet
train of 10 Air Jets
single trial 10 ms bins

▬ Noxious Pinch 5 s
500 ms bins

Figure 2.2 Neurone in the forepaw area of the SI cortex and the effect of CPP against a noxious pinch-evoked response. Single-trial PSTHs represent action potential responses counted in one second bins. The bars above each PSTH correspond to the period of agonist applications (each 10 s) or a noxious pinch stimulus (5 s). Agonist trials were performed first to establish the selectivity of the antagonist followed shortly by noxious stimulus trials. The top row are control responses to iontophoretic application of NMDA and AMPA **(A1)** and to a noxious pinch stimulus applied to the contralateral forepaw digits **(A2)**. Control trials had reproducible responses. During continuous iontophoretic application of CPP at -7 nA for 8 min (last trial shown), the response to NMDA was antagonised selectively **(B1)** and the response to noxious stimulation was replaced by an inhibitory response indicated by a reduction below the baseline activity **(B2)**. The NMDA-evoked response **(C1)** and the sensory-evoked synaptic response **(C2)** recovered following termination of CPP ejection. Note also a reduction in baseline activity during CPP ejection (B1 and B2).

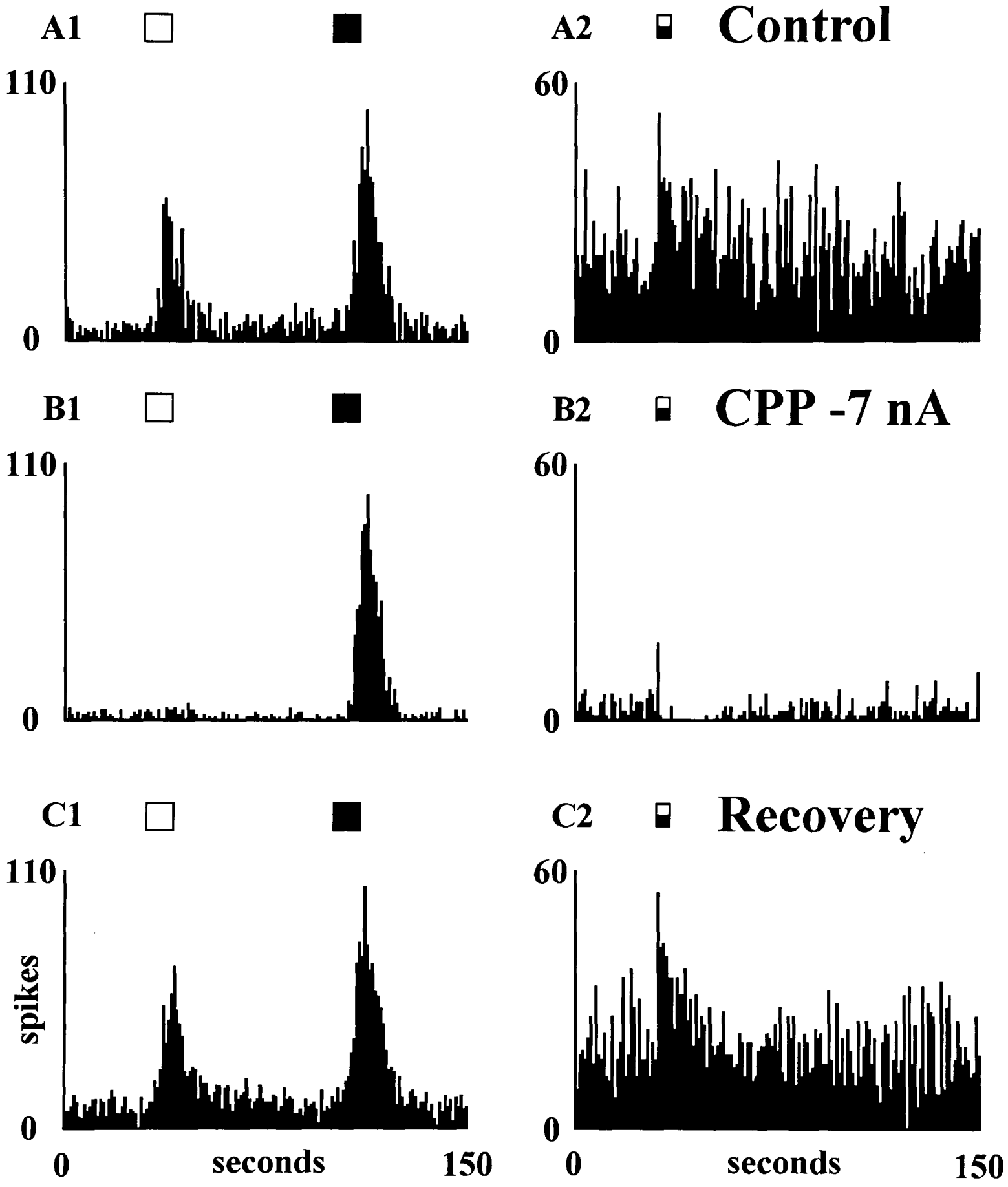
A1
A2
Control
110
0
60
0
B1
B2
CPP -7 nA
110
0
60
0
C1
C2
Recovery
110
spikes
0
60
0
0
seconds
150
0
seconds
150
NMDA -120 nA
AMPA -138 nA
Noxious Pinch 5 s

Fig 2.2

2.3.2 Effects of CPP and NBQX on High-Threshold Responses

Data were pooled for all neurones tested with noxious stimuli (n=31). Twenty-two neurones were investigated for each antagonist used and 13 of these 22 neurones were tested with both antagonists, applied sequentially. Six neurones were tested with a noxious pinch stimulus as well as a noxious thermal stimulus sequentially for one antagonist and in one case for two antagonists. The involvement of NMDA and AMPA/kainate receptors in sensory-evoked responses was tested using CPP and NBQX, selective antagonists at NMDA and AMPA/kainate receptors, respectively. The selectivity of these antagonists at the respective receptors was established by testing their effects against agonist-evoked responses for each recorded neurone. Iontophoresis of CPP caused a marked reduction of the responses evoked by a noxious pinch (21 ± 10 %; n=19/19; Figure 2.2) or noxious thermal stimulus (24 ± 18 %; n=5/5; Figure 2.3). Mechanical (n=9/19) and thermal (n=1/5) HT responses were completely blocked by CPP during which an inhibition replaced the response evoked by the noxious mechanical (n=7/19; Figure 2.2) or thermal (n=1/5) stimulus in comparison to the prestimulus baseline activity. The reductions caused by NBQX were also substantial although smaller than those observed with CPP. The response remaining following NBQX ejection when applying a noxious pinch was 42 ± 12 % (n=19/19; Figure 2.4). The response remaining following NBQX ejection when applying a noxious thermal stimulus was 63 ± 16 % (n=8/8; Figure 2.5). Mechanical HT responses were completely blocked by NBQX in only four neurones and in these neurones, an inhibition replaced the response evoked by the noxious stimulus during application of NBQX. Some neurones had mechanical HT responses which were virtually unaffected by the antagonists (greater than 80 % of control responses; n=3 of 19 neurones for CPP and n=6 of 19 neurones for NBQX).

Figure 2.3 Neurone in the forepaw area of the SI cortex and the effect of CPP against a noxious heat-evoked response. Records are similar to Figure 2.2. The top row are control responses to iontophoretic application of NMDA and AMPA **(A1)** and to a 52°C noxious heat applied to the tail for 15 s **(A2)**. Continuous ejection of CPP at -2 nA for 20 min (last trial shown), selectively antagonised the response to NMDA **(B1)** and substantially reduced the response to noxious stimulation **(B2)**. The NMDA-evoked response **(C1)** and the sensory-evoked synaptic response **(C2)** recovered following termination of CPP ejection.

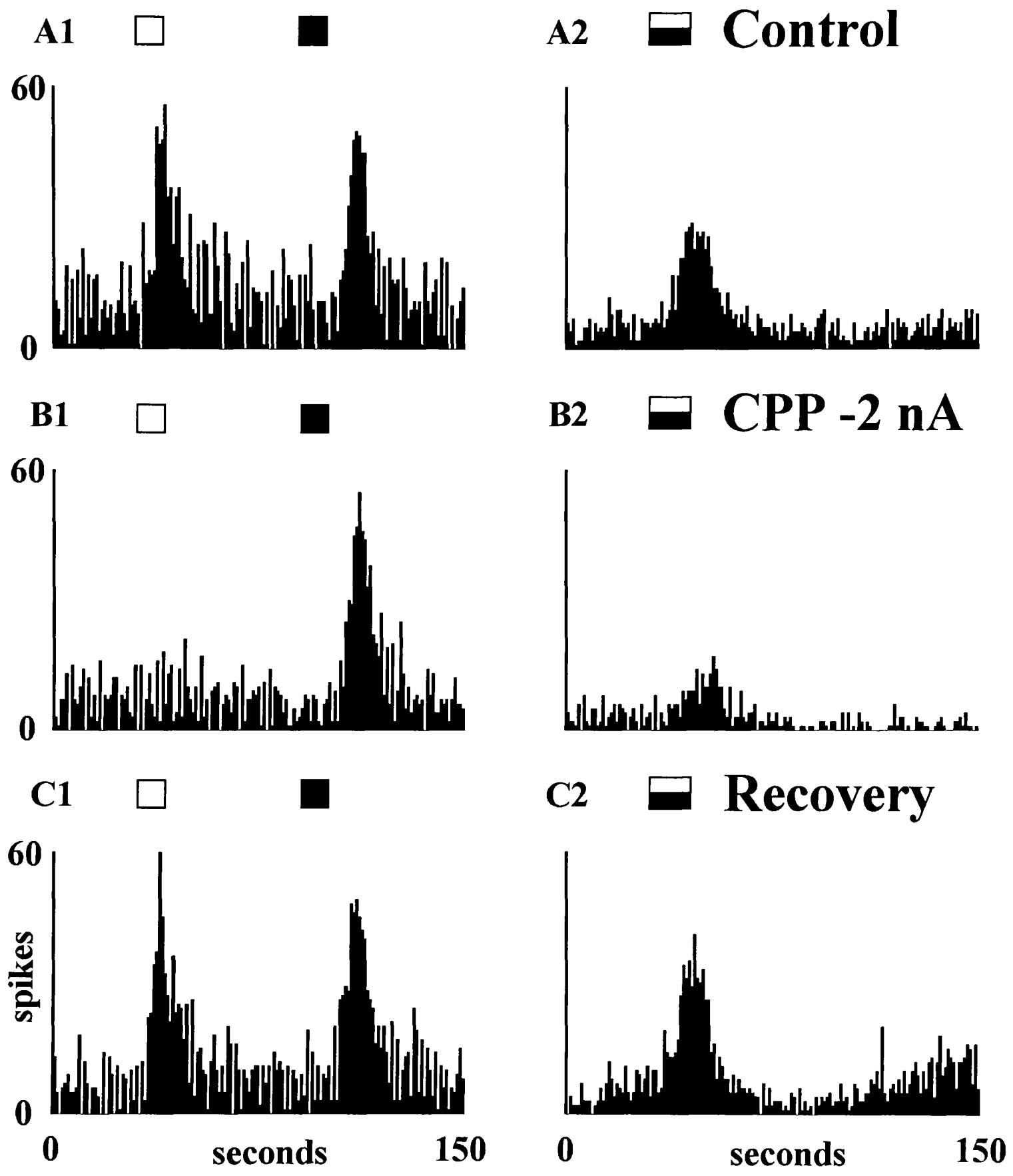
A1
A2
Control
60
0
B1
B2
CPP -2 nA
60
0
C1
C2
Recovery
60
spikes
0
0
seconds
150
0
seconds
150
NMDA -230 nA
AMPA -79 nA
52˚C Noxious Heat 15 s

Fig 2-3

Figure 2.4 Neurone in the hindpaw area of the SI cortex and the effect of NBQX against a noxious pinch-evoked response. Similar representation as in Figure 2.2. The top row are control responses to iontophoretic application of AMPA and NMDA **(A1)** and to a noxious pinch stimulus applied to the contralateral forepaw digits **(A2)**. Continuously ejection of NBQX at -4 nA for 5 min (last trial shown), selectively antagonised the response to AMPA **(B1)** and eliminated the mechanical HT response **(B2)**. The AMPA-evoked response **(C1)** and the sensory-evoked synaptic response **(C2)** recovered following termination of NBQX ejection.

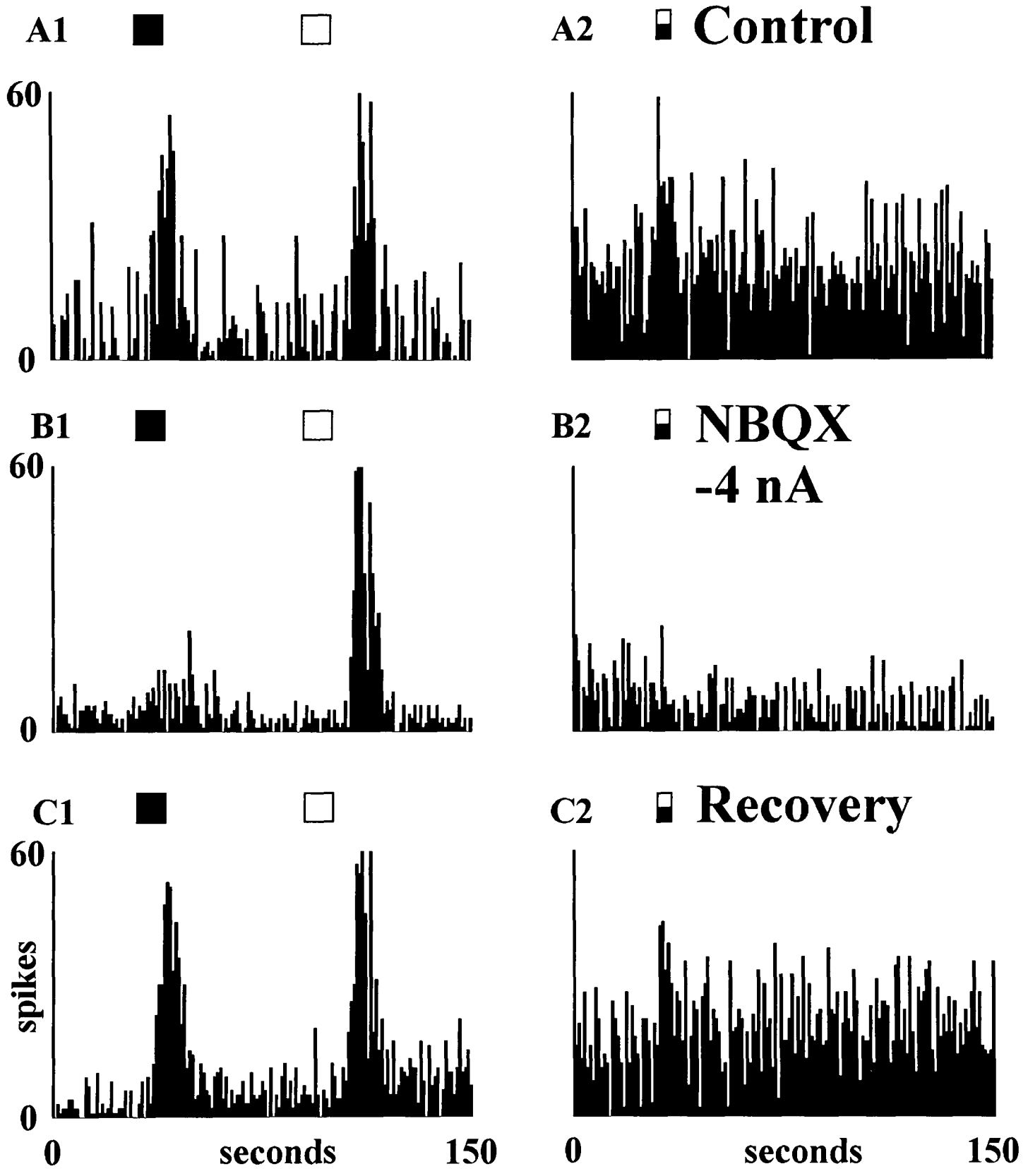
A1
A2
Control
60
0
B1
B2
NBQX
-4 nA
60
0
C1
C2
Recovery
60
spikes
0
0
seconds
150
0
seconds
150
AMPA -30 nA
NMDA -30 nA
Noxious Pinch 5 s

Fig 2 4

Figure 2.5 Neurone in the hindpaw area of the SI cortex and the effect of NBQX against a noxious heat-evoked response. Similar representation as Figure 2.2. The top row are control responses to iontophoretic application of AMPA and NMDA **(A1)** and to a 52°C noxious heat stimulus applied to the tail **(A2)**. Continuous ejection of NBQX at -4 nA for 13 min (last trial shown), selectively antagonised the response to AMPA **(B1)** and reduced the thermal HT response **(B2)**. An increase in baseline activity during NBQX suggests that NBQX may have blocked excitation of nearby inhibitory neurone(s). The AMPA-evoked response **(C1)** and the sensory-evoked synaptic response **(C2)** recovered following termination of NBQX ejection.

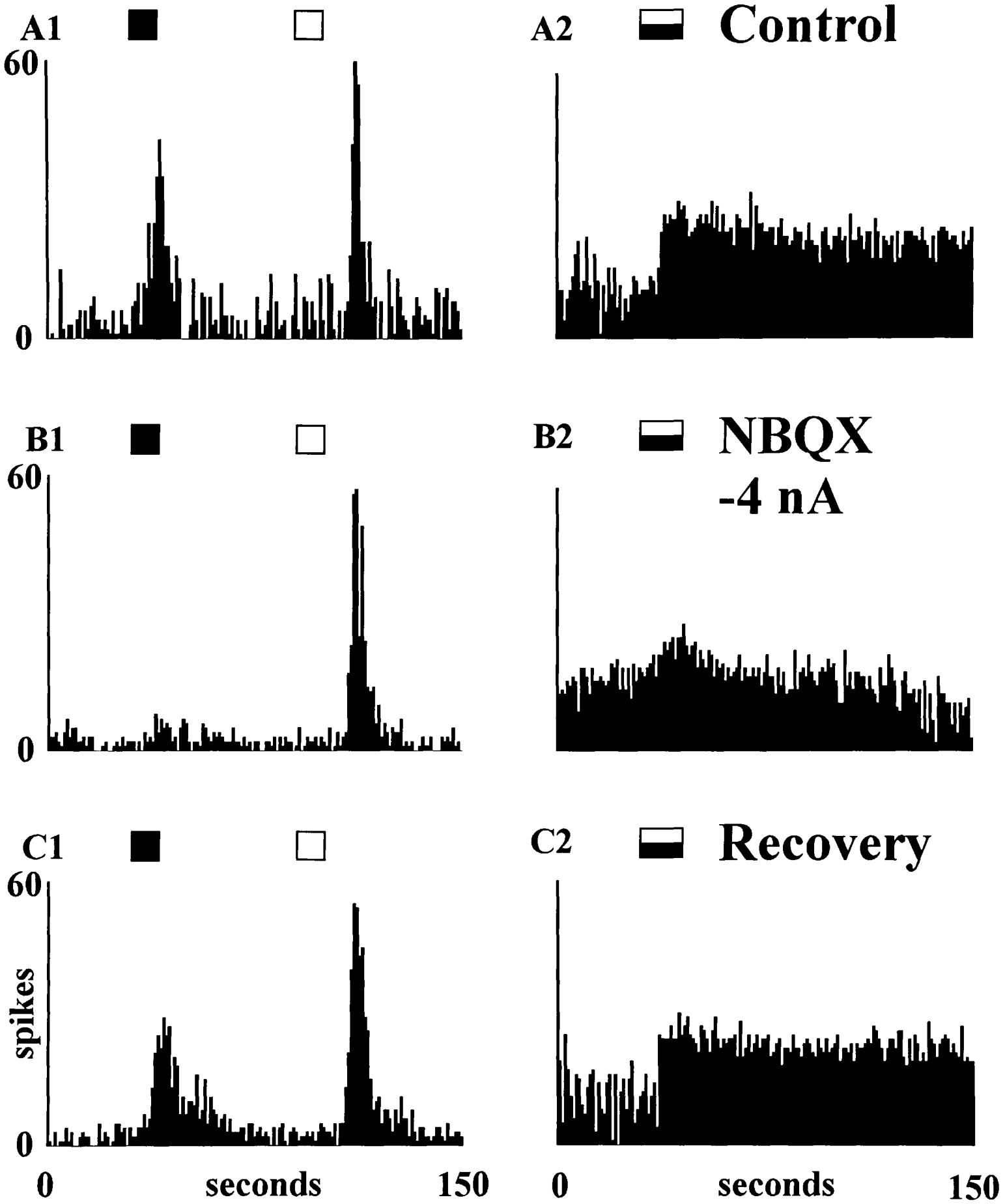
A1
60
0
A2
Control
B1
60
0
B2
NBQX
-4 nA
C1
60
spikes
0
0
seconds
150
C2
Recovery
0
seconds
150
AMPA -52 nA
NMDA -110 nA
52˚C Noxious Heat 15 s

2.3.3 Effects of CPP and NBQX on High-Threshold and Low-Threshold Responses

Neurones with responses evoked by non-noxious as well as noxious stimuli were also analysed so as to compare the involvement of NMDA and AMPA/kainate receptor-mediated responses across somatosensory sub-modalities for individual neurones. Thirteen neurones were tested with innocuous as well as noxious stimuli and 11 of these were tested with both CPP and NBQX, applied sequentially. The fast component of the LT responses was only reduced to 85 ± 4 % (n=12/12; Figure 2.6) by CPP. The slower component of the LT responses which was observed less often was markedly reduced by CPP (15 ± 19 %; n=4/4; Figure 2.6). Similarly, responses evoked by a noxious pinch or a noxious thermal stimulus were markedly reduced by CPP (10 ± 8 %; n=9/9; Figure 2.6) and (11 ± 30 %; n=3/3), respectively. In contrast, NBQX reduced both the fast component and the slower component of the LT responses substantially (43 ± 6 %; n=12/12; Figure 2.7) and (32 ± 20 %; n=6/6), respectively. The pinch-evoked responses were reduced to 13 ± 16 % (n=9/9; Figure 2.7) and the heat-evoked responses were reduced to 58 ± 23 % (n=3/3) following NBQX ejection. The effects of CPP and NBQX on sensory-evoked responses and corresponding selectivity of receptor type are summarised (Figure 2.8).

Figure 2.6 HT and LT responses of a neurone in the SI cortex tested with CPP. Responses evoked by a train of ten, 10 ms air jet stimuli every 2 s followed by responses to ejection of agonists presented in 1 s bins **(A1)**. Cumulative PSTHs over the train of 10 air jet stimuli shown in (A1) has been presented in 10 ms bins **(A2)**. The PSTH of the response evoked by a noxious pinch stimulus is presented in 1 s bins **(A3)**. Bars above the PSTHs correspond to the period of agonist application or sensory stimulation. The air jet stimulus was applied to the ventral aspect of the contralateral forepaw and the noxious pinch stimulus was applied to the contralateral hindpaw digits. An interval of 10 s followed the train of air jets, AMPA was ejected for 10 s followed by an interval of 50 s and NMDA was ejected for 10 s followed by an interval of 50 s. Noxious stimulus trials were performed separately, shortly afterwards. The next row shows selective antagonism of the responses to NMDA **(B1)**, and an elimination of the mechanical HT response **(B3)** and long-latency component of the air jet responses whereas some of the short-latency component of the air jet responses remained **(B2)** during continuous CPP ejection at -5 nA for 12 min (last trial shown). Note also a reduction in baseline activity during CPP ejection between agonist applications (B1) and before the noxious stimulus (B3). After noxious stimulation, baseline activity resumed upon termination of CPP ejection at 70 s (B3).

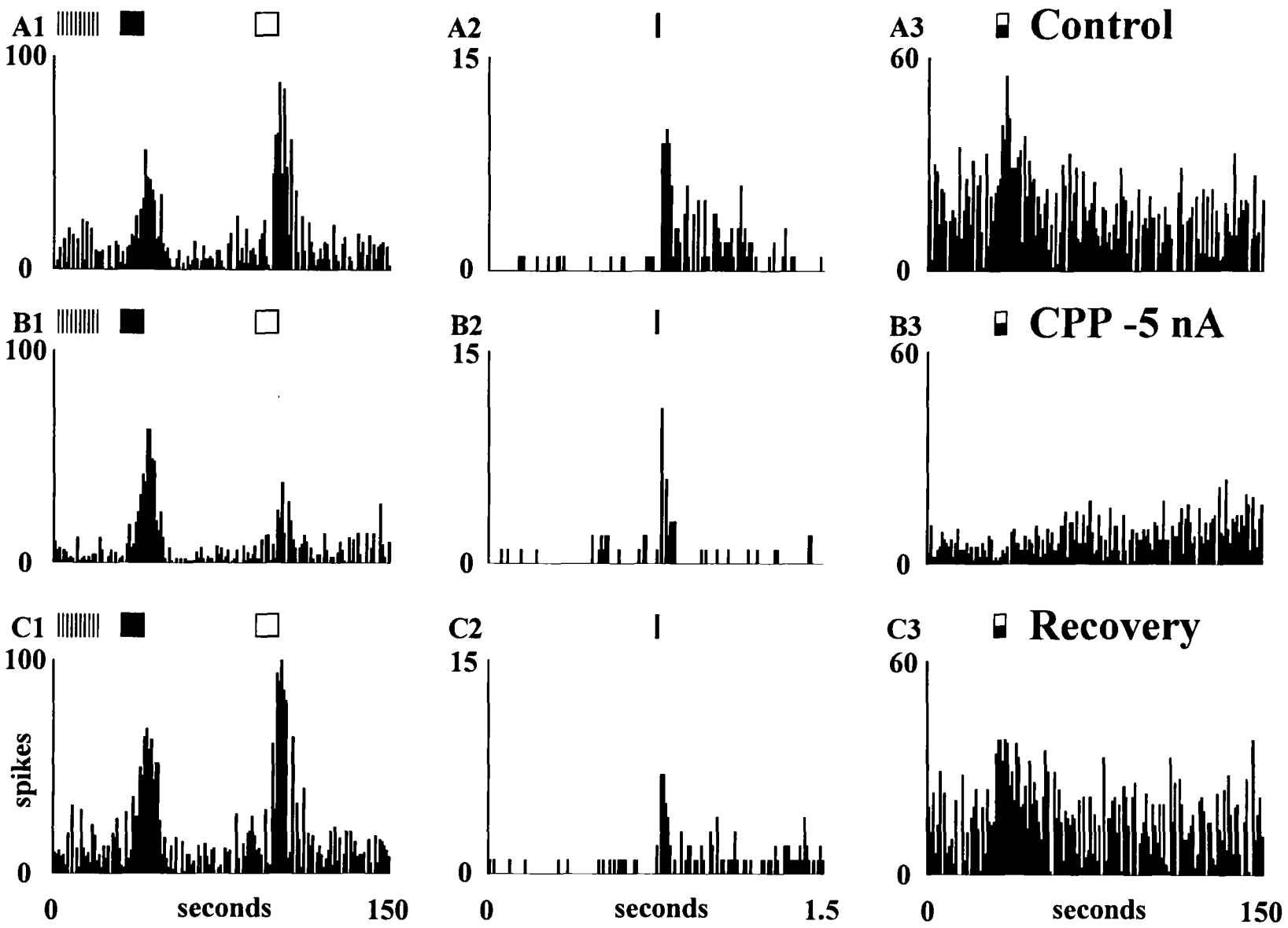
A1
100
0
A2
15
0
A3
Control
60
0
B1
100
0
B2
15
0
B3
CPP -5 nA
60
0
C1
100
spikes
0
0
seconds
150
C2
15
0
0
seconds
1.5
C3
Recovery
60
0
0
seconds
150
10 ms Air Jets
2 s intervals
AMPA -97 nA
NMDA -122 nA
1 s bins
10 Air Jets
cumulated in
single trials
10 ms bins
Noxious Pinch 5 s
1 s bins

Fig 26

Figure 2.7 HT and LT responses of a neurone in the SI cortex tested with NBQX. Records are similar to Figure 2.6 except the responses to the noxious pinch are in 2 s bins for better observation. Responses evoked by agonists **(A1)**, air jet stimuli applied to the dorsal aspect of the contralateral forepaw digit **(A2)** and a noxious pinch applied to the contralateral hindpaw **(A3)**. The next row shows selective antagonism of the responses to AMPA **(B1)** and the disappearance of the mechanical HT response **(B3)** as well as a substantial reduction of the air jet response **(B2)** during continuous NBQX ejection at -8 nA for 12 min (last trial shown). Note an inhibition observed as an action potential rate below baseline activity following the short-latency LT response (A2). Note also a reduction in baseline activity during NBQX ejection (B1, B2 and B3).

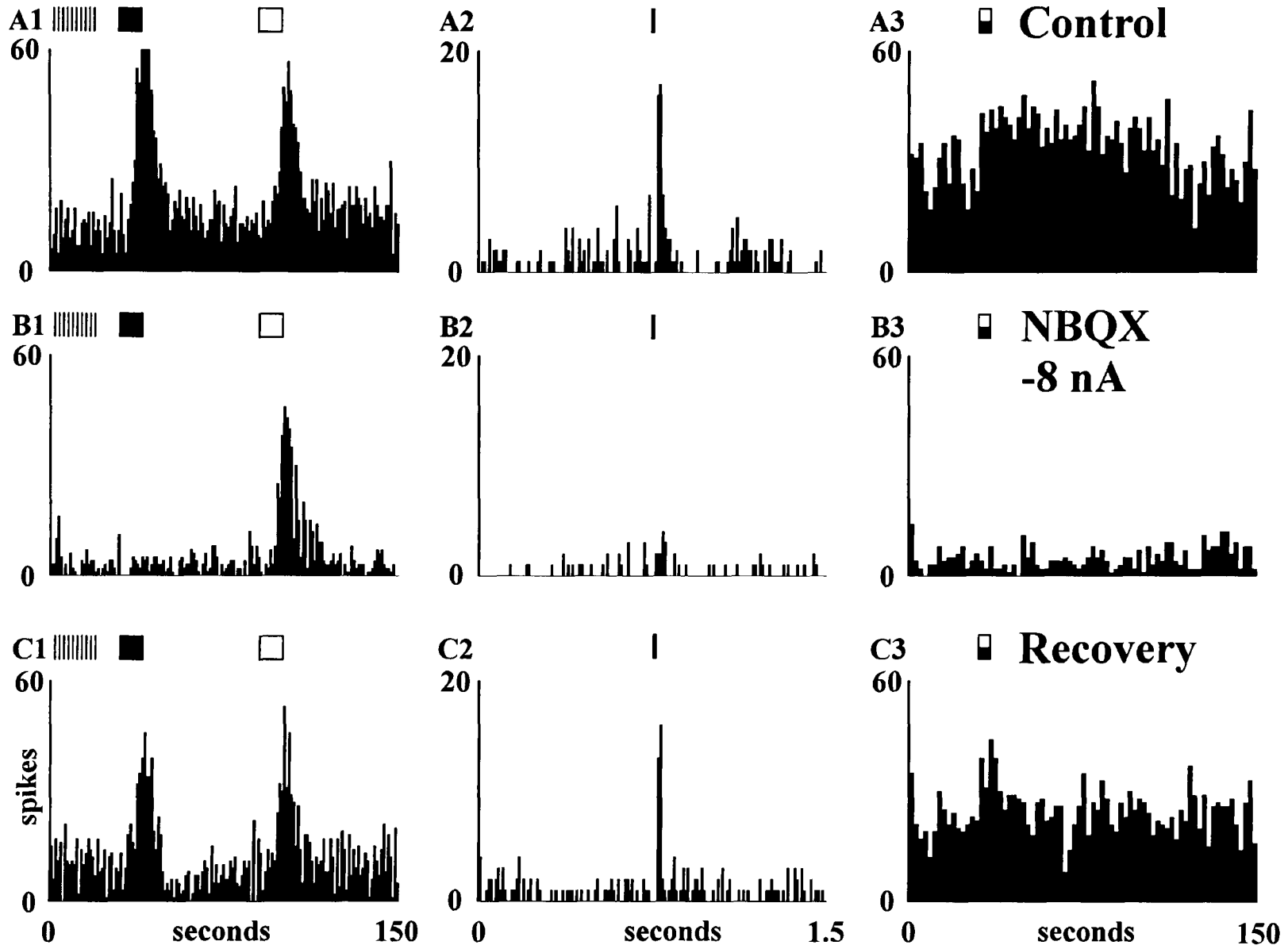
A1
60
0
A2
20
0
A3
Control
60
0
B1
60
0
B2
20
0
B3
NBQX
-8 nA
60
0
C1
60
spikes
0
0
seconds
150
C2
20
0
0
seconds
1.5
C3
Recovery
60
0
0
seconds
150
10 ms Air Jets
2 s intervals
AMPA -136 nA
NMDA -120 nA
1 s bins
10 Air Jets
cumulated in
single trials
10 ms bins
Noxious Pinch 5 s
2 s bins

Fig 2.7

Figure 2.8 Summary of the effects of CPP and NBQX on responses evoked by AMPA, NMDA, air jets and noxious stimuli for SI neurones. Columns represent the mean percent of control responses of the number of neurones (n) investigated. Error bars indicate the SEM. The top row represents the effects of CPP on responses and the bottom row represents the effects of NBQX on responses for groups of neurones tested with only noxious sensory stimulation and neurones tested with both innocuous and noxious sensory stimulation. Some neurones were tested with both types of noxious sensory stimuli sequentially **(A and C)**. Responses evoked by noxious stimuli and the long-latency (L-L) component of the LT response was substantially reduced by CPP at ejection parameters that showed selectivity at NMDA receptors **(A and B)**. The short-latency (S-L) component of the LT response was not markedly reduced by CPP **(B)**. All sensory-evoked responses were reduced by NBQX at ejection parameters that showed selectivity at AMPA/kainate receptors **(C and D)**.

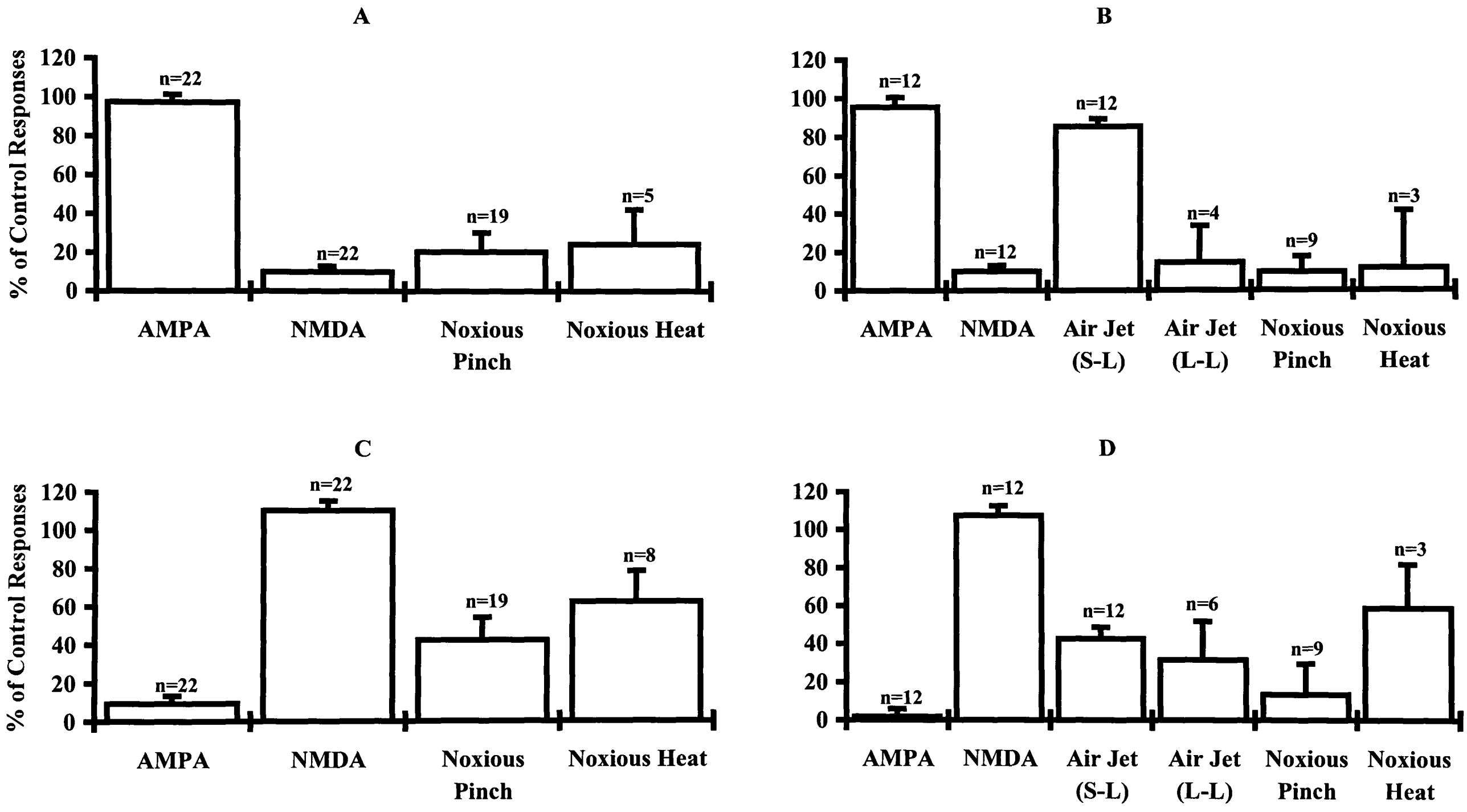
A
B
C
D
% of Control Responses
120
100
80
60
40
20
0
n=22
n=22
n=19
n=5
n=12
n=12
n=12
n=4
n=9
n=3
n=22
n=22
n=19
n=8
n=12
n=12
n=6
n=9
n=3
AMPA
NMDA
Noxious Pinch
Noxious Heat
Air Jet (S-L)
Air Jet (L-L)

2.3.4 Baseline Activity

The baseline activity was quantified for 11 of the 13 neurones above, which were tested with both CPP and NBQX. A comparison of the prestimulus baseline activity between single noxious stimulus trials and single air jet stimulus trials showed that the former was 57 % higher for 11 cells analyzed ($p = 0.06$, Wilcoxon rank sum, two-tailed). In order to establish whether the apparent skewness from the mean of HT responses resulted from changes in baseline activity, correlation coefficients were determined for the two response types for each neurone. The baseline activity correlated well with the magnitude of the responses evoked by a noxious mechanical or thermal stimulus for five neurones (range of r = 0.80 to 0.99; Figure 2.1). Baseline activity and mechanical HT responses were not correlated in the other six neurones (r = -0.66 to 0.49).

Despite some correlation observed between baseline and response magnitudes, it is unlikely that reductions in the baseline activity by either CPP or NBQX accounted for the reductions in the mechanical and thermal HT responses. This is supported by the fact that the normalised ratios of the mechanical and thermal HT response to baseline activity during application of CPP (0.6 ± 0.1; n=11/11) or application of NBQX (0.8 ± 0.1; n=11/11) reflected on average a reduction of the mechanical or thermal HT response below baseline activity. For instance, in some cases, an inhibition replaced the mechanical HT response during application of either CPP (Figure 2.2) or NBQX. For noxious stimulus trials, the baseline activity was reduced to 62 ± 13 % (n=11/11; Figure 2.6) following CPP ejection and to 63 ± 12 % (n=11/11; Figure 2.7) following NBQX ejection. Although not commonly encountered (n=2/22), an increase in the baseline activity was observed following NBQX ejection for the neurone in Figure 2.5. A reduction in baseline activity prior to air jet stimuli

was also observed following CPP and NBQX ejection (48 ± 9 % and 49 ± 7 %, respectively; n=11/11; Figures 2.6 and 2.7).

2.4 Discussion

The main finding was that both NMDA and AMPA/kainate receptors contribute to SI high-threshold responses evoked by noxious somatosensory stimulation. The same receptors were also involved in mediating LT cutaneous responses of neurones showing HT responses but in a temporally differential manner. For LT cutaneous responses, the fast component was mediated predominantly by AMPA/kainate receptors whereas both NMDA and AMPA/kainate receptors were involved in mediating the slower component.

The extension of our results to somatosensory information processing in the normal behaving animal is limited by the use of anaesthesia. There are three reasons for this, based on results of increasing the dose of urethane starting from 1.25 g/kg administered intraperitoneally (Angel et al. 1980). Firstly, the transmission in the sensory volleys from the periphery to the cortex becomes slower. Secondly, there is a decrease in the size or dispersion of the thalamocortical volley. Thirdly, the effectiveness of the thalamocortical volley for triggering firing of the cortical cells decreases.

2.4.1 Temporal Distribution of Responses

These results concerning the temporal aspects of NMDA and AMPA/kainate receptor-mediated LT responses are consistent with those reported for SI low-threshold sensory neurones in the vibrissal representation of the SI cortex (Armstrong et al. 1993) and are thus not a unique attribute of the neurones in our study. It should be noted, however, that in the

present results the slower component of the LT responses did not always occur in each trial. One possible explanation for this is that recordings were made from the forepaw or hindpaw representations of the SI cortex, which unlike other SI areas, contain an overlap of the primary motor cortex representation (Hall and Lindholm 1974). Secondly, LT responses were recorded from neurones that also responded to noxious stimuli and thus, could have differed from neurones responding only to innocuous stimuli. Thirdly, our recordings were made from presumed infragranular layers where LT neurones were shown to have multireceptive fields (Simons 1978; Armstrong-James and Fox 1987) possibly promoting response variability as a result of their spatial organisation. Mechanical and thermal HT responses were not differentiated into separate temporal components because they were typically unimodal, and displayed variable durations between trials in the same neurone as well as between neurones.

2.4.2 Receptive Field

In order to isolate the synaptic pharmacology of somatosensory submodalities, responses evoked by a noxious mechanical stimulus were recorded outside the LT somatosensory receptive fields. Although some mechanical and thermal HT responses were weak, a comparison of mechanical and thermal HT responses within and outside the LT receptive field was not performed. Nevertheless, if activating LT fibres within the vicinity of the recorded neurone's LT receptive field during noxious mechanical or thermal stimuli, it is possible that lateral inhibition would occur and reduce the HT transmission to the SI recorded neurone. Lamour et al. (1983) reported that "convergent" or WDR neurones recorded in the SI were inhibited by light mechanical stimuli and excited by noxious

stimulation in the same receptive field. These neurones could also be inhibited by a noxious stimulus applied outside the receptive field, but such inhibition was less often observed in the present study.

Neurones of the SI cortex responding to noxious stimuli had large receptive fields in the present experiments similar to previous studies recording from nociceptive neurones (Lamour et al. 1982, 1983; Kenshalo and Isensee 1983). In comparison to the results of Lamour et al. (1983), neurones of the SI cortex tested with noxious as well as non-noxious stimulation in the present study usually had larger receptive fields, which were similar to neurones responding only to noxious stimuli in their study. This difference could have resulted from using different anaesthetics. For instance, there is evidence based on the EEG pattern of urethane anaesthetised animals to suggest that urethane does not produce a marked depression of brain activity (Lincoln 1969). Thus, mechanical or thermal HT responses might have resulted from sources other than a specific transmission of nociceptive information. In contrast, slow high voltage activities with periods of depressed activities, recorded by the EEG, could be induced after increasing the proportion of halothane delivered to the rat in the study by Lamour et al. (1983). Under these conditions, no arousal reaction was observed during strong noxious stimuli.

2.4.3 Baseline Activity

During noxious stimulus trials, baseline activity increased and correlated with an increase in mechanical and thermal HT responses of some neurones. Although the noxious stimuli did not cause detectable skin surface damage, tissue trauma cannot be excluded as contributing to

the increase in baseline activity. Care was taken to avoid over stimulating with either a noxious pinch or heat during the search for HT responses. Perhaps using an even longer interstimulus interval would have allowed for the neuronal activity to return to control baseline activity. However, prolonging this period would substantially extend the duration of the experiment and may result in the loss of the reliability of antagonist selectivity tests performed earlier during the experiment.

One possible source for the increased baseline activity may have been the long-lasting nociceptive responses of thalamic relay neurones (Albe-Fessard et al. 1985; Eaton and Salt 1998). Indeed, almost all VB thalamic neurones in the rodent project to the somatosensory cortex (Harris and Hendrickson 1987). However, a long-lasting nociceptive response relay would not impinge upon the present results because mechanical and thermal HT responses in the SI cortex decayed earlier. In addition, the ratios of the mechanical and thermal HT responses to baseline activity during application of either CPP or NBQX showed, on average, that mechanical and thermal HT responses were reduced below the baseline activity. Alternatively, the increase in baseline activity may reflect an overall non-specific cortical excitation via neuromodulatory systems activated by the noxious stimulus. In a previous study, acetylcholine was found to be released in both hemispheres of the sensorimotor cortex after unilateral noxious stimulation of high-threshold afferents of the forelimb nerve in the spinal cord (Mullin and Phillis 1975). Acetylcholine release has also been associated with observed signs of arousal occurring during desynchronisation of the EEG activity (Gadea-Ciria et al. 1973). The fact that CPP and NBQX substantially reduced the baseline activity suggests that NMDA and AMPA/kainate receptors, respectively, are also involved in contributing to the baseline activity. Inhibition was sometimes unmasked during antagonism

of the evoked response as reflected from the average ratios of response to baseline activity. Also, in one neurone recorded, enhancement of baseline activity occurred during the ejection of NBQX which may have resulted from antagonism of AMPA/kainate receptors on nearby inhibitory neurone(s). Thus, it is likely that the increase in the baseline activity during noxious stimulus trials resulted from a summation of excitatory and inhibitory influences arriving from the convergence of prevailing thalamo-cortical and cortico-cortical pathways. Some of these pathways may have involved the neuromodulatory systems mentioned above, although this would need to be verified in future work.

2.4.4 Ionotropic Glutamate Receptors and Responses Evoked by Noxious Stimuli

Although the synaptic pharmacology of nociceptive neurones in the SI cortex has not been previously investigated, other studies have shown evidence for ionotropic glutamate receptor-mediated nociceptive responses in subcortical structures involved in somatosensory processing. For instance, in the dorsal horn of anaesthetised animals, non-NMDA glutamate receptors have been shown to mediate responses evoked by acute noxious thermal stimuli (Dougherty et al. 1992; Cumberbatch et al. 1994) as well as hyperexcitable states induced by inflammation (Neugebauer et al. 1993). NMDA receptors have been mostly implicated in spinal dorsal horn nociceptive responses during sustained noxious stimuli such as peripheral chemical or inflammatory stimuli (Haley et al. 1990; Schaible et al. 1991), or in the 'wind-up' phenomenon induced by repetitive electrical stimulation of C-fibres (Dickenson and Sullivan 1990). Nevertheless, it should be noted that some contrasts exist for the involvement of NMDA receptors in acute or chronic nociceptive responses in the spinal cord which may

depend on the stimulus parameters and preparatory surgery used (Hartell and Headley 1996).

Additionally, NMDA receptors have also been shown to mediate nociceptive responses in the thalamus, including the ventrobasal complex (VB) and the posterior nuclear group (Eaton and Salt 1990), both of which project to the SI cortex (Lu and Lin 1993). Interestingly, antagonists at non-NMDA glutamate receptors did not have any effect on the thalamic nociceptive responses (Eaton and Salt 1990).

The present results together with those from previous studies cited above have shown that NMDA receptors are involved in mediating mechanical and thermal HT responses in the SI cortex as well as nociceptive responses in the spinal cord and thalamus. Although AMPA/kainate receptors were also involved in mediating the present mechanical and thermal HT responses, these receptors were not involved in mediating nociceptive thalamic responses (Eaton and Salt 1990) and were seldom involved in nociceptive responses in the spinal cord. This suggests that NMDA receptors have a common role in mediating responses evoked by noxious stimulation whereas AMPA/kainate receptors may mediate particular aspects of nociceptive transmission.

Following ejection of the antagonist at NMDA receptors, CPP, or the antagonist at AMPA/kainate receptors, NBQX, an inhibition was sometimes observed during noxious stimulation. The antagonism at either NMDA or AMPA/kainate receptors of the recorded neurone may have accounted for the unmasking of inhibition observed. This could be explored further using antagonists acting at inhibitory receptors or using intracellular recordings. Most neurones however, did not exhibit such an effect and in contrast, in a few neurones, mechanical HT responses were unaffected by the antagonists used here. One

possible reason for these variations may be a lack of antagonist diffusion to distant synapses at a sufficient concentration. This would not be surprising as the present recordings were presumably in the infragranular layers and anatomical evidence shows that large layer V pyramidal neurones have extensive dendritic arborisation (Chagnac-Amitai et al. 1990). Yet, there is also the possibility that the variability of responses is due to distinct sets of neurones or the involvement of other receptor types, such as metabotropic glutamate receptors (Taylor and Cahusac 1994).

2.4.5 Conclusions

Within the constraints of anaesthesia, these results point towards a difference in the pattern of receptor involvement during different somatosensory stimulus-evoked responses of individual SI neurones. Both NMDA and AMPA/kainate receptor-mediated components were found during the entire mechanical or thermal HT response, whereas virtually all of the fast component of the LT responses were mediated through AMPA/kainate receptors with NMDA receptors being additionally recruited for any slower component of the LT responses. Ultimately, this may be of relevance for understanding the mechanisms by which somatosensory modalities are differentially processed.

CHAPTER 3: Physiological and Anatomical Classification of Nonpyramidal Cells in Stratum Oriens of the CA1 Hippocampal Area

3.1 Introduction

In the somatosensory cortex, I found that during noxious stimulation, the baseline activity increased and inhibitory influences were detected during antagonism of NMDA receptors. The above results could only be explained if a better definition and understanding of the cortical circuits mediating the sensory-evoked responses and the effects of drugs could be achieved. Unfortunately, with the previous approach, I could not determine the identity of cells anatomically and the circuits of the SI cortex are as yet poorly defined. To gain insight into the organisation of cortical circuits, I chose to study the CA1 area of the hippocampus because it is the best defined area of the cerebral cortex.

Sensory information is processed by the interactions between extrinsic relays and intrinsic circuitry of cells within and across brain regions. In the hippocampus, extensive research has shown that nonpyramidal cells are important in regulating principal cell output via feed-forward and feed-back inhibition (Andersen et al. 1964; Buzsaki 1984; Jefferys 1996). Feed-forward excitation or inhibition results from serial neuronal signalling whereas feed-back excitation or inhibition occurs when a postsynaptic cell signals back to the same cell population. Some nonpyramidal cells which contain vasoactive intestinal polypeptide (VIP) and/or calretinin innervate only other nonpyramidal cells within the hippocampus (Acsady et al. 1996a, 1996b). If the postsynaptic nonpyramidal cell from the above connection contacts a pyramidal cell, this would result in disinhibition of the pyramidal cell. For instance, stimulation of the septal area in a combined septohippocampal slice was shown to suppress spontaneous inhibitory postsynaptic currents (IPSCs) in pyramidal neurones in the presence of atropine, AMPA and NMDA receptor blockers (Toth et al. 1997). However, when excitatory influences are not

blocked, activation of nonpyramidal cells either by intrinsic or extrinsic inputs in a feed-forward and/or feed-back manner may overcome the inhibitory influences originating from other nonpyramidal cells. In addition, some nonpyramidal cells, such as stratum lacunosum-moleculare cells, are solely activated by extrinsic sources and produce feed-forward inhibition onto pyramidal cells (Lacaille and Schwartzkroin 1988a). Other nonpyramidal cells located in stratum oriens (SO)/alveus and stratum pyramidale (SP), inhibit pyramidal cells in both a feed-forward and feed-back manner (Blasco-Ibanez and Freund 1995). Computer models as well as in vitro stimulation paradigms (Traub et al. 1996a, 1999) have shown specific interactions between pyramidal and nonpyramidal cells resulting in certain types of network activity. For example, connections between SP nonpyramidal cells along with tonic excitatory input produce gamma-frequency rhythmicity in pyramidal cells with minimal time lag (Whittington et al. 1995; Traub et al. 1996a). Likewise, NMDA receptor mediated nonpyramidal cell gamma-frequency rhythmicity can be evoked following a synchronised pyramidal cell burst (Traub et al. 1996a). Tetanic stimulation can also induce gamma-frequency network activity but when the stimulation is increased further, pyramidal cell activity alters, reflecting a switch from gamma- to beta-frequency network oscillations (Traub et al. 1999). As a result of the above findings and the fact that some extrinsic inputs may not directly relay sensory-evoked transmission, it is necessary to also investigate factors involved in modulating neuronal signalling, such as intrinsic properties of cells as well as receptor expression of particular cell types.

Nonpyramidal cells can be classified based on their synaptic connections and molecular composition. However, nonpyramidal cells have also been distinguished from pyramidal cells according to other factors such as spontaneous activity, evoked responses, and passive membrane properties (Ranck 1973; Fox and Ranck 1981; Buzsaki and Eidelberg 1982; Ashwood et al. 1984; Lacaille et al. 1987). In addition, there are several distinctive features between nonpyramidal cells. Basket cells and axo-axonic cells in SP have afterhyperpolarisation

potentials (AHPs) which are larger in amplitude than those of pyramidal cells but smaller than those of other nonpyramidal cells (Kawaguchi and Hama 1988; Buhl et al. 1994b, 1995). In addition, basket cells can fire action potentials (APs) at very high frequencies with little accommodation (Schwartzkroin and Mathers 1978; Kawaguchi and Hama 1988; Ylinen et al. 1995b) and axo-axonic cells have been shown to fire doublets in response to depolarising current pulses (Buhl et al. 1994b). Basket and axo-axonic cells are also less responsive to group I mGluR agonists than SO/alveus nonpyramidal cells (McBain et al. 1994). Large inward current responses to group I mGluR activation and a prominent depolarising 'sag' in response to hyperpolarising current pulses appear to be characteristics of oriens-lacunosum moleculare (O-LM) nonpyramidal cells in SO/alveus but not other nonpyramidal cells with similar somatodendritic domains (McBain 1994; McBain et al. 1994; Sik et al. 1994). Stratum lacunosum-moleculare cells were shown to have longer duration APs as compared to SP and SO/alveus nonpyramidal cells (Kawaguchi and Hama 1988; Lacaille and Schwartzkroin 1988b). The above list is not expended as there are at least 10 anatomically distinguished nonpyramidal cell types in any area of the hippocampus promoting the necessity for more stringent physiological classification schemes.

In particular, I studied O-LM and oriens-bistratified (O-Bi) nonpyramidal cells because their synaptic organisation is ideal for investigating underlying mechanisms of functional diversity. For instance, the similar somatodendritic location as well as expression of somatostatin in O-LM and O-Bi cells (Somogyi et al. 1984; McBain et al. 1994; Maccaferri et al. 2000) may be a target for particular types of extrinsic inputs, yet O-LM and O-Bi cells have distinct axonal projections co-aligned with the entorhinal and CA3 glutamatergic inputs onto pyramidal cells, respectively (Maccaferri et al. 2000). Additionally, in the subiculum, which contains somatostatin-immunoreactive boutons (Aylward and Totterdell 1993) cells were shown to be distinguished by their sensitivity to somatostatin-modulated $GABA_B$ IPSPs (Greene and

Mason 1996a, 1996b). As O-LM and O-Bi cells are in a position to receive pyramidal cell feedback (Blasco-Ibanez and Freund 1995), it is probable that both cell types are activated under similar conditions. However, due to spatial constraints of their axonal projections, it is likely that O-LM and O-Bi cells influence pyramidal cells differentially. Moreover, somatostatin-immunoreactive fibres were shown to be mostly located in stratum lacunosum-moleculare (Aylward and Totterdell 1993), in correspondence to O-LM but not O-Bi cell axonal projections. Nevertheless, it is not known whether intrinsic membrane properties and expression of glutamate receptors in O-LM and O-Bi cells may also lead to functional differences between these two cell types. Therefore, intrinsic membrane properties of O-LM and O-Bi cells were investigated. The tracer, biocytin, was included in the recording pipette for subsequent anatomical identification of the cells. Afterwards, immunocytochemical analysis for somatostatin and mGluR1α was also carried out.

3.2 Methods

3.2.1 Slice Preparation

Sprague-Dawley rats, aged 14-20 postnatal days, were anaesthetised with isoflurane followed by decapitation and removal of the brain in ice-cold artificial cerebrospinal fluid (ACSF). The ACSF consisted of (mM): 130 NaCl, 3.5 KCl, 0.8 $CaCl_2$, 2.4 $MgSO_4$, 1 NaH_2PO_4, 24 $NaHCO_3$, 10 glucose, saturated with 95% O_2 and 5% CO_2 (pH 7.4, 310 mOsm). After about 2 min in ACSF, bubbled with carbogen (95% O_2 and 5% CO_2), the brain was transferred to a petri dish where it was prepared for sectioning. The cerebellum and part of the underlying brain stem tissue was removed by a cut approximately 45° to the horizontal plane. A vertical cut along the midline of the brain was made and each hemisphere was placed with the midline plane facing down. A cut, angled parallel to the frontocaudal axis, was made along the dorsal side of each hemisphere and this surface was glued onto the stage of the vibrating microtome. Horizontal (300 μm) slices were cut from both hemispheres simultaneously from the ventrocaudal to ventrofrontal portion of the brain in carbogen bubbled ACSF surrounded by an ice jacket. Single slices were transferred to a holding chamber with ACSF at room temperature using an inverted Pasteur pipette attached to a suction bulb. The slices were kept in the holding chamber to equilibrate for at least 1 hour prior to recording.

3.2.2 Recording

In the recording chamber, ACSF containing 2mM $CaCl_2$ and 1mM $MgSO_4$ was pumped through the recording chamber at 1.2 ml/min using a peristaltic pump (Minipuls3; Gilson, France). The temperature control of the Peltier device (Luigs & Neumann, Germany) was set at 35.5-37.5 °C, but actual thermometer readings in the recording chamber were 32-34 °C. Slices

were submerged in the bath and held under two nylon threads glued to a small platinum wire frame. A Zeiss Axioskop microscope (Zeiss, Germany) equipped with a x40 water immersion DIC objective connected to an infrared camera (Hamamatsu, Japan) was used to view the positioning of the electrode onto cells in stratum oriens of the CA1 area. Whole-cell recording electrodes were made from 1.2 mm outer diameter standard wall borosilicate capillary glass pulled with a laser puller (Sutter Instrument Co., USA) to electrode resistances of 6-12 MΩ. The internal solution of the electrode consisted of (mM): 126 potassium gluconate, 4 KCl, 4 ATP-Mg, 0.3 GTP-Na, 10 phosphocreatine-Na_2, 10 HEPES and 0.5% biocytin (pH 7.4 adjusted with KOH, 310 mOsm adjusted with potassium gluconate). As the electrode was lowered into the bath, positive pressure was applied. The extracellular reference potential in the bath was offset to 0 mV in voltage-clamp mode. The electrode and sealing resistances were measured in voltage-clamp mode using –5 mV steps. The electrode was manoeuvred onto the cell and negative pressure was applied followed by a quick change of the holding potential to –70 mV. Pressure was released when a resistance of ~200 MΩ was reached to allow easier formation of a GΩ seal. In order to obtain whole-cell configuration, pulses of negative pressure were applied to break the membrane patch. Recordings were obtained in current-clamp bridge mode via a headstage (bias current = 0.1 nA) and an AxoClamp 2B amplifier (gain x10, Axon Instruments, USA). The recorded signal was further amplified and filtered with an amplifier made in house (gain x10, DC-5 kHz). Recordings were transmitted at a sampling rate of 10 kHz via a Digidata 1200 A/D board to a PC running pClamp 8.0 software (Axon Instruments, USA).

3.2.3 Data Analysis

Compensation of the electrode capacitance was achieved using 5 ms hyperpolarising square current pulses in discontinuous current-clamp mode by turning the capacitance compensation dial until the initial part of the voltage response appeared square. The series resistance (R_s) was compensated using –0.1 nA steps of 80 ms duration in bridge mode by turning the bridge balance dial until the fast transient resulting from the capacitance compensation disappeared. Recordings were rejected if R_s was above 50 MΩ. Data were analysed with the Axograph software (Axon Instruments, USA) and digital filtering was applied at 1 kHz in cases of exponential fits or voltage 'sag' measurements. All traces were offset from resting or holding membrane potential (-57 to –64 mV) to 0 mV except in the case of action potential (AP) and afterhyperpolarisation potential (AHP) measurements, which were offset to AP threshold. The mean ± standard deviation of measured parameters is given for clarity of the response variability, although the data are not normally distributed. Separate groups of data were compared using the unpaired nonparametric Mann-Whitney *U* test. The separate groups of data were considered to be significantly different at $p<0.05$. Linear regression was used to determine potential relationships between separate groups of data.

In order to characterise the intrinsic properties of nonpyramidal cells under investigation, three different protocols were employed. The first protocol consisted of a –20 pA current injection lasting 200 ms performed in one to three trials or in some cases repeated over 50 trials. This was used to obtain values for the time constant and input resistance. The apparent time constant was estimated from a single or double exponential fit to the data points between the first 20% of the peak to the peak voltage response (Figure 3.1). As a comparison, the time constant was also estimated as the time from pulse onset to 63% of the peak voltage response. The electrotonic length was estimated from the model for a sealed end cylinder (Rall 1969) using the equalising time constant (tau_1) and the passive membrane time constant (tau_2) obtained

from the double exponential fit (Figure 3.1). The equalising time constant is the rapid time course for electrotonic spread of charging of the membrane charge over regions where the membrane potential is farthest from resting value. The passive membrane time constant is the slower time course of charging the membrane over a region of uniform polarisation. The apparent input resistance was calculated from Ohm's law using the peak voltage response and the current injected (Figure 3.1).

The second protocol consisted of applying current pulses of 5 ms duration repeated over 10 or 30 times in order to elicit single APs in about 50% of the sweeps which could then be subtracted from the subthreshold voltage response which occurred on other sweeps. This procedure avoided contamination of the AP and AHP by potential changes due to the current injection alone. In those cases where APs were elicited on all sweeps, subthreshold voltage responses were scaled and subtracted from the AP, which was carried by a depolarising plateau. The AP and AHP were analysed for peak amplitude and duration at half-amplitude. The AHP time-to-peak was measured from AP onset and the AP rise time was measured at 10-90% of the AP peak amplitude (Figure 3.2).

The third protocol consisted of current injection ranging between 0.4 to –0.26 nA in –0.015 nA steps lasting 1 sec with 2.5 sec intervals between current pulses and was used to analyse the firing pattern and current to voltage relationship of cells over three trials. Linear fits were applied using the least squares method to the early and late firing rates, peak amplitude and duration at half-amplitude data in order to obtain the slopes (m) and Y-intercepts (b) for calculating changes between particular data points (Figure 3.3). The linear fit was used to determine a trend in the data and account for the occurrence of random changes such as the frequent occurrence of opposing values. Exponential fits were not used for three reasons. Firstly, the data did not always follow an exponential curve. Secondly, due to the in vitro technicalities, comparison between analysed parameters were made rather than presented as absolute

measurements. Thirdly, percent changes are mathematically expressed as a linear relationship. Early and late spike rate accommodation were estimated as $(m_e f_i - m_e f_{200})/(m_e f_i + b_e)$ and $(m_l f_{200} - m_l f_f)/(m_e f_i + b_e)$ [1], respectively, (Figure 3.3). The changes in peak amplitude and duration at half-amplitude of APs were also measured using linear fits between the 1st AP, the AP occurring closest to 200 ms after the onset of the current step and the final AP (Figure 3.3). The cut-off point at 200 ms corresponded to the observed depolarisation occurring particularly at high frequency firing of O-LM cells during a depolarising current step. Values for the firing rate, peak amplitude and duration at half-amplitude were obtained from the elicited train of APs aligned at the peak based on an initial guess of rise time followed by actual measurements using an Axograph built-in procedure (Figure 3.3). The percent changes in firing rate, peak amplitude and duration at half-amplitude are given for cells at similar average firing frequencies (19 to 26 Hz). Comparison of the voltage 'sag' in response to hyperpolarising current pulses between cells was obtained over three trials by taking the rectification ratio comprising the peak voltage response divided by the steady state response (averaged over the last 5 ms before the end of the stimulus) at approximately -90 mV for each cell (Figure 3.4). A rebound depolarisation was sometimes observed and measured as the peak occurring after stepping from -90 mV back to resting membrane potential (Figure 3.4). When action potentials occurred, the rebound depolarisation was reported as the membrane potential at threshold for AP generation. Total recording time ranged between 30 min and 1 hr.

---

[1] m_e/m_l = slope of the early/late line
f_i = firing rate between the first two spikes
f_{200} = firing rate between spikes occurring closest to 200 ms after the current pulse
f_f = firing rate between the last two spikes
b_e = y-intercept of the early line

Figure 3.1 Procedure for estimation of time constant and input resistance using a –0.02 nA current pulse of 200 ms duration. The nonpyramidal cell recorded could not be classified anatomically. The apparent time constant was estimated from a single or double exponential fit to the data points between the first 20% of the peak to the peak voltage response with a constraint for the fit to reach the peak voltage response (V_P) where a and b are constants and t is time. As a comparison, the time to 63% of the peak voltage response was also measured. The apparent input resistance was calculated from Ohm's law using V_P divided by the current (I) injected. The electrotonic length (L) was estimated from the sealed end cylinder model using the equalising time constant (τ_1) and the passive membrane time constant (τ_2). The rapid time course of electrotonic spread of charging the membrane over a region deviating from resting membrane potential is τ_1. The slower time course of charging the membrane over a region of uniform membrane polarisation is τ_2.

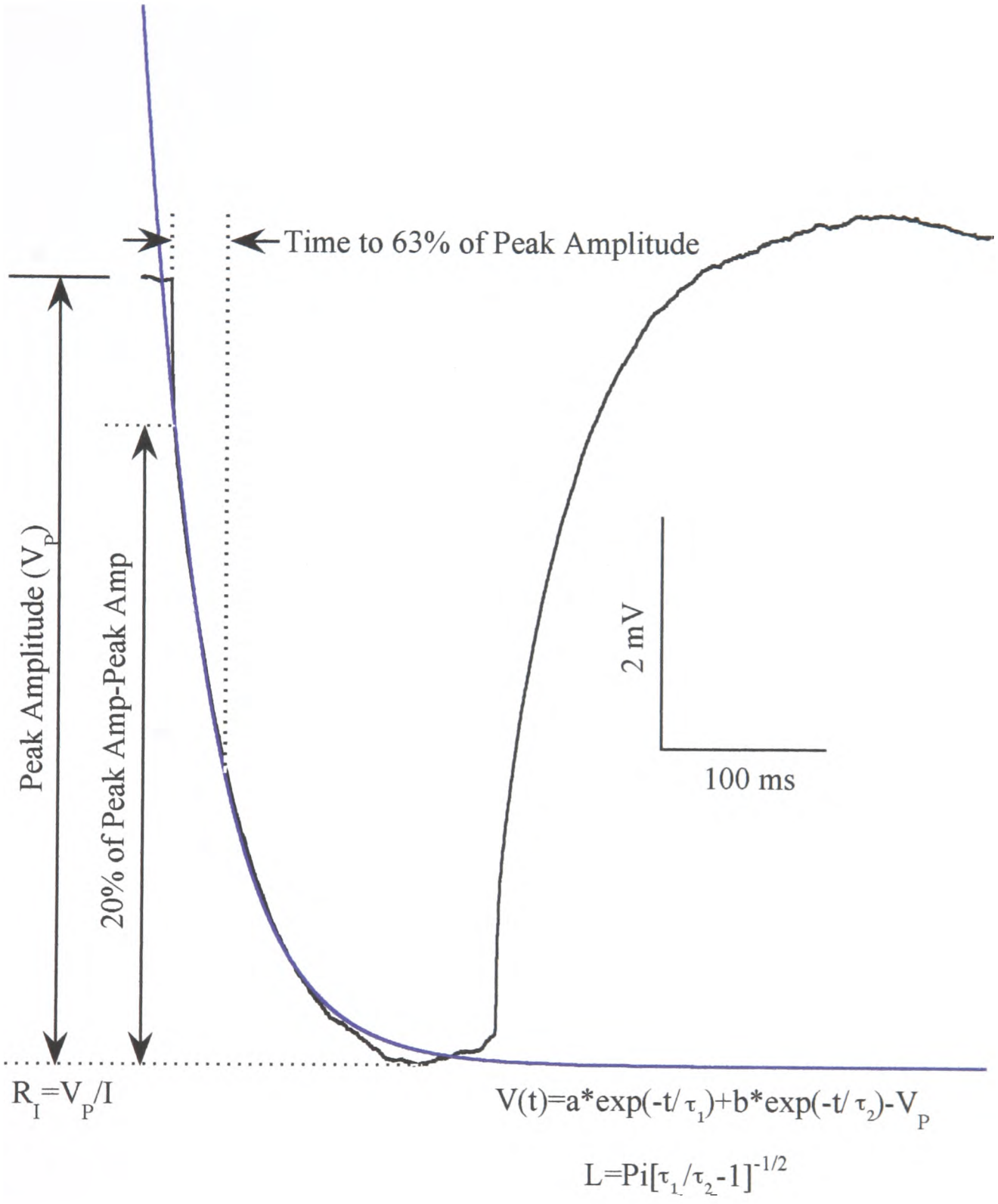
Time to 63% of Peak Amplitude
Peak Amplitude (V_p)
20% of Peak Amp-Peak Amp
2 mV
100 ms
$R_I=V_P/I$
$V(t)=a*\exp(-t/\tau_1)+b*\exp(-t/\tau_2)-V_P$
$L=Pi[\tau_1/\tau_2-1]^{-1/2}$

Fig 3.1

Figure 3.2 Single APs followed by AHPs obtained from current pulses of 5 ms duration. Same nonpyramidal cell as in Figure 3.1. **(A)** The subthreshold depolarisation due to the current pulse was subtracted from each trace. **(B)** All values are referenced from the AP threshold voltage offset to 0 mV. The peak amplitude of the AP and AHP was measured from the AP threshold voltage. The duration of AP and AHP was measured at half-amplitude for each. The AP rise time was measured between 10-90% of the AP peak. The AHP time-to-peak was measured from the onset of the AP threshold voltage.

A

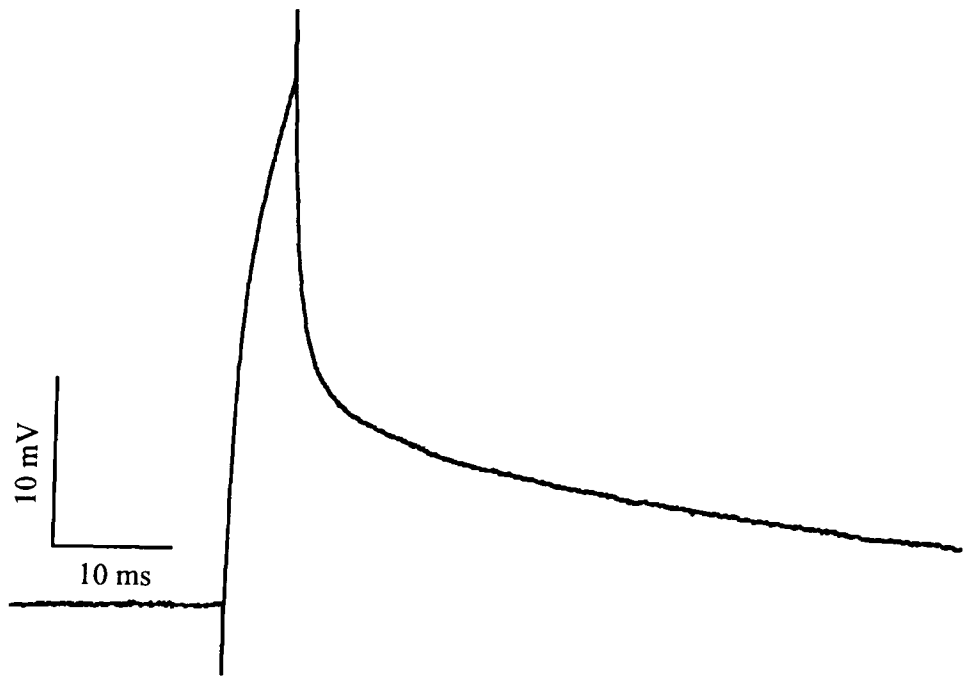
10 mV
10 ms

B

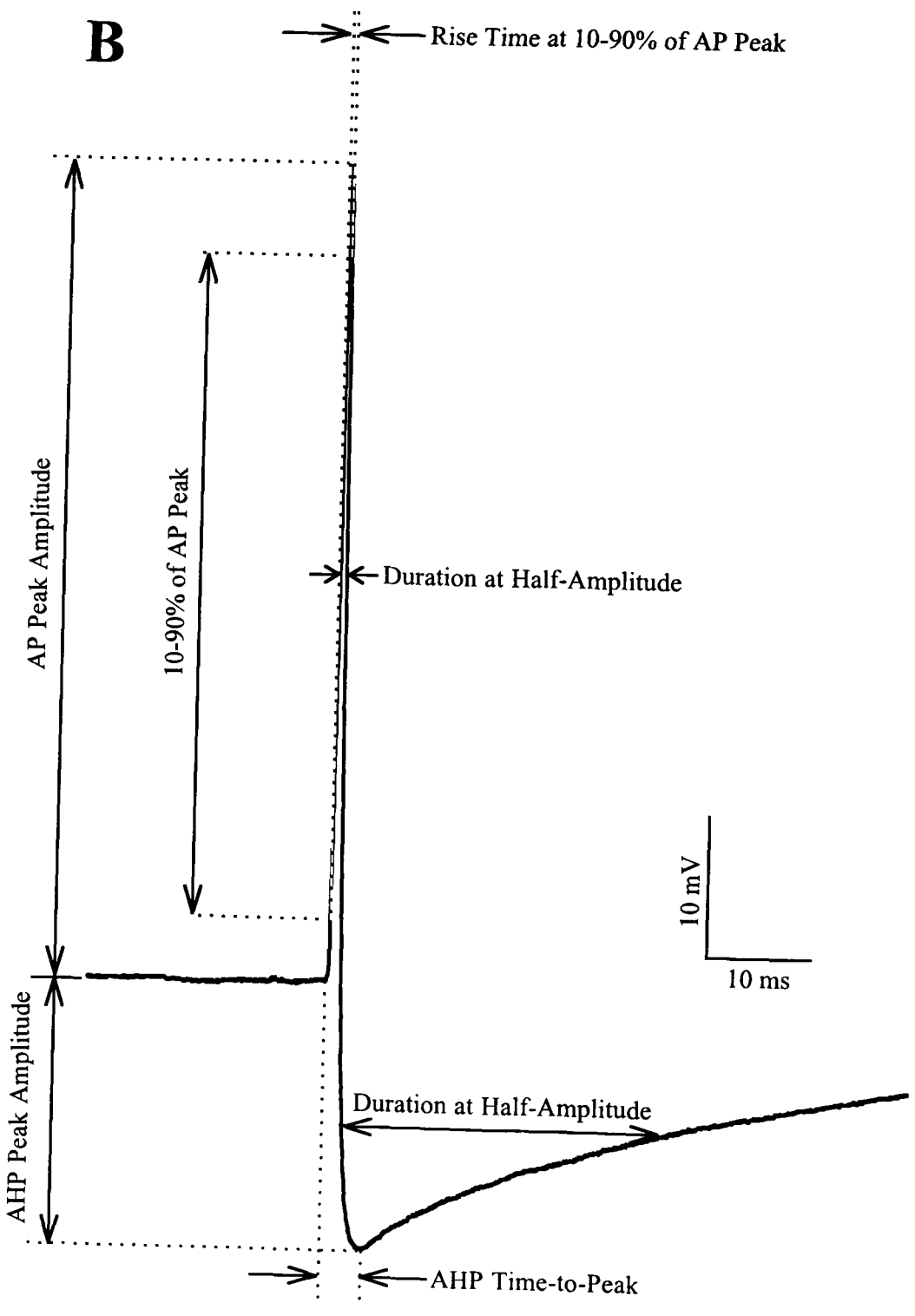
Rise Time at 10-90% of AP Peak
AP Peak Amplitude
10-90% of AP Peak
Duration at Half-Amplitude
10 mV
10 ms
AHP Peak Amplitude
Duration at Half-Amplitude
AHP Time-to-Peak

Figure 3.3 Methodology for the changes in instantaneous firing rate (f), absolute amplitude, and duration at half-amplitude. Same nonpyramidal cell as in Figure 3.1 with similar firing pattern to O-LM cells. **(A)** Action potential train evoked by a depolarising current injection of 1 s duration. Early changes were calculated between the initial AP and the AP occurring closest to 200 ms. Late changes were calculated between the AP occurring closest to 200 ms and the final AP relative to the initial AP. Instantaneous frequency was measured between two APs at each of the above data points considered. **(B)** Captured train of APs elicited by depolarising current injection of 1 sec duration. A train of APs were aligned at peak amplitude by providing a best estimate of AP rise time at 10-90% of absolute AP amplitude. This allowed for multiple measurements of parameters relative to resting membrane potential (V_{rmp}) needed for calculating increments or decrements of firing rate, amplitude and duration at half-amplitude for a train of APs. **(C)** A linear fit employing the least squares method was applied to the early (green) and late segments (red) of the data under consideration. **(D)** Early (e) and late (l) changes between two data points (x) were estimated from the slope (m) and Y-intercept (b) of the linear fit.

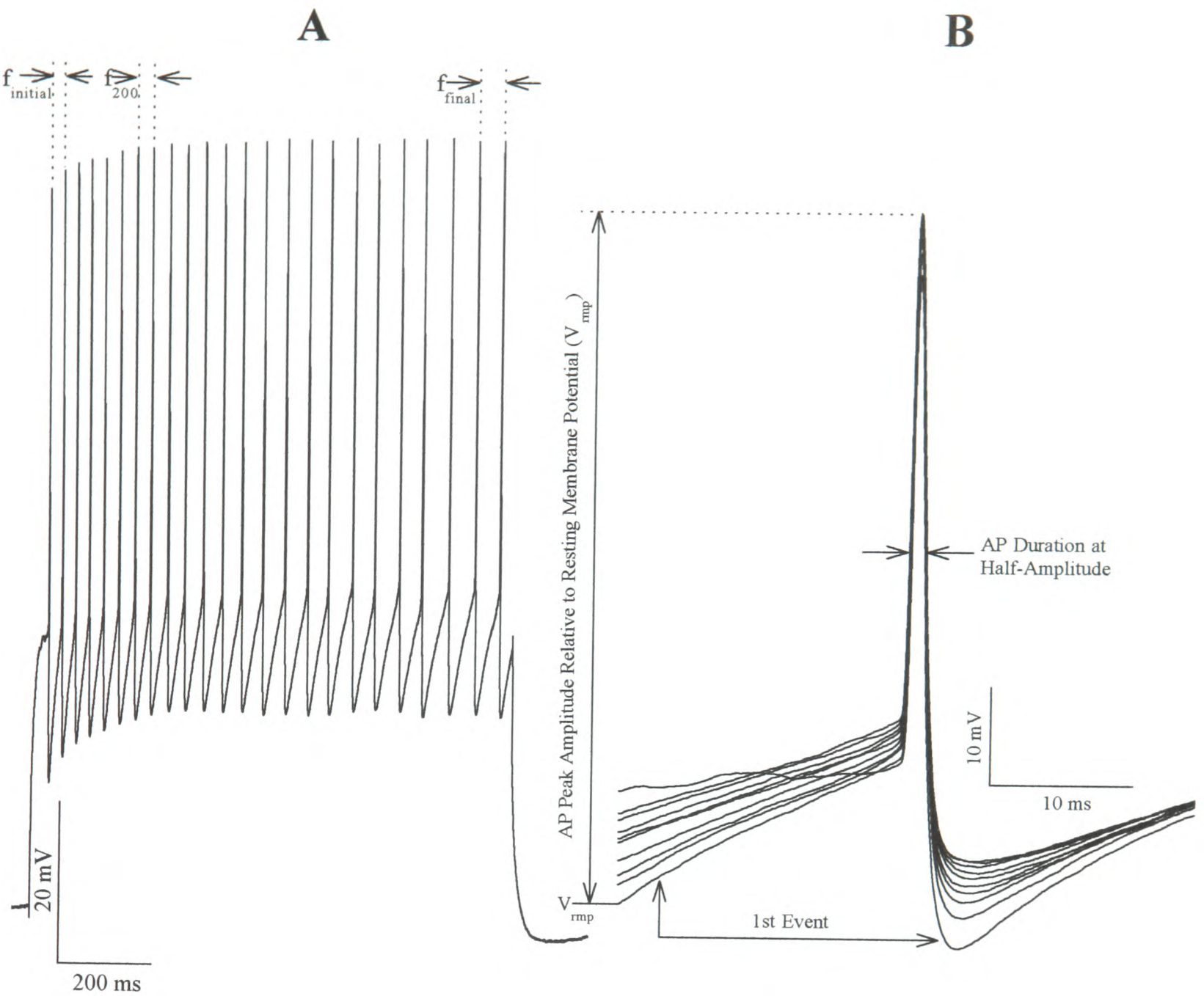

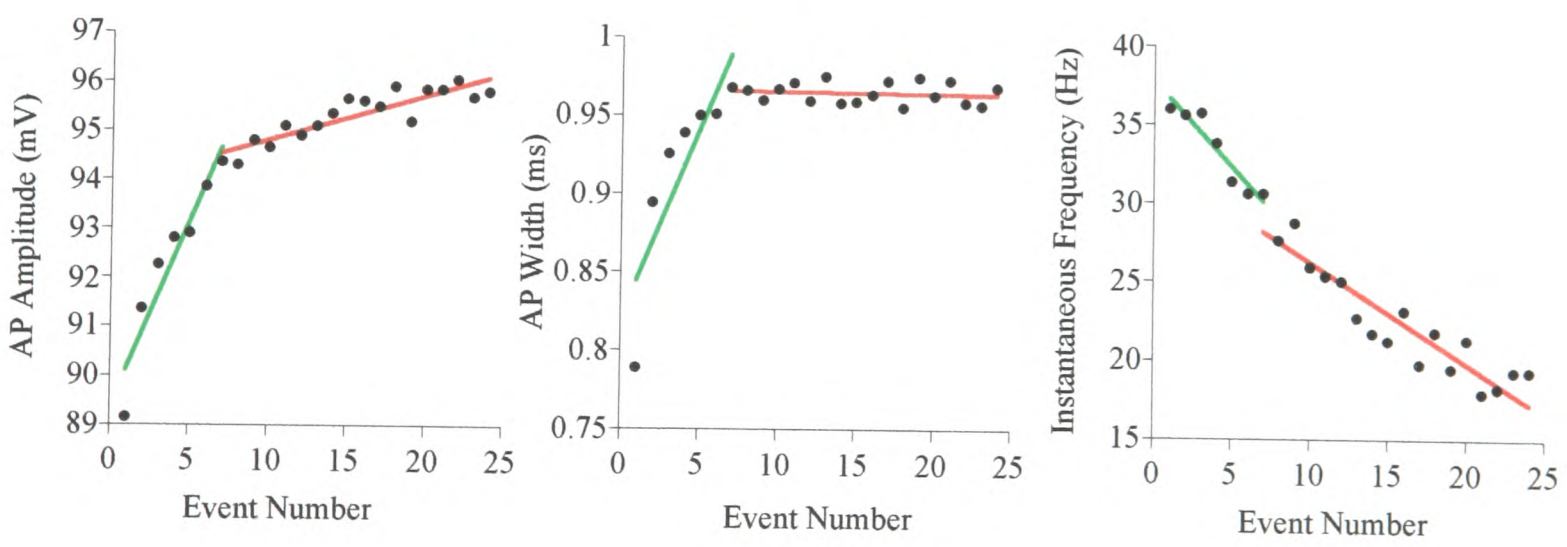

D

Early Linear Fit

$y_e = m_e * x + b_e$

Late Linear Fit

$y_l = m_l * x + b_l$

Early Changes

$(m_e * x_{initial} - m_e * x_{200}) / (m_e * x_{initial} + b_e)$

Late Changes

$(m_l * x_{200} - m_l * x_{final}) / (m_e * x_{initial} + b_e)$

x=event number for below:
instantaneous frequency (f)
AP duration at half-amplitude
AP amplitude relative to V_{rmp}

Fig 3.3

Figure 3.4 Voltage 'sag' evoked by a hyperpolarising current injection of 1 sec duration followed by a rebound depolarisation from resting membrane potential (V_{rmp}). Same nonpyramidal cell as in Figure 3.1. The magnitude of rectification was calculated as a ratio of the peak voltage response to the steady state voltage response averaged over 5 ms from the end of the current injection. This rectification ratio represents the amount of voltage 'sag' that occurred. The rebound depolarisation sometimes observed immediately after termination of the current injection was measured as a peak voltage response. All measurements were taken with reference to approximately -90 mV peak membrane potential (V_m).

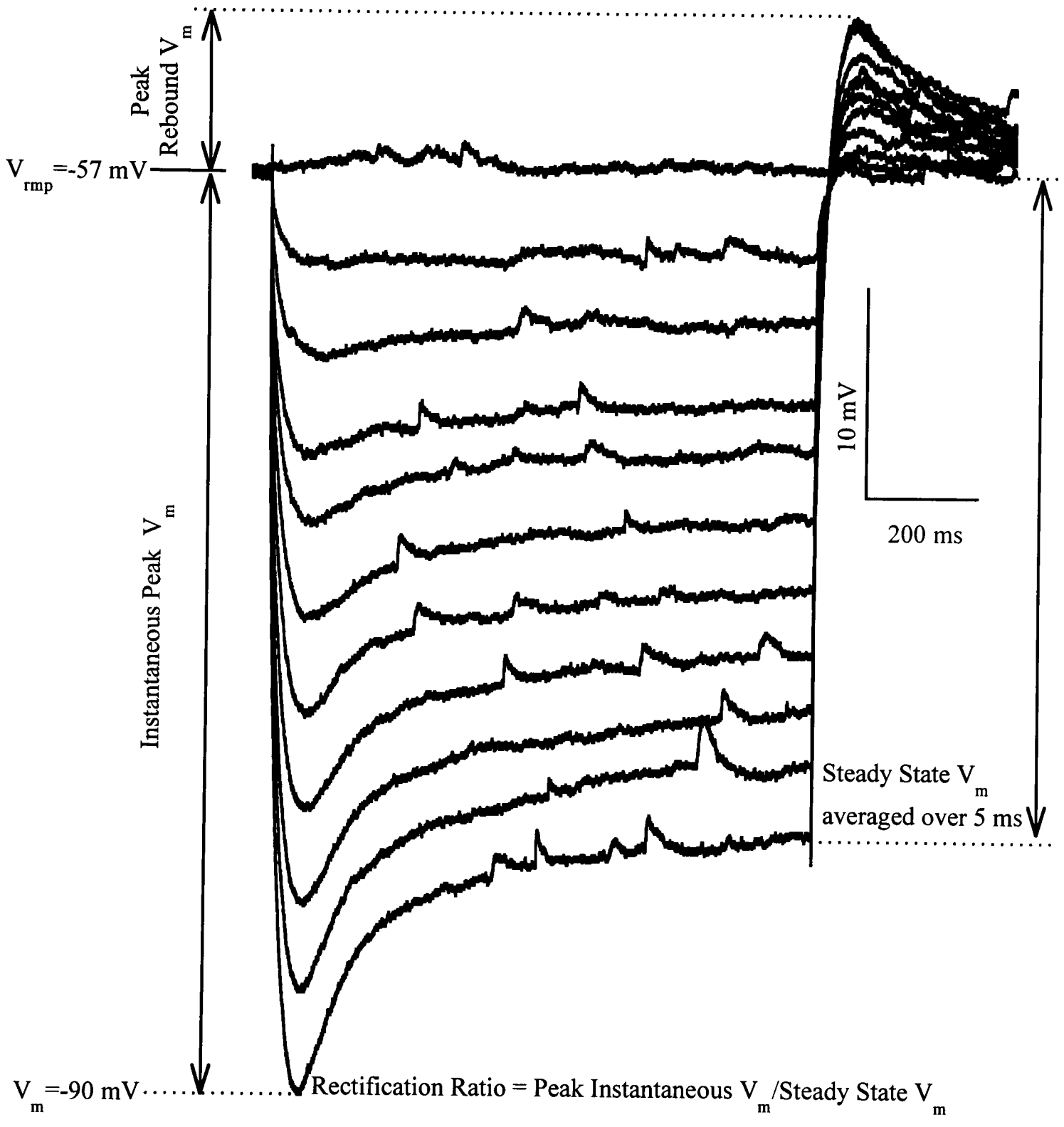
Peak
Rebound V m
V rmp =-57 mV
10 mV
200 ms
Instantaneous Peak V m
Steady State V m
averaged over 5 ms
V m =-90 mV
Rectification Ratio = Peak Instantaneous V m /Steady State V m

Fig 3.4

3.2.4 Immunocytochemistry

Recorded cells were labelled with biocytin included in the recording electrode. After recording, the slice was transferred to a glass slide using an inverted pasteur pipette filled with ACSF. The slice was sandwiched between two millipore filters and placed in fixative solution consisting of 4% paraformaldehyde, 0.05% glutaraldehyde, 15% (v/v) picric acid and 0.1 M phosphate buffer (pH 7.0). Slices were left in fixative solution between two to three hours and then thoroughly rinsed with 0.1 M phosphate buffer (PB) to avoid decrease in immunoreactivity caused by long fixation. In order to achieve adequate penetration of antibodies the slices were re-sectioned. The slices were mounted in gelatin and placed in fixative for hardening the gelatin. A slice was placed on top of a dry copper plate chilled with ice. Excess liquid was removed with filter paper. A well was made around the slice using three cut glass slides. A large drop of 10% gelatin dissolved in warm distilled water was placed over the entire window. A plastic square was then rubbed on the skin and quickly placed on top of the window adding light pressure to make a gelatin block. When condensation started to form, the plastic cover was easily removed with a dry cold blade due to the oily surface produced upon rubbing. The gelatin was cut around the slice and quickly transferred into cold fixative solution where it was left for 30 minutes to harden. A vibratome was used to obtain 60 μm sections of the gelatin-coated slice in 0.1 M PB surrounded by an ice jacket. In order to ensure that the antibodies or technical procedures work, a control section from a perfused rat brain was placed in a vial along with the other sections. Two sections from a perfused rat brain were place in a separate vial as negative controls to test whether incubation with secondary antibodies alone produced non-specific reactions. Prior to incubation with primary antibodies, all sections were given repeated washes with 0.1 M PB followed by repeated washes in Tris-buffered saline (TBS pH 7.4). After removal of the washing buffer, 700 μl of 20% Normal Goat Serum (NGS) in 0.1 % Triton X-100 in TBS was added to each vial to block sites in the tissue susceptible to non-specific binding of the

antibodies. The vials were left on the shaker for 2 hours at room temperature. After removal of the blocking agent, 500 µl of the primary antibodies and streptavidin-conjugated Aminomethylcoumarin (AMCA; 1 µg/ml; Vector Laboratories, Inc.) made up in 1% NGS in 0.1% Triton X-100 in TBS were added to each vial, which were left on a shaker for 24 hours at 4°C. Primary antibodies consisted of an ascites fluid monoclonal mouse IgG anti-somatostatin (1:500 coutesy of Dr A. Buchan; characterisation by Maccaferri et al. 2000) and affinity purified polyclonal rabbit IgG anti-mGluR1α (0.19 µg/ml; courtesy of Dr S. Alaluf and Dr E. Mulvihill; characterisation by Baude et al. 1993). Following repeated washes in TBS, the washing buffer was removed from each vial and 500 µl of goat anti-mouse IgG conjugated to Indocarbocyanine (CY3) (3.5 µg/ml; Jackson ImmunoResearch Laboratories, Inc.) and goat anti-rabbit IgG conjugated to Alexa488 (2 µg/ml; Molecular Probes Inc., USA) made up in 1% NGS in 0.1% Triton X-100 in TBS was added to each vial. Due to a decrease of immunoreactivity in slices kept in vitro, signal amplification was used to test for mGluR1α in most cells. This procedure involved incubation of sections with HRP conjugated swine anti-rabbit IgG (2.4 µg/ml; DAKO, Denmark) instead of the Alexa488 conjugated secondary antibody. After addition of secondary antibodies, the vials were left on a shaker covered from light for 24 hours at 4°C. Sections with the Alexa488 conjugated secondary antibody were given repeated washes in TBS and mounted on microscope slides with Vectashield, an anti-fading medium for fluorescing sections (Vector Laboratories, Inc.). Sections with the HRP conjugated secondary antibody were given repeated washes in 0.1% Triton X-100 in TBS followed by 5 minutes incubation with 500 µl of Fluorescein isothiocyanate (FITC) conjugated to tyramide (NEN Kit, Life Science Products, Inc.) and left in the dark on the shaker at room temperature. The horseradish peroxidase present at the mGluR1α sites catalyzes the formation of tyramide radicals that bind covalently to tyrosine residues present in the tissue. Due to the short half-life of tyramide radicals, only

tyrosine residues in the direct surroundings of HRP will be bound by the FITC conjugated tyramide. Sections were given one wash in 0.1% Triton X-100 in TBS followed by repeated washes in TBS before mounting with Vectashield.

Images were taken with a digital camera attached to a Leitz DMR fluorescence microscope (Leica, Germany) compatible with the software Openlab (Improvision Image Processing & Vision Company, Ltd. UK). Fluorescence filters used were AMCA (excitation filter BP 340-380 nm), CY3 (excitation BP 515-560 nm) and Alexa488 (excitation BP 460-500). Some images were scanned with argon (488 nm) and helium/neon (543 and 633 nm) lasers using an Axiovert 100 M confocal microscope and LSM 510 software (Zeiss, Germany). A combination of streptavidin-conjugated AMCA (1 μg/ml) and streptavidin-conjugated CY5 (1.8 μg/ml) was required to first detect the cell with fluorescent filters and then scan the same area for CY5 in the invisible spectrum.

3.2.5 Histological Processing of Sections for Light Microscopy

In order to identify the recorded cells anatomically, a peroxidase reaction using 3,3'-diaminobenzidine tetrahydrochloride (DAB) as a chromogen was performed on the above sections. Sections were demounted, placed into vials and given repeated washes with 0.1% Triton X-100 in TBS followed by TBS alone. Sections were then incubated with 500 μl of biotinylated horseradish peroxidase (1:100 in TBS, ABC Vector) in order to bind to the pre-existing streptavidin-conjugated AMCA labelled cell. The vials were left on a shaker overnight at 4°C. Sections were washed repeatedly in TBS while a 1% avidin-biotinylated horseradish peroxidase complex in TBS (ABC Kit, Vector Laboratories, Inc.) was prepared 30 min prior to use. The washing buffer was removed from each vial and 500 μl of the complex was added to

each vial. The vials were left on a shaker at room temperature for 4 hours. The sections were washed repeatedly with TBS followed by TB (pH 7.4). After removal of the washing buffer the vials were incubated with 2 ml of DAB solution (0.5 mg/ml TB) for 15 min on a shaker at room temperature. Hydrogen peroxide was added to each vial to make a 0.01% solution with the buffered DAB in the vials. The reaction was stopped after 3 min by repeated washes with TB. Sections were mounted on microscopic slides with gelatin and placed for 5 min in 50 ml of 0.1 M phosphate buffer containing 5 drops of 4% osmium tetroxide in order to increase the contrast between the labelled cell and surrounding tissue. Afterwards, the sections were rinsed in 0.1 M phosphate buffer once and 3 times in distilled water followed by dehydration in an ascending series of ethanol solutions (50%, 70%, 95%, 100%x2; 10 minutes in each). The remaining ethanol was then cleared from the sections by immersing in xylene twice for 10 minutes each and then mounted under a coverslip with XAM mounting medium.

Recovered cells were visualised under a light microscope and classified according to somatodendritic orientation and axonal projection. Some labelled cells were reconstructed with the aid of a drawing tube using a x100 oil objective. Drawings were scanned into the Adobe Photoshop software (Adobe Systems, Inc.) for further image processing.

3.3 Results

3.3.1 Intrinsic Membrane Properties

Nonpyramidal cells were physiologically characterised according to intrinsic membrane properties. The intrinsic membrane properties analysed included firing pattern, voltage 'sag' and rebound depolarisation, single AP and AHP parameters, time constant and electrotonic length constant. Oriens lacunosum-moleculare (O-LM) nonpyramidal cells and oriens bistratified (O-Bi) nonpyramidal cells both named for their somatodendritic location and orientation as well as their axonal projections, were investigated in this study. Similarities in the somatodendritic placement and differences in the axonal projections of O-LM and O-Bi cells suggest that they receive similar inputs but functionally control different pyramidal dendritic fields. A total of 37 nonpyramidal cells were recorded and immunolabelled. To my knowledge, the present O-LM (n=11) and O-Bi anatomically verified cells (n=8) are the largest sample to be recorded and immunolabelled at the time of submission. As explained in the methods section of this chapter, all cells were analysed at similar membrane potentials and firing frequencies.

3.3.1.1 O-LM Nonpyramidal Cells

Eleven anatomically verified O-LM cells out of the total 37 cells were recorded and analysed for intrinsic membrane properties (Table 3.1). These cells typically showed a prominent late accommodation (25.23 ± 8.57 %; n=11/11) in comparison to a smaller early one (8.68 ± 14.94 %; n=11/11; Figure 3.5). The large variation with respect to the mean for the early accommodation reflects three outliers showing large early accommodation (>20%). Cells (n=4/11) showing an early accommodation greater than the mean were recorded from P19 or P24 animals except one case (M0131) in which the animal was P15 indicating that the postnatal days are not correlated with the larger early accommodation observed in some cells. In two

(M0131 and M1221) out of three cells showing a prominent early as well as late accommodation, the AP amplitude decrement was larger than all other cells. Action potential width increase (Figure 3.5) was larger for the early part of the AP train (11.80 ± 3.69 %; n=11/11) than for the late (4.33 ± 2.66 %; n=11/11). However, the AP width increase was not significantly correlated with the accommodation observed since less accommodation occurred (sometimes slight increases in firing rate) during larger increases in AP width (early r=0.28; P=0.41 and late r=-0.10; P=0.76). Typically, O-LM cells exhibited a prominent voltage 'sag' at –90 mV (1.47 ± 0.22 rectification ratio; n=11/11) and relatively large rebound depolarisation (6.58 ± 4.16 mV; n=11/11). The average amplitude of single APs (Figure 3.6) was 89.18 ± 10.24 mV (n=5/5) with one cell (M1231) accounting for the large standard deviation. As a subthreshold response was not recorded and therefore could not be subtracted for the remaining cells, parameters based on the single AP could not be analysed for these cells. Specifically, the single AP and AHP coincided in these cases with the end of the current pulse, which decayed back to resting membrane potential exponentially. The cell (M1231) with the smallest AP amplitude had a more negative resting membrane potential (-67 mV), which could have contributed to a reduction of AP amplitude arriving at the soma. The AHP width and time constants obtained from both the single and double exponential fits were also larger for this cell. However, these outliers were not excluded on the basis that other single AP and AHP parameters were similar to the rest of the cells. Other parameters (Figure 3.5) such as AP width (0.45 ± 0.08 ms; n=5/5), AP rise time (0.22 ± 0.04 ms; n=5/5), AHP amplitude (18.18 ± 2.72 mV; n=5/5) and AHP time to peak (3.92 ± 1.60 ms; n=5/5) were less skewed compared to those with outliers. The AHP width (33.03 ± 9.08 ms; n=5/5; Figure 3.5) had a large standard deviation as a consequence of the cell with the more negative resting membrane potential (M1231) described above. Time constants obtained from double exponential fits (57.9 ± 27.7

ms; n=6/6) were the largest followed by time constants obtained from single exponential fits (48.2 ± 24.4 ms; n=6/6) and time constants obtained from the time to reach 63% of the peak voltage response (35.8 ± 14.1 ms; n=6/6). Time constants obtained from the time to reach 63% of the peak voltage response rely on single point measurements, which can be easily influenced by synaptic activation of membrane channels. Moreover, as the time constant obtained from the double exponential fit accounts for variability in the membrane potential of the cell, it was used as a more accurate measure. The influence of the equalising time constant in the double exponential fit is used in Rall's model for the electrotonic length of a sealed end cylinder (Rall, 1969). Therefore, the length constant also provided a good check as to whether the time constant was best obtained from a single or double exponential fit. For example, one cell (M1621) had a large electrotonic length constant indicating that the two time constants were similar (τ_1=20.9 ms; τ_2=26.1 ms) and thus a double exponential fit was not necessary. One cell (M1711) had a very short electrotonic length constant indicating that the equalising time constant was too short to estimate accurately (τ_1=0.50 ms; τ_2=53.6 ms) and thus a single exponential fit would suffice. The input resistance for one cell (M0121) was very large but this was likely due to poor electrode resistance compensation because all other parameters are similar to the other cells with lower input resistance values. Additionally, the cell soma size observed was not any smaller than that of other cells as would be expected for cells with a large input resistance and a large time constant (Kawaguchi 1993). The average value of input resistance (255.0 ± 44.8 MΩ; n=5/6), time constants (59.2 ± 26.1 ms; n=6/6) and length constants (2.1 ± 1.4; n=4/6) are presented (Table 3.2) with the exclusion of the aforementioned outliers.

Table 3.1 Comparison of data for all O-LM and O-Bi cells recorded in the CA1 area of the hippocampus.

Experiment	Cell Type	Age(P)	V_m	Avg Hz	early Accommodation	late Accommodation	early APamp	late APamp	early APwidth	late APwidth	rectification ratio	rebound peak(mV)	single AP amp(mV)	single AP width(ms)	single AP rise time(ms)	single AHP peak(mV)	single AHP width(ms)	single AHP time-to-peak(ms)	1exponential 20%-peak Time const.	2exponential 20%-peak Time const.	63% Time const.	R_i(Mohms)	electrotonic length (L)
M0121	O-LM	15	-57	25	-0.0508	0.2102	-0.0291	-0.0180	-0.0867	-0.0423	1.24	2.10							73.6	66.6	54.4	407.8	1.5
M0131	O-LM	15	-62	22.5	0.2942	0.2634	0.0256	0.0242	-0.0773	-0.0734	1.84	9.63							21.4	28.2	21.2	269.7	4.2
M0311	O-LM	17	-63	18.75	-0.0480	0.4476	0.0178	0.0121	-0.1081	-0.0222	1.41	4.53											
M0321	O-LM	17	-63	23.75	-0.0416	0.3305	-0.0142	0.0127	-0.1627	-0.0632	1.71	13.13											
M0521	O-LM	16	-65	20.83	-0.0802	0.1962	0.0051	0.0131	-0.1034	-0.0347	1.62	5.88											
M0611	O-LM	19	-64	18.75	0.3588	0.1981	0.0087	0.0140	-0.0890	-0.0077	1.18	3.51											
M1221	O-LM	19	-64	21.25	0.2005	0.2725	0.0584	0.0366	-0.1252	-0.0784	1.22	2.32	92.13	0.39	0.20	-15.98	32.51	3.38	27.8	75.9	22.9	214.3	1.6
M1231	O-LM	19	-67	24.58	0.1115	0.1724	0.0086	0.0163	-0.1532	-0.0726	1.31	3.43	71.16	0.53	0.27	-15.47	47.75	4.37	79.3	96.9	31.2	269.2	1.2
M1621	O-LM	24	-58	22.67	0.1404	0.1928	0.0083	0.0034	-0.0821	-0.0015	1.57	6.93	96.84	0.33	0.18	-22.21	23.51	2.49	33.7	26.1	34.0	206.7	6.3
M1711	O-LM	15	-62	22.66	-0.0039	0.1723	0.0146	0.0090	-0.1196	-0.0315	1.54	14.22	93.10	0.47	0.22	-18.03	33.06	6.49	53.6	53.6	51.3	315.1	0.3
M1821	O-LM	15	-61	22.33	0.0735	0.3193	0.0097	0.0163	-0.1905	-0.0483	1.55	6.68	92.68	0.51	0.27	-19.20	28.30	2.84					
MEAN		**17.4**	**-62.32**	**22.10**	**8.68%**	**25.23%**	**1.03%**	**1.27%**	**-11.80%**	**-4.33%**	**1.47**	**6.58**	**89.18**	**0.45**	**0.22**	**-18.18**	**33.03**	**3.92**	**48.2**	**57.9**	**35.8**	**280.5**	**2.5**
SD		**2.8**	**2.83**	**2.07**	**14.94%**	**8.57%**	**2.19%**	**1.33%**	**3.69%**	**2.66%**	**0.22**	**4.16**	**10.24**	**0.08**	**0.04**	**2.72**	**9.08**	**1.60**	**24.4**	**27.7**	**14.1**	**74.1**	**2.3**
n		**11**	**11**	**11**	**11**	**11**	**11**	**11**	**11**	**11**	**11**	**11**	**5**	**5**	**5**	**5**	**5**	**5**	**6**	**6**	**6**	**6**	**6**
M0111	O-Bi	15	-60	20	0.3900	0.2186	-0.1737	0.0050	0.0054	-0.0312	1.08	1.28							26.9	62.1	26.8	325.0	2.4
M0411	O-Bi	14	-60	20	0.0480	0.0688	0.0039	0.0051	-0.0154	-0.0257	1.14	4.02	84.65	0.38	0.20								
M1011	O-Bi	16	-65	19.17	0.2051	0.0995	0.0403	0.0180	-0.0812	-0.0579	1.13	6.34	78.32	0.47	0.20	-19.74	99.69	21.59					
M1431	O-Bi	17	-60	24	0.3370		0.1988		-0.6183		1.04		85.84	0.32	0.16	-10.48	13.76	3.41	53.8	76.9	21.8	239.8	1.2
M1511	O-Bi	16	-52	22	0.5934	-0.1973	0.0663	0.0073	-0.1504	-0.0355			83.40	0.29	0.16								
n4621	O-Bi	14	-60	22.5	0.2180	0.3277	-0.0570	-0.0042	-0.0787	0.0252	1.49	6.28							49.5	43.6	42.5	362.3	2.3
n4921	O-Bi	14	-60	22.5	0.2951	0.0202	-0.0057	0.0098	-0.0867	-0.0515	1.18	2.24							49.4	57.7	19.8	220.3	1.0
n5341	O-Bi	13	-60	26.25	0.1914	0.0604	0.0867	0.0166	-0.2260	-0.0838	1.21	16.76											
MEAN		**14.9**	**-59.63**	**22.05**	**28.47%**	**8.54%**	**1.99%**	**0.82%**	**-15.64%**	**-3.72%**	**1.18**	**6.15**	**83.05**	**0.36**	**0.18**	**-15.11**	**56.73**	**12.50**	**44.9**	**60.1**	**27.7**	**286.9**	**1.7**
SD		**1.4**	**3.54**	**2.35**	**16.24%**	**16.42%**	**10.91%**	**0.76%**	**20.03%**	**3.38%**	**0.15**	**5.59**	**3.31**	**0.08**	**0.02**	**6.55**	**60.76**	**12.86**	**12.2**	**13.7**	**10.3**	**67.8**	**0.7**
n		**8**	**8**	**8**	**8**	**7**	**8**	**7**	**8**	**7**	**7**	**6**	**4**	**4**	**4**	**2**	**2**	**2**	**4**	**4**	**4**	**4**	**4**

P = postnatal days
V_m = resting or holding membrane potential
Avg Hz = average firing frequency of the AP train
AP train parameters obtained from V_m
single AP and AHP parameters obtained from AP threshold
rise time obtained from 10-90% of the peak AP amplitude
width obtained at half-amplitude
1st and 2nd exponential fits obtained from 20% to the peak of the response
R_i = input resistance
(-%) = increasing
(-AHP) = below AP threshold

Figure 3.5 Physiological characteristics of a typical O-LM cell (M1821) with a V_{rmp} of –61 mV recorded in the stratum oriens of the CA1 area of the hippocampus in vitro. **(A)** A train of APs at an average firing frequency of 22 Hz were elicited using a 0.235 nA current injection of 1 s duration. The sixth AP separates the early and late firing of APs because it occurred closest to the time (200 ms) when changes could be readily observed for most cells studied. During a hyperpolarising response of –91 mV elicited by current injection of –0.125 nA for 1 s, a prominent voltage 'sag' was apparent followed by a rebound depolarisation upon termination of the current step. **(B)** A single AP after subtraction of a subthreshold response elicited by a current pulse of 5 ms duration. The single AP and AHP parameters were referenced from AP threshold: AP width (0.51 ms), AHP width (28.30 ms), and AHP peak (19.20 mV). The AP amplitude (92.68 mV) is larger compared to most O-Bi cells recorded. **(C)** Linear fit analysis of AP amplitudes, AP widths and AP accommodation as a function of event number including the early (green) and late (red) components of the train of APs in (A). The AP amplitude and width at half amplitude were referenced from V_{rmp}. A larger AP accommodation occurred during the late part of the response compared to the earlier part of the response. The AP amplitude decrement was not as large as the AP accommodation for both the early and late responses, however the late part of the response has a larger AP amplitude decrement than the earlier part of the response. Note that a small y-axis range can account for linear fits to appear steeper. The AP width at half amplitude increased more during the earlier part of the response compared to the late part of the response. Scale: 20 mV applies to both (A) and (B).

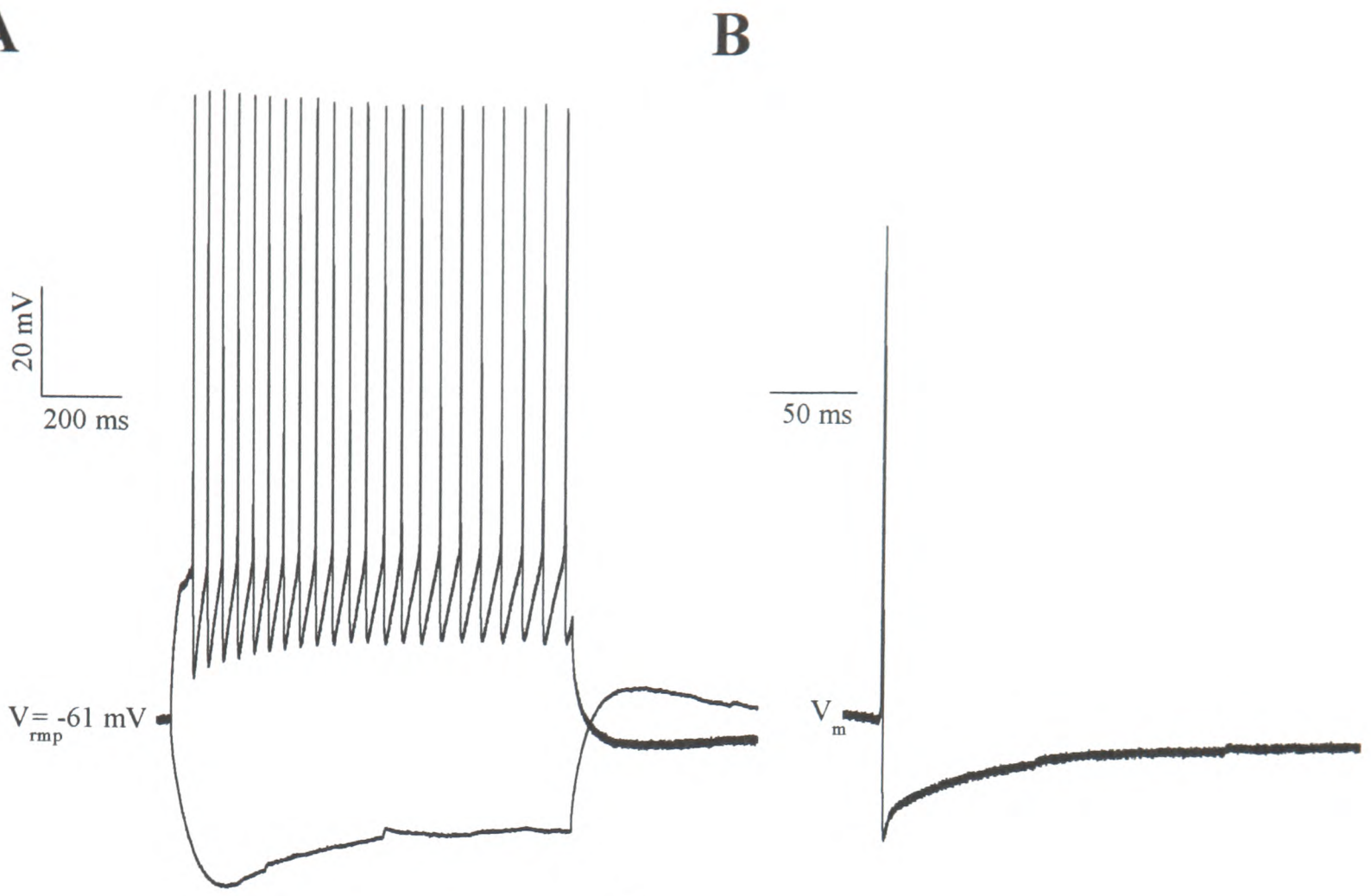
A
B
20 mV
200 ms
V= -61 mV
rmp
50 ms
V
m

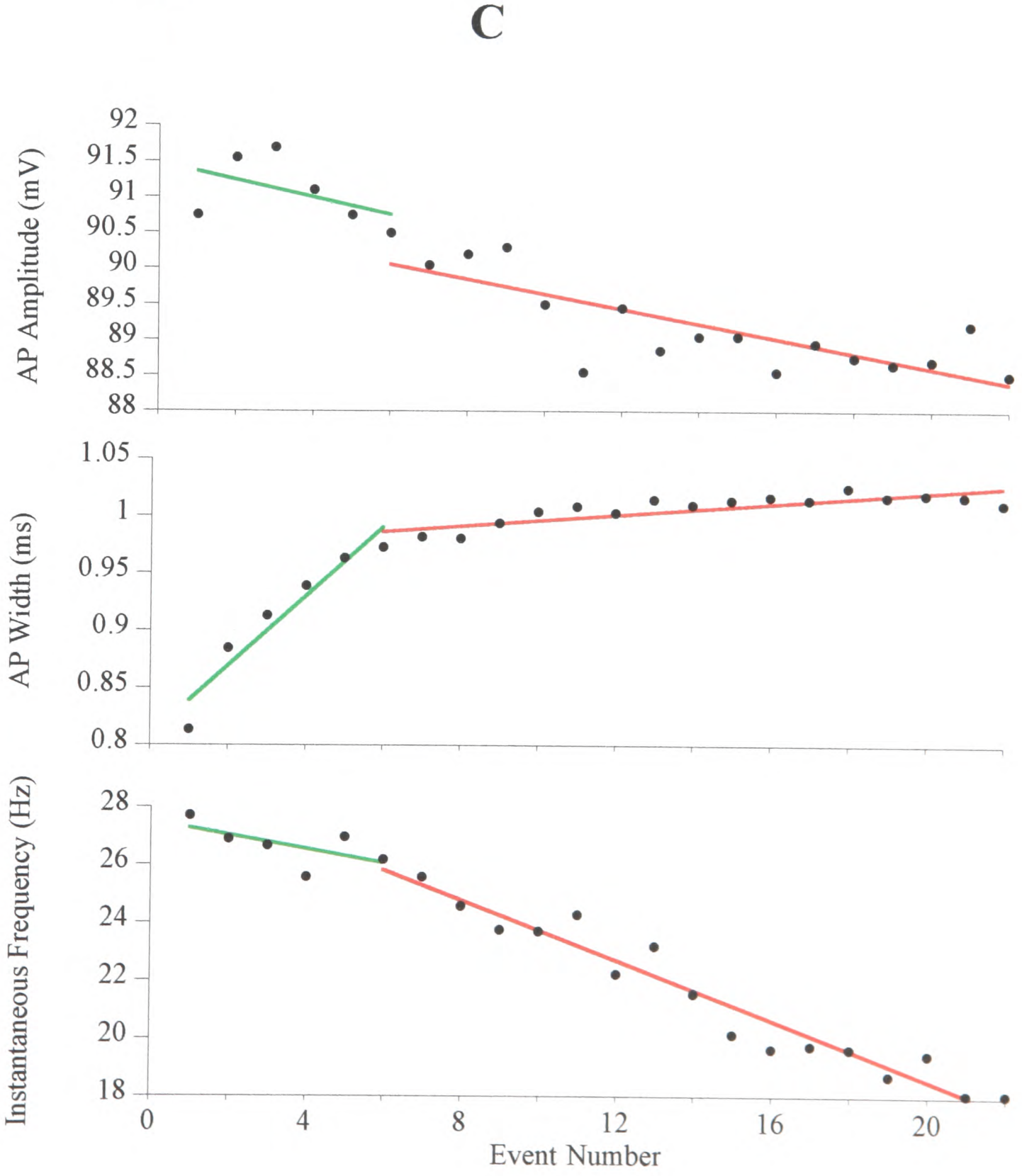
C
AP Amplitude (mV)
92
91.5
91
90.5
90
89.5
89
88.5
88
AP Width (ms)
1.05
1
0.95
0.9
0.85
0.8
Instantaneous Frequency (Hz)
28
26
24
22
20
18
0
4
8
12
16
20
Event Number

Fig 3.5

Table 3.2 Comparison of data analysis for O-LM and O-Bi cells **excluding outliers**.

Experiment	Cell Type	Age(P)	V_m	Avg Hz	early accommodation	late accommodation	early APamp	late APamp	early APwidth	late APwidth	rectification ratio	rebound peak(mV)	single AP amp(mV)	single AP width(ms)	single AP rise time(ms)	single AHP peak(mV)	single AHP width(ms)	single AHP time-to-peak(ms)	20%-peak Time const.	R_I(Mohms)	electrotonic length (L)
M0121	O-LM	15	-57	25	-0.0508	0.2102	-0.0291	-0.0180	-0.0867	-0.0423	1.24	2.10							66.6		1.5
M0131	O-LM	15	-62	22.5	0.2942	0.2634	0.0256	0.0242	-0.0773	-0.0734	1.84	9.63							28.2	269.7	4.2
M0311	O-LM	17	-63	18.75	-0.0480	0.4476	0.0178	0.0121	-0.1081	-0.0222	1.41	4.53									
M0321	O-LM	17	-63	23.75	-0.0416	0.3305	-0.0142	0.0127	-0.1627	-0.0632	1.71	13.13									
M0521	O-LM	16	-65	20.83	-0.0802	0.1962	0.0051	0.0131	-0.1034	-0.0347	1.62	5.88									
M0611	O-LM	19	-64	18.75	0.3588	0.1981	0.0087	0.0140	-0.0890	-0.0077	1.18	3.51									
M1221	O-LM	19	-64	21.25	0.2005	0.2725	0.0584	0.0366	-0.1252	-0.0784	1.22	2.32	92.13	0.39	0.20	-15.98	32.51	3.38	75.9	214.3	1.6
M1231	O-LM	19	-67	24.58	0.1115	0.1724	0.0086	0.0163	-0.1532	-0.0726	1.31	3.43	71.16	0.53	0.27	-15.47	47.75	4.37	96.9	269.2	1.2
M1621	O-LM	24	-58	22.67	0.1404	0.1928	0.0083	0.0034	-0.0821	-0.0015	1.57	6.93	96.84	0.33	0.18	-22.21	23.51	2.49	33.7	206.7	
M1711	O-LM	15	-62	22.66	-0.0039	0.1723	0.0146	0.0090	-0.1196	-0.0315	1.54	14.22	93.10	0.47	0.22	-18.03	33.06	6.49	53.6	315.1	
M1821	O-LM	15	-61	22.33	0.0735	0.3193	0.0097	0.0163	-0.1905	-0.0483	1.55	6.68	92.68	0.51	0.27	-19.20	28.30	2.84			
MEAN		**17.4**	**-62.32**	**22.10**	**8.68%**	**25.23%**	**1.03%**	**1.27%**	**-11.80%**	**-4.33%**	**1.47**	**6.58**	**89.18**	**0.45**	**0.22**	**-18.18**	**33.03**	**3.92**	**59.2**	**255.0**	**2.1**
SD		**2.8**	**2.83**	**2.07**	**14.94%**	**8.57%**	**2.19%**	**1.33%**	**3.69%**	**2.66%**	**0.22**	**4.16**	**10.24**	**0.08**	**0.04**	**2.72**	**9.08**	**1.60**	**26.1**	**44.8**	**1.4**
n		**11**	**11**	**11**	**11**	**11**	**11**	**11**	**11**	**11**	**11**	**11**	**5**	**5**	**5**	**5**	**5**	**5**	**6**	**5**	**4**
M0111	O-Bi	15	-60	20	0.3900			0.0050	0.0054	-0.0312	1.08	1.28							62.1	325.0	2.4
M0411	O-Bi	14	-60	20	0.0480	0.0688	0.0039	0.0051	-0.0154	-0.0257	1.14	4.02	84.65	0.38	0.20						
M1011	O-Bi	16	-65	19.17	0.2051	0.0995	0.0403	0.0180	-0.0812	-0.0579	1.13	6.34	78.32	0.47	0.20	-19.74	99.69	21.59			
M1431	O-Bi	17	-60	24	0.3370						1.04		85.84	0.32	0.16	-10.48	13.76	3.41	76.9	239.8	1.2
M1511	O-Bi	16	-52	22			0.0663	0.0073		-0.0355			83.40	0.29	0.16						
n4621	O-Bi	14	-60	22.5	0.2180		-0.0570	-0.0042	-0.0787	0.0252	1.49	6.28							43.6	362.3	2.3
n4921	O-Bi	14	-60	22.5	0.2951	0.0202	-0.0057	0.0098	-0.0867	-0.0515	1.18	2.24							57.7	220.3	1.0
n5341	O-Bi	13	-60	26.25	0.1914	0.0604	0.0867	0.0166	-0.2260	-0.0838	1.21	16.76									
MEAN		**14.9**	**-59.63**	**22.05**	**24.07%**	**6.22%**	**2.24%**	**0.82%**	**-8.05%**	**-3.72%**	**1.18**	**6.15**	**83.05**	**0.36**	**0.18**	**-15.11**	**56.73**	**12.50**	**60.1**	**286.9**	**1.7**
SD		**1.4**	**3.54**	**2.35**	**11.24%**	**3.27%**	**5.26%**	**0.76%**	**8.10%**	**3.38%**	**0.15**	**5.59**	**3.31**	**0.08**	**0.02**	**6.55**	**60.76**	**12.86**	**13.7**	**67.8**	**0.7**
n		**8**	**8**	**8**	**7**	**4**	**6**	**7**	**6**	**7**	**7**	**6**	**4**	**4**	**4**	**2**	**2**	**2**	**4**	**4**	**4**

P = postnatal days
V_m = resting or holding membrane potential
Avg Hz = average firing frequency of the AP train
AP train parameters obtained from V_m
single AP and AHP parameters obtained from AP threshold
rise time obtained from 10-90% of the peak AP amplitude
width obtained at half-amplitude
1st and 2nd exponential fits obtained from 20% to the peak of the response
R_I = input resistance
(-%) = increasing
(-AHP) = below AP threshold

3.3.1.2 O-Bi Nonpyramidal Cells

Eight anatomically verified O-Bi cells out of the total 37 cells were recorded and analysed for intrinsic membrane properties (Table 3.1). There appear to be two O-Bi cell groups emerging from the physiological data. Altogether, O-Bi cells typically showed a larger early accommodation (28.47 ± 16.24 %; n=8/8) compared to the late accommodation (8.54 ± 16.42 %; n=7/7) as well as a relatively small voltage 'sag' at –90 mV (1.18 ± 0.15 rectification ratio; n=7/7). Three (M0111, M1431 and M1511) of the eight cells showed intermittent firing of a train of APs elicited whereas the others responded with a continuous train of APs. Consequently, these three cells showed differences in the analysed parameters for the train of APs elicited. However, most of the differences in parameters analysed do not correlate with each other and in fact, some differences are similar to one or two other cells which did not show intermittent firing of APs. For example, two (M1431 and M1511) of the three cells showed large increases in the early AP width compared to the others although one cell (n5341) which did not show intermittent firing exhibited the same property. A combination of two other cells (M0111 and M1431) showed a large increase and a large decrease in early AP amplitude respectively compared to all other cells showing little change. Also, another combination of two cells (M0111 and M1511) had similar opposite attributes of late accommodation, although the cell with a large late accommodation (M0111) was similar to another cell, which did not show intermittent firing (n4621). Nonetheless, the cell without intermittent firing (n4621) was the only cell of its kind to have a similar AHP waveform to the three cells with intermittent firing, typically a large peak with faster kinetics. The AHP kinetic differences of a cell with intermittent firing (M1511) were apparent from the smaller AHP width and AHP time to peak after eliciting a single AP as compared to a cell (M1011) without intermittent firing. However, having only two examples does not permit exclusion of one or the other for cell classification. Based on the similar AHP shape (Figure 3.6) but different firing patterns between cells with

(M0111, M1431 and M1511) and without (n4621) intermittent firing, it appears that these two properties result from more than one mechanism. Caution should be taken however with respect to two cells (M0411 and n5341) which had typical continuous APs and AHPs elicited but unique properties of accommodation and AP width during the early part of the AP train, respectively. The age of the animals used for recordings were similar for each experiment and could thus not account for any large variability observed. It is possible that these differences could be inherent of the in vitro conditions where some channels may not be operational or diminished. Therefore, unique data from cells belonging to the group with intermittent firing of APs and large AHPs were excluded, leaving data from cells on which there was no apparent basis for exclusion (Table 3.2). Comparisons of the three unique cells could not be made as one of them (M1511) had a resting membrane potential (-52 mV) considerably different from the others to be representative of the small sample. From the new data set with exclusions, statistical significance did not change although the averages are more representative of a population mean for the parameters analysed. Early accommodation of O-Bi cells (Figure 3.7) was still larger (24.07 ± 11.24 %; n=7/8) than late accommodation (6.22 ± 3.27 %; n=4/7). Early AP amplitude decrease (2.24 ± 5.26 %; n=6/8) was larger than the late AP amplitude decrease (0.82 ± 0.76 %; n=7/7; Figure 3.7). However, the AP amplitude decrease did not correlate with the accommodation observed (early r=0.16; P=0.76 and late r=0.45; P=0.55). As in O-LM cells the early AP width increase (8.05 ± 8.10 %; n=6/8) was larger than the late AP width increase (3.72 ± 3.38 %; n=7/7; Figure 3.7). Also, the AP width increase did not correlate with the accommodation observed (early r=0.15; P=0.78 and late r=-0.26; P=0.74). The rectification ratio at –90 mV (1.18 ± 0.15; n=7/7) was relatively small but the rebound voltage depolarisation (6.15 ± 5.59 mV; n=6/6) was similar to that of O-LM cells (Figure 3.7). The AP amplitude (83.05 ± 3.31 mV; n=4/4), AP width (0.36 ± 0.08 ms; n=4/4), AP rise time (0.18 ± 0.02 ms;

n=4/4) and AHP amplitude (15.11 ± 6.55 mV; n=2/2) were similar to that of O-LM cells (Figure 3.7). Single AHP width (56.73 ± 60.76 ms; n=2/2) and single AHP time to peak (12.50 ± 12.86 ms; n=2/2) were larger than those of O-LM cells, presumably reflecting the two types of O-Bi firing patterns observed. The time constant (60.1 ± 13.7 ms; n=4/4), input resistance (286.9 ± 67.8 MΩ; n=4/4) and length constant (1.7 ± 0.7; n=4/4) were also similar to those of O-LM cells.

Figure 3.6 Recording of an O-Bi cell (M0111) at a V_{rmp} of –60 mV in stratum oriens of the CA1 area of the hippocampus in vitro. The cell had different physiological characteristics from the majority of O-Bi cells. **(A)** A train of APs at an average firing frequency of 20 Hz was elicited using a 0.1 nA current injection of 800 ms duration. The fifth AP separates the early and late firing of APs because it occurred closest to the time (200 ms) when changes could be readily observed for most cells studied. Note also the prominent AHP peak. During a hyperpolarising response of -92 mV elicited by current injection of –0.1 nA for 800 ms a small voltage 'sag' was observed followed by a small rebound depolarisation upon termination of the current step. **(B)** Linear fit analysis of AP amplitudes, AP widths and AP accommodation as a function of event number including the early (green) and late (red) components of the train of APs in (A). The AP amplitude and width at half amplitude were referenced from V_{rmp}. This cell shows intermittent AP firing exemplified by both the large early and late accommodation. Amplitude fluctuations were observed throughout the response. The AP width for the early part of the response was unaltered but a slight increase occurred for the late part of the response. Note that a small y-axis range can account for linear fits to appear steeper.

A

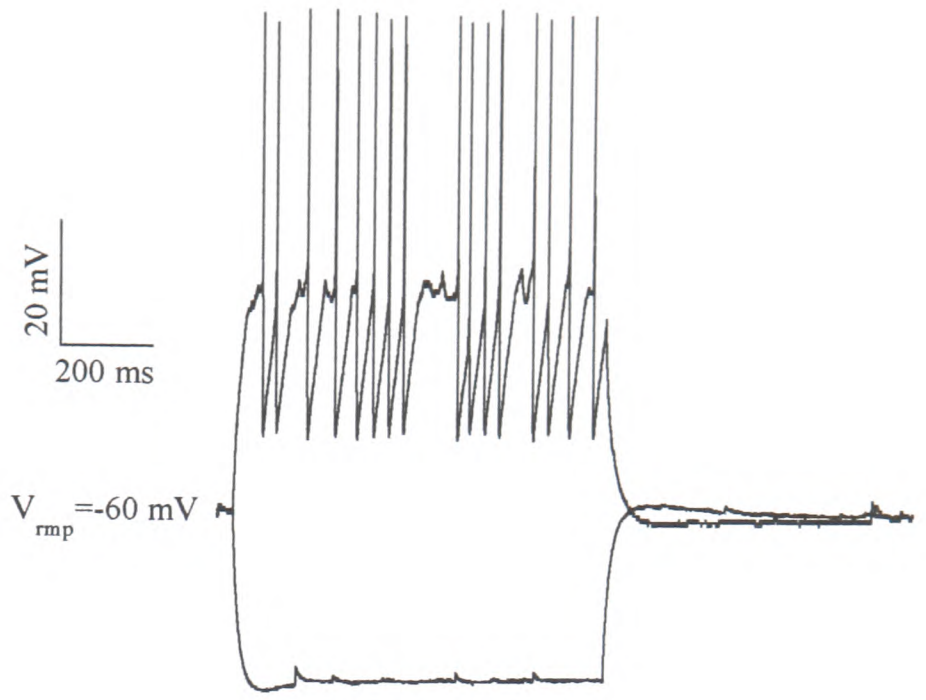
20 mV
200 ms
V rmp =-60 mV

B

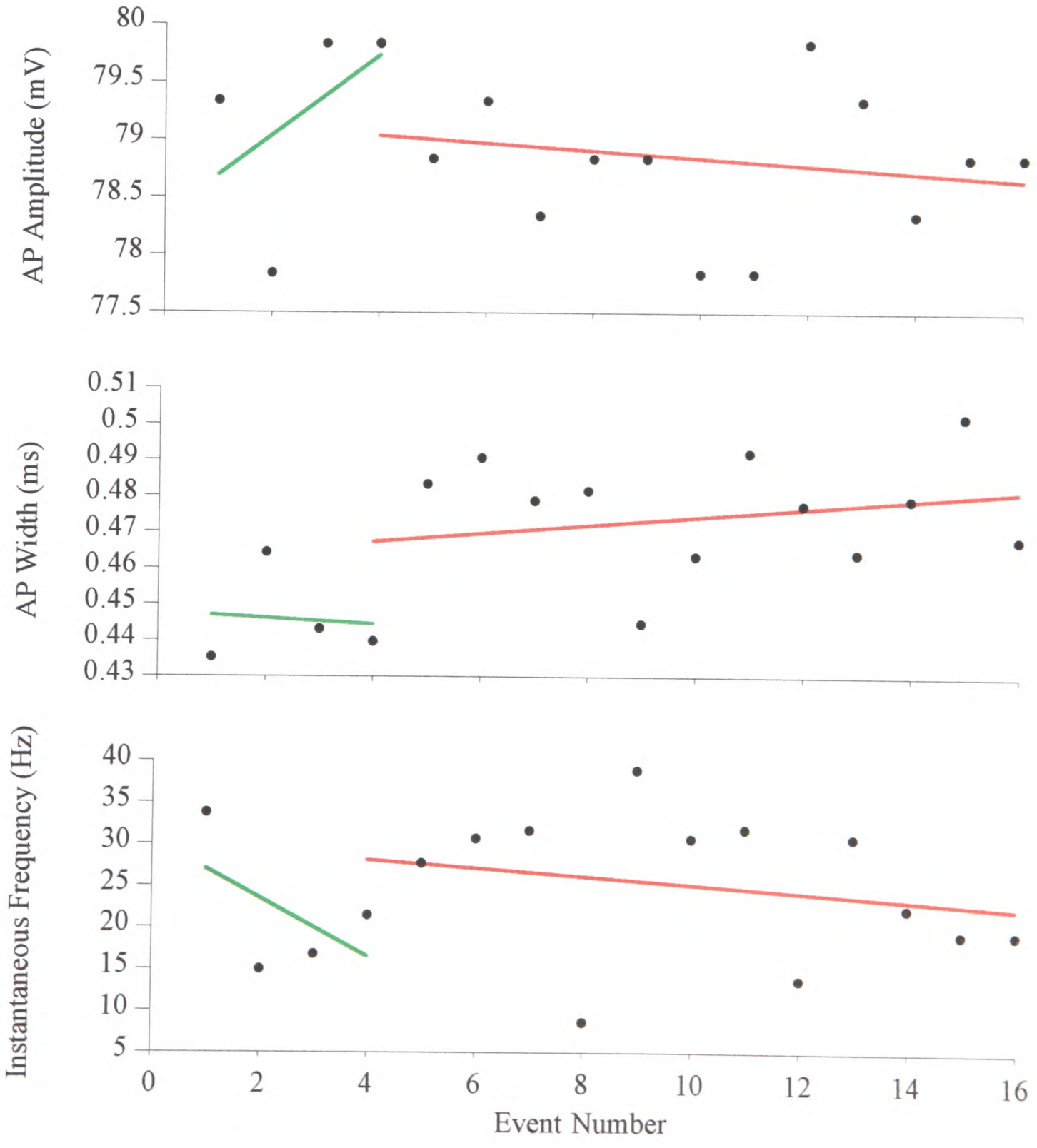
AP Amplitude (mV)
80
79.5
79
78.5
78
77.5
AP Width (ms)
0.51
0.5
0.49
0.48
0.47
0.46
0.45
0.44
0.43
Instantaneous Frequency (Hz)
40
35
30
25
20
15
10
5
0
2
4
6
8
10
12
14
16
Event Number

Fig 36

Figure 3.7 Physiological characteristics of a typical O-Bi cell (M1011) recorded at a V_{rmp} of –65 mV in the stratum oriens of the CA1 area of the hippocampus in vitro. **(A)** A train of APs at an average firing frequency of 19 Hz was elicited by a current injection of 0.15 nA for 800 ms. The seventh AP separates the early and late firing of APs because it occurred closest to the time (200 ms) when changes could be readily observed for most cells studied. The voltage 'sag', although quite small, was inevitably influenced by the synaptic activity present during a hyperpolarising response of-90 mV elicited by current injection of –0.15 nA for 800 ms. This was followed by a large rebound depolarisation at threshold to elicit an AP. **(B)** A single AP after subtraction of a subthreshold response elicited by a current pulse of 5 ms duration. The single AP and AHP parameters were referenced from AP threshold. In this case, the AP amplitude (78.32 mV) was smaller than the rest of the O-Bi cells. The AHP width (99.69 ms) and AHP time to peak (21.59 ms) were quite large in comparison to other O-LM or O-Bi cells. However, data on single AHP parameters exist for only this cell as subthreshold responses were not recorded in other cells to subtract the decay phase of the subthreshold response affecting the AHP amplitude and kinetics. **(C)** Linear fit analysis of AP amplitudes, AP widths and AP accommodation as a function of event number including the early (green) and late (red) components of the train of APs in (A). The AP amplitude and width at half amplitude were referenced from V_{rmp}. This cell had a much larger early accommodation compared to the late part of the response. The AP amplitude also decreased more in the early part of the response compared to the late part of the response. The AP width increased more in the early part of the response than in the late. Typically, most O-Bi cells without intermittent firing of APs or prominent AHPs had larger changes occurring for the early part of the response in all categories analysed. Note that a small y-axis range can account for linear fits to appear steeper. Scale: 20 mV applies to both (A) and (B).

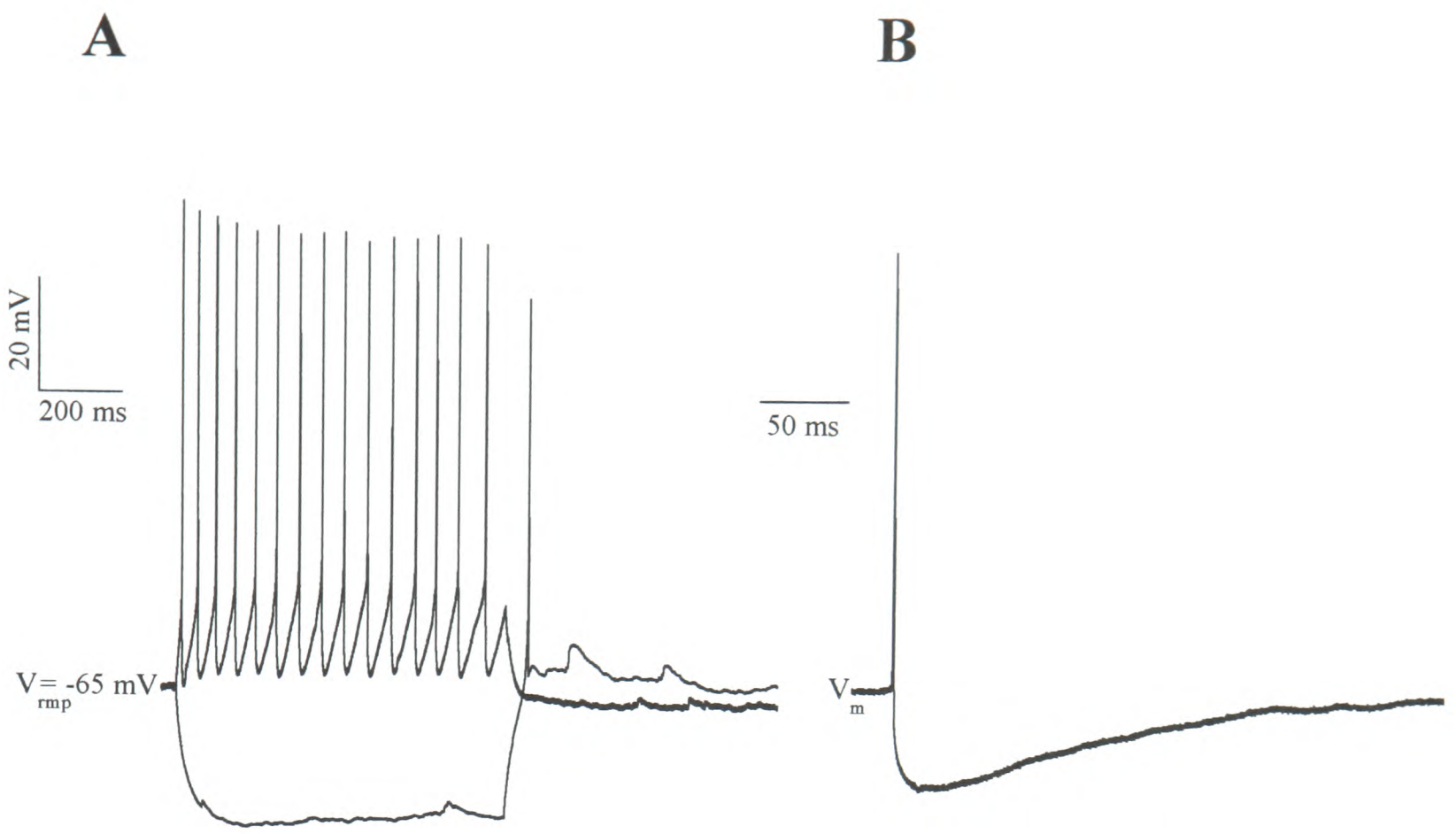
A
B
20 mV
200 ms
50 ms
V= -65 mV
rmp
V
m

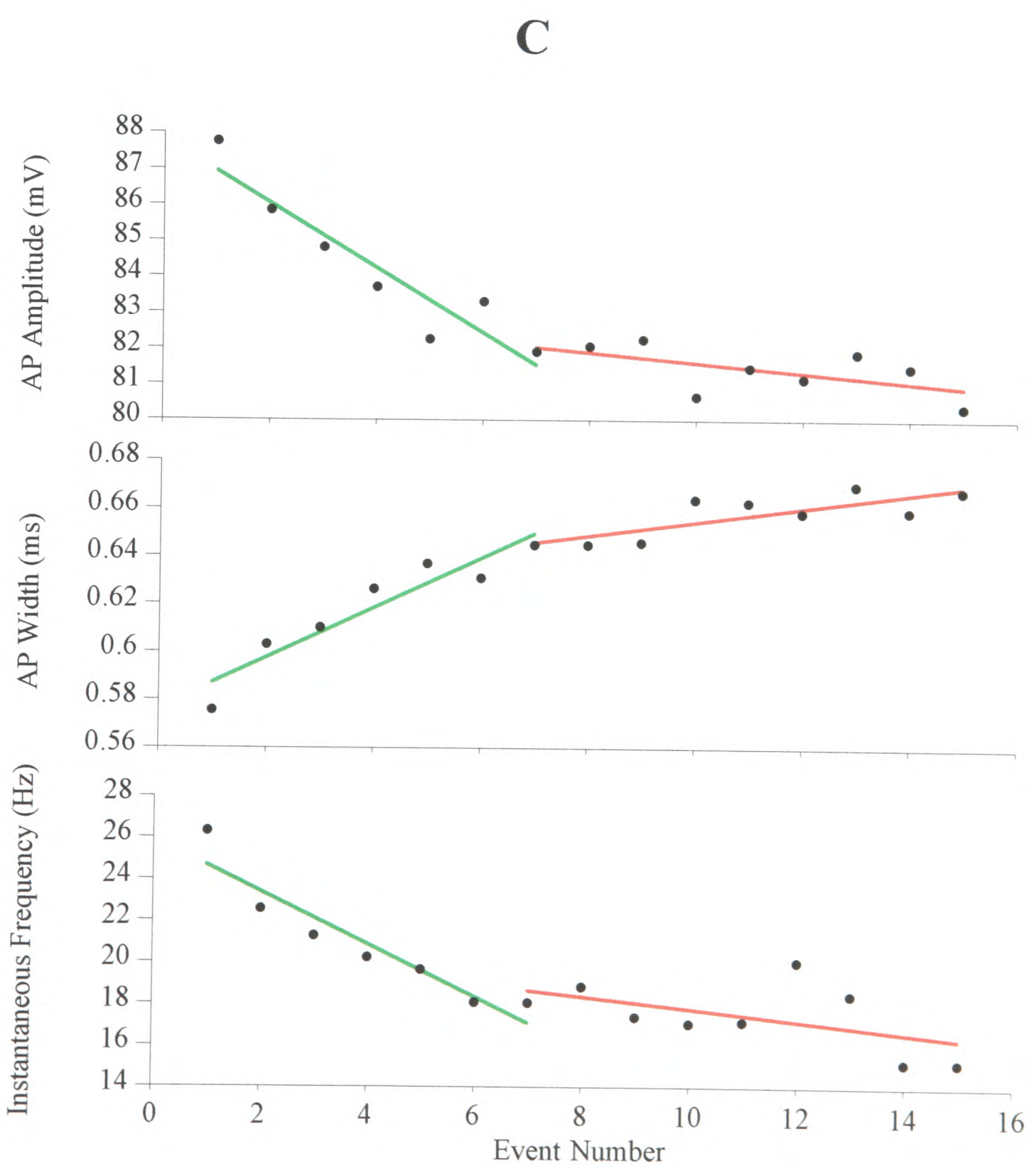
C
AP Amplitude (mV)
88
87
86
85
84
83
82
81
80
AP Width (ms)
0.68
0.66
0.64
0.62
0.6
0.58
0.56
Instantaneous Frequency (Hz)
28
26
24
22
20
18
16
14
0
2
4
6
8
10
12
14
16
Event Number

Fig 3.7

3.3.1.3 Statistical Comparisons of O-LM and O-Bi Cells

There were three statistically significant physiological differences between O-LM cells and O-Bi cells obtained from the compressed data in Table 3.3. It should be noted that significant differences are presented for data excluding outliers on the basis that two or more measured parameters of a cell were substantially different from the mean. As one aim of this study was to group cells based on their similar intrinsic properties, the uncertainty of including either potentially different cells or cells affected by the in vitro procedures was reduced by excluding outliers. However, the inclusion of outliers does not alter the significant differences. The early accommodation of O-LM cells (8.68 ± 14.94 %; n=11/11) was significantly less (P<0.05; Figure 3.8) than that of O-Bi cells (24.07 ± 11.24 %; n=7/8). In contrast, the late accommodation of O-LM cells (25.23 ± 8.57 %; n=11/11) was significantly greater (P=<0.01; Figure 3.8) than that of O-Bi cells (6.22 ± 3.27 %; n=4/7). The larger early increase in AP width in O-Bi cells was not correlated (r=0.15; P=0.78) with the large early accommodation observed in these cells (Figure 3.8). The voltage 'sag' quantified as the rectification ratio was also significantly greater (P<0.01; Figure 3.8) in O-LM cells (1.47 ± 0.22; n=11/11) than in O-Bi cells (1.18 ± 0.15; n=7/7). The rebound depolarisation amplitudes in O-LM (6.58 ± 4.16 mV; n=11/11) and O-Bi (6.15 ± 5.59 mV; n=6/6) cells were not significantly different (P=0.62; Figure 3.8) indicating that the presumed hyperpolarisation-activated cationic current (I_h) underlying the voltage 'sag' (Maccaferri and McBain 1996) is not the only current driving the rebound depolarisation in O-Bi cells. Moreover, the rebound depolarisation was not significantly correlated with the rectification in O-Bi cells (r=0.15; P=0.78; Figure 3.8). In the case of O-LM cells however, there was a significant correlation between rectification ratio and rebound depolarisation (r=0.76; P<0.01). Although there appeared to be differences in AP amplitudes and AP widths between the two cell types, these were not statistically significant.

Table 3.3 Intrinsic properties significantly differing between O-LM and O-Bi cells **excluding outliers** *(see note below)* .

Experiment	Cell Type	Age(P)	V_m	Avg Hz	early accommodation	late accommodation	rectification ratio	rebound peak(mV)
M0121	O-LM	15	-57	25	-0.0508	0.2102	1.24	2.10
M0131	O-LM	15	-62	22.5	0.2942	0.2634	1.84	9.63
M0311	O-LM	17	-63	18.75	-0.0480	0.4476	1.41	4.53
M0321	O-LM	17	-63	23.75	-0.0416	0.3305	1.71	13.13
M0521	O-LM	16	-65	20.83	-0.0802	0.1962	1.62	5.88
M0611	O-LM	19	-64	18.75	0.3588	0.1981	1.18	3.51
M1221	O-LM	19	-64	21.25	0.2005	0.2725	1.22	2.32
M1231	O-LM	19	-67	24.58	0.1115	0.1724	1.31	3.43
M1621	O-LM	24	-58	22.67	0.1404	0.1928	1.57	6.93
M1711	O-LM	15	-62	22.66	-0.0039	0.1723	1.54	14.22
M1821	O-LM	15	-61	22.33	0.0735	0.3193	1.55	6.68
MEAN		**17.4**	**-62.32**	**22.10**	**8.68%**	**25.23%**	**1.47**	**6.58**
SD		**2.8**	**2.83**	**2.07**	**14.94%**	**8.57%**	**0.22**	**4.16**
n		**11**	**11**	**11**	**11**	**11**	**11**	**11**
M0111	O-Bi	15	-60	20	0.3900		1.08	1.28
M0411	O-Bi	14	-60	20	0.0480	0.0688	1.14	4.02
M1011	O-Bi	16	-65	19.17	0.2051	0.0995	1.13	6.34
M1431	O-Bi	17	-60	24	0.3370		1.04	
M1511	O-Bi	16	-52	22				
n4621	O-Bi	14	-60	22.5	0.2180		1.49	6.28
n4921	O-Bi	14	-60	22.5	0.2951	0.0202	1.18	2.24
n5341	O-Bi	13	-60	26.25	0.1914	0.0604	1.21	16.76
MEAN		**14.9**	**-59.63**	**22.05**	**24.07%**	**6.22%**	**1.18**	**6.15**
SD		**1.4**	**3.54**	**2.35**	**11.24%**	**3.27%**	**0.15**	**5.59**
n		**8**	**8**	**8**	**7**	**4**	**7**	**6**

P = postnatal days
V_m = resting or holding membrane potential
Avg Hz = average firing frequency of the AP train
AP train parameters obtained from V_m
(-%) = increasing
Note: significant differences were obtained with or without outliers

Figure 3.8 Statistical comparisons between O-LM and O-Bi cells. (**A-C**) Box plots displaying the 10th, 25th, 50th, 75th and 90th percentiles of early accommodation, late accommodation and rectification ratio for O-LM and O-Bi cells. Most O-Bi cells showed more significant early accommodation (**A**) whereas most O-LM cells showed more late accommodation than O-Bi cells (**A**). Statistical significance was tested using the Mann-Whitney *U* test for unpaired variables with a nonparametric distribution. Significant differences were obtained for both the early accommodation ($P<0.05$) and the late accommodation ($P<0.01$). (**B**) Most O-LM cells showed a larger rectification ratio compared to O-Bi cells ($P<0.01$). (**C-E**) A linear regression was performed between independent and dependent variables including 95 % confidence intervals for the mean and slope. (**C**) The larger early accommodation of the O-Bi cells did not depend on their large early increase in AP width ($r=0.15$ $P=0.77$). This is represented by the many points that fall outside of the 95 % confidence interval bounds for either the increasing or decreasing slope of the data. None of the points could be excluded because they were between the bounds of the means of both variables. (**D**) In O-LM cells, the rebound depolarisation appeared to be dependent upon their larger rectification ($r=0.76$ $P<0.01$). The two outliers were not excluded as this did not significantly alter the y-intercept value and statistical significance was achieved with their inclusion (**E**) In O-Bi cells however, the rebound depolarisation was not dependent upon their amount of rectification ($r=0.22$ $P=0.67$). This is also evident by the data falling outside the 95 % confidence intervals.

A

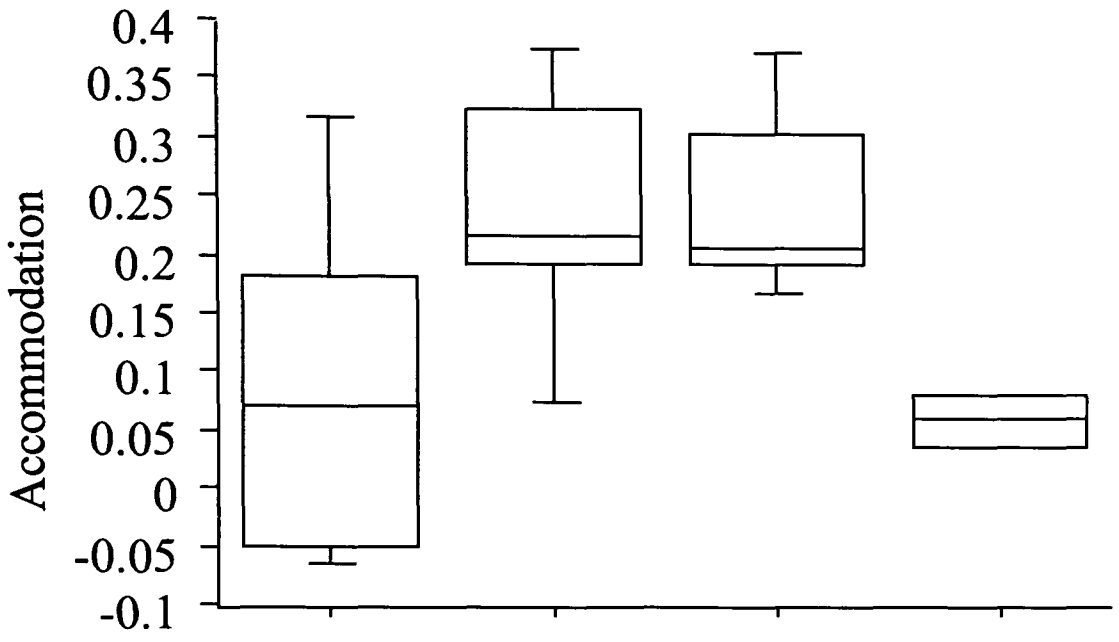

B

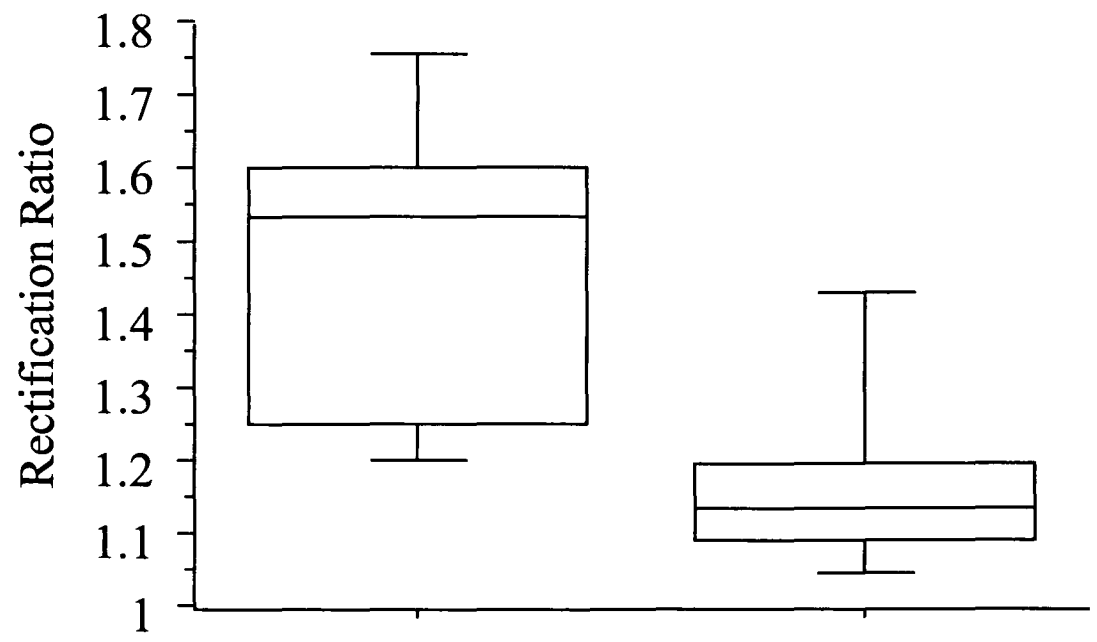

C

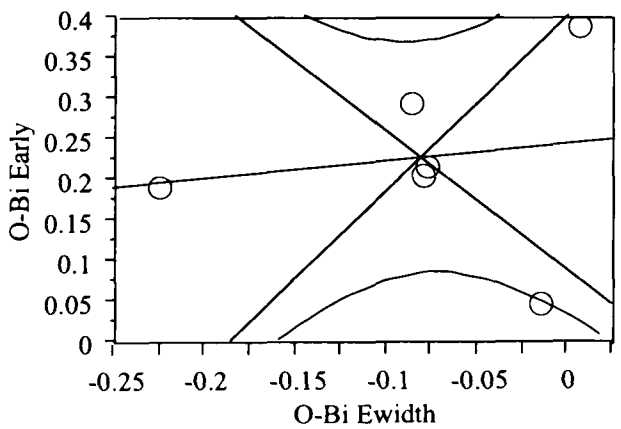

O-Bi Early = 0.242 + 0.216 * O-Bi Ewidth; R^2 = 0.024

D

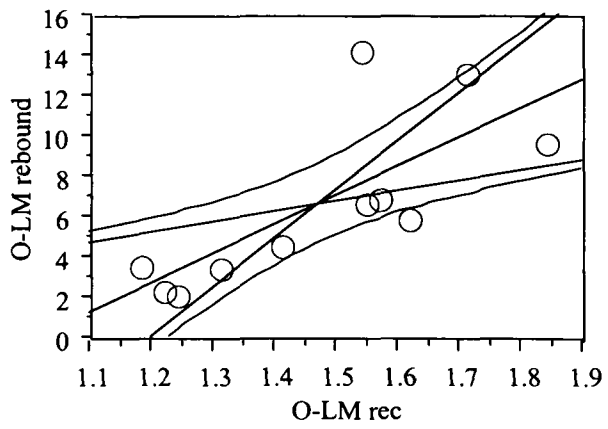

O-LM rebound = -14.811 + 14.532 * O-LM rec; R^2 = .57

E

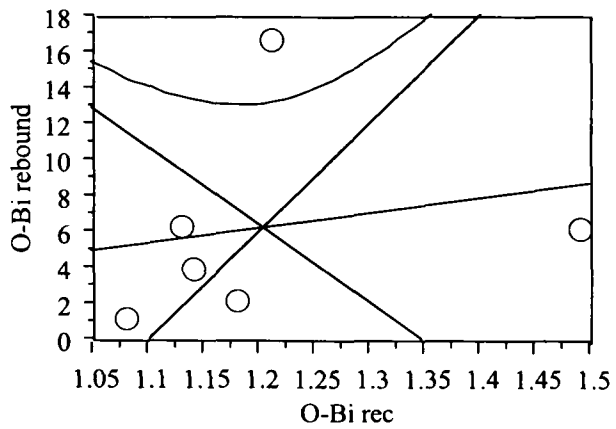

O-Bi rebound = -4.183 + 8.578 * O-Bi rec; R^2 = .051

3.3.2 Anatomical Classification

As new physiological findings on nonpyramidal cells emerge, it is necessary to have more stringent criteria for anatomical classification. Apart from somatodendritic orientation, axonal projections and distribution of boutons which can all be observed in the light microscope, immunohistochemical techniques can be used in combination to determine the expression of receptor (sub)types, neuropeptides, calcium-binding proteins and other molecules in cells filled with a tracer. Nevertheless, variables in the slice preparation can affect physiological responses and also anatomical identification from one experiment to the next if robust measures are not used for analysis. Therefore, the following anatomical descriptions of O-LM and O-Bi cells are based on the minimum criterion of sufficient dendritic and axonal arborisations present in the slice to allow for broad groupings of orientation and direction. Also, during immunohistochemistry, attempts were made to minimise false negatives resulting from the length of the recording or effectiveness of the primary antibody in the recorded slice.

3.3.2.1 Anatomical Heterogeneity of O-LM and O-Bi Nonpyramidal Cells

Several criteria were used to describe the cellular characteristics of O-LM (n=11) and O-Bi (n=8) cells in the CA1 area of the hippocampus. Previously, it has been shown that O-LM (McBain et al. 1994; Sik et al. 1995) and O-Bi cells (Maccaferri et al. 2000) have their soma and dendrites confined to stratum oriens and alveus with dendrites oriented tangential to the CA1 pyramidal layer and have been distinguished on the basis of their axonal projections. Oriens lacunosum-moleculare cells are characterised by a main axon forming few collaterals in stratum oriens (SO) and mainly projecting, sometimes after several bifurcations, to stratum lacunosum-moleculare (SL-M) where it forms dense collaterals containing many boutons (Figure 3.9). Oriens bistratified cells have many axon collaterals with boutons in both SO and stratum radiatum (SR) with only a sparse amount of axon crossing stratum pyramidale (SP) and few if

any found in SL-M (Figure 3.10). Hence, O-LM (Sik et al. 1995) and O-Bi cells (Maccaferri et al. 2000) were so named based on their somatodendritic orientation and axonal projections. However, there exist several differences within and across the two cell groups when features for classification were analysed in the present study. The presence or absence of several anatomical categories were examined for the in vitro recorded cells: i) tangential dendrites (parallel to SP in the CA1 area) ii) radial dendrites (extending through SP in the CA1 area) iii) beaded dendrites iv) spiny dendrites v) round or fusiform perikarya vi) axonal origin, projection and direction referenced from the placement of the soma.

Anatomical characteristics of recorded O-LM cells were similar to those described previously in addition to novel observations (Table 3.4). From the eleven O-LM cells recorded, nine had tangential dendrites and two had in addition, one dendrite remaining in SO but perpendicular to SP. Along with all cells having smooth dendrites, three were medium spiny, three were beaded and the other five exhibited all dendritic characteristics. Nine cells had a fusiform soma and two had a round soma. Five out of 11 cells had axons originating from or near the soma whereas five other cells had axons originating from a proximal dendrite. In one cell, the origin of the axon could not be determined due to loss of the soma after histological processing. One (M0131) out of the five cells with axons originating from a proximal dendrite had two main axons (Figure 3.9). These two axons projected in different directions. The first axon projected below the soma towards SL-M where it ramified. The second axon sent a collateral through SO towards but not reaching the CA3 area and from there it projected to SL-M where it ramified and sent back a collateral tangential to the somatodendritic position (Figure 3.9). Interestingly, this cell was one of the three cells to show a large early accommodation of firing rate (Figure 3.9) in comparison to the majority of cells which had minimal early accommodation. A second cell (M0611) out of the three showing early accommodation had an axon projecting to SL-M where it continued tangentially to the sharp border between the CA1

and CA3 area. The third cell (M1221) showing early accommodation had an axon projecting along the stratum oriens/alveus border towards but not reaching the CA3 area and traversed diagonally back towards SL-M where it ramified tangential to the somatodendritic position. However, the axonal direction towards the CA3 area cannot be taken as a marker for the physiological findings observed since two cells (M0521 and M1821) with typical firing patterns, as those of the majority of O-LM cells sampled, had similar axonal projections. The first cell (M0521) with typical firing patterns had an axon branch projecting to SL-M where it ramified below the somatodendritic position and another branch in SO projecting towards but not reaching the CA3 area and then reaching SL-M where it ramified. The second cell (M1821) with typical firing patterns had an axonal projection to SL-M where it ramified below the somatodendritic position as well as an axon collateral traversing diagonally through SR towards but not reaching the CA3 area. One cell (M0121) was unlike all of the analysed cells in that it had an axon projecting towards but not reaching the subiculum and traversing back diagonally towards SL-M where it ramified tangential to the somatodendritic position. The direction of the axon towards the subiculum is not surprising as some axons have been shown to enter the subiculum from an O-LM cell recorded in vivo (Sik et al. 1995). The other five cells remaining of the eleven recorded had an axonal projection to SL-M where it ramified tangential to the somatodendritic position. In contrast to previous findings (McBain et al. 1994), none of the cells had collaterals originating in SR which projected back to SO, although this may have depended on the tissue sectioning.

Figure 3.9 Reconstruction of a somatostatin and mGluR1α-immunopositive O-LM cell recorded in vitro (M0131; see also Figure 3.11 for immunoreactivity). The soma and dendrites (red) are located in SO of the CA1 area of the hippocampus. Two main axons (arrows) branch from a proximal dendrite. One axon projects towards but not reaching the CA3 area and reaches SL-M where it arborises tangential to the somatodendritic position. The other axon as typically seen in most O-LM cells projects straight to SL-M where it produces dense collaterals tangential to the somatodendritic position. Inset is the firing pattern and voltage 'sag' of the cell, which is typical of O-LM cells with the exception of the prominent early accommodation observed for this cell as compared to others.

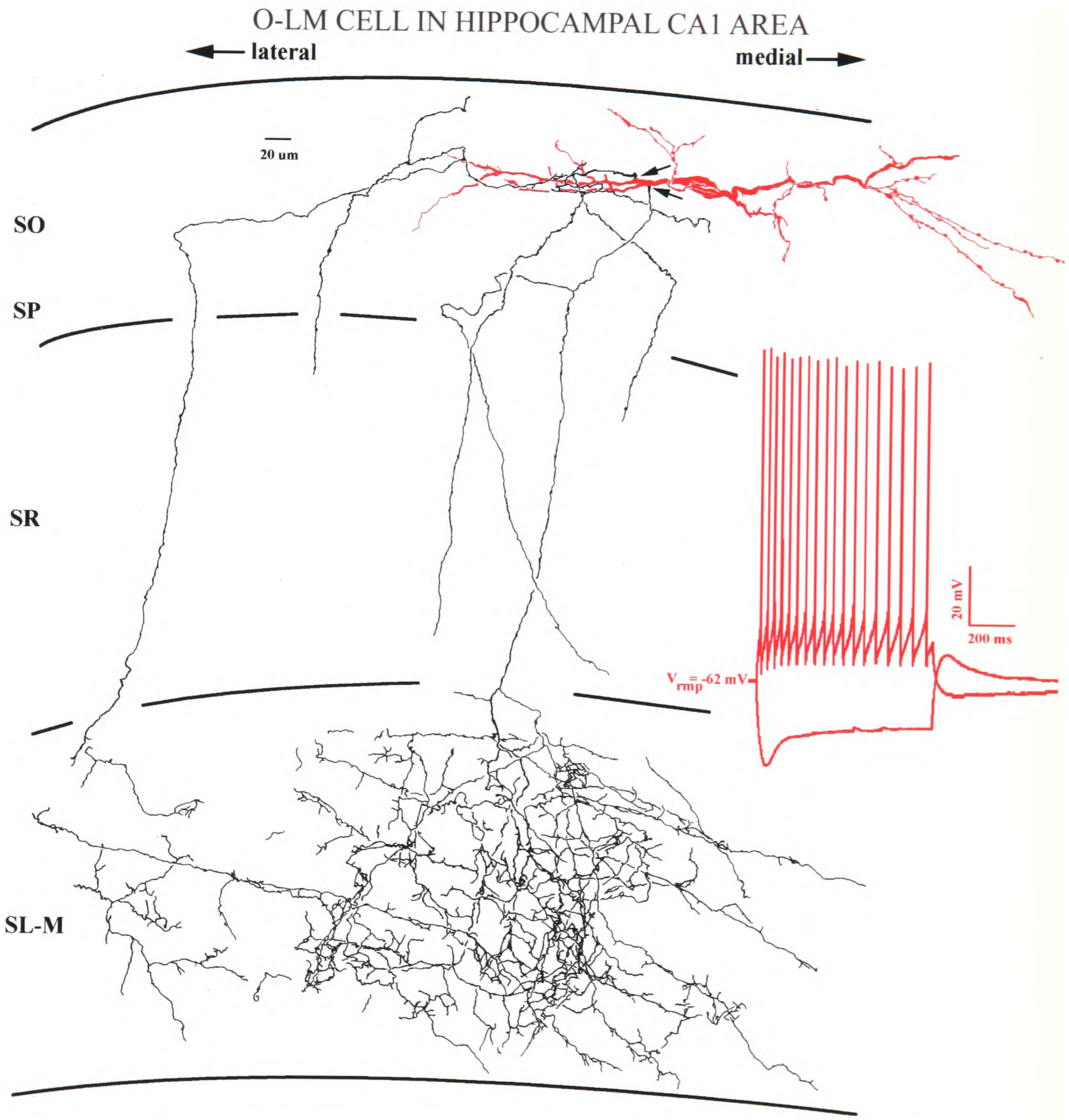
O-LM CELL IN HIPPOCAMPAL CA1 AREA
lateral
medial
20 um
SO
SP
SR
SL-M
20 mV
200 ms
V rmp =-62 mV

Fig 3.4

All eight O-Bi cells analysed had similar anatomical characteristics as previously described and, as in O-LM cells, additional features were uncovered (Table 3.4). Along with smooth dendrites, two cells had one beaded radial dendrite extending into mid SR (M0111) or SL-M (M0411). Both of these cells also had round perikarya whereas all other cells had fusiform perikarya. One of these cells (M0111) showed intermittent firing of APs and pronounced AHPs (Figure 3.6). All three cells showing the same firing pattern did not have similar anatomical characteristics. However, this was anticipated as the intrinsic properties analysed in the present study did not correlate between the three cells either. Considering all cells analysed, only two (M1011 and n4921) had a few spines and large perikarya as well as axon collaterals that were widespread as opposed to forming a dense plexus. One of these cells (M1011) had two axon collaterals in SR and at the border with SL-M, which projected tangentially towards but did not reach the CA3 area (Figure 3.10). In addition, it had an axon collateral in SO almost reaching the subiculum border (Figure 3.10). The other cell (n4921) had a collateral in SO that projected towards but did not reach the CA3 region and a long collateral along the stratum oriens/alveus border. Both cells had several radial axon collaterals entering SR where they divided further. Three other cells (M0111, n4621 and n5341) had axon collaterals projecting towards but not reaching the CA3 area in both SR and SO. Two other cells (M0411 and M1431) had axon collaterals projecting towards but not reaching the subiculum and one cell (M1511) had only previously described features of O-Bi cells such as dense collaterals in SR and SO surrounding the position of its soma. The main axon originated either from the soma (n=5/8) or proximal dendrite (n=2/8) and for one cell (M1431) the origin could not be established due to biocytin spill over.

Table 3.4 Anatomical characteristics of O-LM and O-Bi cells recorded in the hippocampus. The direction of axonal projections (not innervation) are represented using arrows.

Experiment	Cell Type	Soma	Dendrites	Axon Origin	Axon
M0121	O-LM	F	T;S	dendrite	SO → sub SL-M ↻
M0131*	O-LM	F	T;B;S	dendrite	SO → CA3 → SL-M
M0521	O-LM	F	T;B;S	soma	SO → CA3 → SL-M SO → SL-M
M0611	O-LM	F	T;B	soma	SO → SL-M SL-M → CA3
M1821	O-LM	F	T;B;S	dendrite	SO → SL-M SR → CA3
M1221	O-LM	F	T;B	soma	A → CA3 SL-M ↻
M0311	O-LM	N/A	P;T;B;S	N/A	SO → SL-M
M0321	O-LM	R	P;T;B;S	soma	SO → SL-M
M1231	O-LM	R	T;B	soma	SO → SL-M
M1621	O-LM	F	T;S	dendrite	SO → SL-M
M1711	O-LM	F	T;S	dendrite	SO → SL-M
M0111	O-Bi	R	R;T;B	dendrite	SO & SR SO → CA3 SR → CA3
M0411	O-Bi	R	R;T;B	soma	SO & SR SR → sub
M1431	O-Bi	F	T;B	N/A	SO & SR SR → sub
M1511	O-Bi	F	T;B	soma	SO & SR
n5341	O-Bi	F	T;B	soma	SO & SR SR → CA3
n4621	O-Bi	F	T	soma	SO & SR SO → CA3
n4921	O-Bi	F;large	T	soma	SO & SR SO → CA3
M1011	O-Bi	F;large	T;B;S	dendrite	SO & SR SO → sub SR → CA3

*Axon 2 O → SL-M

F = fusiform

R = radial dendrites or round soma

T = tangential to pyramidal layer

P = perpendicular to pyramidal layer

S = some spiny dendrites

B = some beaded dendrites

A = alveus

SO = stratum oriens

SL-M = stratum lacunosum-moleculare

SR = stratum radiatum

sub = subiculum

N/A = not available

→ forward direction

↻ tangential to the somatodendritic region

Figure 3.10 Reconstruction of a somatostatin-immunopositive O-Bi cell (M1011; see also Figure 3.12 for immunoreactivity) with intrinsic properties represented in Figure 3.7. The soma (red) is near the alveus. The axon (black) originates from one proximal dendrite and branches into two directions. One branch remains in SO and projects close to the subiculum border. In addition to projecting around its own dendrites another branch traverses through SR where it gives off widespread collaterals, mostly in the direction of the CA3 area and another more distal axon branch follows this same pattern.

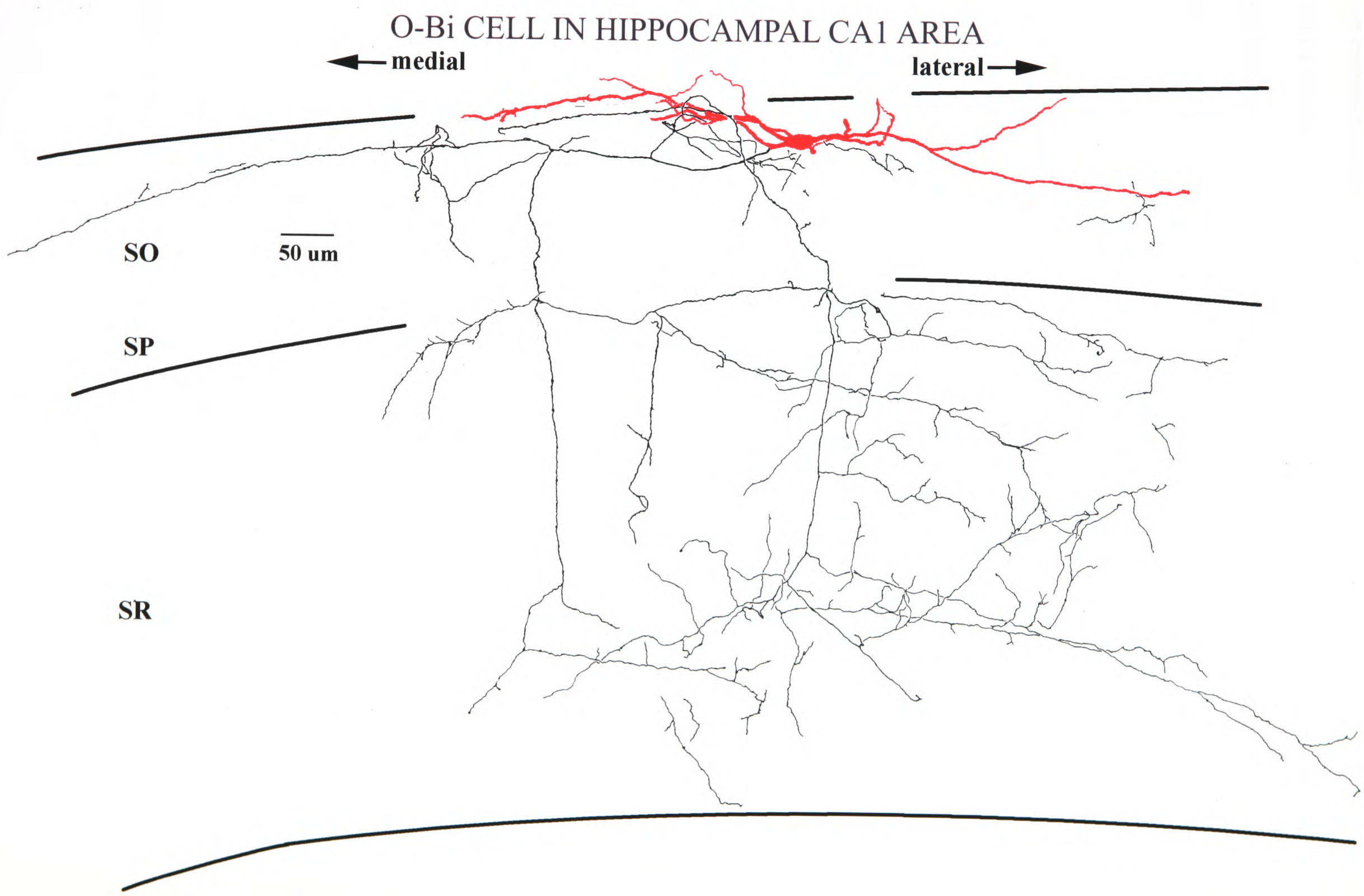
O-Bi CELL IN HIPPOCAMPAL CA1 AREA
medial
lateral
SO
50 um
SP
SR
SL-M

Fig 3.10

In summary, most O-LM and O-Bi cells had axon collaterals projecting in the direction of the CA3 area but remaining in the CA1 area. Spiny dendrites were more common for O-LM cells than for O-Bi cells. Interestingly, the only two O-Bi cells which had spiny dendrites, albeit few, had a large somatodendritic domain as well as more radial axon branches traversing SR forming disperse collaterals with some reaching the SL-M border. These cells do not appear to have common characteristics with O-LM cells based on the physiological parameters analysed or the majority of O-Bi based on anatomy. In addition, although loss of collaterals from sectioning cannot be ruled out, the unique soma and dendrites compared to all other O-Bi cells would suggest that the anatomical features are representative of a separate population of cells, albeit with similar intrinsic membrane properties to O-Bi cells.

3.3.3 Somatostatin and mGluR1α Immunoreactivity of O-LM and O-Bi Nonpyramidal Cells

Previous studies have shown in the hippocampus that most somatostatin expressing cells are found in SO/alveus and the hilus and that the majority of these cells also express mGluR1α (Baude et al. 1993). However, there is no direct evidence as to which cell types, as defined by axonal patterns, are mGluR1α-immunopositive although there is direct evidence showing that O-LM and O-Bi cells express somatostatin (Maccaferri et al. 2000). In order to resolve whether either or both O-LM and O-Bi somatostatin expressing cells also express mGluR1α, somatostatin and mGluR1α immunohistochemistry was performed on recorded cells. To my knowledge this is the first time that a receptor has been detected from recorded cells using immunohistochemistry. Although one study (van Hooft et al. 2000) employed single-cell reverse transcription-PCR, I used direct detection of receptor protein expression through antibodies conjugated to fluorophores. The presence of mGluR1α on these cell types could

potentially result in their similar activation, although information processing would be differentially affected based on their different axonal projections. Eight out of the eleven O-LM cells recorded were immunopositive for somatostatin, one was not reacted for somatostatin and two were not tested, because although the reaction worked well in the control section, no immunofluorescent labelling was detected in the recorded slice. Seven O-LM cells were immunopositive and one was immunonegative for mGluR1α, one cell was not reacted for mGluR1α and two could not be tested due to the failure of the reaction in the slice. Six O-LM cells were both positive for somatostatin and mGluR1α (Figure 3.11).

In the case of the O-Bi cells, only positive results are acceptable as some of the cells were recorded for a long period of time possibly resulting in lower immunoreactivity. To this end, out of the eight O-Bi cells recorded and tested, three were positive for somatostatin and all others showed inconclusive immunoreactivity for somatostatin. Cells with (M0111) or without (M1011 and n5341) intermittent firing patterns were found to be somatostatin positive (Figure 3.12). Only four cells could be tested for mGluR1α and they were all immunonegative. Immunoreactivity for mGluR1α was absent in the remaining four sections containing the recorded O-Bi cells. In comparison to O-LM cells, the lack of immunoreactivity of mGluR1α observed for O-Bi cells did not correlate with the recording time or amount of time of slice incubation in ACSF or fixative solution. Therefore, other parameters have to be considered which might fluctuate between experiments. For instance, changes in the room temperature where the slices were kept in a holding chamber. As the recording time did not affect immunoreactivity of mGluR1α for O-LM cells, it is possible that O-Bi cells pertain to the weakly mGluR1α immunolabelled cells closer to SP. I have observed such cells, which are somatostatin-immunopositive or immunonegative and weakly immunolabelled for mGluR1α in the Ammon's horn of the hippocampus from control sections of rats perfused with fixative

(Figure 3.13). These cells would thus be more susceptible to the dialysing of intracellular contents during recordings and possibly explain the lack of immunolabelling of mGluR1α for the O-Bi cells recorded.

Figure 3.11 Fluorescence images of the O-LM cell shown in Figure 3.9. Streptavidin conjugated AMCA (blue) was used for fluorescence detection of the biocytin filled cell, which was immunopositive for both somatostatin detected by CY3 conjugated goat anti-mouse IgG (red) and mGluR1α detected by FITC conjugated to tyramide for signal amplification via HRP conjugated to swine anti-rabbit IgG (green). The bottom is a superimposed image of the AMCA labelled cell, somatostatin and mGluR1α immunofluorescence. Scale bar is 25 μm for all images.

AN O-LM CELL IDENTIFIED BY BIOCYTIN FOLLOWING RECORDING IN VITRO IS IMMUNOPOSITIVE FOR mGluR1α AND SOMATOSTATIN IN THE CA1 AREA

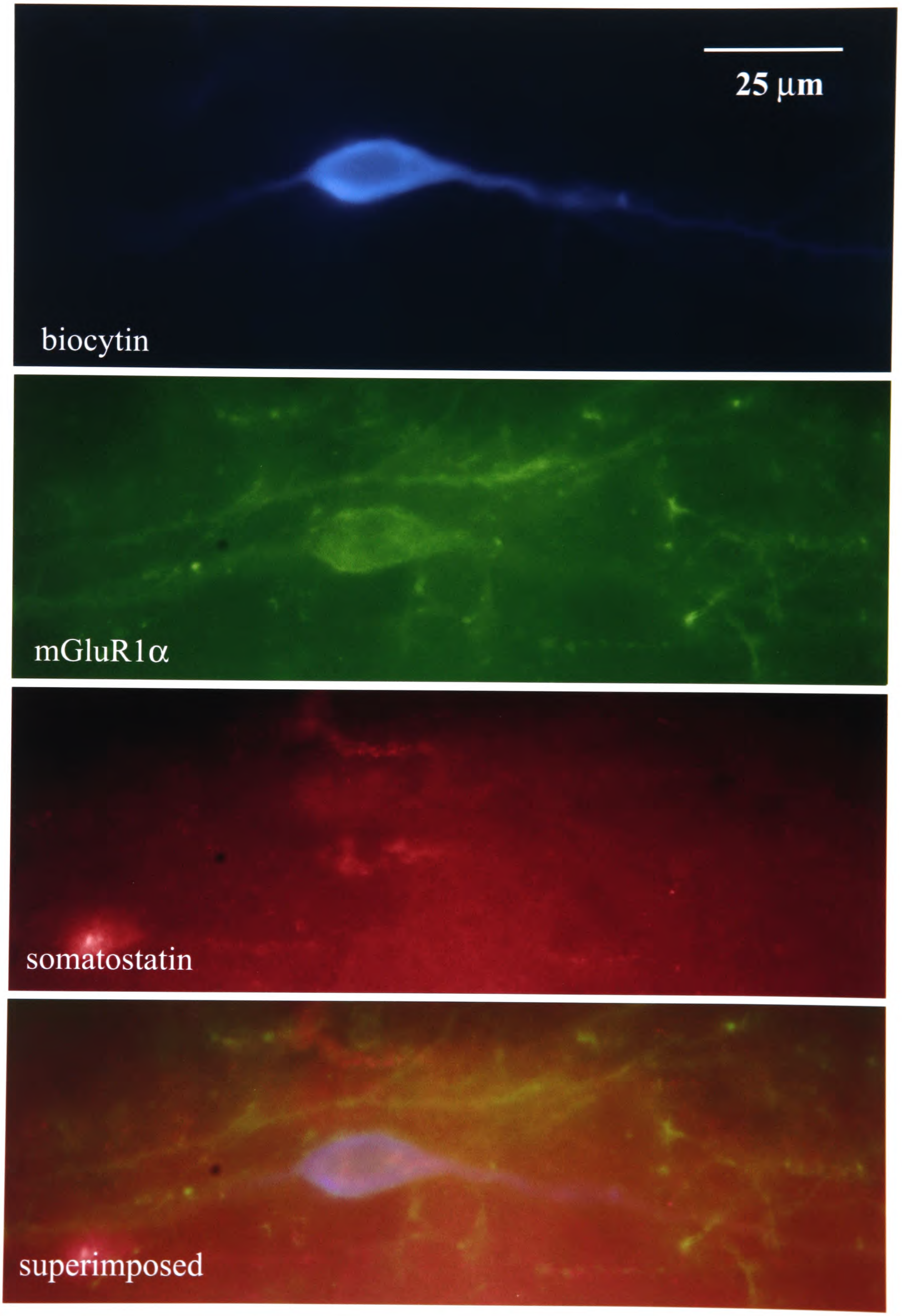

Fig 3.11

Figure 3.12 Somatostatin immunoreactivity of an O-Bi cell (M1011). Streptavidin conjugated AMCA (blue) was used for fluorescence detection of the biocytin filled O-Bi cell as shown in Figure 3.10, which was immunopositive for somatostatin detected by CY3 conjugated to goat anti-mouse CY3 (red). Scale bar is 25 μm for all images.

AN O-Bi CELL IDENTIFIED BY BIOCYTIN FOLLOWING RECORDING IN VITRO IS IMMUNOPOSITIVE FOR SOMATOSTATIN IN THE CA1 AREA

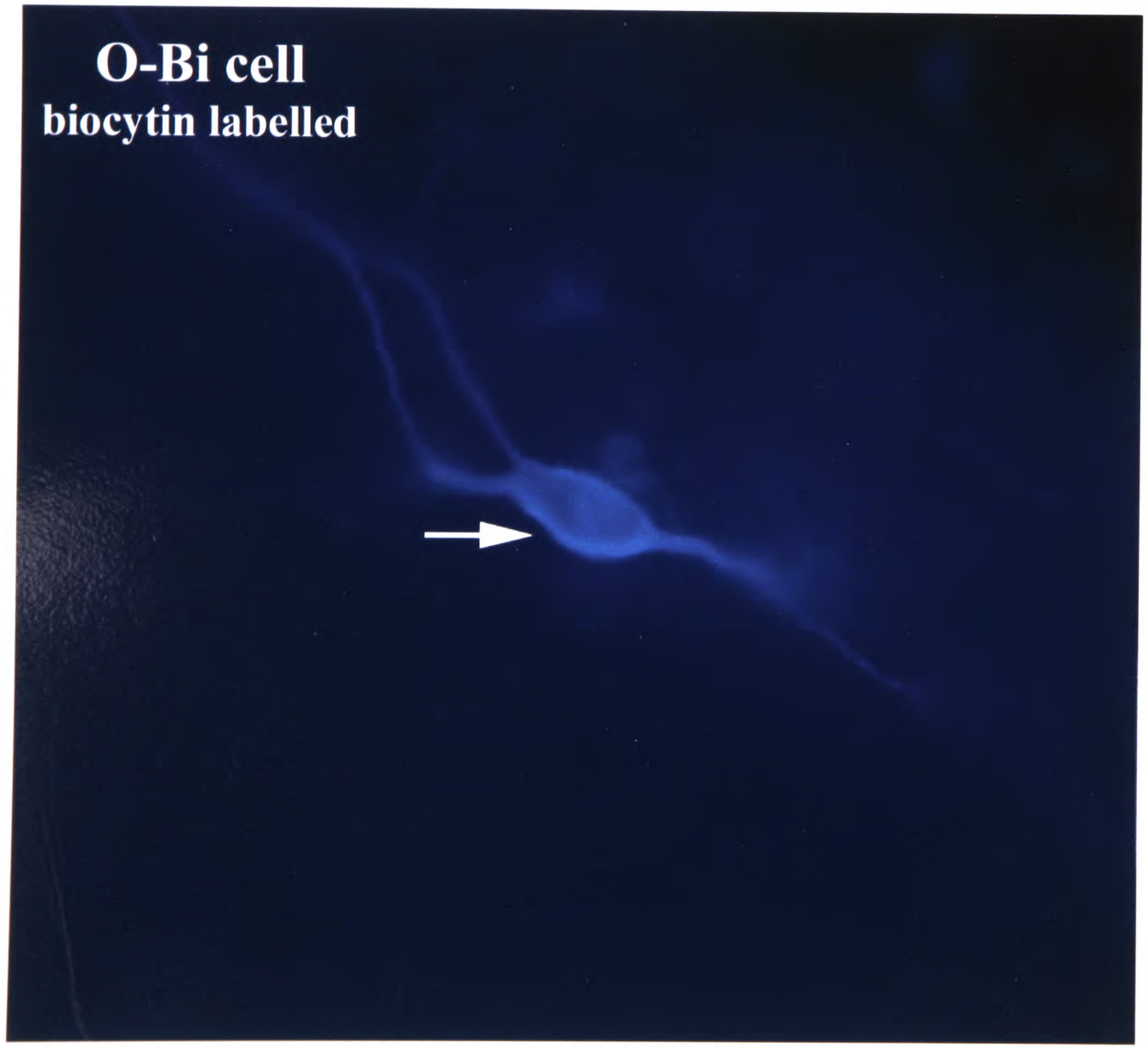

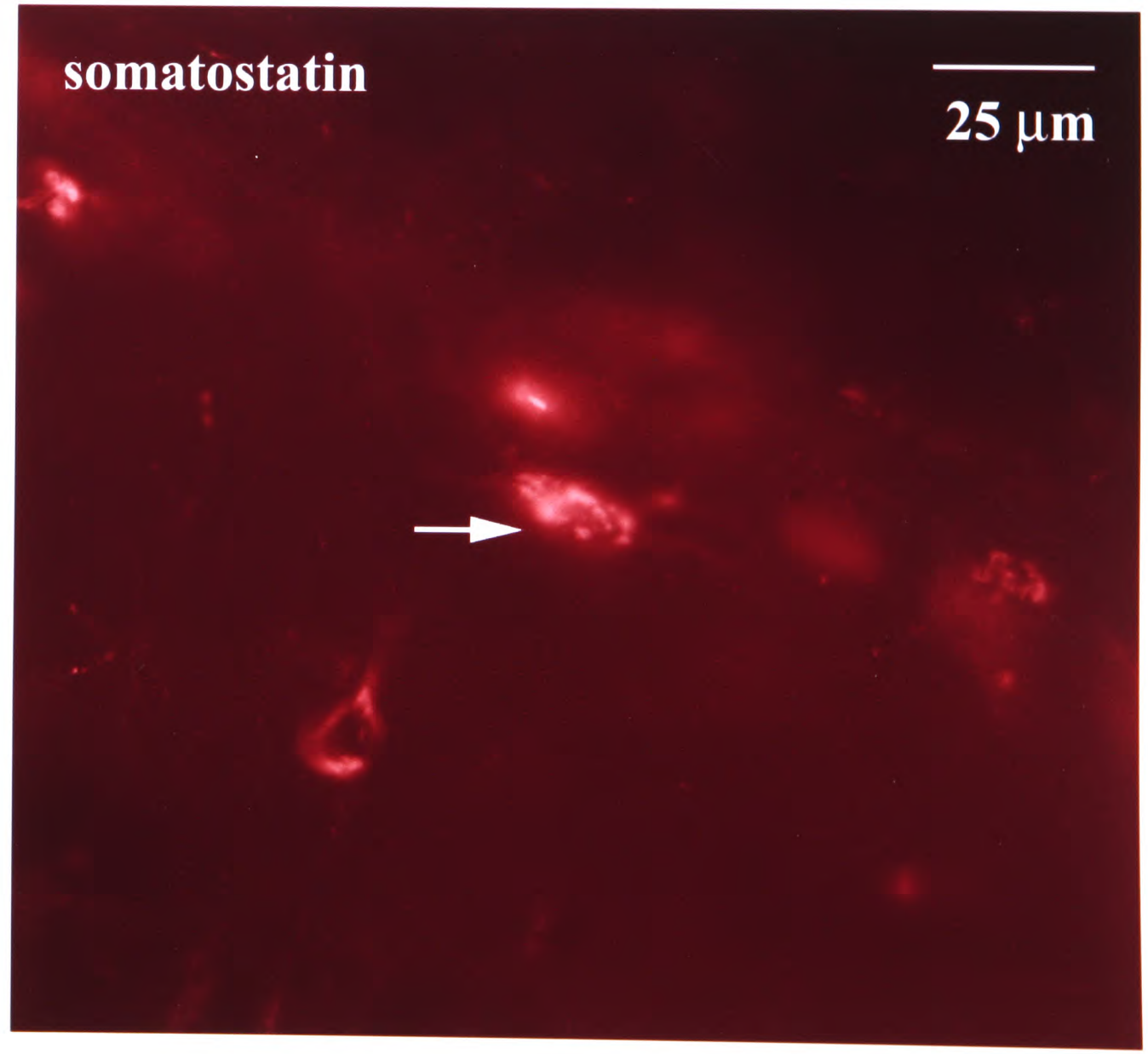

Figure 3.13 Image of somatostatin (red) and mGluR1α (green) immunoreactivity in the dorsal hippocampus taken from a control section. White arrows designate two, somatostatin-immunopositive cells weakly immunolabelled for mGluR1α in the stratum oriens/alveus and near stratum pyramidale. Red arrows designate three, somatostatin-immunopositive cells strongly immunolabelled for mGluR1α in the alveus. Scale bar is 25 μm.

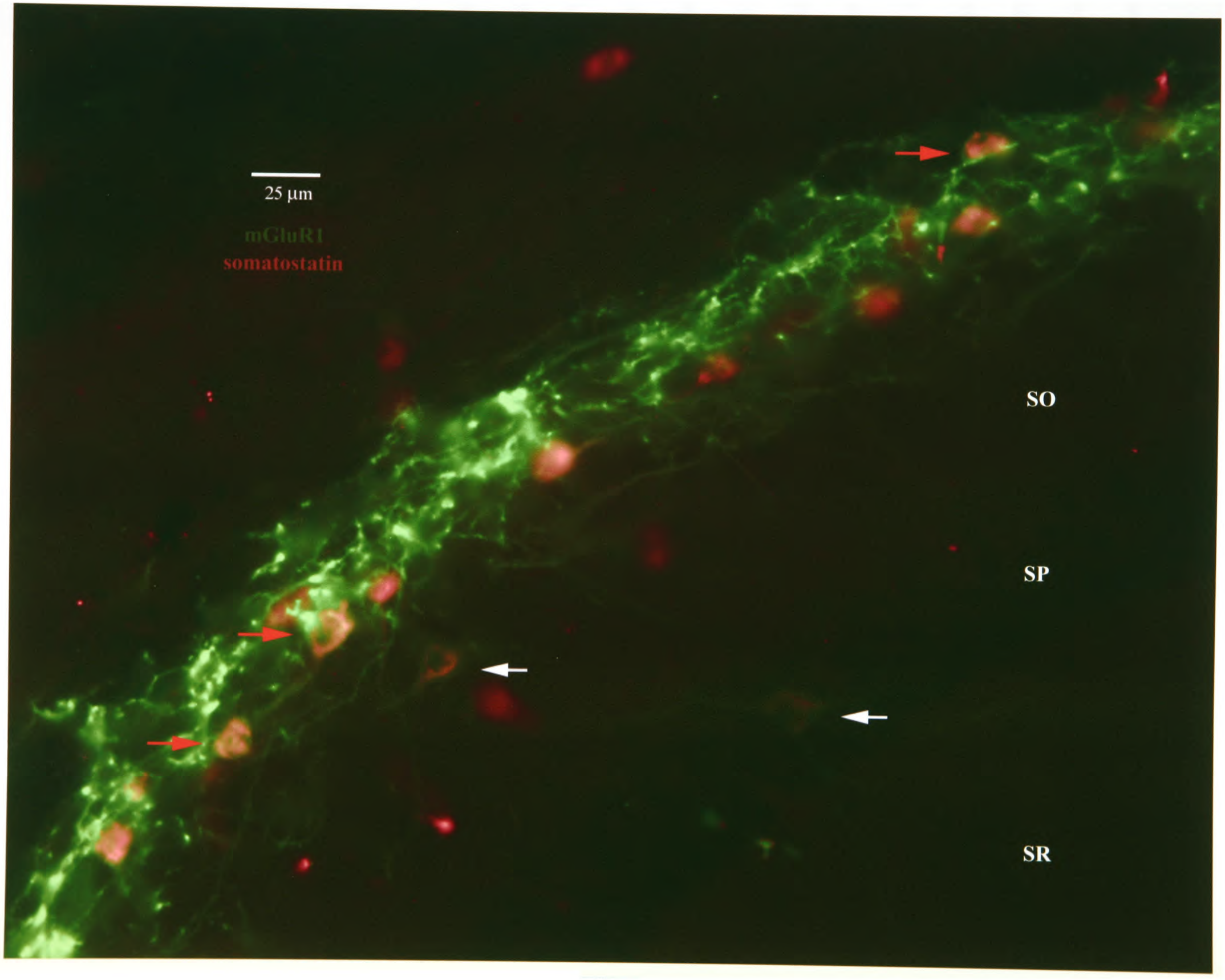
25 µm
mGluR1
somatostatin
SO
SP
SR

3.4 Discussion

3.4.1 Intrinsic Membrane Properties

Differences in accommodation of AP firing and voltage 'sag' properties were observed between two anatomically distinguished nonpyramidal cell types, namely O-LM and O-Bi cells. These differences are likely to result from distinct expression of membrane channels and not somatic size given that both cell types had similar time constants and input resistances. The possible influence of Na^+ channel inactivation on the accommodation of APs will be considered first. Inactivation of Na^+ channels could be observed through increases in absolute AP amplitude provided that this coincided with an increase in AP threshold. Large increases in absolute AP amplitude only occurred in two O-Bi cells (M0111 and n4621) but this is unlikely to reflect the accommodation of APs observed for the following reasons. Firstly, AP amplitudes barely changed during the large late accommodation of APs observed in the two cells. Secondly, most O-LM and O-Bi cells had small changes in AP amplitude during both the early and late train of APs, yet prominent differences between the early and late accommodation of their APs. Given the small changes in AP amplitude observed in most cells, it is likely that these changes resulted from errors in sampling at the AP peak rather than inactivation of Na^+ channels. Likewise, the two O-LM cells (M0131 and M1221), which showed relatively large decreases in AP amplitude, likely resulted from a sampling error because their AP thresholds did not decrease concomitantly and synaptic inhibition was not observed throughout the sustained depolarisation pulse. However, it is not possible to exclude inactivation of Na^+ channels influencing the accommodation of APs as an increase in AP threshold was observed for most cells, particularly during the late part of the train of APs. In addition, O-LM and O-Bi cells may express different densities of Na^+ channels accounting for their differences between early and late accommodation of APs, although this remains to be proven.

A large variety of potassium channels have been isolated (Storm 1990; Zhang and McBain 1995; Erisir et al. 1999) and will be considered next as possible influences of AP accommodation. Overall, both cell types displayed a larger early increase in AP width compared to the late part of the AP train but this did not correlate significantly with the early accommodation of APs observed. The fact that increases in AP width were observed would exclude the involvement of fast-activating K^+ channels, shown to decrease AP width (Storm 1990; Zhang and McBain 1995). As the increase in AP width did not correlate with the observed accommodation, then the possible K^+ channel candidates for delaying APs are those which influence the duration of the AHPs. In SO/alveus nonpyramidal cells of the CA1 hippocampal area, K^+ conductances underlying AHPs have been studied (Zhang and McBain 1995). It was shown that apamin, a selective antagonist of the low-conductance Ca^{2+}-activated K^+ channels, reduced the duration of slow AHPs in SO/alveus nonpyramidal cells (Zhang and McBain 1995). Moreover, an increase in cell excitability of SO/alveus nonpyramidal cells during a sustained depolarising pulse was observed following apamin application without an effect on the resting membrane potential (Zhang and McBain 1995). These data indicate that the K^+ conductance responsible for the I_{AHP}, participates in influencing the frequency of AP firing elicited by a sustained depolarising pulse (Zhang and McBain 1995). The fact that AP widths increased in the present study supports the existence of a slowly-activating K^+ channel as discussed above. Interestingly, when blocking K^+ channels mediating transient current (I_A) or Ca^{2+}-activated K^+ channels mediating large-conductances (I_C), an increase in AP amplitude was observed in the previous study (Zhang and McBain 1995). However, it is unlikely that the overall decreases in AP amplitudes observed in the present study resulted from I_A or I_C for the following reasons. Firstly, I_C is involved in decreasing AP width (Zhang and McBain 1995), which was not observed in the present study. Secondly, the AP width and amplitude changes observed in the present study did not correlate linearly. Nevertheless, it is possible that other K^+ channel

conductances underly the accommodation observed as over 100 different pore-forming subunits of mammalian K^+ channels have been discovered (Coetzee et al. 1999). Clearly, the differences in accommodation observed between the early and late parts of the AP trains for both cell types implicate the involvement of more than one mechanism, perhaps acting in concert.

A depolarising voltage 'sag' was observed in both O-LM and O-Bi cells during a hyperpolarising current pulse. However, the voltage 'sag' in O-LM cells was significantly greater than that in O-Bi cells. It is possible that the voltage 'sag' in both cell types resulted from the hyperpolarisation-activated cationic current (I_h) for the following reasons. Firstly, a previous study (Maccaferri and McBain 1996), showed that the voltage 'sag' in SO/alveus nonpyramidal cells of the CA1 hippocampal area was blocked by a specific antagonist of I_h. Secondly, the voltage 'sag' in O-LM and O-Bi cells of the present study occurred within the voltage range (~-50 to -120 mV) for the activation of I_h in SO/alveus nonpyramidal cells previously recorded (Maccaferri and McBain 1996). Interestingly, when blocking I_h in the previous study (Maccaferri and McBain 1996), a differential increase in the firing frequency of current-evoked APs occurred early in the train (first two APs) compared with those occurring late in the train (last two APs). This would imply that I_h exerts a larger influence during the early part of a train of APs, presumably because at a resting membrane potential of –60 mV, I_h is tonically activated until the voltage crosses the deactivation range for I_h (Maccaferri and McBain 1996). However, one would expect that I_h increases the firing frequency (shown for spontaneous APs; Maccaferri and McBain 1996) if it has not reached its reversal potential. Otherwise, a reduction in firing frequency would likely result if I_h has reversed before K^+ channel activation due to a reduction in the driving force for K^+ through voltage-gated K^+ channels. The latter would be a possible explanation as to why O-Bi cells showed a larger early accommodation compared to the late part of the AP train where I_h may be deactivated. Despite the above relationship between I_h and firing frequencies of O-Bi cells, the existence of I_h in O-

Bi cells is uncertain due to the prevalence of synaptic activity occurring during hyperpolarising current pulses in these cells. Moreover, the rebound depolarisation occurring at the end of a hyperpolarising current pulse correlated with the voltage 'sag' measurement in O-LM but not O-Bi cells. Therefore, it is likely that the voltage 'sag' observed in O-LM cells resulted from I_h, whereas in O-Bi cells I_h or other factors such as synaptic activity could have caused the voltage 'sag' along with low-threshold Ca^{2+} conductances for the rebound depolarisation.

3.4.1.1 Previous Findings

Based on existing evidence and the present findings, one can assume that anatomically distinguished cell types may also have distinct physiological properties when more stringent analytical methods are used. Certainly, significant accommodation differences between O-LM and O-Bi cells would have been missed if the early and late component of the AP train were not analysed separately. Broad classifications of intrinsic membrane properties between pyramidal and nonpyramidal cells in the neocortex have been well documented (McCormick et al. 1985; Agmon and Connors 1989; Connors and Gutnick 1990). This was followed by subgroupings of neocortical nonpyramidal cell types based on firing properties (Kawaguchi 1993) correlating with their differences in expression of calcium-binding proteins and dendritic and axonal organisation (Kawaguchi and Kubota 1993). As in the neocortex, there are general response characteristics of nonpyramidal cells, which distinguish them from pyramidal cells in the hippocampus as well as the subiculum (Greene and Totterdell 1997). In addition, hippocampal nonpyramidal cells have been classified into three distinct groups based on intracellular response characteristics (Schwartzkroin and Mathers 1978; Knowles and Schwartzkroin 1981; Lacaille et al. 1987; Kawaguchi and Hama 1988; Morin et al. 1996). One study (Parra et al. 1998), claiming that most nonpyramidal cells cannot be classified into groups presented no anatomical data, only schematic conclusions. For instance, nonpyramidal cells should not be

anatomically analysed unless the main axon arborises into collaterals and sufficient projection exists to designate laminar specificity. Moreover, bath application of agonists in the same study (Parra et al. 1998) did not allow precise temporal activation of receptors as would occur under physiological conditions, which also inevitably involves intrinsic properties of cells. One may argue that hippocampal nonpyramidal cell classifications could be erroneous due to experimental variability between several studies. However, general measurements of intrinsic properties of pyramidal cells remained robust between studies implying that, valid comparisons between pyramidal cells and nonpyramidal cells could at least exist. Also, nonpyramidal cells have been identified in separate studies based on their intrinsic properties and verified by anatomical analysis. It is also possible that more intrinsic properties between nonpyramidal cells could have been distinguished in some studies if broad anatomical groupings were not employed. The present study has further differentiated two anatomically distinct cell types within the broad grouping of SO/alveus nonpyramidal cells.

Several intrinsic membrane properties of O-LM and O-Bi cells were different from those of the broadly grouped SO/alveus nonpyramidal cells of the CA1 hippocampal area previously recorded in whole-cell current-clamp mode (Morin et al. 1996). For instance, the resting membrane potential and membrane time constant were larger for both O-LM and O-Bi cells as compared to previously recorded SO/alveus nonpyramidal cells (Morin et al. 1996). Also, the previous study showed that SO/alveus nonpyramidal cells had both a fast AHP and medium AHP following single APs. In the present study, O-LM and O-Bi cells displayed only a fast AHP, which was larger in amplitude as well as longer in duration as compared to both the fast and medium AHPs in the previous findings (Morin et al. 1996). The AP amplitude, at least for O-LM cells, was also larger compared to SO/alveus nonpyramidal cells in the previous report. These discrepancies can be explained mainly by the fact that the previous recordings of SO/alveus nonpyramidal cells encompassed not only O-LM cells, but a variety of other cell

types with axonal projections to SP and/or SR (Morin et al. 1996). Also, with regard to the AHP measurments, the present study subtracted the subthreshold response from the APs that occurred 50 % of the time using the same current pulse. In this way, the resulting AHP was a consequence of the AP and not the membrane properties, which would otherwise occlude the AHP. Other studies elicit APs at a current pulse above that which evokes a subthreshold response, which avoids the occlusion of the AHP. Although this would not affect the AP amplitude, it would allow for variability of the AHP measurements between studies. Another difference is that the inclusion of $MgCl_2$ in the pipette of the previous study (Morin et al. 1996) may have excluded effects from NMDA receptors during a depolarising current pulse and presynaptic glutamate release. In addition, the previous recordings may have been more affected by the dialysing of intracellular contents than in the present recordings. In support of this, noninvasive measurements of membrane potential in hippocampal nonpyramidal cells were performed by determining the reversal potential of K^+ currents through a cell-attached patch (Verheugen et al. 1999). The noninvasive method showed that the resting membrane potential of hippocampal nonpyramidal cells was more hyperpolarised than during whole-cell current-clamp recordings. The resting membrane potential during intracellular recording with sharp electrodes was similar to that during whole-cell recordings for the same group (Lacaille et al. 1987) but this could have been attributed to current leak around the sharp electrode. The more depolarised resting membrane potentials in previous recordings (Morin et al. 1996) likely resulted in the lower AP amplitudes observed and consequently differences in the K^+ currents underlying the AHP. Furthermore, as the input resistances of cells were similar between the present and previous study, the only possible account of differences in the membrane time constant observed is the dialysing of intracellular contents. Thus, provided that experimental variabilities are kept at a minimum, it is more appropriate to focus on comparisons between cell types rather than absolute measurements of the parameters under investigation.

Nevertheless, it is not possible to assume that every cell can be classified into one group. There are of course parameters which overlap between groups of cells and also cells which are distinct anatomically but appear to lack differentiation in intrinsic membrane properties or vice versa. However, until all relevant physiological and anatomical criteria are analysed, it is not possible to deem certain cells as unclassifiable. Objective, statistical cluster analysis of nonpyramidal cells has already led to unequivocal groupings purely on anatomical grounds (Tamas et al. 1997; Somogyi et al. 1998).

3.4.2 Anatomical Features

The different axonal projections in apposition to two separate excitatory input pathways, namely the perforant path projection and Schaffer collateral input, suggests that O-LM and O-Bi cells could alter physiological states depending on their specific activation. What remains to be determined is whether both cell types are activated via similar synaptic inputs. The answer to this is not easy to obtain given that there are at least two main extrinsic inputs (perforant path and medial septal) to SO/alveus nonpyramidal cells involved in physiologically-relevant activity as well as local circuit interactions. Nevertheless, there is some segregation of inputs to the CA1 hippocampal area. For instance, an indirect layer II entorhinal cortical input to CA1 pyramidal cells arises via Schaffer collaterals of CA3 pyramidal cells (Schaffer 1892; Steward 1976; Claiborne et al. 1986; Ishizuka et al. 1990), which target the same dendritic zone as O-Bi cells. On the other hand, direct entorhinal projections to the CA1 area originate from layer III cells and terminate in close apposition to axonal targets of O-LM cells (Steward 1976) as well as also projecting to SO/alveus (Deller et al. 1996), where both O-LM and O-Bi cells are located. Further specificity of entorhinal connections to and from the hippocampus may occur based on the present anatomical classifications of O-LM and O-Bi cells. For example, both O-LM and O-Bi cells had axon collaterals remaining in the CA1 area but skewed towards the CA3 area

(proximal part of the CA1 area) where the pyramidal cell output has been shown to target the medial entorhinal area rather than the lateral entorhinal area (Tamamaki and Nojyo 1995). The proximal part of the CA1 area was also shown to receive perforant path projections originating from the medial entorhinal area as opposed to the lateral entorhinal area (Tamamaki and Nojyo 1995). However, it is not possible to exclude a direct or indirect lateral entorhinal projection to O-LM or O-Bi cells either.

3.4.3 Somatostatin and mGluR1α Immunoreactivity

The present and previous findings (Baude et al. 1993; Maccaferri et al. 2000) have shown that both O-LM and O-Bi cells contain somatostatin. Evidence of the actions of somatostatin suggest that this neuropeptide acts both presynaptically to reduce GABAergic transmission to principal cells in the hippocampus (Scharfman and Schwartzkroin 1989) and sensory thalamus (Leresche et al. 2000) as well as postsynaptically (Schweitzer et al. 1998). This is in contrast to the excitatory action of locally applied somatostatin to SO/alveus and SP nonpyramidal cells (Scharfman and Schwartzkroin 1988). Given that both O-LM and O-Bi cells have axon collaterals in SO/alveus, sometimes innervating their somatodendritic regions, somatostatin may have a postsynaptic action in these cells, which in turn affects pyramidal cells as an indirect presynaptic action. Indeed immunolabelling for one somatostatin receptor subtype (sst4) was found on axon collaterals located in SL-M (Selmer et al. 2000). Immunolabelling of the same receptor subtype was also found on the soma and dendrites of cells located in SO, SP and SR (Selmer et al. 2000). If the described excitation/inhibition occurs sequentially, then it may have implications in oscillatory activity. Others (Boehm and Betz 1997; Tallent and Siggins 1997) reported that somatostatin reduces glutamatergic transmission to hippocampal pyramidal cells by a presynaptic mechanism on excitatory terminals. Nevertheless, this would depend on somatostatin spillover from nonpyramidal cells.

In addition to somatostatin, O-LM cells recorded in the present study were directly shown to express mGluR1α. This is also supported by direct physiological evidence of large oscillatory inward currents evoked in O-LM cells by the group I and II mGluR agonist, (1S,3R)-ACPD (McBain et al. 1994). The prominent inward current likely reflects pre- and post-synaptic actions of the agonist (McBain et al. 1994). Others (van Hooft et al. 2000), classified SO/alveus nonpyramidal cells with distinct anatomical features and neurochemical markers into groups based on responses to (1S,3R)-ACPD and expression of group I mGluRs using reverse-transcription PCR. Although this study (van Hooft et al. 2000) showed a similar prominent mGluR-mediated oscillatory response in O-LM cells, several inconsistencies exist. For example, another group of cells in the above study (van Hoof et al. 2000) expressed group I mGluRs but lacked an inward current upon application of a group I mGluR agonist. This suggests that there may be some alteration in the slicing procedure, which could account for different physiological effects depending on the existing circuitry. Also, the inward currents recorded for some cells may be due to activation of presynaptic group II mGluRs rather than group I receptors, due to the non-specific agonist used. Moreover, the study's criteria for grouping cells based on anatomical features was questionable due to minimal amount of axon evaluated as evidenced in the figures (van Hoof et al. 2000). As a result of the above discrepancies, it is not possible to determine from the previous study (van Hooft et al. 2000) that cells morphologically similar to O-Bi cells actually expressed group I mGluRs. In the present study, O-Bi cells were not found to be immunopositive for mGluR1α, but this may have been attributed to a weak expression of mGluR1α in these cells, which would be more susceptible to loss in the in vitro preparation. However, additional recordings of O-Bi cells along with testing of different experimental factors could be used to evaluate their immunoreactivity for mGluR1α further.

CHAPTER 4: Physiological and Anatomical Characteristics of Nonpyramidal Cells and Hippocampal Network Activity In Vivo

4.1 Introduction

Different specialised brain areas may interact efficiently through state-dependent synchronous activity between populations of neurones. Neuronal synchrony is facilitated by oscillatory activity. Several forms of oscillatory activity have been described in the hippocampus based on waveform, amplitude and frequency. Population activity, such as sharp wave bursts (SPWs) and θ-frequency oscillations, have been shown to occur both during awake and sleep states in animals (Buzsaki et al. 1983).

Sharp wave bursts reflect a propagation of highly synchronous excitatory drive throughout the CA3-CA1-entorhinal cortex axis, which is usually accompanied by fast rhythmic spindle-like field oscillations (ripples) in the CA1 pyramidal layer (Chrobak and Buzsaki 1994; Ylinen et al. 1995a). Sharp wave bursts are observed during consumatory or still behaviours of the animal and are also observed when the animal is anaesthetised (Ylinen et al. 1995a). During anaesthesia, the SPW amplitude in stratum radiatum remains the same (1-5 mV) but the ripple frequency is reduced (90-130 Hz) compared to that during awake states (180-200 Hz; Ylinen et al. 1995a). Theta-frequency oscillations (3-12 Hz) can be up to 2 mV in amplitude (Bland et al. 1996) and are observed when the animal is exploring its environment or during movement and paradoxical sleep (Vanderwolf 1969). Both the frequency and amplitude of θ-frequency oscillations may be reduced depending on the depth of anaesthesia (Kramis et al. 1975; Soltesz and Deschenes 1993).

4.1.1 Mechanisms of SPW Activity

Sharp wave bursts are likely to emanate from strong excitatory input via Schaffer collaterals as evidenced by large amplitude field potentials and prominent current sink observed in SR of the CA1 area (Suzuki and Smith 1987; Ylinen et al. 1995a). Moreover, during SPWs, CA3 pyramidal cells increase their firing rate, which can predict ripple amplitude in the CA1 area (Csicsvari et al. 2000). Given the voltage independence of ripple frequency and the high frequency discharge of nonpyramidal cells recorded in SP during SPWs, it has been suggested that ripples reflect summed IPSPs in pyramidal cells (Ylinen et al. 1995a). It appears that local circuit interactions in the CA1 area are necessary for generating ripple oscillations for the following reasons. Firstly, ripple oscillations in the CA1 area are not correlated temporally with unit activity in the CA3 area (Ylinen et al. 1995a). Secondly, CA1 pyramidal cells show a larger increase in synchrony during SPWs as compared to nonpyramidal cells in SP and SO/alveus (Csicsvari et al. 1998), where CA3 pyramidal cells also innervate (Ishizuka et al. 1990; Li et al. 1994). During SPWs however, an increase in CA1 pyramidal cell synchrony was less reliable in activating nonpyramidal cells than in the absence of SPWs (Csicsvari et al. 1998). This would imply that nonpyramidal cells are activated directly by CA3 pyramidal cells during SPWs. Furthermore, in addition to the prominent current sink in SR, a smaller current sink is also observed in SO during SPWs (Ylinen et al. 1995a). Given their extensive axonal projections, nonpyramidal cells could indeed promote ripple oscillations via input from CA3 pyramidal cells. This may be further facilitated by the presence of gap junctions between parvalbumin positive hippocampal nonpyramidal cells (Katsumaru et al. 1988) as halothane, an anaesthetic which blocks gap junctions, also blocked ripple activity during SPWs (Ylinen et al. 1995a). On the contrary, computer modelling showed that axon-axon gap junctions between pyramidal cells allow for the generation of ripple oscillations and in turn, nonpyramidal cells were phased due to the convergence of pyramidal cell inputs (Traub and Bibbig 2000). However, nonpyramidal

cells show more synchrony than pyramidal cells regardless of network activity (Csicsvari et al. 1998). In order for the computational model (Traub and Bibbig 2000) to explain the experimental results (Csicsvari et al. 1998), the converging inputs of pyramidal cells would have to be greater than the divergent output of nonpyramidal cells, thus questioning the role of nonpyramidal cells during SPW activity.

4.1.2 Mechanisms of Theta-Frequency Activity in Anaesthetised Animals

Theta-frequency activity involves cholinergic activation in anaesthetised animals as evidenced by a block in θ-frequency oscillations after application of atropine, an antagonist at muscarinic receptors (Kramis et al. 1975). During anaesthesia, nonpyramidal cells near SP of the CA1 area fire in conjunction with the positive peak of θ-frequency waves opposite to pyramidal cells (Fox et al. 1986; Ylinen et al. 1995b). Such out-of-phase activity between pyramidal cells and nonpyramidal cells may be a consequence of nonpyramidal cells pacing pyramidal cell activity in conjunction with cholinergic activation. Four groups of evidence support this notion. Firstly, current-source density analysis has shown that the prominent sink in SL-M was strongly attenuated under anaesthesia, thereby reducing the influence from entorhinal cortical inputs (Buzsaki et al. 1986; Brankack et al. 1993). Secondly, muscarinic action of acetylcholine on pyramidal cells is too slow to carry a θ-frequency oscillatory signal without additional excitatory influences (Dodd et al. 1981; MacVicar 1985; MacVicar and Tse 1989). However, nonpyramidal cell firing can be phase locked to θ oscillations after application of acetylcholine (Stewart et al. 1992). Thirdly, muscarinic induction of θ-frequency membrane potential oscillations were shown in CA1 nonpyramidal cells and their stimulation at θ frequency paced intrinsically generated membrane potentials in CA1 pyramidal cells (Chapman and Lacaille 1999). Fourthly, $GABA_A$ receptor-mediated IPSPs were shown to phase

spontaneous firing and subthreshold oscillations of CA1 pyramidal cells at θ-frequency in combination with intrinsic properties of pyramidal cells (Cobb et al. 1995). One discrepancy however, is the occurrence of θ-frequency dendritic oscillations of CA1 pyramidal cells, which are in phase with the field θ oscillations recorded in SP but out of phase with θ-frequency somatic oscillations of CA1 pyramidal cells in anaesthetised rats (Kamondi et al. 1998). Layer III entorhinal cortical neurones shown to discharge phase-locked to θ-frequency oscillations (Mitchel and Ranck 1980) are unlikely to contribute to θ-frequency oscillations observed in CA1 pyramidal cell dendrites due to the attenuated sink in SL-M during anaesthesia (Buzsaki et al. 1986; Brankack et al. 1993). The voltage dependence of the frequency of dendritic θ-frequency oscillations (Kamondi et al. 1998) would support a role for dendritic channels. In addition, the phase shift of θ-frequency oscillations in the dendrites as compared to the soma would suggest that the dendritic oscillations were triggered by synaptic influences instead of oscillations propagating from the soma.

4.1.3 Mechanisms of Theta-Frequency Activity in Unanaesthetised Animals

In unanaesthetised animals, θ-frequency oscillations are abolished by applying atropine and at the same time lesioning the entorhinal cortex projection to the hippocampus (Vanderwolf and Leung 1982; Lee et al. 1994). Both nonpyramidal cells and pyramidal cells near SP of the CA1 area of the hippocampus typically fire APs in conjunction with the negative peak of the locally recorded θ-frequency field oscillations in unanaesthetised animals (Fox et al. 1986; Csicsvari et al. 1999). Therefore, in addition to the direct cholinergic influence in θ-frequency oscillations, the entorhinal cortical projection would provide a much stronger excitatory input via glutamatergic synapses during θ-frequency oscillations in unanaesthetised animals. The entorhinal cortical input may also have a prominent role in the minimal time lag of firing

between pyramidal cells and nonpyramidal cells as this was not observed in anaesthetised animals. One possible mechanism is that entorhinal cortical input to pyramidal cells and nonpyramidal cells is paced by medial septal input resulting from feedback hippocampo-septal nonpyramidal cells. The following evidence would support this hypothesis, at least for the CA1 area of the hippocampus. Firstly, medial entorhinal cortical projections (Deller et al. 1996) and medial septal projections, encompassing the vertical limb of the diagonal band of Broca (Nyakas et al. 1987), target all layers in the CA1 area. Secondly, projections to the medial septum from the hippocampus mainly originate from nonpyramidal cells in SO (Toth et al. 1993). Thirdly, θ-frequency depolarisations can be elicited by cholinergic activation in combination with Na^+-dependent currents in pyramidal cells (MacVicar 1985; MacVicar and Tse 1989). Fourthly, the activity of the majority of medial septal neurones correlates with the maximum discharge probability of CA1 pyramidal cells and nonpyramidal cells during θ-frequency oscillations in unanaesthetised rats (Dragoi et al. 1999). In addition, an entorhino-septo-supramammilary nucleus feedback connection could also influence θ-frequency oscillations observed in the hippocampus (Leranth et al. 1999).

4.1.4 Aims

From the above, it is clear that nonpyramidal cells may play a prominent role in patterning hippocampal pyramidal cell activity. Because more than ten types of GABAergic cells have been described in the hippocampus, it would be important to establish if their anatomical differences correlate with the differential responses observed during network activity (Ylinen et al. 1995a, 1995b; Fox et al. 1986; Csicsvari et al. 1998, 1999). Therefore, I attempted to record from nonpyramidal cells in SO and SP during network activity and determine their anatomical identity. Nonpyramidal cells in SO have been reported to express a high level of

mGluR1α (Baude et al. 1993). The activation of this receptor results in oscillatory activity in the cell via calcium mobilisation (Woodhall et al. 1999). Such an oscillatory activity demonstrated in vitro may contribute to the patterned neuronal activity in vivo. Therefore, I also explored which nonpyramidal cell populations express mGluR1α in addition to the ones described in the literature (Baude et al. 1993).

4.2 Methods

4.2.1 Animal Preparation for In Vivo Recording

Sprague-Dawley rats (350-650g) were anaesthetised with halothane in a fume hood followed by an intraperitoneal injection of urethane (1.5 g/kg, 33%w/v). The whiskers were shaved on one side to allow for easier swivelling of the electrode into position and the cranial area was shaved for subsequent surgical procedures. The rat was placed on a heated water blanket and puncturing ear bars were inserted so as to center the head in the stereotaxic frame. Lidocaine powder with saline (150mM) was applied over the area of the skin to be opened. An anterior to posterior scalp incision ending below the cerebellum was made and the skin was splayed back with coarse forceps on both sides. A bone scraper was used to scrape away all connective tissue and also remove the muscle surrounding the skull. Tissue paper was placed within the gaps of the bone and muscle to absorb bleeding and to keep the incised skin away from the bone. The coarse forceps, which held the skin were then removed.

4.2.2 Electrode Entry

An insulated bifilar tungsten electrode (California Fine Wire Company Inc., USA) for stimulating the commisure from the fimbria was cut at the tip to make an approximate 45° angle with one wire protruding. The electrode was bent 5 mm from the tip to form a step, which allowed for the bent end to contact the skull after insertion. The electrode was kept in place with dental acrylic. The flat skull position was established by aligning the tip of the stimulating electrode just above lamda and comparing the height difference with the alignment over bregma under microscopic control. The mouth bar was adjusted accordingly. The fimbria (AP=-1.3, ML=-1.0, H=3.95) and a position over the CA1 area of the hippocampus (AP=-3.5, ML=+2.5 and –2.5 co-ordinates from bregma) were marked first with the bone scraper using the position

of the stimulating electrode under microscopic visualisation. The mark was made larger with a large drill bit. All the marks were drilled first with a large drill bit followed by a smaller drill bit with care to gradually thin the bone. A needle glued to a syringe plunge and bent at the tip to form a hook (in-house) was used to remove the thinned bone by hooking broken pieces and scraping them up against the wall of the opening (1.5 mm diameter). Any blood was removed with small pieces of tissue paper and saline. Occasionally, a cauteriser was used to dry the ends of the blood vessels found in the dura. This allowed for only a small degree of bleeding when the dura was cut for electrode entry. A small diameter stainless steel wire glued to a wooden stick (in-house) had a hook that was used to cut the dura where the electrode would be placed. A similar larger diameter stainless steel wire with a hook was used to make the dura opening wider and to fold the sides away from the opening. The small hook was again used to poke a hole through the pia (away from blood vessels) for easier electrode entry. Any subsequent bleeding from capillaries was removed with saline and a piece of tissue paper. In order to insert the stimulating electrode, saline was removed with a tissue paper and the electrode was quickly lowered to the surface noting the scale value of the manipulator. The stimulating electrode was then lowered manually to the appropriate depth. Once the stimulating electrode was lowered to the level of the fimbria, the skull opening was filled with dental acrylic powder dissolved with glue to keep the electrode in place. The dental acrylic solution was also added over all visible sutures to provide a well around drilled areas as well as reduce brain pulsation effects. When the dental acrylic solution dried, the stimulating wire holder was removed and the wire was bent out of the way.

A small drill bit was used to drill two holes to the surface of the cerebellum. An earth and indifferent stainless steel screws were soldered to an insulated copper wire with the aid of zinc chloride, which served as an intermediary bond between the stainless steel, otherwise immune to surface erosion, and the soldering metal. The screws went into the holes and served

as a reference to the field electrode. The other end of the wires had male soldered pins that were later inserted into female pins of the extracellular preamplifier. The preamplifier (gain=1, Texas Instruments) with copper shielding was mounted on a manipulator rod and assembled (in-house) together with the nichrome field tetrode for field recordings (4 twisted wires, 12 μm diameter). After one of the marks over the CA1 area was drilled to allow electrode entry as described above, the field electrode assembly was clamped into the manipulator which was angled at 10° from the vertical plane and the reference pins were inserted into the preamplifier. In order to avoid drying of the cortex, a mixture of heated 50/50% solid/liquid paraffin was applied as a solution to the drilled opening. The paraffin solution was held by the dental acrylic well and hardened within seconds.

Intracellular electrodes (60-90 MΩ) were made from 2.0 mm outer diameter standard wall borosilicate capillary glass (World Precision). This glass was cleaned in ethanol prior to pulling with a horizontal Flaming-Brown puller using a heated silver filament. The intracellular electrode was back-filled with 2% biocytin in 1M potassium acetate. Any bubbles in the electrode were removed with a thin tungsten wire. A silver wire was inserted subcutaneously along the dorsal side of the neck to serve as a reference for the intracellular electrode.

4.2.3 Recording

The paraffin wax, covering the opening over the CA1 area, was removed with fine forceps. Saline was added to the opening and a piece of tissue paper was placed over the saline to remove any remaining paraffin oil. The saline was removed with tissue paper and the field electrode was lowered onto the surface of the brain noting the scale value of the micromanipulator. The field electrode was manually lowered to the depth of the stratum pyramidale determined by the Paxinos and Watson atlas (1986) as well as observing the unit activity, reversal of the sharp wave population burst and reversal of the population discharge

evoked by stimulation (20 mA; 50 μs). Saline was added again in order to measure and compensate the intracellular electrode resistance and offset the intracellular voltage using the Axoclamp-2A amplifier. The intracellular voltage signal was recorded in bridge mode via an Axoclamp-2A amplifier (gain=10; LP=3kHz) connected to a headstage (biased current = 0.1 nA) which was mounted on a stationary micromanipulator close enough for the silver/silver chloride wire to reach the electrode which was mounted on a Burleigh motor drive. The signal was further amplified and filtered using a Warner DC Amplifier (gain=5; LP=2 kHz). All recordings including intracellular, field, stimulation and current injection were recorded using the Enhanced Graphics Acquisition and Analyisis (EGAA) software interfaced with an RC analog/digital converter (RC Electronics Inc., USA). Field recordings were filtered using a Grass Model 12 Neurodata Acquisition System (Braintree Inc., USA). Four channels from the tetrode recordings were amplified and filtered (gain=5000; 1Hz-3kHz band width) and one of the four channels was amplified and filtered at different settings (gain=20,000; 300 Hz-10kHz band width) for extracellular unit activity. After the intracellular electrode resistance was compensated and the voltage was offset, the electrode was withdrawn and the saline removed. The intracellular electrode was then lowered onto the surface of the brain using the Burleigh motor drive and the depth was offset to zero. The electrode was stepped at slow to medium speed to a depth of approximately 500 μm followed by addition of paraffin solution into the well. The capacitance of the intracellular electrode was compensated using the Axoclamp-2A and subsequent spontaneous activity was recorded as well as responses evoked by positive or negative current injection. Field recordings consisted of stimulation evoked population activity; slow wave activity; occasional episodes of theta-frequency oscillations (4-8 Hz) evoked by a manual tail pinch with perforated curved forceps; sharp wave bursts and associated ripples also monitored by the high pass filtered tetrode channel.

4.2.4 Juxtacellular Recording Methods

In some experiments male Wistar rats (300-550 g) under the same anaesthesia as described above were used for juxtacellular recordings along with iontophoretic application of L-Quisqualic acid (5 mM in NaOH; pH 8) an AMPA and group I mGluR agonist. The electrode design consisted of three borosilicate glass capillaries with filament (1.5 mm OD) glued under microscopic control with one glass protruding approximately 10 μm (in-house). The electrode arrangement was reinforced with two to three smaller pieces of glass capillary glued over the gaps and covered with molten wax. The protruding electrode served to record cells juxtacellularly and the other two electrodes were used for drug application and current balancing with 1M NaCl, respectively. The juxtacellular electrode contained 1.5% neurobiotin tracer in 0.5 M NaCl. As a result of the large resistances sometimes observed with the iontophoretic electrodes, large ejection currents of approximately –30 nA were needed for the drug to produce an effect. Consequently, a low retaining current between +4 to +10 nA was used. However, currents used for ejection and retaining were above the minimum for obtaining a linear relationship between current and efflux (Purves, 1979). As the recording electrode was farther away from the iontophoretic application, the juxtacellular responses recorded did not directly result from extracellular potential changes due to current application but were either due to the drug itself or indirect activation by other cells near the iontophoretic electrode. Animal preparation and equipment are similar to that described in the methods section of chapter 1. A craniotomy was performed over the CA1 area of the hippocampus (1.5 x 3 mm) to allow entry of the recording/iontophoretic electrode (AP=-4.16, ML=+2.5 from bregma) and a field electrode (AP=-4.3, ML=+2.5 from bregma) angled at 30° from the vertical plane. In order for the field electrode to reach SL-M at the specified co-ordinates from bregma, the electrode was positioned 3.2 mm posterior to this point obtained from the geometric equations concerning (right) triangles with the known values for the electrode angle (30°) and depth of interest (H=2.8

mm). Juxtacellular recordings were separated into two channels at the level of the Axoprobe-1A amplifier. The first channel was amplified (x10, Axoprobe-1A ;x100, Neurolog System and filtered (500 Hz to 3 kHz band width, Neurolog System) for single cell recording. The second channel was amplified (x10, Axoprobe-1A) and filtered (5kHz LP, Axoprobe-1A) in order to record any phase reversal of oscillatory activity which would serve as a reference to the placement of the field electrode. The field electrode was also amplified (x100) and filtered (500 Hz LP) using the Axoprobe-1A amplifier but via a separate headstage. The ECG recording (Neurolog System) in this case served not only as a monitor of the animal's welfare but also as a basis for discriminating behaviourally-relevant rhythmic activity. Data was stored on DAT tapes and transferred onto the Spike2 software via the 1401 CED interface (Cambridge Electronic Design) for investigation.

4.2.5 Histological Processing

At the end of the recording, positive current pulses (300 ms on and 500 ms off) were applied for 15 minutes in order to release neurobiotin from the juxtacellular electrode at a magnitude that evoked a train of APs. The animal was given additional urethane anaesthesia and perfused through the heart with 150 mM NaCl followed by fixative consisting of 4% paraformaldehyde, 0.05% glutaraldehyde, 15% (v/v) saturated picric acid and 0.1 M phosphate buffer (pH 7.0). The brain was removed and left in a fixative consisting of 4% paraformaldehyde, 15% (v/v) picric acid and 0.1 M PB until sectioning. Coronal sections of 70 to 90 μm thickness were made in 0.1 M PB surrounded by an ice jacket using a Vibratome. The sections were thoroughly rinsed with 0.1 M PB and then 0.1% Triton X-100 in TBS (pH 7.4). The sections were then incubated with avidin-biotinylated horseradish peroxidase complex in TBS (ABC Kit, Vector Laboratories) and left overnight on a shaker at 4°C. The following day, the sections were washed repeatedly with TBS followed by TB and were incubated in a solution

of DAB (0.5 mg/ml TB) for 15 min on a shaker at room temperature. Hydrogen peroxide was added to each vial to make a 0.01% solution with the buffered DAB solution. The reaction was stopped after 5 to 8 minutes by repeated washes with TB. Sections were mounted on microscopic slides with gelatin and placed in 50 ml of 0.1M phosphate buffer containing 5 drops of 4% osmium tetroxide for 10 min. The sections were then rinsed in 0.1 M PB followed by distilled water before being dehydrated and mounted under a coverslip as specified in the histology section of chapter 3. One juxtacellularly recorded and labelled cell was reconstructed with a drawing tube using an x100 oil objective.

4.2.6 Immunocytochemistry

In order to determine any histological correlates with one juxtacellularly labelled cell, co-localisation of calretinin and vasoactive intestinal polypeptide (VIP) was investigated in the CA1 area of adult Wistar rat dorsal hippocampal sections. In addition, the soma sizes of the immunolabelled cells were compared to the juxtacellularly labelled cell. Immunocytochemical procedures are similar to those described in chapter 3 methods. Briefly, one animal was perfused through the heart as described above and serial sections of 60 μm thickness were made in 0.1 M PB using a Vibratome. Sections were washed in buffer and incubated in 20% NGS in 0.1% Triton X-100 in TBS for 1 hr on a shaker at room temperature. Sections were incubated with mouse anti-VIP IgG (1:10,000; Cat. No. 9535-0504; Lot No. EA980907A; Biogenesis Ltd., UK) and rabbit anti-calretinin IgG (1:800; Cat. No. AB149; Lot No. 25797041; Chemicon International Inc., USA) made up in 1% NGS in 0.1% Triton X-100 in TBS and left for two days on a shaker at 4°C. After washing with buffer, Alexa488 conjugated to goat anti-mouse IgG (2 μg/ml; Molecular Probes Inc., USA) and CY3 conjugated to goat anti-rabbit IgG (IgG (3.5 μg/ml; Jackson ImmunoResearch Laboratories, Inc.) made up in 1% NGS in 0.1% Triton

X-100 in TBS was added to each vial and kept in the dark for 24 hrs on a shaker at 4°C. The sections were then rinsed in buffer and mounted with Vectashield.

Images were taken using a fluorescence microscope with a digital camera via the Openlab software and somatic areas were determined using the NIH Image software (National Institute of Health, USA). Expression of VIP only, calretinin only or co-localisation of VIP and calretinin were quantified as a percent with respect to the total VIP positive cells and the total calretinin positive cells counted. In order to compensate for any shrinkage due to the dehydration procedure for the juxtacellularly labelled cell, intrasection distances were measured for 10 cells before and after dehydration and these values are reported as a mean ± SD including a *P* value for significant differences (Wilcoxon rank sum test).

The distribution of the processes of the juxtacellularly labelled cell were also compared to calretinin immunopositive cells, one of which was demonstrated by light microscopic reconstruction (x100 oil objective). This procedure required a biotinylated goat anti-rabbit IgG (3 μg/ml; Vector Laboratories Inc., USA) as a secondary antibody followed by incubations with avidin-biotinylated horseradish peroxidase complex in TBS and later buffered DAB as specified in the histological section above.

Further analysis of VIP positive cells were performed by determining the degree of co-localisation with mGluR1α in the CA1 area of the dorsal hippocampus of adult Wistar rat hippocampal sections. The primary antibodies consisted of mouse anti-VIP IgG (1:10,000; Cat. No. 9535-0504; Lot No. EA980907A; Biogenesis Ltd., UK) and the affinity purified polyclonal rabbit anti-mGluR1α IgG (1:500; Cat. No. 24426; Lot No. 007016; DiaSorin, USA) tested for specificity in mGluR1 knockout mice (Dr Francesco Ferraguti, personal communication). The secondary antibodies used were CY3 conjugated to goat anti-mouse IgG (3.5 μg/ml; Jackson ImmunoResearch Laboratories, Inc.) and swine anti-rabbit IgG (2.4 μg/ml; DAKO, Denmark).

An enhancing agent containing FITC conjugated to tyramide was used to detect mGluR1α. Immunofluorescence procedures are similar to and fully described in chapter 3.

4.3 Results

4.3.1 State-dependent Activity In Vivo

In chapter 3, two anatomically distinguished nonpyramidal cell types were found to also differ in their firing rates and voltage 'sag' properties. Such differences could underly specific physiological roles between cell types during population activity. Interestingly, O-LM and O-Bi cells, which are found in SO and described in chapter 3, contain axonal projections in proximity to the synaptic origin of θ activity and SPWs, respectively. Therefore, I investigated whether different types of anatomically defined nonpyramidal cells in SO had specific firing patterns during two physiologically-relevant population activities, namely θ-frequency oscillations and SPWs. In order to obtain physiologically-relevant population activity for correlating with nonpyramidal cell firing patterns, extracellular and intracellular recordings in anaesthetised rats were performed in SP and SO of the CA1 area, respectively. Juxtacellular recordings were also performed and, in this case, the simultaneous extracellular recording was obtained from SP/SR of the CA1 area. In total, 27 cells were recorded and anatomically verified. Four of the total cells recorded were nonpyramidal cells.

4.3.1.1 Nonpyramidal Cells Recorded In Vivo

Four nonpyramidal cells were recorded in vivo including one recorded juxtacellularly and three recorded intracellularly. One (d150) of the four cells was recorded intracellularly by Dr Darrell Henze (Rutgers University, Newark, New Jersey, USA). This cell (d150) was included in the present study because I was present during the recordings and subsequent interpretation of the recordings was performed by me. During evoked θ-frequency field oscillations, one cell (m11) fired in phase with the negative peak of the θ-frequency waves; two

cells (m24 and mt47) recorded were 'silent', one of which was the juxtacellularly recorded cell (mt47) and in the case of the d150 cell, θ-frequency oscillations could not be tested. Two cells (m24 and d150) fired during SPWs, however, during the juxtacellular recordings and recording of the cell (m11) that fired during theta-frequency field oscillations, SPWs did not occur. Intrinsic membrane properties of the cells recorded in vivo could not be compared to the cells recorded in vitro (chapter 3) for two reasons. Firstly, cells recorded in vivo had different resting membrane potentials from those recorded in vitro. Secondly current pulses tested during in vivo recordings were minimal in order to avoid cell loss and consequently allow more time for the assessment of population activity. Moreover, in vivo state-dependent network activity cannot be excluded from the firing patterns of in vivo recorded cells. Nevertheless, current evoked firing patterns are presented for the intracellularly recorded cells as examples of firing characteristics and also in the presence of SPWs as a test for underlying mechanisms.

In the first cell (m11) recorded intracellularly (Figure 4.1), an AP train (average frequency 59 Hz) was evoked by 0.16 nA current for 400 ms. Some slow rhythmic activity (3.3 Hz) was simultaneously occurring but did not appear to have modulated the firing pattern. In the absence of current steps, θ-frequency field oscillations (4 Hz) were evoked by a tail pinch and the cell entered into a rhythmic firing pattern in conjunction with the negative peak of the θ-frequency waves. The threshold of AP generation was reduced around the centre of the peak without attenuation of AP amplitude, which was usually largest at the centre. The fact that the cell's resting membrane potential was unusually close to AP threshold (-48 mV) may have been actual or a consequence of current leak around the electrode. The undershooting APs suggest a dendritic recording.

Figure 4.1 In vivo intracellular recording of a presumed backprojection nonpyramidal cell (m11) in SO of the CA1 area of the hippocampus. The top traces are extracellular wide band pass recordings of oscillatory activity in SP. The middle traces are high pass (HP) filtered recordings of the top trace for extracellular unit activity. The bottom traces are the intracellular recording of the cell. **(A)** The cell had a resting membrane potential of –48 mV and responded to 0.16 nA or 0.32 nA current steps of 400 ms duration. This firing did not appear to be modulated during spontaneous slow rhythmic field activity (3.3 Hz). **(B)** During pinch-evoked θ-frequency episodes (4 Hz), the cell fired in phase with the negative peak of θ. Note the reduction in AP threshold and increase in AP amplitude towards the centre of the burst epoch.

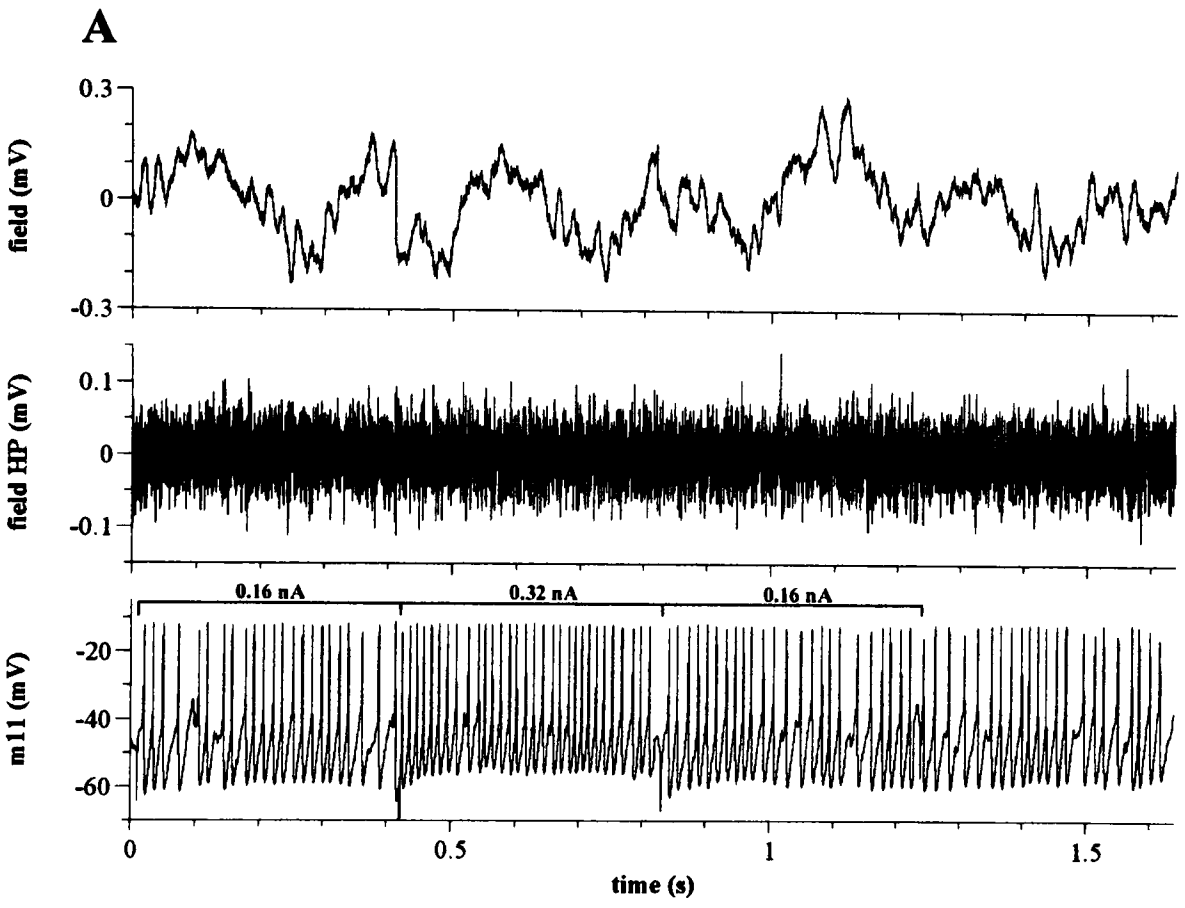
A
field (mV)
0.3
0
-0.3
field HP (mV)
0.1
0
-0.1
0.16 nA
0.32 nA
0.16 nA
m11 (mV)
-20
-40
-60
0
0.5
1
1.5
time (s)

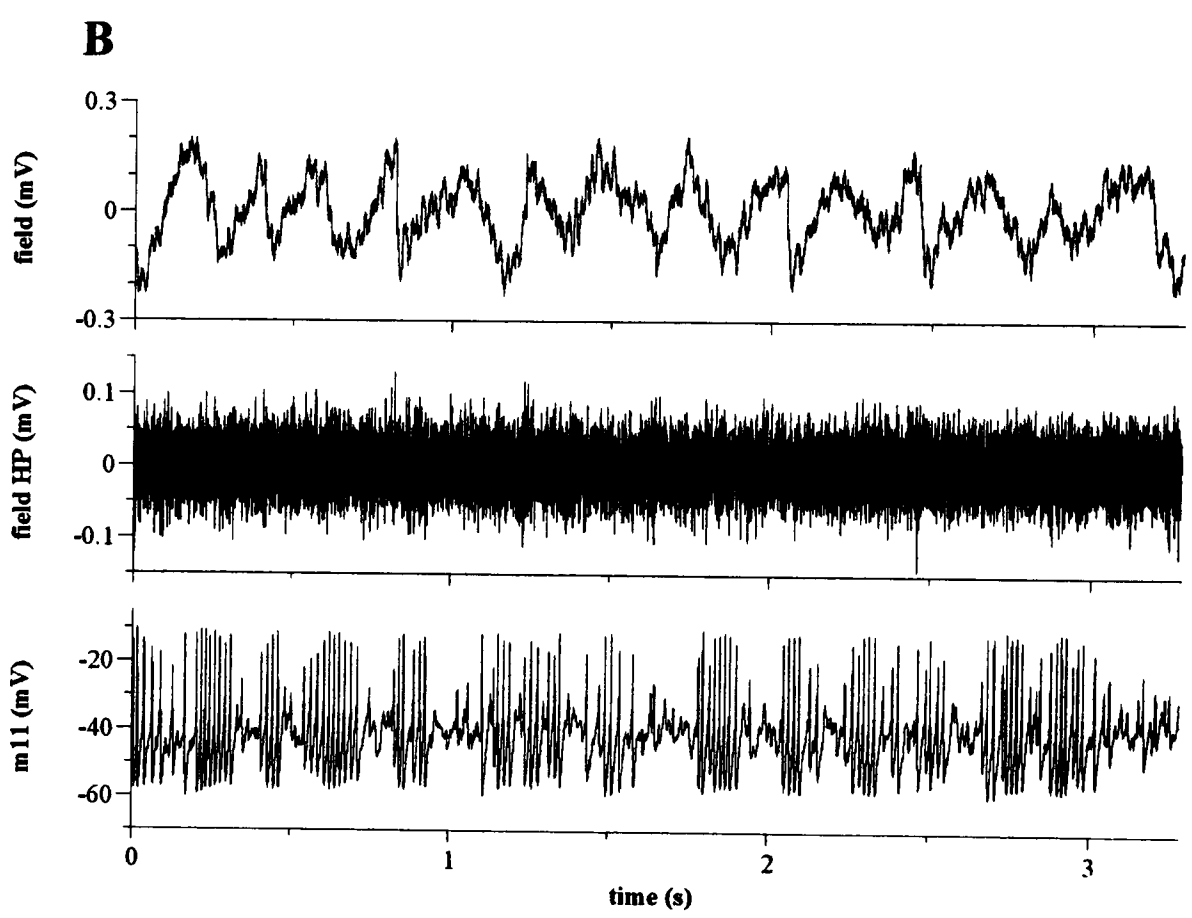
B
field (mV)
0.3
0
-0.3
field HP (mV)
0.1
0
-0.1
m11 (mV)
-20
-40
-60
0
1
2
3
time (s)

The second cell (m24), which had a resting membrane potential of –70 mV, was 'silent' during the few, rather slow (3 Hz) evoked θ-frequency episodes (Figure 4.2.2.A). However, there are several interesting features of the cell's activity observed during SPWs. Firstly, a SPW occurring at the beginning of a current-evoked (0.7 nA; 500 ms) train of APs delayed firing of the cell (Figure 4.2.1.A). When the SPW occurred during the train of APs, the cell increased its firing rate in the form of doublets just after the large excitatory population peak (Figure 4.2.1.B). The doublet interval ranged between 6.5 and 7.9 ms, which was longer than that recorded from axo-axonic cells in vitro (Buhl et al. 1994b). Also unlike axo-axonic cells, depolarising afterpotentials did not follow single evoked APs during the train, instead, membrane depolarisations occurred prior to the suprathreshold evoked APs. Doublet firing was not observed in periods of current injection without the occurrence of SPWs. Nevertheless, the cell exhibited a large decrease in firing rate (Figure 4.2.1.C) after 200 ms implying the need for a large excitatory drive such as a SPW to overcome either the presumed slowly inactivating K^+ channels or inhibition occurring at the site for AP generation. The second observation was that during a SPW the cell showed strong depolarisations and in some cases the smaller depolarisations were the carriers of a single AP coinciding with the strongest excitatory drive of the extracellular unit activity (Figure 4.2.2.B). This would indicate along with the undershooting of APs observed that it was a dendritic recording. Sometimes, the depolarisation diminished in decrements which in most cases coincided with the activity of different cells extracellularly recorded in SP and distinguished on the basis of AP height (Figure 4.2.2.C). The diminishing depolarisation occurs after the negative peak of the SPW and an after-hyperpolarisation potential appears often after a SPW episode and usually in conjunction with a positive wave in the extracellular recording. The third observation was that SPWs would often elicit APs riding on top of depolarising waves with both usually coinciding with the observed ripples when

present (Figures 4.2.3.A and 4.2.3.B). Some of the nonpyramidal cell APs were only 0.8 ms lagging from the positive peak of the ripples but in most cases depolarisation and APs were in temporal correlation with the extracellular field events (Figures 4.2.3.A and 4.2.3.B). However, not every depolarising wave recorded from the cell contained an AP and this appeared to correlate with a smaller amplitude of the observed ripples (Figures 4.2.3.A and 4.2.3.B). Therefore, it appears that the present cell is engaged in activity during SPWs (Figures 4.2.3.A, 4.2.3.B, 4.2.3.C and 4.2.3.D) and is perhaps prone to control by synaptic influences from pyramidal cells evidenced by ripple amplitude and coinciding of pyramidal cell activity with the diminishing membrane depolarisations observed in the nonpyramidal cell during SPWs (Figures 4.2.3.A, 4.2.3.B and 4.2.2.C).

Figure 4.2.1 In vivo intracellular recording of a nonpyramidal cell (m24) in SO of the CA1 area of the hippocampus. Traces are represented similar to Figure 4.1. **(A)** The resting membrane potential of the cell was –70 mV. During a SPW accompanied by extracellular multiple unit activity, the cell delayed its firing evoked by a 0.7 nA current step of 500 ms. **(B)** A SPW accompanied by multiple unit activity occurring midway through the current-evoked train of APs induced doublet firing (arrows) in the recorded cell. **(C)** Current-evoked responses of the cell during slow wave sleep. Note that the firing rate decreases after about 200 ms.

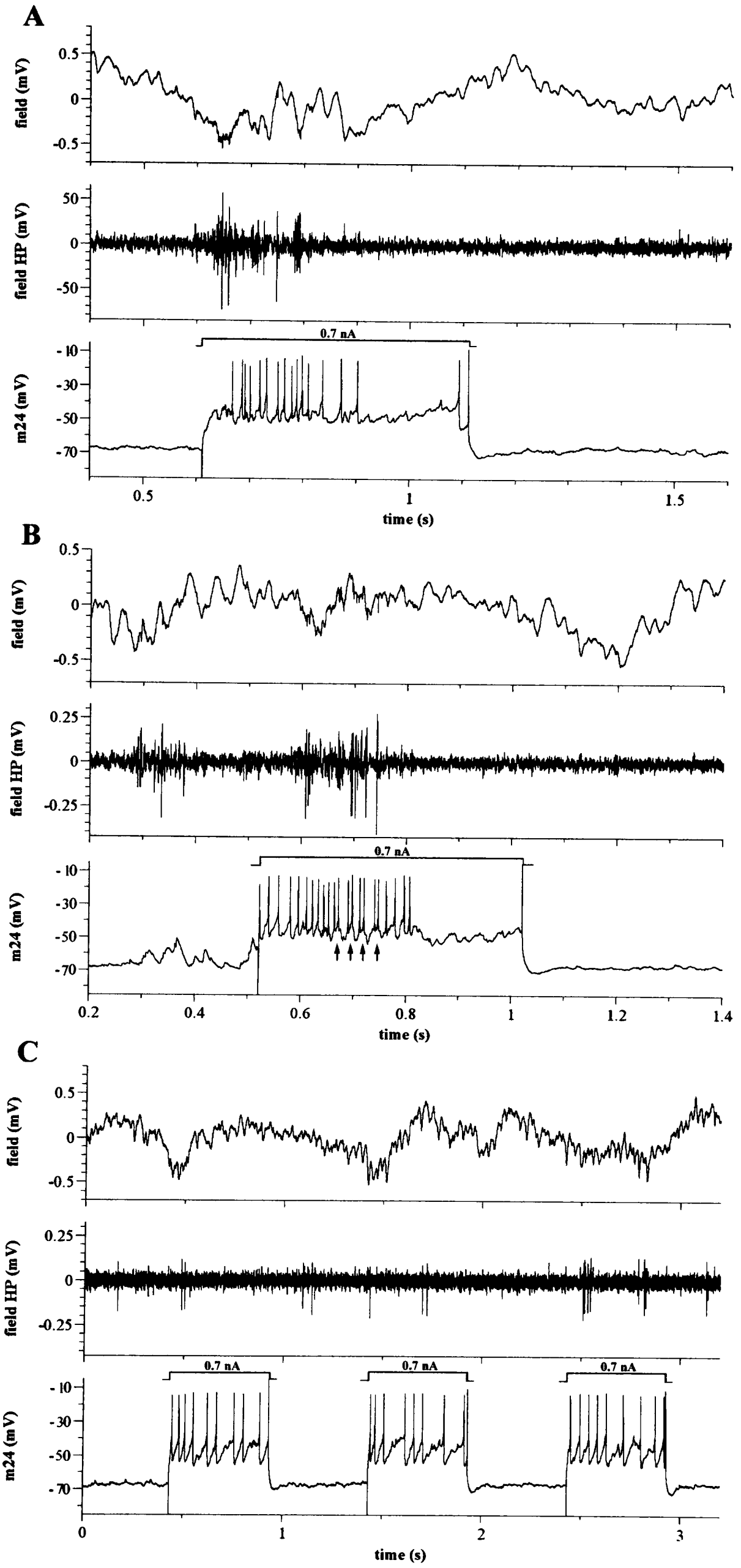
A
field (mV)
0.5
0
-0.5
field HP (mV)
50
0
-50
0.7 nA
m24 (mV)
-10
-30
-50
-70
0.5
1
1.5
time (s)
B
field (mV)
0.5
0
-0.5
field HP (mV)
0.25
0
-0.25
0.7 nA
m24 (mV)
-10
-30
-50
-70
0.2
0.4
0.6
0.8
1
1.2
1.4
time (s)
C
field (mV)
0.5
0
-0.5
field HP (mV)
0.25
0
-0.25
0.7 nA
0.7 nA
0.7 nA
m24 (mV)
-10
-30
-50
-70
0
1
2
3
time (s)

Fig 4.2.1

Figure 4.2.2 Same nonpyramidal cell (m24) as in Figure 4.2.1. **(A)** Evoked θ-like activity (3 Hz) did not correlate with firing of the cell, whereas some of the extracellular unit activity in SP coincided mostly with the negative peaks of the oscillations. **(B)** A SPW evoked an AP in the cell occurring on a relatively small membrane depolarisation in conjunction with the extracellular unit activity. The arrows denote coinciding of intracellular hyperpolarisation with a positive extracellular deflection reflecting outward current. **(C)** A SPW evoked a large depolarisation of the cell, which diminished in decrements. The multiple unit activity appeared to coincide with the membrane depolarisations of the cell. Arrows denote coinciding intracellular hyperpolarisation with outward population currents.

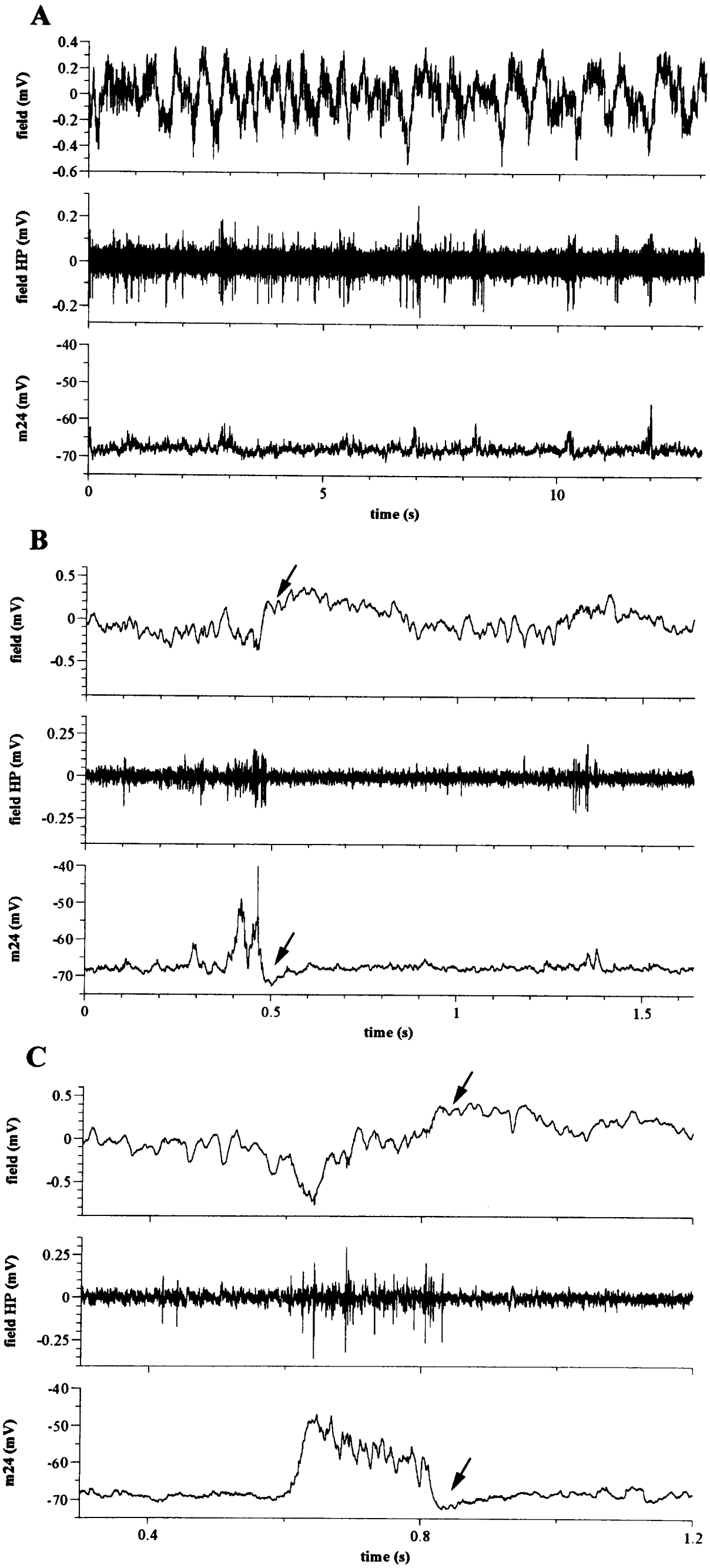
A
field (mV)
field HP (mV)
m24 (mV)
time (s)
B
field (mV)
field HP (mV)
m24 (mV)
time (s)
C
field (mV)
field HP (mV)
m24 (mV)
time (s)

Fig 4.2.2

Figure 4.2.3 Same nonpyramidal cell (m24) as in Figures 4.2.1 and 4.2.2. Arrows denote the coinciding population outward current with the return to resting membrane potential (-70 mV) or hyperpolarisation of the cell. **(A)** Clear ripples observed during a SPW with shorter amplitude ripples coinciding with the absence of APs on depolarising waves in the cell (star *). **(B)** Another SPW with clear ripples producing a similar mode of activity as in (A). The nonpyramidal cell fired APs, which had a maximum lag of 0.8 ms from the ripple peak to the peak of the APs. **(C)** The cell fired APs riding on a membrane depolarisation, which lasted as long as the SPW. Action potential firing increased concomitantly with the occurrence of ripples. **(D)** A SPW evoked similar activity as in (C) but with a different recruitment of multiunit activity.

Fig 6

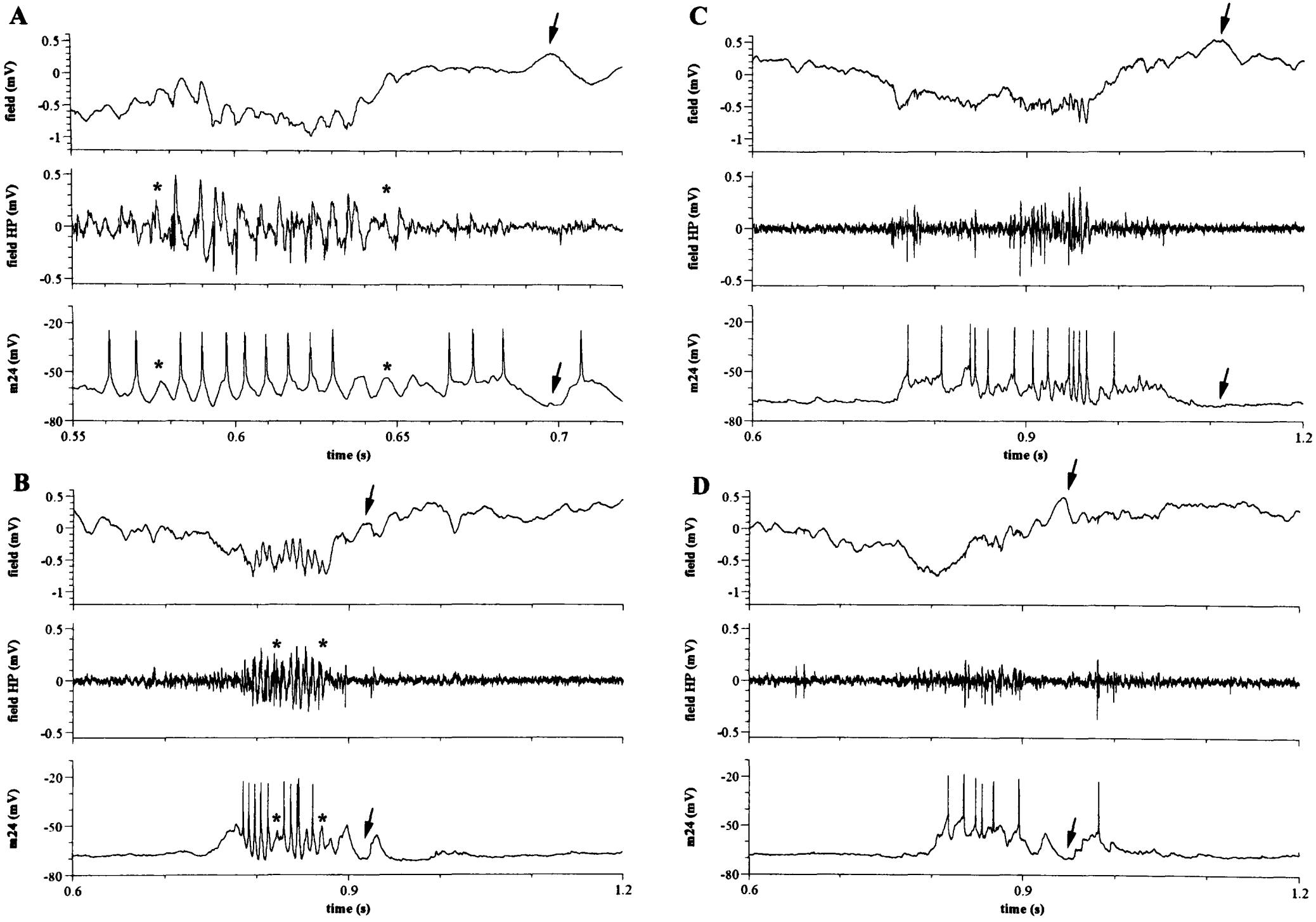
A
B
C
D
field (mV)
field HP (mV)
m24 (mV)
time (s)
0.5
0
-0.5
-1
-20
-50
-80
0.55
0.6
0.65
0.7
0.9
1.2

The third intracellularly recorded nonpyramidal cell (d150) showed different responses during SPW activity and in this case, θ-frequency oscillations could not be elicited. Based on the cell's widespread axonal projections it will be referred to as a projection cell. During 1 nA current pulses of 500 ms duration, the hyperpolarisation observed during a SPW appeared greater than the excitatory drive of the cell which had a resting membrane potential of –72 mV (Figure 4.3.1.A). Multiunit activity was not always accompanied by a sharp extracellular voltage deflection reflecting a SPW but could elicit, in the projection cell, a single AP followed by a relatively long duration hyperpolarisation resulting from synaptic inhibition (Figure 4.3.1.B). The delayed onset of the evoked train of APs (Figure 4.3.1.B) resulted from synaptic inhibition arising during the occurrence of multiunit activity. This is confirmed by the fact that hyperpolarisation of the cell membrane negative to that observed during the train of AHPs, suggesting a synaptic origin, always occurred during prominent multiunit activity (Figures 4.3.1.A and 4.3.1.B). Several reasons indicate that the multiunit activity resulted from a SPW. Firstly, the multiunit activity present (Figure 4.3.1.B) was similar to that observed during a SPW deflection (Figure 4.3.1.A). Secondly, the projection cell usually fired a single AP followed by a relatively long duration hyperpolarisation during SPWs (Figure 4.3.2.B). Thirdly, SPWs may or may not be observed as a sharp deflection depending on the strength of the excitatory drive. Fourthly, as the strongest dipole observed during the SPW occurs in SR (Ylinen et al. 1995a), the position of the electrode closer to SO would support the third reason. Further observations were that the absence of extracellular unit activity coincided with the hyperpolarisation or lack of firing of the projection cell as well as the positive deflection of slow oscillatory waves indicative of inhibitory influences (Figure 4.3.2.A). Whereas the previous recorded cell (m24) appeared to be activated by nearby pyramidal cells, the present cell (d150) appears to be influenced differently. For instance, inhibition of nearby pyramidal cells could have rendered

the projection cell (d150) silent during the observed positive deflection within the SPW event (Figure 4.3.2.A). Also, direct inhibition was frequently observed as periods of hyperpolarisation of the projection cell during a SPW (Figure 4.3.2.B). Sometimes the projection cell fired several APs during a SPW although this did not occur often (Figure 4.3.2.C). Stimulation in the hippocampal commissure (0.2 mA; 50 μs) evoked an AP in the cell 1.6 ms after the prominent excitatory population depolarisation (Figure 4.3.2.D). There was a lack of an antidromic response observed from both the extracellular and intracellular recordings indicating that the cells recorded did not project to the area of stimulation.

Figure 4.3.1 In vivo intracellular recording of a projection cell (d150) in SO of the CA1 area of the hippocampus. Traces are represented similar to Figure 4.1. A current step of 1 nA applied for a duration of 500 ms evoked a train of APs in the projection cell having a resting membrane potential of–72mV. **(A)** A SPW evoked a fast accommodation and hyperpolarisation during a current-evoked train of APs. **(B)** A single AP response (arrow) followed by a relatively long duration hyperpolarisation resulting from synaptic inhibition was evoked by the multiunit activity. Note that the prominent multiunit activity, also observed as fast oscillations in the field trace, indicates that the simultaneous extracellular voltage deflection is a SPW.

A

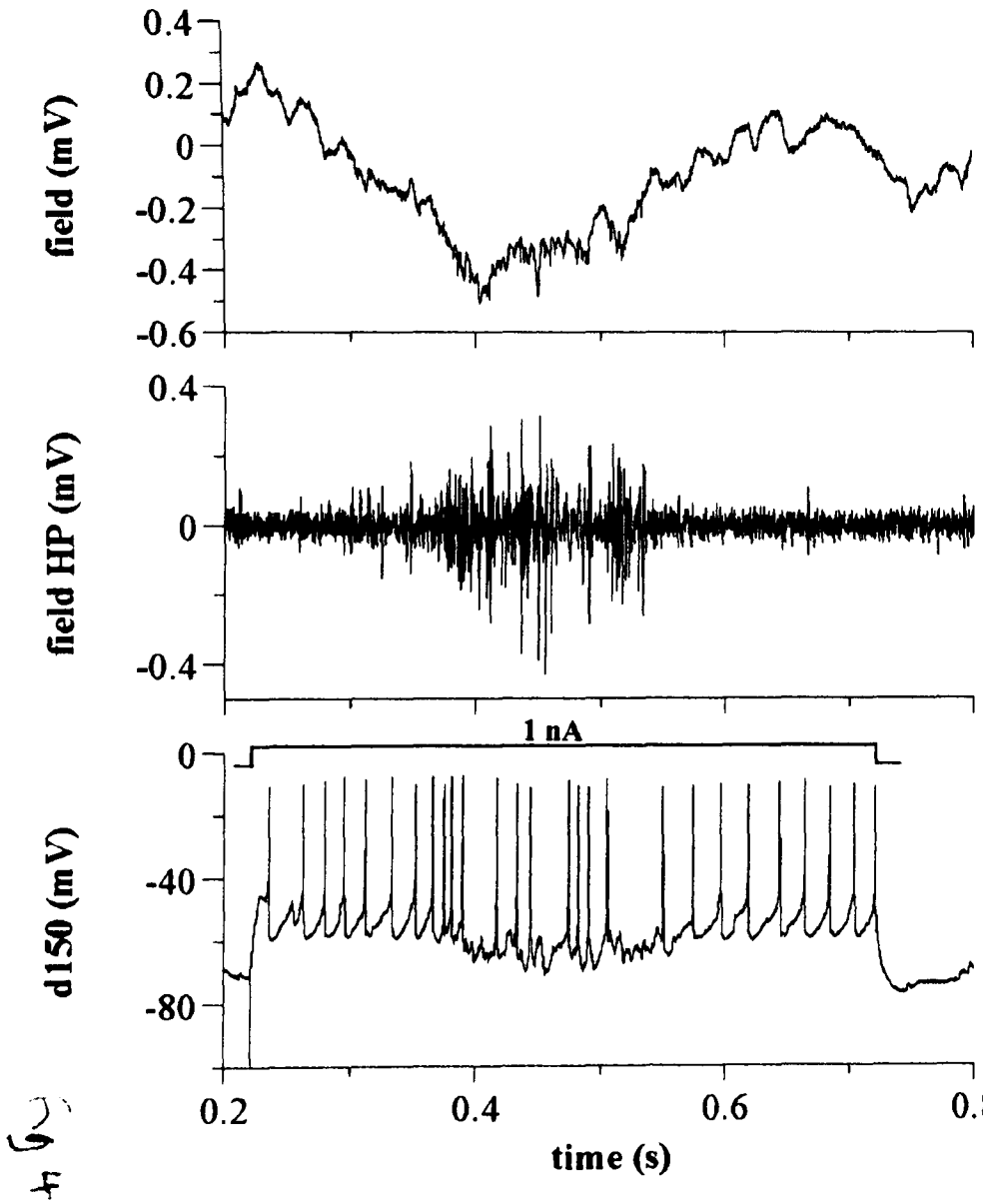
field (mV)
0.4
0.2
0
-0.2
-0.4
-0.6
field HP (mV)
0.4
0
-0.4
d150 (mV)
1 nA
0
-40
-80
0.2
0.4
0.6
0.8
time (s)

B

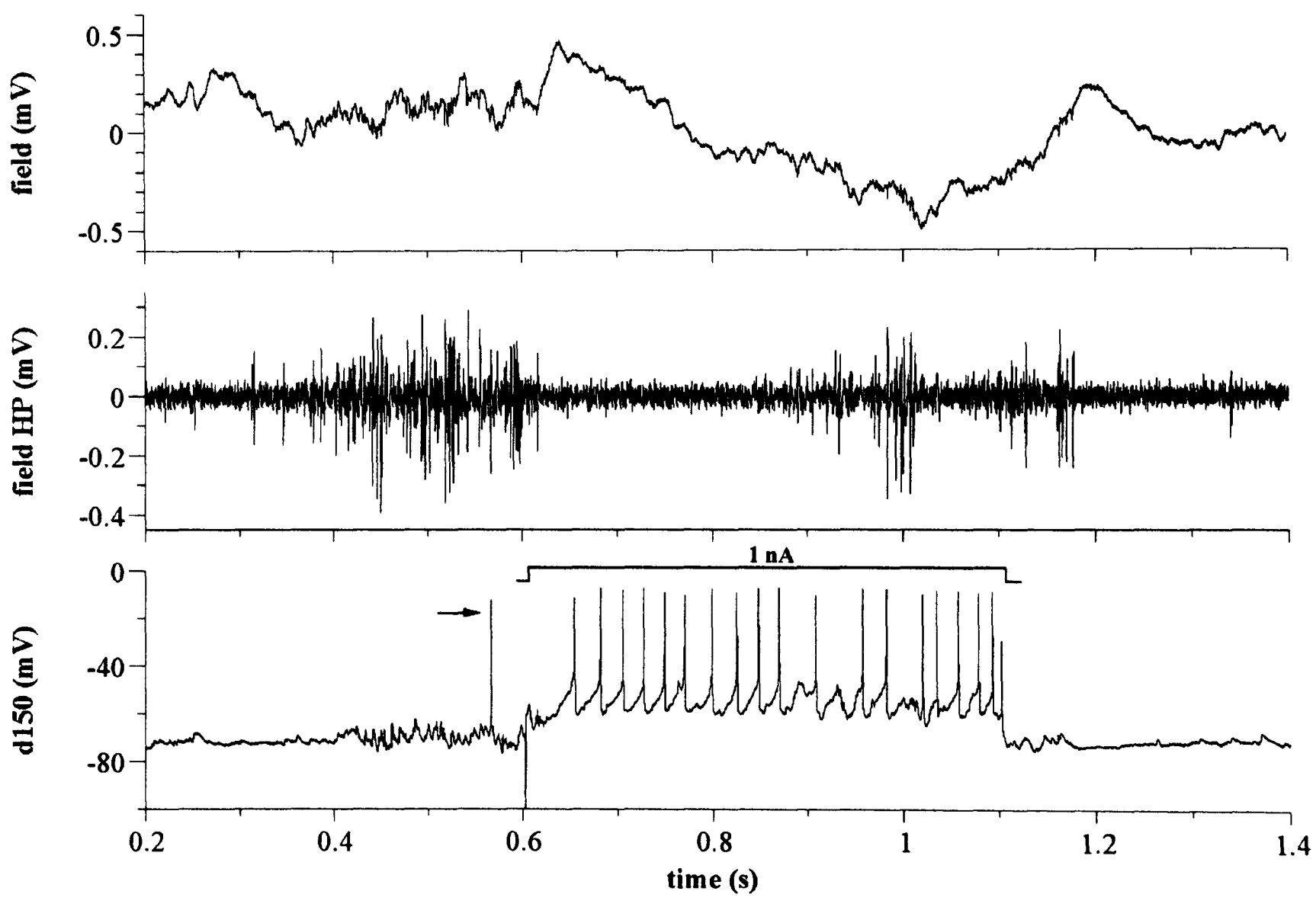
field (mV)
0.5
0
-0.5
field HP (mV)
0.2
0
-0.2
-0.4
d150 (mV)
1 nA
0
-40
-80
0.2
0.4
0.6
0.8
1
1.2
1.4
time (s)

Figure 4.3.2 Same projection cell as in Figure 4.3.1. **(A)** The cell fires single APs during epochs of extracellular unit activity during a SPW. **(B)** Typical response of the projection cell during a SPW: a single AP preceded and followed by hyperpolarisation of the membrane potential. **(C)** A SPW produces a mixture of hyperpolarisation and AP firing in the cell. **(D)** Stimulation (star *; 0.2 mA; 50 μs) in the hippocampal commissure produces a prominent excitatory population potential observed in the extracellular recording (arrow). This was followed (1.6 ms) by an AP evoked in the projection cell.

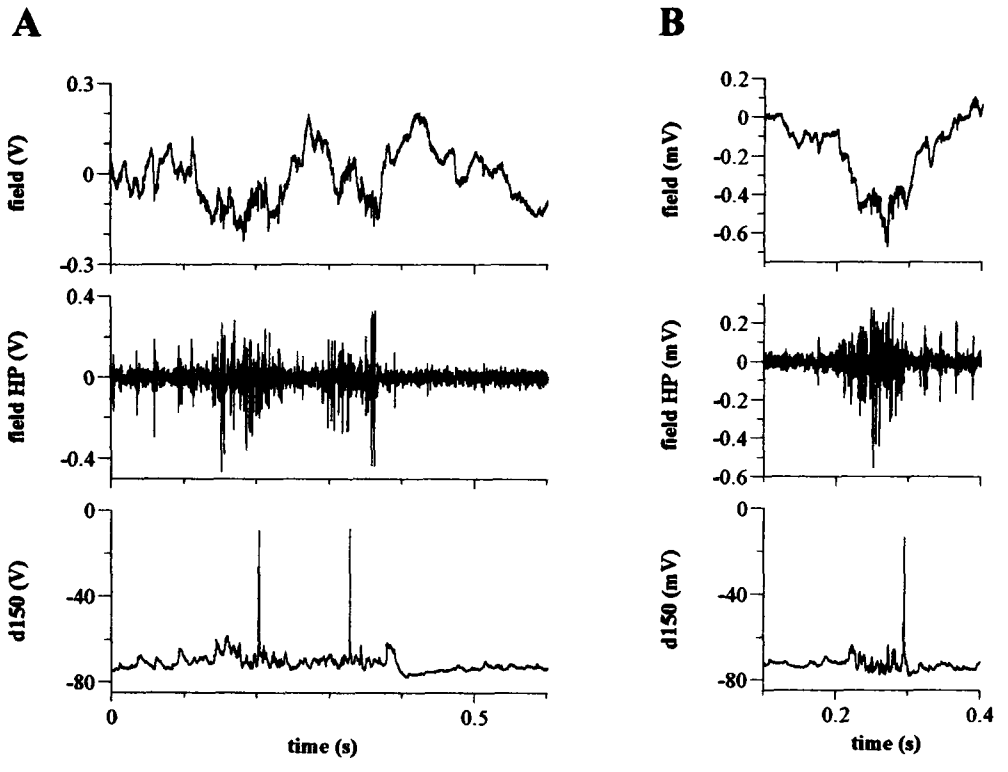
A
field (V)
field HP (V)
d150 (V)
time (s)
B
field (mV)
field HP (mV)
d150 (mV)
time (s)
C
field (mV)
field HP (mV)
d150 (mV)
time (s)
D
field (mV)
field HP (mV)
d150 (mV)
time (ms)

Fig 4.3.2

The last nonpyramidal cell (mt47) was recorded juxtacellularly (Figure 4.4) and an agonist acting at AMPA and group I mGluRs (L-Quisqualic acid) was used to detect otherwise 'silent' cells in the SO region as the electrode was stepped into the hippocampus. The juxtacellular recorded cell fired only after a barrage of extracellular unit activity and the cell's (mt47) firing did not last for the entire ejection of the agonist. Therefore, it is likely that the cell (mt47) was influenced indirectly by cells nearby which were directly activated by the agonist. The cell rarely fired APs amidst the surrounding activity indicating the specificity of this cell to particular inputs. Theta-frequency field oscillations (6 Hz; 5 to 10 s) were evoked three times during recording of the cell, however, the cell always remained 'silent'.

Figure 4.4 In vivo juxtacellular recording and reconstruction of a presumed VIP/calretinin expressing cell in SP of the CA1 area of the dorsal hippocampus. The top two traces are APs of the cell evoked by L-quisqualic acid, the AMPA and group I mGluR agonist, at slower and faster time scales, respectively. The large arrow denotes continuous application of the drug to termination. The small arrow denotes the AP represented in the faster time scale. The bottom four traces are the electrocardiogram (ECG) recording; extracellular wide band pass recording in SP/SR; the juxtacellular wide band pass recording in SP and the juxtacellular high pass recording of the cell. The arrow denotes the start and end of the tail pinch, which evoked field θ activity (6Hz). During θ-frequency field oscillations, the cell was 'silent'. The cell has four main beaded, radial dendrites terminating in tufts in SO and SL-M. The soma is relatively small and fusiform. The main axon descends into SR and branches from SR to SL-M and projects back to SO, densely innervating the alveus. The axon was weakly filled and could only be partially reconstructed in SO/alveus.

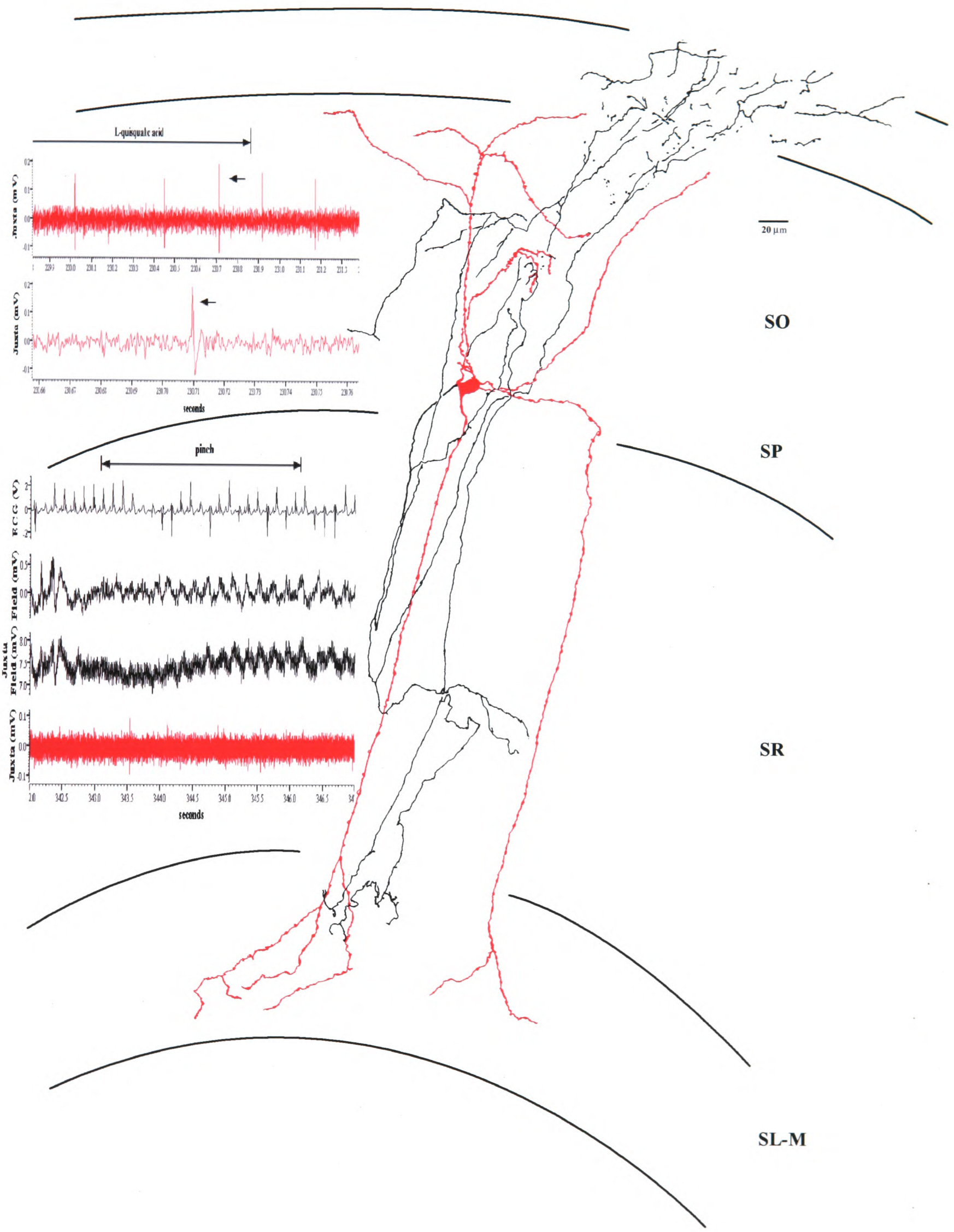
L-quisqualic acid
Juxta (mV)
seconds
pinch
ECG (V)
Field (mV)
Juxta Field (mV)
Juxta (mV)
seconds
20 µm
SO
SP
SR
SL-M

Fig 4-4

4.3.2 Anatomical Analysis of Nonpyramidal Cells Recorded In Vivo

In order to relate the observed cellular activity to the underlying circuitry, cells were labelled and anatomically analysed. The soma and dendrites of one cell (m11) were not recovered after histological processing. The axon, however, was labelled and its projections were similar to previously described backprojection cells recorded in vivo (Sik et al. 1994, 1995). The main axon, bifurcated and radially projected to the SL-M border. At the SL-M border the farthest radial branch became oriented diagonally and produced a tangential collateral along the SL-M border, which reached the CA3a area forming collaterals in SR. The other branch continued diagonally in the same direction crossing the upper blade of the dentate gyrus and forming several collaterals in the hilus. The present cell also had few collaterals in SO as well as a tangential axon collateral along the alveus. On the basis of its projection to the CA3 area and hilus, this cell appears to be a backprojection cell similar to two previously recorded cells (Sik et al. 1994, 1995) although this cannot be unequivocally established due to the missing somatodendritic area and the limited extent of the recovered axon. The present cell has a biased axonal direction, both in its projection to the CA3 area as well as the hilus. However, the weak labelling of the cell could have accounted for bias in axonal direction due to missing collaterals.

The second cell (m24) was not recovered after histological processing, therefore its firing modulation during SPWs could not be interpreted in terms of connections. The third cell (d150) had similar anatomical features to two O-Bi cells recorded in vitro with large somas. For example, large somatodendritic domain including tangential and radial dendrites in SO, widespread axon collaterals in SR including one tangential collateral along the SR and SP border and two axonal branches in the alveus projecting caudolaterally towards the dorsal subiculum. Sections more caudal were lost and so it is not known whether the axon entered the entorhinal cortex. The projection towards the subiculum is similar to the axonal projection in SO

towards the subiculum for one of the O-Bi cells (M1011) recorded in vitro. In addition to these similar features, the projection cell (d150) had some boutons in SP and two axonal branches along with collaterals in SR and SL-M reaching the most rostral tip of the CA3 area, presumably continuing to the septum or commissurally, although sections further rostral were lost to confirm this.

The last cell labelled in vivo (mt47) was juxtacellularly recorded. This cell had anatomical characteristics similar to previously studied VIP positive CA1 hippocampal cells (Acsady et al. 1996a). Features such as the ascending axon originating proximally in SP and innervating SO as well as four primary dendrites, which branched distally from the soma forming a tuft in SL-M and SO, were evident in the cell recorded in vivo (Figure 4.4). Additionally, the cell (mt47) had dense axonal innervation in the alveus and smaller axonal arborisations in SR reaching SL-M (Figure 4.4), which were missed in the previous reports (Acsady et al. 1996a) due to the different preparations.

4.3.3 Anatomical Characteristics of VIP and Calretinin Immunopositive Cells

As there are no previous reports on recordings or single cell labelling of any cell similar to the above cell (mt47), I compared its dendritic and axonal arbours to cell populations labelled by antibodies to VIP and calretinin. Similarities between the cell labelled juxtacellularly (mt47) and calretinin-positive cells are presented using a reconstruction of a calretinin-immunopositive cell (Figure 4.5). An antibody to calretinin was used instead of an antibody to VIP for two reasons. One is that full labelling of the dendritic and at least partial axonal tree can be achieved with the calretinin antibody. Secondly, calretinin has been shown to co-localise preferentially with VIP in cells densely innervating the border of SO and the alveus (Acsady et al. 1996a). All VIP positive boutons in the SO/alveus border have been shown to innervate only other GABAergic cells (Acsady et al. 1996b).

Figure 4.5 Reconstruction of a calretinin-immunopositive cell in the CA1 area of the adult rat dorsal hippocampus. Similar to the juxtacellularly recorded cell, this cell is characterised by beaded, radial dendrites with terminating tufts in SO and SL-M. The soma was relatively small and round. The axon branced in SR and projected back to SO.

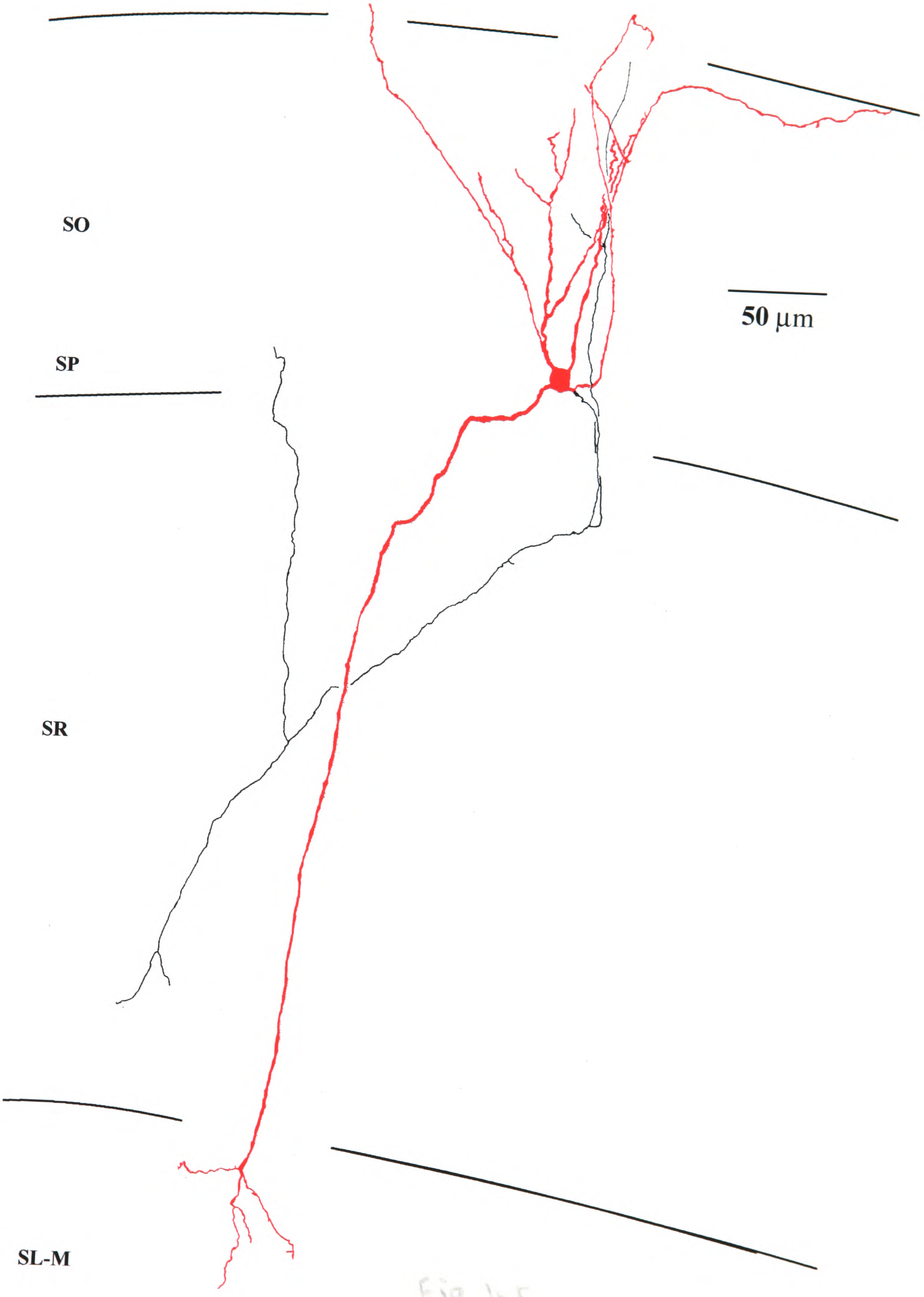

Fig 4.5

4.3.3.1 Co-localisation of VIP and Calretinin in Nonpyramidal Cells

The cell labelled juxtacellularly (mt47) was not tested for neurochemical characteristics, but its axonal and dendritic features suggest that it was an interneurone selective type III cell (Freund and Buzsaki 1996). These have been reported to express calretinin and VIP (Acsady et al. 1996a, 1996b). If the cell labelled juxtacellularly (mt47) was a member of this population, then its somatic area would fall into the range pertaining to cells expressing both calretinin and VIP. However, calretinin and VIP are not completely co-localised. Therefore, I first tested the extent of co-localisation of the two proteins, then I measured the soma area of the different populations. In order to test the extent of colocalisation of calretinin and VIP in the layers having such cells which innervate SO/alveus (i.e. SP and proximal SR), double immunofluorescence was performed on adult rat hippocampal sections and quantified in the CA1 area of the dorsal hippocampus close to SP. Out of a total of 70 cells counted, 43 % were both VIP- and calretinin-positive, 13 % were VIP-positive only and 44 % were calretinin-positive only (Figure 4.8). Therefore, most cells encountered either contain both VIP and calretinin or calretinin only. Out of the total VIP positive cells counted, 77 % also contained calretinin immunoreactivity and out of the total calretinin-positive cells counted, 49 % also showed VIP immunoreactivity. It is thus more likely for a cell with VIP to also contain calretinin than vice versa. VIP-immunolabelled images for calretinin and VIP immunofluorescence are presented along with immunoperoxidase labelling for several calretinin positive cells with similar anatomical characteristics to the cell (mt47) recorded juxtacelluluarly (Figure 4.4 and 4.6). Cells immunolabelled for VIP only, calretinin only and both VIP and calretinin were measured for the area of the soma along with the juxtacellularly recorded cell (Figure 4.7). Typically, cells positive for VIP only had the largest somatic area (172.7 ± 44.6 μm^2; n=9) followed by cells positive for calretinin only (130.2 ± 31.2 μm^2; n=31) and lastly

cells positive for both VIP and calretinin (92.6 ± 20.0 μm^2; n=30; Figure 4.9). After testing for shrinkage of tissue caused by the dehydration process, it was found that there was no significant difference in shrinkage measured for cells in ten sections during immunofluorescence and after histological processing (P=0.11; Wilcoxon Signed Rank). Therefore, a shrinkage factor was not needed for the comparison of the somatic area obtained for the cell recorded juxtacellularly (109.2 μm^2), which deviated least from the mean area of the cells expressing both VIP and calretinin (Figure 4.9). Although there was overlap between the three groups in somatic area, it is unlikely that the recorded cell (mt47) could only express VIP alone because its somatic area deviated out of the SD range calculated for cells expressing VIP only (Figure 4.9).

Figure 4.6 Immunolabelling of VIP- and calretinin-positive cells in the CA1 area of adult rat dorsal hippocampus. The left column shows immunofluorescence images of cells positive for calretinin and/or VIP. Arrows show cells labelled for both calretinin and VIP. The right column shows cells expressing calretinin after processing by the immunoperoxidase method. Note that the dendritic distribution of cells is very similar to the reconstructed juxtacellularly labelled cell in Figure 4.4. Scale bar is 50 μm.

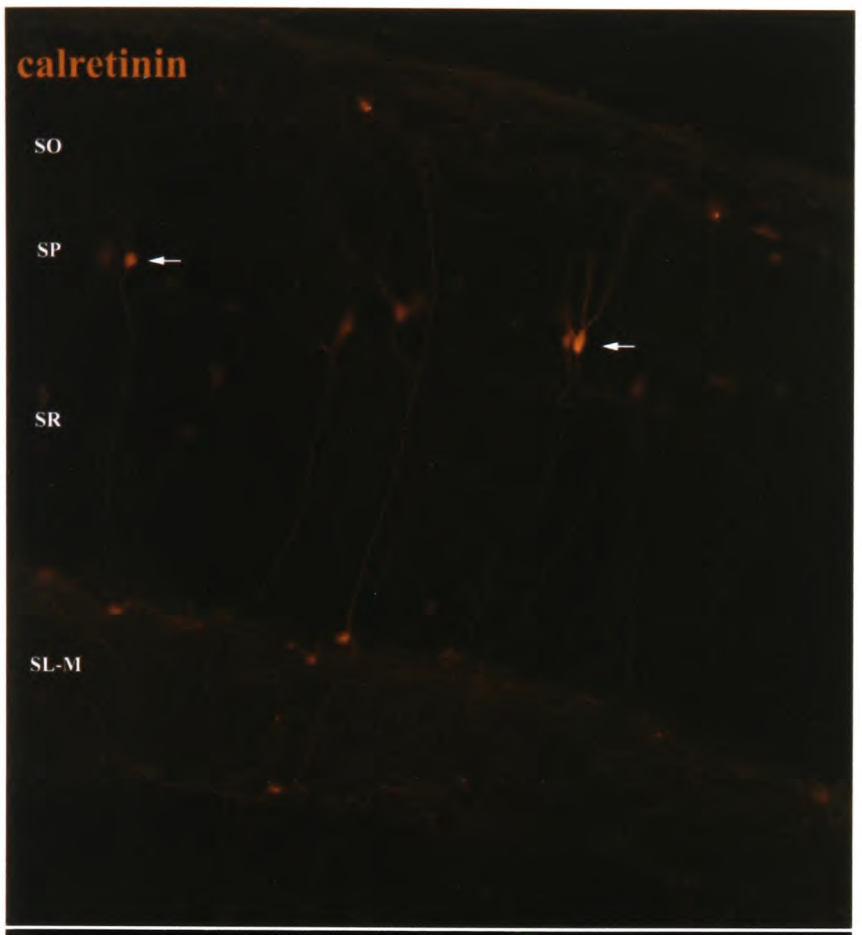

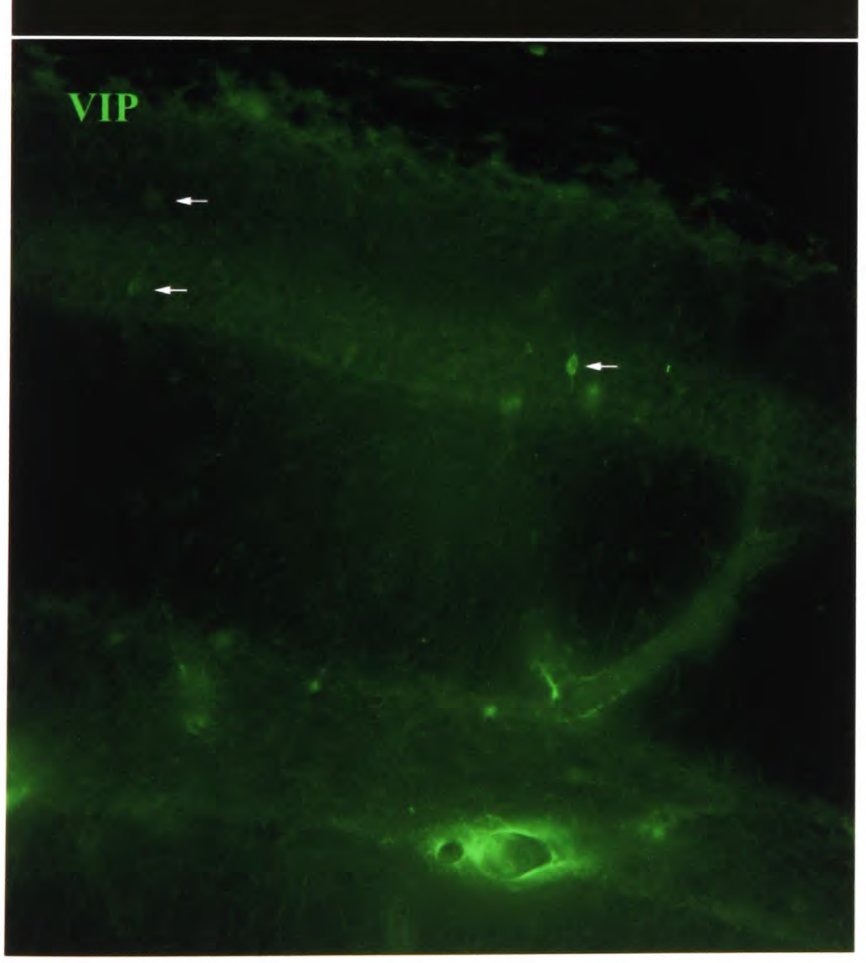

50 µm

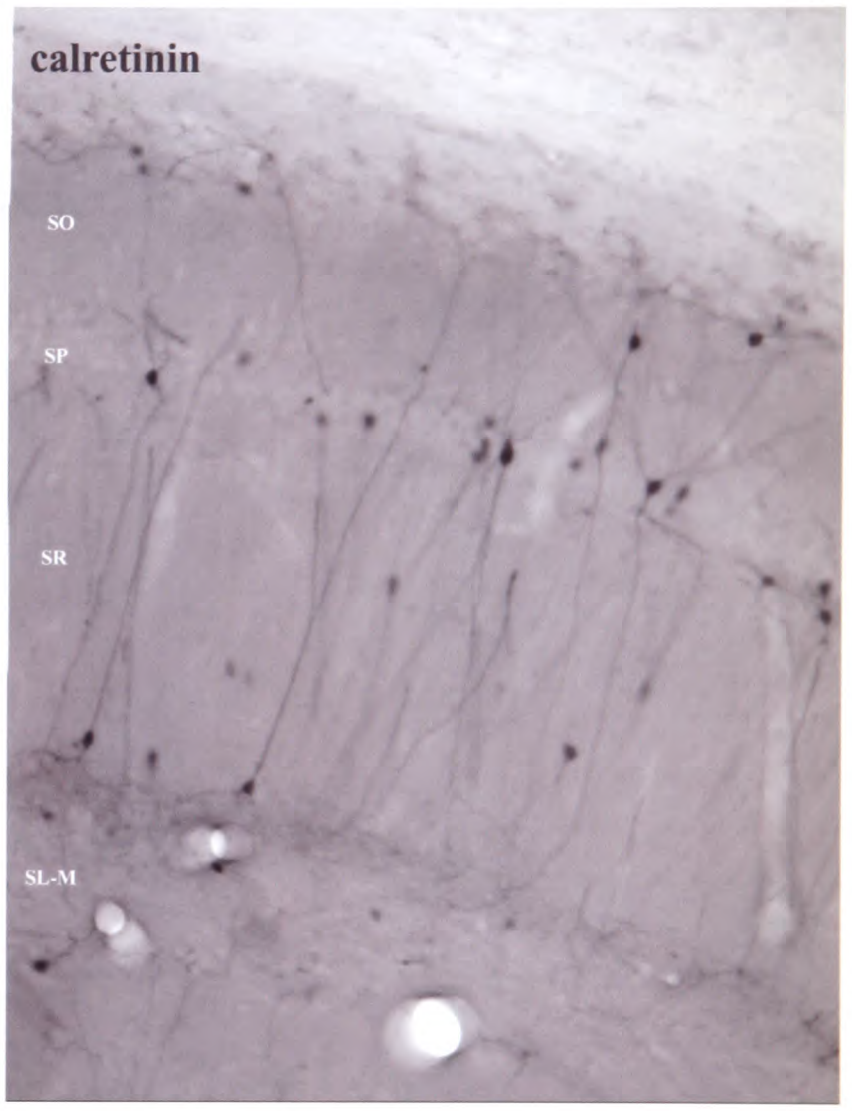

Fig 4.6

Figure 4.7 Measurements of somatic area of calretinin- and/or VIP-immunolabelled cells near SP from the CA1 area of adult rat dorsal hippocampus. The left column shows images of cells immunopositive for both calretinin and VIP with designated somatic area. The bottom image is a superposition of the top two. The middle column shows images of a cell immunopositive for calretinin only with designated somatic area. The last column shows images of a cell immunopositive for VIP only with designated somatic area. Scale bar is 25 μm.

VIP positive

calretinin positive

VIP positive
calretinin positive

92 μm²

VIP negative

calretinin positve

128 μm²

25 μm

calretinin negative

VIP positive

214 μm²

Figure 4.8 Proportion of cells co-localising VIP and mGluR1α (top) or VIP and calretinin (bottom) in and close to stratum pyramidale of the CA1 area in the adult rat dorsal hippocampus. Percentages were obtained with respect to the total VIP cells and total mGluR1α or total calretinin immunoreactive cells, and the total cells counted for both groups (top and bottom).

PROPORTION OF VIP AND/OR mGluR1α IMMUNOREACTIVE CELLS IN AND CLOSE TO STRATUM PYRAMIDALE OF THE CA1 AREA

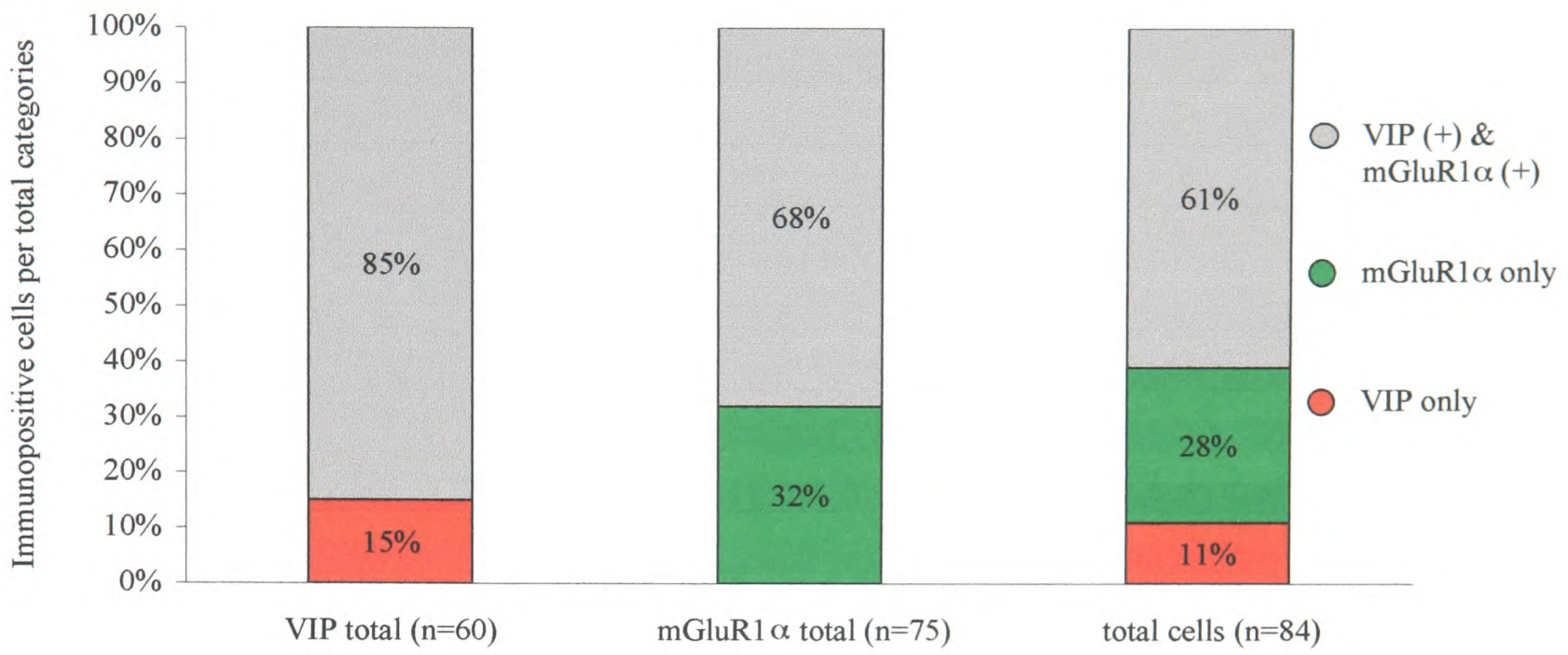

PROPORTION OF VIP AND/OR CALRETININ IMMUNOREACTIVE CELLS IN AND CLOSE TO STRATUM PYRAMIDALE OF THE CA1 AREA

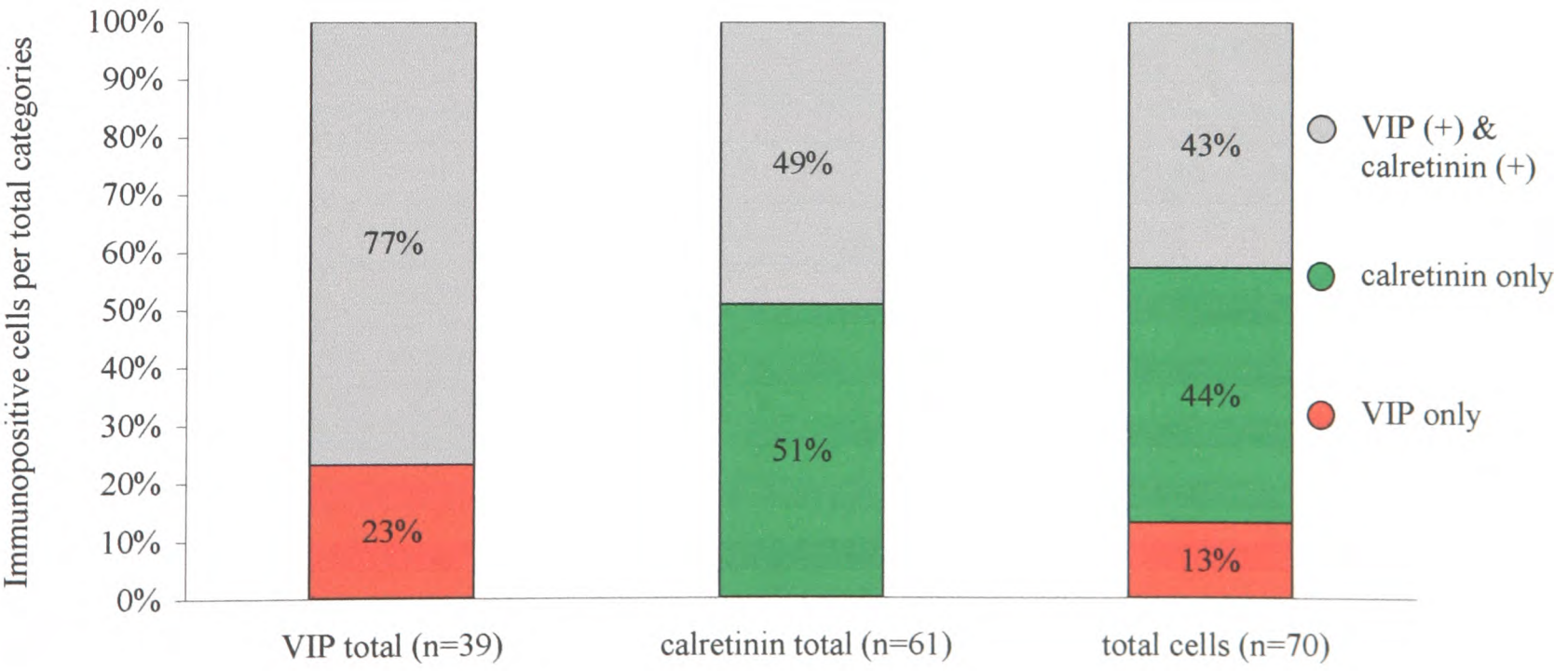

Fig 4.3

Figure 4.9 Graphic representation of projected somatic areas for calretinin- and/or VIP-immunopositive cells. The somatic area of the juxtacellularly labelled cell deviated least from the mean of the somatic area of cells expressing both calretinin and VIP, although there is overlap between all three groups. Note that the deviation of the somatic area for the juxtacellularly labelled cell fell outside of the SD range of cells expressing VIP only (40%).

Somatic area μm²	VIP only	VIP + cal.	cal. only
Mean	172.7	92.6	130.2
SD	44.6	20.0	31.2
n	9.0	30.0	31.0

Juxta cell area (μm²)

109.2

difference from mean	63.5	16.6	21.0
ratio from SD	0.4	0.2	0.3

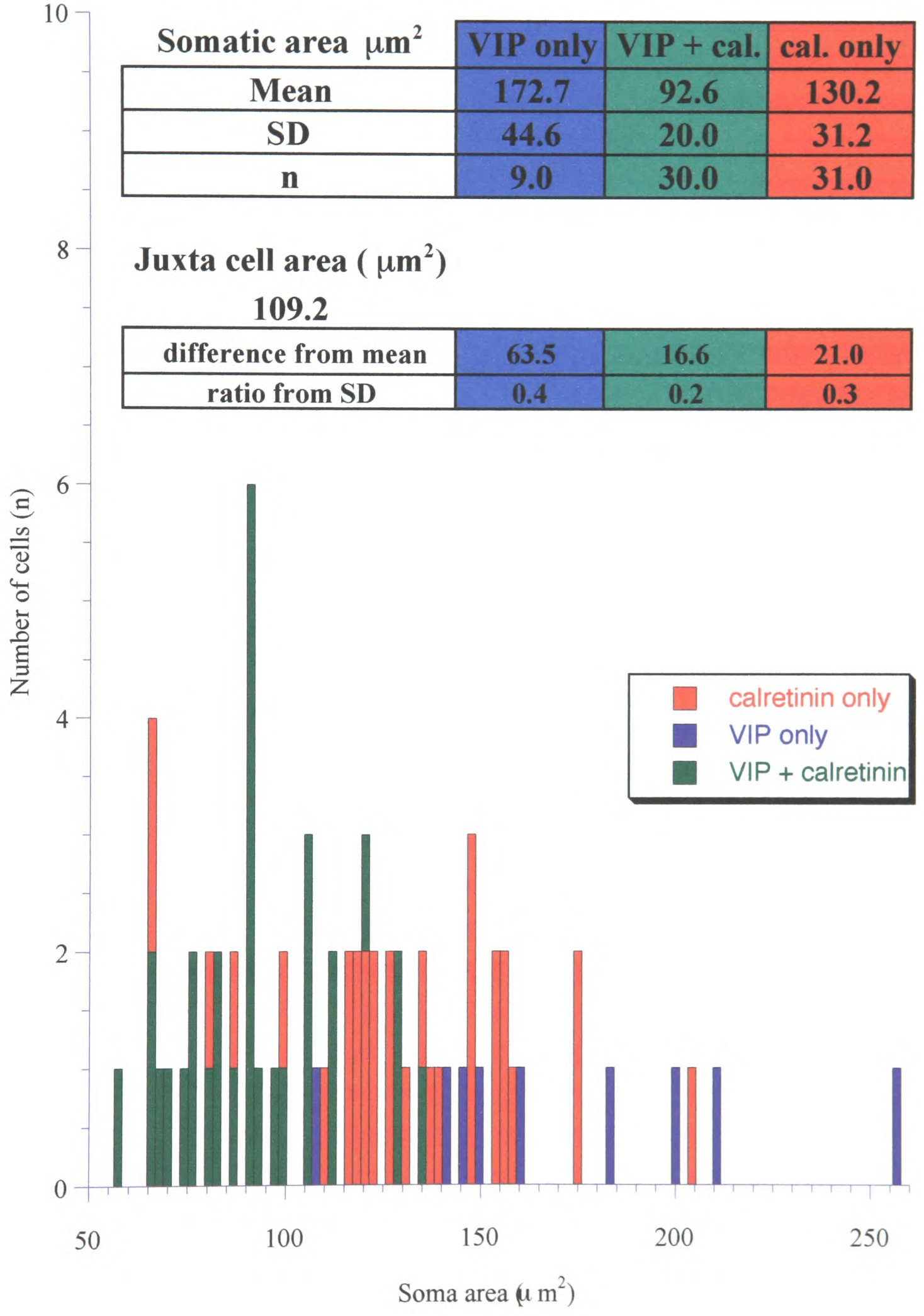

Fig 4 a

4.3.4 Co-localisation of VIP and mGluR1α in Nonpyramidal Cells

Several of the in vivo recorded cells (mt47, m24 and d150) are either silent or inhibited during extracellular θ activity or SPWs. As group I mGluRs have been shown to be involved in oscillatory activity via Ca^{2+} mobilisation in SO nonpyramidal cells of the hippocampus (Woodhall et al. 1999), the next experiment was performed to determine whether cells expressing VIP also expressed mGlu receptors. In particular, mGluR1α receptors were studied because they are abundantly expressed by cells also expressing somatostatin in SO/alveus (Baude et al. 1993) and these cells are innervated by cells expressing VIP and calretinin (Acsady et al. 1996a, 1996b). Out of a total of 84 cells counted in the CA1 area of the dorsal hippocampus close to SP, 61 % were both VIP- and mGluR1α-positive, 11 % were VIP-positive only and 28 % were mGluR1α-positive only (Figure 4.8; Figure 4.10). Therefore, most of the VIP-positive cells express mGluR1α. This is apparent in the extent of co-localisation with respect to the total VIP cells counted (85 %) and the total mGluR1α cells counted (68 %).

Figure 4.10 Immunofluorescence images of VIP (red) and mGluR1α (green) positive cells in the CA1 area of adult rat dorsal hippocampus. Arrows denote co-localisation of VIP and mGluR1α immunoreactivity. Triangle denotes an mGluR1α-immunopositive cell, which was immunonegative for VIP. Scale bar is 25μm.

IMMUNOFLUORESCENCE IMAGES OF VIP AND/OR mGluR1α POSITIVE CELLS IN STRATUM PYRAMIDALE OF THE CA1 AREA

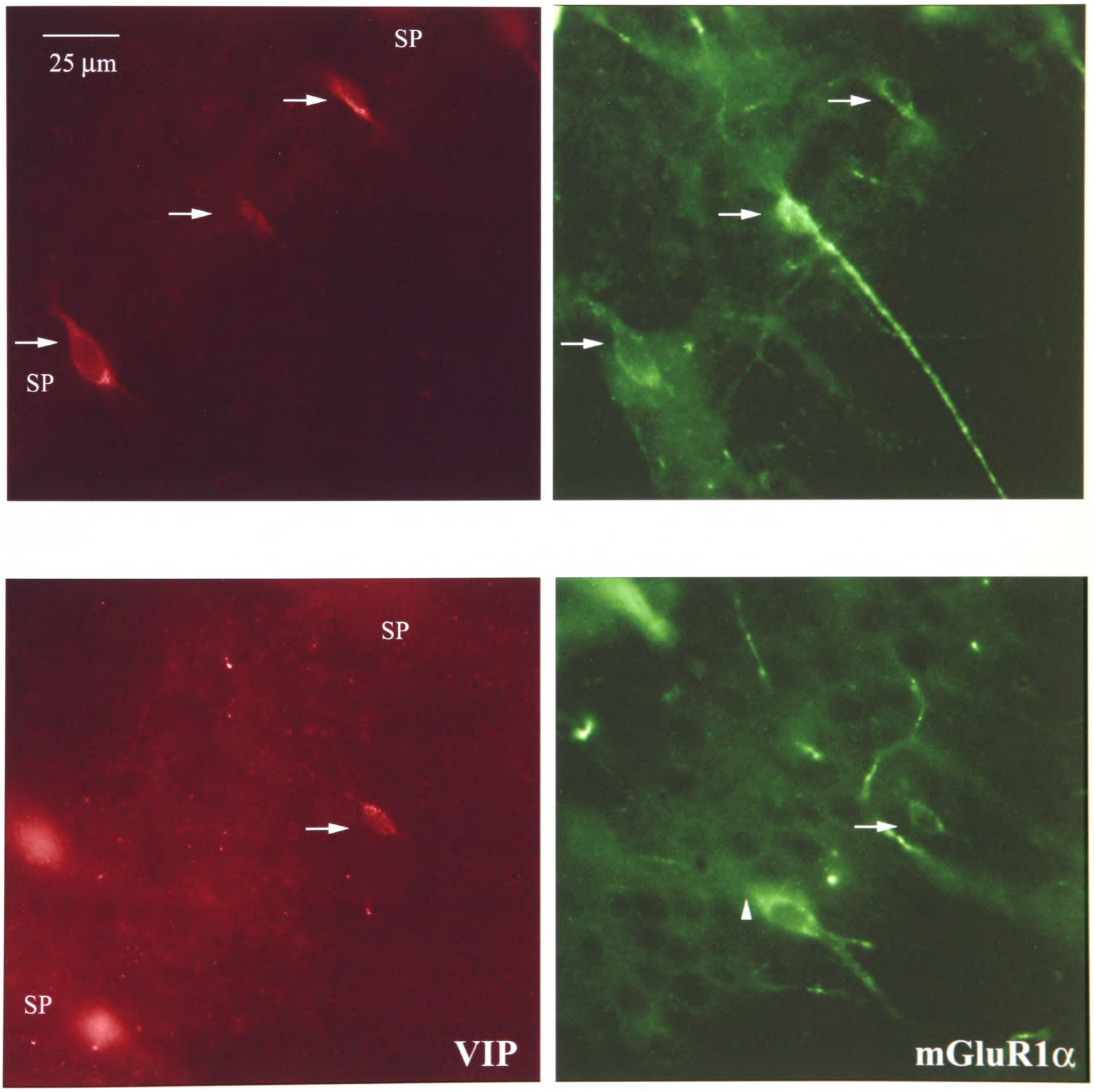

Fig 4.10

4.4 Discussion

4.4.1 State-dependent Modulation of Nonpyramidal Cell Activity

Overall, the recordings of nonpyramidal cells obtained during θ-frequency field oscillations under urethane anaesthesia are different from previous findings in unanaesthetised animals (Csicsvari et al. 1999). For instance, only one nonpyramidal cell was entrained into θ-frequency bursts of APs whereas the activity of the other three nonpyramidal cells was unaltered during θ-frequency field oscillations. Given that nonpyramidal cells in SO/alveus were shown to increase their activity during θ episodes (Csicsvari et al. 1999), it is interesting that a glutamate receptor agonist but not θ-frequency evoked activity could elicit neuronal firing in SO/alveus cells, which were otherwise 'silent' when searching for cells during juxtacellular recordings. Three possibilities could explain these contradictory findings. Firstly, the cells recorded may in fact pertain to a minority group of cells, which are not modulated by θ-frequency activity. Secondly, a lower resistance electrode used in the previous study (Csicsvari et al. 1999) could have been more amenable to recording activity amongst such widely-spaced cells found in SO. Thirdly, anaesthesia could have caused the lack of θ-frequency dependent modulation in the activity of the present nonpyramidal cells recorded. The latter is supported by a previous study showing that cells with high frequency firing increase their firing rates during atropine-resistant but not atropine-sensitive θ-frequency activity in rabbits (Sinclair et al. 1982). The most parsimonious explanation however, is that the present recorded cells constitute a separate group of cells because they showed minimal spontaneous activity throughout the recording time.

During SPWs, the variability of SO/alveus nonpyramidal cell activity (Csicsvari et al. 1999) was evidenced in the two presently recorded cells. For instance, some SO/alveus nonpyramidal cells increase their firing rates during SPWs whereas others decrease their firing

rates (Csicsvari et al. 1999). The advantage of the present study is that it includes information on membrane potentials during population activity. Neither cell in the present study decreased its firing rates during SPWs but one cell (d150) exhibited more hyperpolarisation or absence of firing. The absence of firing usually corresponded to periods without multiunit activity, indicating a direct influence from presumed pyramidal cells when the nonpyramidal cell (d150) was firing. The other nonpyramidal cell (m24) also likely received a direct influence from presumed pyramidal cells as it showed little lag of APs with respect to ripple activity and the amplitude of ripples appeared to determine the occurrence of an AP in the nonpyramidal cell. It was also observed that the activity of both nonpyramidal cells recorded was strongly curtailed by recruited network inhibition resulting from SPW activity. This was evidenced by the correspondence between extracellular positive voltage deflections reflecting outward current and the hyperpolarisations of the recorded cells.

4.4.2 Mechanisms for Modulation by Population Activity

One nonpyramidal cell recorded (m11) was entrained into θ-frequency burst of APs when θ-frequency field oscillations were evoked. Furthermore, the AP threshold was lowered and the amplitude increased at the centre of the burst of APs in correspondence to the negative peak of the extracellular θ-frequency waves. Overall, AP amplitude was small, indicating a dendritic recording. In light of existing evidence for pyramidal cells, it is possible that a persistent Na^+ channel (I_{NaP}) could have been involved in amplifying backpropagating APs (Lipowsky et al. 1996). Indeed, I_{NaP} channels are activated at lower thresholds than transient Na^+ channels and computer simulations showed that stronger synaptic potentials (i.e. during the negative peak of the θ-frequency waves) are more enhanced by I_{NaP} channels (Lipowsky et al. 1996). Moreover, previous work has demonstrated that the I_{NaP} in principal neurones of

entorhinal-cortex layer II has a key role in sustaining low-threshold, θ-like membrane voltage oscillations in single cells (Alonso and Llinas 1989; Klink and Alonso 1993). In the present case, dendritic hyperpolarisation could have set the activation/inactivation sequence of transient and persistent Na^+ channels although the same could have occurred at a site other than the recording site. It is not known whether the inhibition results from intrinsic or extrinsic nonpyramidal cells given that hippocampal nonpyramidal cells recorded in anaesthetised animals were found to fire APs during the positive peak of the θ-frequency waves. Also, the juxtacellularly recorded cell (mt47), presumed to be a hippocampal interneurone selective type III cell innervating only other GABAergic cells, did not fire during three θ-evoked episodes. Another possible and perhaps more probable account for the AP firing pattern observed in the recorded cell (m11) is that prominent simultaneous excitatory influences (i.e. during the negative peak of the θ-frequency waves) could have allowed for faster activation of Na^+ channels as compared to random excitation, which can also be easily countered by gradual increases in inhibition (i.e. towards the positive peak of θ-frequency waves).

During SPWs, one cell fired AP doublets, which appeared to involve a slowly activating mechanism as doublet firing failed to occur during the early stages of the SPW. One possibility is the involvement of slowly inactivating K^+ channels as the cell decreased its firing rate during the late stages of current-evoked AP trains. However, it is not possible to exclude the recruitment of inhibitory influences at the site of AP generation in both instances, especially when nonpyramidal cell activity during SPWs was typically curtailed by inhibition. Indeed, doublet firing occurred during the positive voltage deflection of the extracellular wave indicating outward current. Inhibition could have set the excitatory drive necessary for doublet firing. The most revealing example of inhibitory influences was the large depolarisation in a nonpyramidal cell, which was diminished in large decrements throughout a SPW event. The

implications for doublet firing may be to enhance synaptic efficacy at specialised synapses or as indicated in a previous study (Traub et al. 1996b), to reduce phase lag over long-range circuits by means of matching the doublet interval to the conduction delay. As APs were presumably backpropagating and no spikelets were observed during recording, the first hypothesis seems more probable.

4.4.3 Anatomical and Physiological Comparisons of Nonpyramidal Cells

The presumed backprojection cell (m11) recorded in vivo is similar to one of the O-Bi cells with a large soma described in chapter 3 (M1011) on the basis of its axonal branches in the SL-M border tangentially projecting towards the CA3 area. However, the cell recorded in vivo is probably not an O-Bi cell for three reasons. One is that the tangential axon of the O-Bi cell (M1011) never reached the CA3 area. Secondly, the O-Bi cell did not have an axonal projection to the hilus. Thirdly, another O-Bi cell with a large soma (n4921) did not have a similar axon in SL-M. Instead, the cell's (m11) axonal projection to the CA3 area and the hilus is more indicative of a backprojection cell type as has been previously studied (Sik et al. 1994, 1995). However, the cell (m11) cannot be classified unequivocally due to the missing somatodendritic region and limited extent of recovered axon after histological processing. Additionally, the presumed backprojection cell's current-evoked firing pattern cannot be directly compared to a previously recorded backprojection cell (Sik et al. 1994) due to their different resting membrane potentials (-48 mV versus –60 mV), respectively. Nevertheless, both cells showed a similar mode of delay in AP repolarisation. If the cell (m11) is indeed a backprojection cell, it would be the first of its kind to show θ-frequency dependent modulation of APs. Therefore, it still remains to be determined whether a lowering of AP threshold during the negative peak of θ-frequency oscillations occurs specifically in backprojection cells. The fact that its θ-frequency phase

related firing was opposite to that of basket cells (Sik et al. 1995; Ylinen et al. 1995b), emphasises input and output specificities in distinct cell types.

The nonpyramidal projection cell recorded in vivo (d150) also had some similar anatomical features to the two O-Bi cells with large somas described in chapter 3. The fact that the projection cell had two axonal branches reaching the most rostral tip of the CA3 area sets it apart from the O-Bi cells. However, due to their widespread axons, it is possible that the two O-Bi cells also had projections to the CA3 area, which may have been lost due to the in vitro process. Unfortunately, the intrinsic membrane properties of the projection cell and the anatomically most similar O-Bi cell (M1011) could not be compared due to their differences in current pulse duration, average firing frequency (48 Hz versus 19 Hz) and resting membrane potential (-72 mV versus –65 mV), respectively. Most importantly, in vivo state-dependent network activity cannot be excluded from influencing the neuronal firing pattern of the in vivo recorded neurone. Nevertheless, it is interesting to note that cells with a larger early versus late accommodation, as shown for O-Bi cells in vitro, could influence synaptic targets transiently. One example being the fast accommodation of APs during simultaneous SPWs and current-evoked firing observed in the projection cell (Figure 4.3.1).

The juxtacellularly recorded cell (mt47) was presumed to be an interneurone selective type III cell containing both VIP and calretinin. The basis for this assumption lies in the similar anatomical features between the recorded cell and cells immunopositive for both VIP and calretinin (Acsady et al. 1996a). Also, the somatic area of the recorded cell fell within the range of somatic areas of cells immunopositive for both VIP and calretinin. Some caveats exist in the above supporting evidence. Firstly, in the previous study (Acsady et al. 1996a) cells that had axonal projections to both SO/alveus and SR as in the recorded cell (mt47) were not reported. This discrepancy can be explained by the technical challenges of obtaining adequate immunoreactivity in separate serial sections (three reacted for VIP and the last reacted for

calretinin) and having a minimal quantity of VIP-immunopositive cells to choose from for reconstruction (Acsady et al. 1996a). Secondly, some overlap occurred between the somatic area measurments for the different cell categories tested. One might attribute the overlap to factors such as a surface cut of the immunolabelled cells or the poor outline of some cells due to weak labelling. This is unlikely because all cells were observed to be within the section and images were digitally contrasted to determine the outline of any weakly labelled cells. It is likely that the recorded cell (mt47) is not a cell that only expresses VIP as its somatic area lay outside the standard deviation of the somatic areas for cells expressing VIP only. In addition, the recorded cell (mt47) and the reconstructed calretinin-immunopositive cell both have small somatic areas. If interneurone selective type III cells can be classified as one group in terms of their physiology, then it is interesting to note that the recorded cell (mt47) was 'silent' during evoked θ field activity. This would imply that the presumed backprojection cell (m11) was not inhibited by interneurone selective type III cells during θ-frequency field oscillations, although this assumption is based on a presumed VIP/calretinin cell (mt47) and only three θ-frequency evoked episodes lasting between 5 to 10 s are available to correlate with the cell's activity.

4.4.4 Implications for a Possible Role for mGluR1α

It is still unknown under what physiologically-relevant conditions are mGluR1α positive cells activated and how their spatial arrangement would influence their output patterns. Based on a few episodes of θ activity and the indirect assumption for the juxtacellularly recorded cell (mt47) to be an interneurone selective type III cell does not suffice to classify these cell types as inactive during θ-frequency activity. In addition, mGluR1α positive cells may not necessarily only affect the entorhinal cortical input based on the prevalence of mGluR1α positive O-LM cells innervating the distal dendrites of pyramidal cells. According to the present findings some

cells weakly immunopositive for mGluR1α were not VIP-immunopositive whereas O-LM cells, which are SOM positive, typically contain strong immunolabelling for mGluR1α (Baude et al. 1993; present study). Therefore, it is likely that there is an additional group of mGluR1α-positive cells, which may project to areas other than the entorhinal cortical input zones. Although a small percentage of VIP-immunopositive cells were not mGluR1α-immunopositive, these cells originated from one animal in which the mGluR1α immunoreaction was considerably weaker than in the other. Therefore, VIP-immunopositive cells, which were mGluR1α-immunonegative are considered to be false negatives. Finally, it cannot be assumed that VIP and SOM positive cells are activated during the same physiological conditions via mGluR1α. The fact that Woodhall et al. 1999 showed Ca^{2+}-mediated oscillatory activity in SO nonpyramidal cells resulting from an mGluR group I agonist applied in an in vitro bath preparation would suggest the involvement of group I mGluRs in rhythmic activity. Whether the circuitry involved includes pyramidal cells or not remains to be determined by testing agonists specific to mGluR1.

CHAPTER 5: Conclusion

5.1 Low-Threshold Responses and Intrinsic Properties of Cortical Cells

The present study has shown that cortical information processing is shaped by the organisation of neuronal circuits, the receptors involved in mediating neuronal signalling and the intrinsic properties of cells involved in the transfer of information. In the SI cortex, low-threshold responses evoked by innocuous stimuli were biphasic, consisting of short-latency short duration and long duration responses. Both components were mediated by AMPA/kainate and NMDA receptors differentially. The short-duration response was mostly mediated by AMPA/kainate receptors whereas NMDA receptors were additionally recruited for the long duration response. The involvement of NMDA receptors in the long duration response may be a consequence of intracortical activity. For instance, layer IV cells, which receive the densest thalamocortical projections, show short-latency responses mediated by AMPA/kainate receptors (Armstrong-James et al. 1993). A minor projection from the thalamus to supragranular (Jensen and Killackey 1987) and infragranular layers (Chmielowska et al. 1989) in the SI cortex may explain the involvement of AMPA/kainate receptors in the short-latency as well as long duration responses. However, SI cortical cells in layer II/III and V showed delayed NMDA receptor mediated responses compared to thalamocortical inputs to layer IV cells (Armstrong-James et al. 1992). Moreover, the expression of NMDA receptors is highest in layers II/III, followed by layers V/VI and IV (Petralia et al. 1994). In the present study, inhibition or a reduction below the baseline activity was observed inbetween the short-latency and long duration responses. Such reduction in baseline activity is most likely a result of intracortical interactions in the SI cortex because inhibitory influences resulting from activation of surround receptive fields were shown to occur less often in the ventrobasal thalamus (Simons and Carvell 1989). In addition, the peak response latencies between activation of a centre and surround receptive field are

shorter in the ventrobasal thalamus as compared to the SI cortex, implying that long duration responses in the SI cortex result from intracortical interactions (Armstrong-James and Callahan 1991). Overall, the likely scenario is that intracortical projections, perhaps originating from layer II/III SI cortical cells might make synapses with layer V cells containing a high density of NMDA receptors. In support of this, layer II/III cells project to layer V cells which have apical dendrites extending into supragranular layers (Akers and Killackey 1978; Fonseca et al. 1988). In this way, dendritic spatial delays may also contribute to the long duration responses. As timing is essential in the response patterns observed for low-threshold responses, it would be interesting to determine the involvement of intrinsic membrane properties in modulating the activity through particular receptor types.

In order to understand the role of intrinsic properties of cells in physiologically-relevant activity, it is necessary to elucidate properties in a cortical area with less complex circuitry than the SI cortex. For this reason, I chose the CA1 area of the hippocampus as the basis for understanding some mechanisms underlying physiologically-relevant activity. Inhibitory cells have been implicated in regulating principal cell excitation during state-dependent activities as a result of their widespread projections and multiple synaptic release sites (Buhl et al. 1994a). Indeed, several lines of physiological evidence support the above notion. For instance, SP nonpyramidal cells fire at high frequencies and are likely responsible for ripple oscillations observed in pyramidal cells during SPWs (Ylinen et al. 1995a). Given that nonpyramidal cells show more synchrony than pyramidal cells during SPWs (Csicsvari et al. 1998), it is unlikely that gap junctional coupling between pyramidal cells is involved in ripple field oscillations, as predicted from a computer model for high-frequency (125-182 Hz) synchronised oscillations (Traub et al. 1999). Gamma-frequency network activity is sustained by nonpyramidal cell coupling alone and can entrain pyramidal cell activity (Whittington et al. 1995; Jefferys et al.

1996). Also, nonpyramidal cells show more synchronous firing of APs than pyramidal cells, regardless of whether θ field activity or SPWs exist (Csicsvari et al. 1998).

Based on the present findings, I suggest that two SO/alveus nonpyramidal cell types can affect pyramidal cell activity differentially due to their axonal patterns and intrinsic membrane properties. Oriens-lacunosum moleculare and O-Bi nonpyramidal cells both contain somatostatin and are located in SO/alveus (Somogyi et al. 1984; McBain et al. 1994; Maccaferri et al. 2000) where pyramidal cell axons are likely to innervate them (Blasco-Ibanez and Freund 1995). As most CA1 pyramidal cells in SP have similar dendritic arrangements and extrinsic inputs, it is likely that O-LM and O-Bi cells receiving pyramidal cell feed-back would be activated under the same physiological conditions. The similar somatodendritic position of both O-LM and O-Bi cells might also be suitable for particular extrinsic inputs such as the one from the entorhinal cortex. In addition, both O-LM and O-Bi cells express somatostatin allowing for output specificity that acts comparable to GABAergic influences. However, O-LM and O-Bi cells may display differences in their density of mGluR1α, which may be an explanation for the lack of mGluR1α immunoreactivity observed in O-Bi cells. There were also differences in intrinsic properties between O-LM and O-Bi cells. A larger late accommodation of AP firing occurred in O-LM cells whereas O-Bi cells showed a larger early accommodation during depolarising current pulses. Therefore, during tonic activation, the point of change in the firing rate of O-LM cells may result in triggering a shift from one state to another. On the contrary, O-Bi cells may be involved in sustaining a particular frequency-dependent episode. Similar cells could exist in the SI cortex and account for the occurrence of a biphasic low-threshold response. Additionally, O-LM cells displayed a larger voltage 'sag' during hyperpolarising current pulses, which correlated with the rebound depolarisation occurring after the end of the current pulse. The role of the presumed I_h current is not clear in these cell types as it has been shown to

increase spontaneous AP firing rates but decrease AP firing rates evoked by depolarising current injection (DiFrancesco 1991; Hughes et al. 1998; Maccaferri and McBain 1996). However, I_h is known as a pacemaker current (DiFrancesco 1991; McCormick and Pape 1990; Soltesz et al. 1991) which in combination with inhibitory influences or low-threshold Ca^{2+} currents, could promote oscillatory activity in the absence of tonic activation.

5.2 Summary of High-Threshold Responses and Synchronous Activity of Cortical Cells

A noxious pinch, which evoked an increased excitation in SI layer V cortical cells also evoked θ-frequency population oscillations in the hippocampus. High-threshold responses in the SI cortex were unimodal and mediated by both AMPA/kainate and NMDA receptors. The onset latency of high-threshold responses was also longer as compared to short-latency low-threshold responses. Therefore, it is not possible to exclude a polysynaptic contribution to high-threshold responses. The fact that high-threshold responses were unimodal, even in wide dynamic range cells, which also responded to innocuous stimuli, indicates separate modes by which somatosensory submodalities can be distinguished. However, after a noxious stimulus was delivered, the baseline activity of single cells recorded in the SI cortex increased and this too was mediated by AMPA/kainate and NMDA receptors. It is not known as to whether other receptors were involved in the increase in baseline activity and whether intracortical circuits or extrinsic inputs played a role. There are several likely candidates for contributing to the increase in baseline activity. Cells in the medial thalamic nuclei respond to noxious stimuli, have large receptive fields (Dostrovsky and Guilbaud 1990) and receive spinomesencephalic tract inputs originating from cells which show long afterdischarges and high rates of background activity during noxious stimuli (Yezierski and Schwartz 1986). In addition, medial thalamic neurones send diffuse projections to widespread cortical areas but specifically to infragranular layers (Jones and Leavitt 1974; Herkenham 1980). Due to their large receptive fields but more

importantly, their projections to and from limbic areas, cells in the medial thalamic nuclei are implicated in the affective-motivational aspects of nociceptive transmission (Willis 1985; Yoshida et al. 1992). Although the SI cortex is accepted as having a sensory-discriminative function, it is likely that information processing in the SI cortex also involves cognitive-evaluative aspects given that descending cortical projections signal behavioural reactions to take place.

Septal cholinergic and GABAergic projections to the hippocampus have a main involvement in maintaining θ-frequency rhythmicity in hippocampal cells (Kramis et al. 1975; Lee et al. 1994). Although recordings during θ-frequency activity were performed in anaesthetised animals, this is not considered unphysiological because θ-frequency activity has been shown to occur during paradoxical sleep (Vanderwolf 1969). As there was a relatively long delay in the occurrence of θ-frequency population activity when a noxious stimulus was applied, it is possible that cortico-hippocampal projections may have a role in promoting θ-frequency field oscillations in the hippocampus. Although the SI cortex shows mostly desynchronised EEG patterns during somatosensory stimuli (Thompson et al. 1991) there is evidence of gamma-frequency field oscillations in the SI and SII cortex evoked by stimulating multiple vibrissa in unanaesthetised rats (Jones and Barth 1997). Other cortical areas, including the hippocampus, typically exhibit network oscillations during sensory stimulation (Sannita 2000; Vanderwolf 1969). In addition, the combined activation of cortical areas (i.e. audio-visual stimulation) results in synchronous EEG oscillations at θ frequency (Sakowitz et al. 2000). The differences in the effects of sensory stimulation between the SI cortex and other cortical areas are still not well understood but may reflect the difference between single-site and multiple-site stimuli (Jones and Barth 1997). However, desynchronisation and synchronisation of EEG patterns have been shown to correspond to planning and execution of motor tasks (Pfurtscheller and Neuper

1992). It should also be noted that synchronous oscillations in the visual cortex were shown to correlate with discharge rates in the inferotemporal cortex (Newman and Grace 1999) implying that associational information processing can also involve asynchronous activity. For instance, the increased baseline activity observed in SI cortical cells after noxious stimulation could have been involved in hippocampal θ-frequency activity, which also occurred with a delay after a noxious stimulus. There is evidence of projections from the SI cortex to the medial thalamus (Wise and Jones 1977) and parietal association areas (Fabri and Burton 1991), which are reciprocally connected with limbic areas (Kolb and Walkey 1987; Yoshida et al. 1992). Furthermore, interactions between the hippocampus and neocortex have been observed from temporal correlations of population bursts such as SPWs and neocortical spindle oscillations (Siapas and Wilson 1998). It has been suggested that the transition between θ-frequency activity and SPWs, allows for the formation, consolidation and retrieval of memories (Chrobak and Buzsaki 1994). Indeed, θ-frequency activity has been implicated in memory formation by promoting long-term potentiation (Huerta and Lisman 1993, 1995) or by modulating AP firing into episodes of gamma-frequency activity (Lisman and Idiart 1995).

There are several ways in which cells may be activated synchronously. One mechanism is the timing of events through synaptic inhibition (Cobb et al. 1995; Jefferys et al. 1996). Another mechanism is the modulation of neuronal activity through ephaptic transmission or field effects (Jefferys 1995). Gap junctional coupling, which allows for fast simultaneous activation of cells also may promote synchrony (Draguhn et al. 1998; Tamas et al. 2000). Both experimental and computational evidence suggest that doublet firing, which can overcome long-distance conduction delays can promote population synchrony (Traub et al. 1996b; Whittington et al. 1997; Stanford et al. 1998). Doublet firing during a SPW in the present study was observed in one nonpyramidal cell recorded. Moreover, the projection nonpyramidal cell, which was also

activated during SPWs had axonal projections extending close to the entorhinal cortex as well as the most frontal part of the CA3 area. The presumed backprojection cell fired a burst of APs during θ episodes and had axonal projections to the CA3 area as well as the hilus. Such widespread axonal projections could result in synchronous activation amongst a population of cells within and perhaps beyond the hippocampus. However, further experiments are necessary to link sensory-evoked neuronal signalling in the SI cortex to associational information processing.

5.3 Glutamate Receptors

Further analysis of the glutamate receptors involved at each stage of neuronal processing may elucidate the molecular mechanisms of cortical interactions. For instance, some NMDA receptors display slower activation kinetics due to the voltage-dependent Mg^{2+} block (Hestrin et al. 1990; McBain and Mayer 1994) and AMPA/kainate receptors desensitise faster (Hestrin 1992). These characteristics are exemplified in the present results where long duration low-threshold responses as well as long duration high-threshold responses involved NMDA receptors in addition to AMPA/kainate receptors. As it has been previously shown that mGluRs are located perisynaptically and extrasynaptically (Baude et al. 1993; Lujan et al. 1996), their activation is likely to increase during stronger excitatory drive. It would be interesting to know whether mGluRs are activated during prominent excitatory population bursts such as SPWs given that such activity represents strong synchrony across the cortical to hippocampal loop (Buzsaki et al. 1983; Chrobak and Buzsaki 1994). It has already been shown that gamma-frequency network oscillations can be induced by group I mGluR activation in CA1 nonpyramidal cells (Whittington et al. 1995) or CA3 pyramidal cells in the presence of GABA receptor antagonists (Taylor et al. 1995). Interestingly, the present study showed that most VIP-expressing nonpyramidal cells, which only contact other nonpyramidal cells, were

immunopositive for mGluR1α. In addition, mGluR-induced oscillations including the activation of both nonpyramidal and pyramidal cells are phased by $GABA_A$ receptor mediated synaptic events (Jefferys et al. 1996; Traub et al. 1996a) and synchronised by AMPA/kainate receptor mediated synaptic events in the case of CA3 pyramidal cells (Taylor et al. 1995). In contrast, slower synchronous oscillations (8-12 Hz) are mediated by NMDA receptors (Flint and Connors 1996). However, depending on the membrane potential of a cell, NMDA receptors can mediate rhythmic bursts in single cells with an intraburst frequency occurring within the gamma-frequency range (Khateb et al. 1995). In addition, mGluRs and NMDA receptors are involved in the generation or maintenance of long-lasting synaptic efficacy (Dudek and Bear 1992; Huang et al. 1999; Cohen et al. 1999; Raymond et al. 2000) which can arise during θ oscillations. Thus, the spatiotemporal characterisitics of neuronal signalling determine the activation of particular glutamate receptors, which as shown from the present findings, mediate different aspects of neuronal signalling.

REFERENCES

Abe T, Sugihara H, Nawa H, Shigemoto R, Mizuno N, Nakanishi S (1992) Molecular characterization of a novel metabotropic glutamate receptor mGluR5 coupled to inositol phosphate/Ca2+ signal transduction. J Biol Chem 267: 13361-13368

Abraham WC, Goddard GV (1983) Asymmetric relationships between homosynaptic long-term potentiation and heterosynaptic long-term depression. Nature 305: 717-719

Acsady L, Arabadzisz D, Freund TF (1996a) Correlated morphological and neurochemical features identify different subsets of vasoactive intestinal polypeptide-immunoreactive interneurons in rat hippocampus. Neuroscience 73: 299-315

Acsady L, Gorcs TJ, Freund TF (1996b) Different populations of vasoactive intestinal polypeptide- immunoreactive interneurons are specialized to control pyramidal cells or interneurons in the hippocampus. Neuroscience 73: 317-334

Agmon A, Connors BW (1989) Repetitive burst-firing neurons in the deep layers of mouse somatosensory cortex. Neurosci Lett 99: 137-141

Agmon A, O'Dowd DK (1992) NMDA receptor-mediated currents are prominent in the thalamocortical synaptic response before maturation of inhibition. J Neurophysiol 68: 345-349

Akers RM, Killackey HP (1978) Organization of corticocortical connections in the parietal cortex of the rat. J Comp Neurol 181: 513-538

Albe-Fessard D, Berkley KJ, Kruger L, Ralston HJ III, Willis WD Jr (1985) Diencephalic mechanisms of pain sensation. Brain Res Rev 9: 217-296

Alonso A, Llinas RR (1989) Subthreshold Na+-dependent theta-like rhythmicity in stellate cells of entorhinal cortex layer II. Nature 342: 175-177

Andersen P, Eccles JC, Loyning Y (1964) Pathways of postsynaptic inhibition in the hippocampus. J Neurophysiol 27: 608-619

Angel A, Gratton DA, Halsey MJ, Wardley-Smith B (1980) Pressure reversal of the effect of urethane on the evoked somatosensory cortical response in the rat. Br J Pharmac 70: 241-247

Aniksztejn L, Otani S, Ben-Ari Y (1992) Quisqualate metabotropic receptors modulate NMDA currents and facilitate induction of long-term potentiation through protein kinase C. Eur J Neurosci 4: 500-505

Aniksztejn L, Sciancalepore M, Ben Ari Y, Cherubini E (1995) Persistent current oscillations produced by activation of metabotropic glutamate receptors in immature rat CA3 hippocampal neurons. J Neurophysiol 73: 1422-1429

REFERENCES

Aramori I, Nakanishi S (1992) Signal transduction and pharmacological characteristics of a metabotropic glutamate receptor, mGluR1, in transfected CHO cells. Neuron 8: 757-765

Armstrong-James M, Callahan CA (1991) Thalamo-cortical processing of vibrissal information in the rat. II. spatiotemporal convergence in the thalamic ventroposterior medial nucleus (VPm) and its relevance to generation of receptive fields of S1 cortical "barrel" neurones. J Comp Neurol 303: 211-224

Armstrong-James M, Fox K (1987) Spatiotemporal convergence and divergence in the rat S1 "barrel" cortex. J Comp Neurol 263: 265-281

Armstrong-James M, Fox K, Das-Gupta A (1992) Flow of excitation within rat barrel cortex on striking a single vibrissa. J Neurophysiol 68: 1345-1358

Armstrong-James M, Welker E, Callahan CA (1993) The contribution of NMDA and non-NMDA receptors to fast and slow transmission of sensory information in the rat SI barrel cortex. J Neurosci 13: 2149-2160

Artola A, Singer W (1993) Long-term depression of excitatory synaptic transmission and its relationship to long-term potentiation. Trends Neurosci 16: 480-487

Ashwood TJ, Lancaster B, Wheal HV (1984) In vivo and in vitro studies on putative interneurones in the rat hippocampus: possible mediators of feed-forward inhibition. Brain Res 293: 279-291

Aylward RLM, Totterdell S (1993) Neurons in the ventral subiculum, amygdala and entorhinal cortex which project to the nucleus accumbens: Their input from somatostatin-immunoreactive boutons. J Chem Neuroanat 6: 31-42

Baskys A, Bernstein NK, Barolet AW, Carlen PL (1990) NMDA and quisqualate reduce a Ca-dependent K+ current by a protein kinase-mediated mechanism. Neurosci Lett 112: 76-81

Baude A, Nusser Z, Roberts JD, Mulvihill E, McIlhinney RA, Somogyi P (1993) The metabotropic glutamate receptor (mGluR1 alpha) is concentrated at perisynaptic membrane of neuronal subpopulations as detected by immunogold reaction. Neuron 11: 771-787

Benveniste M, Mayer ML (1993) Multiple effects of spermine on N-methyl-D-aspartic acid receptor responses of rat cultured hippocampal neurones. J Physiol (Lond) 464: 131-163

Bettler B, Boulter J, Hermans-Borgmeyer I, O'Shea-Greenfield A, Deneris ES, Moll C, Borgmeyer U, Hollmann M, Heinemann S (1990) Cloning of a novel glutamate receptor subunit, GluR5: expression in the nervous system during development. Neuron 5: 583-595

Bettler B, Egebjerg J, Sharma G, Pecht G, Hermans-Borgmeyer I, Moll C, Stevens CF, Heinemann S (1992) Cloning of a putative glutamate receptor: a low affinity kainate-binding subunit. Neuron 8: 257-265

REFERENCES

Birse EF, Eaton SA, Jane DE, Jones PL, Porter RH, Pook PC, Sunter DC, Udvarhelyi PM, Wharton B, Roberts PJ, et al. (1993) Phenylglycine derivatives as new pharmacological tools for investigating the role of metabotropic glutamate receptors in the central nervous system. Neuroscience 52: 481-488

Bland BH, Trepel C, Oddie SD, Kirk IJ (1996) Intraseptal microinfusion of muscimol: effects on hippocampal formation theta field activity and phasic theta-ON cell discharges. Exp Neurol 138: 286-297

Blasco-Ibanez JM, Freund TF (1995) Synaptic input of horizontal interneurons in stratum oriens of the hippocampal CA1 subfield: structural basis of feed-back activation. Eur J Neurosci 7: 2170-2180

Bleakman D, Rusin KI, Chard PS, Glaum SR, Miller RJ (1992) Metabotropic glutamate receptors potentiate ionotropic glutamate responses in the rat dorsal horn. Mol Pharmacol 42: 192-196

Boehm S, Betz H (1997) Somatostatin inhibits excitatory transmission at rat hippocampal synapses via presynaptic receptors. J Neurosci 17: 4066-4075

Bortolotto ZA, Bashir ZI, Davies CH, Collingridge GL (1994) A molecular switch activated by metabotropic glutamate receptors regulates induction of long-term potentiation. Nature 368: 740-743

Bortolotto ZA, Clarke VR, Delany CM, Parry MC, Smolders I, Vignes M, Ho KH, Miu P, Brinton BT, Fantaske R, Ogden A, Gates M, Ornstein PL, Lodge D, Bleakman D, Collingridge GL (1999) Kainate receptors are involved in synaptic plasticity. Nature 402: 297-301

Boss V, Conn PJ (1992) Metabotropic excitatory amino acid receptor activation stimulates phospholipase D in hippocampal slices. J Neurochem 59: 2340-2343

Boulter J, Hollmann M, O'Shea-Greenfield A, Hartley M, Deneris E, Maron C, Heinemann S (1990) Molecular cloning and functional expression of glutamate receptor subunit genes. Science 249: 1033-1037

Brankack J, Stewart M, Fox SE (1993) Current source density analysis of the hippocampal theta rhythm: associated sustained potentials and candidate synaptic generators. Brain Res 615: 310-327

Buhl EH, Cobb SR, Halasy K, Somogyi P (1995) Properties of unitary IPSPs evoked by anatomically identified basket cells in the rat hippocampus. Eur J Neurosci 7: 1989-2004

Buhl EH, Halasy K, Somogyi P (1994a) Diverse sources of hippocampal unitary inhibitory postsynaptic potentials and the number of synaptic release sites [published erratum appears in Nature 1997 May 1;387(6628):106]. Nature 368: 823-828

REFERENCES

Buhl EH, Han ZS, Lorinczi Z, Stezhka VV, Karnup SV, Somogyi P (1994b) Physiological properties of anatomically identified axo-axonic cells in the rat hippocampus. J Neurophysiol 71: 1289-1307

Buhl EH, Tamas G, Fisahn A (1998) Cholinergic activation and tonic excitation induce persistent gamma oscillations in mouse somatosensory cortex in vitro. J Physiol (Lond) 513: 117-126

Burnashev N, Khodorova A, Jonas P, Helm PJ, Wisden W, Monyer H, Seeburg PH, Sakmann B (1992) Calcium-permeable AMPA-kainate receptors in fusiform cerebellar glial cells. Science 256: 1566-1570

Buzsaki G (1984) Feed-forward inhibition in the hippocampal formation. Prog Neurobiol 22: 131-153

Buzsaki G, Czopf J, Kondakor I, Kellenyi L (1986) Laminar distribution of hippocampal rhythmic slow activity (RSA) in the behaving rat: current-source density analysis, effects of urethane and atropine. Brain Res 365: 125-137

Buzsaki G, Eidelberg E (1982) Direct afferent excitation and long-term potentiation of hippocampal interneurons. J Neurophysiol 48: 597-607

Buzsaki G, Leung LW, Vanderwolf CH (1983) Cellular bases of hippocampal EEG in the behaving rat. Brain Res 287: 139-171

Cahusac PM B, Morris R, Salt TE, Hill RG (1990) Sensory responses of caudal trigeminal neurons to thermal and mechanical stimuli and their behavioural correlates in the rat. Neuroscience 36: 543-551

Castro-Alamancos MA, Calcagnotto ME (1999) Presynaptic long-term potentiation in corticothalamic synapses. J Neurosci 19: 9090-9097

Cerne R, Jiang M, Randic M (1992) Cyclic adenosine 3'5'-monophosphate potentiates excitatory amino acid and synaptic responses of rat spinal dorsal horn neurons. Brain Res 596: 111-123

Chagnac-Amitai Y, Luhmann HJ, Prince DA (1990) Burst generating and regular spiking layer 5 pyramidal neurons of rat neocortex have different morphological features. J Comp Neurol 296: 598-613

Chapin JK, Lin C-S (1984) Mapping the body representation in the SI cortex of anesthetized and awake rats. J Comp Neurol 229: 199-213

Chapman CA, Lacaille JC (1999) Cholinergic induction of theta-frequency oscillations in hippocampal inhibitory interneurons and pacing of pyramidal cell firing. J Neurosci 19: 8637-8645

Charpak S, Gahwiler BH, Do KQ, Knopfel T (1990) Potassium conductances in hippocampal neurons blocked by excitatory amino-acid transmitters. Nature 347: 765-767

REFERENCES

Chavis P, Shinozaki H, Bockaert J, Fagni L (1994) The metabotropic glutamate receptor types 2/3 inhibit L-type calcium channels via a pertussis toxin-sensitive G-protein in cultured cerebellar granule cells. J Neurosci 14: 7067-7076

Chmielowska J, Carvell GE, Simons DJ (1989) Spatial organization of thalamocortical and corticothalamic projection systems in the rat SmI barrel cortex. J Comp Neurol 285: 325-338

Chrobak JJ, Buzsaki G (1994) Selective activation of deep layer (V-VI) retrohippocampal cortical neurons during hippocampal sharp waves in the behaving rat. J Neurosci 14: 6160-6170

Chudler EH, Anton F, Dubner R, Kenshalo DR Jr (1990) Responses of nociceptive SI neurons in monkeys and pain sensation in humans elicited by noxious thermal stimulation: Effect of interstimulus interval. J Neurophysiol 63: 559-569

Claiborne BJ, Amaral DG, Cowan WM (1986) A light and electron microscopic analysis of the mossy fibers of the rat dentate gyrus. J Comp Neurol 246: 435-458

Cobb SR, Buhl EH, Halasy K, Paulsen O, Somogyi P (1995) Synchronization of neuronal activity in hippocampus by individual GABAergic interneurons. Nature 378: 75-78

Coetzee WA, Amarillo Y, Chiu J, Chow A, Lau D, McCormack T, Moreno H, Nadal MS, Ozaita A, Pountney D, Saganich M, Vega-Saenz de Miera E, Rudy B (1999) Molecular diversity of K+ channels. Ann N Y Acad Sci 868: 233-285

Cohen AS, Coussens CM, Raymond CR, Abraham WC (1999) Long-lasting increase in cellular excitability associated with the priming of LTP induction in rat hippocampus. J Neurophysiol 82: 3139-3148

Collingridge GL, Kehl SJ, McLennan H (1983) Excitatory amino acids in synaptic transmission in the Schaffer collateral-commissural pathway of the rat hippocampus. J Physiol (Lond) 334: 33-46

Connors BW, Gutnick MJ (1990) Intrinsic firing patterns of diverse neocortical neurons. Trends Neurosci 13: 99-104

Courtney MJ, Nicholls DG (1992) Interactions between phospholipase C-coupled and N-methyl-D-aspartate receptors in cultured cerebellar granule cells: protein kinase C mediated inhibition of N-methyl-D-aspartate responses. J Neurochem 59: 983-992

Cox CL, Metherate R, Weinberger NM, Ashe JH (1992) Synaptic potentials and effects of amino acid antagonists in the auditory cortex. Brain Res Bull 28: 401-410

Csicsvari J, Hirase H, Czurko A, Buzsaki G (1998) Reliability and state dependence of pyramidal cell-interneuron synapses in the hippocampus: an ensemble approach in the behaving rat. Neuron 21: 179-189

REFERENCES

Csicsvari J, Hirase H, Czurko A, Mamiya A, Buzsaki G (1999) Oscillatory coupling of hippocampal pyramidal cells and interneurons in the behaving Rat. J Neurosci 19: 274-287

Csicsvari J, Hirase H, Mamiya A, Buzsaki G (2000) Ensemble patterns of hippocampal CA3-CA1 neurons during sharp wave- associated population events [In Process Citation]. Neuron 28: 585-594

Cumberbatch MJ, Chizh BA, Headley PM (1994) AMPA receptors have an equal role in spinal nociceptive and non-nociceptive transmission. Neuroreport 5: 877-880

Davies J, Francis AA, Jones AW, Watkins JC (1981) 2-amino-5 phosphovalerate (2APV), a potent and selective antagonist of amino acid-induced and synaptic excitation. Neurosci Lett 21: 77-81

Davies J, Jones AW, Sheardown MJ, Smith DA, Watkins JC (1984) Phosphono dipeptides and piperazine derivatives as antagonists of amino acid-induced and synaptic excitation in mammalian and amphibian spinal cord. Neurosci Lett 52: 79-84

Davies J, Miller AJ, Sheardown MJ (1986) Amino acid receptor mediated excitatory synaptic transmission in the cat red nucleus. J Physiol 376: 13-29

Davies J, Watkins JC (1983) Role of excitatory amino acid receptors in mono- and polysynaptic excitation in the cat spinal cord. Exp Brain Res 49: 280-290

Debanne D, Gahwiler BH, Thompson SM (1998) Long-term synaptic plasticity between pairs of individual CA3 pyramidal cells in rat hippocampal slice cultures. J Physiol (Lond) 507: 237-247

Deller T, Adelmann G, Nitsch R, Frotscher M (1996) The alvear pathway of the rat hippocampus. Cell Tissue Res 286: 293-303

Derrick BE, Weinberger SB, Martinez JL, Jr. (1991) Opioid receptors are involved in an NMDA receptor-independent mechanism of LTP induction at hippocampal mossy fiber-CA3 synapses. Brain Res Bull 27: 219-223

Dickenson AH, Sullivan AF (1990) Differential effects of excitatory amino acid antagonists on dorsal horn nociceptive neurones in the rat. Brain Res 506: 31-39

DiFrancesco D (1991) The contribution of the 'pacemaker' current (if) to generation of spontaneous activity in rabbit sino-atrial node myocytes. J Physiol (Lond) 434: 23-40

Dingledine R, Hume RI, Heinemann SF (1992) Structural determinants of barium permeation and rectification in non- NMDA glutamate receptor channels. J Neurosci 12: 4080-4087

Dodd J, Dingledine R, Kelly JS (1981) The excitatory action of acetylcholine on hippocampal neurones of the guinea pig and rat maintained in vitro. Brain Res 207: 109-127

REFERENCES

Dostrovsky JO, Guilbaud G (1990) Nociceptive responses in medial thalamus of the normal and arthritic rat. Pain 40: 93-104

Dougherty PM, Palecek J, Paleckova V, Sorkin LS, Willis WD (1992) The role of NMDA and non-NMDA excitatory amino acid receptors in the excitation of primate spinothalamic tract neurons by mechanical, chemical, thermal, and electrical stimuli. J Neurosci 12: 3025-3041

Dragoi G, Carpi D, Recce M, Csicsvari J, Buzsaki G (1999) Interactions between hippocampus and medial septum during sharp waves and theta oscillation in the behaving rat. J Neurosci 19: 6191-6199

Draguhn A, Traub RD, Schmitz D, Jefferys JG (1998) Electrical coupling underlies high-frequency oscillations in the hippocampus in vitro. Nature 394: 189-192

Dudek SM, Bear MF (1992) Homosynaptic long-term depression in area CA1 of hippocampus and effects of N-methyl-D-aspartate receptor blockade. Proc Natl Acad Sci U S A 89: 4363-4367

Dumuis A, Pin JP, Oomagari K, Sebben M, Bockaert J (1990) Arachidonic acid released from striatal neurons by joint stimulation of ionotropic and metabotropic quisqualate receptors. Nature 347: 182-184

Durand GM, Gregor P, Zheng X, Bennett MV, Uhl GR, Zukin RS (1992) Cloning of an apparent splice variant of the rat N-methyl-D-aspartate receptor NMDAR1 with altered sensitivity to polyamines and activators of protein kinase C. Proc Natl Acad Sci U S A 89: 9359-9363

Duvoisin RM, Zhang C, Ramonell K (1995) A novel metabotropic glutamate receptor expressed in the retina and olfactory bulb. J Neurosci 15: 3075-3083

Eaton SA, Birse EF, Wharton B, Sunter DC, Udvarhelyi PM, Watkins JC, Salt TE (1993) Mediation of thalamic sensory responses in vivo by ACPD-activated excitatory amino acid receptors. Eur J Neurosci 5: 186-189

Eaton SA, Salt TE (1990) Thalamic NMDA receptors and nociceptive sensory synaptic transmission. Neurosci Lett 110: 297-302

Eaton SA, Salt TE (1998) Neurotransmitter receptor mechanisms involved in nociceptive processing in the thalamus. In: Ayrapetyan SN , Apkarian AV (eds) Pain Mechanisms and Management. IOS Press, Amsterdam, pp 237-251

Egebjerg J, Bettler B, Hermans-Borgmeyer I, Heinemann S (1991) Cloning of a cDNA for a glutamate receptor subunit activated by kainate but not AMPA. Nature 351: 745-748

Egebjerg J, Heinemann SF (1993) Ca2+ permeability of unedited and edited versions of the kainate selective glutamate receptor GluR6. Proc Natl Acad Sci U S A 90: 755-759

REFERENCES

Egger V, Feldmeyer D, Sakmann B (1999) Coincidence detection and changes of synaptic efficacy in spiny stellate neurons in rat barrel cortex. Nat Neurosci 2: 1098-1105

Erisir A, Lau D, Rudy B, Leonard CS (1999) Function of specific K(+) channels in sustained high-frequency firing of fast-spiking neocortical interneurons [published erratum appears in J Neurophysiol 2000 Jul;84(1):following table of contents]. J Neurophysiol 82: 2476-2489

Fabri M, Burton H (1991) Ipsilateral cortical connections of primary somatic sensory cortex in rats. J Comp Neurol 311: 405-424

Fisahn A, Buhl EH (2000) A role of kainate receptors in the induction of gamma frequency oscillations in the rodent somatosensory cortex in vitro. In: Cavalheiro EA et al. (eds) Excitatory Amino Acids: Ten Years Later. IOS Press, Amsterdam, pp 147-157

Fisher K, Coderre TJ (1998) Hyperalgesia and allodynia induced by intrathecal (RS)-dihydroxyphenylglycine in rats. Neuroreport 9: 1169-1172

Flint AC, Connors BW (1996) Two types of network oscillations in neocortex mediated by distinct glutamate receptor subtypes and neuronal populations. J Neurophysiol 75: 951-957

Flint AC, Dammerman RS, Kriegstein AR (1999) Endogenous activation of metabotropic glutamate receptors in neocortical development causes neuronal calcium oscillations. Proc Natl Acad Sci U S A 96: 12144-12149

Flint AC, Maisch US, Kriegstein AR (1997) Postnatal development of low [Mg2+] oscillations in neocortex. J Neurophysiol 78: 1990-1996

Fonseca M, DEFilipe J, Fairen A (1988) Local connections in transplanted and normal cerebral cortex of rats. Exp Brain Res 69: 387-398

Fox K, Schlaggar BL, Glazewski S, O'Leary DD (1996) Glutamate receptor blockade at cortical synapses disrupts development of thalamocortical and columnar organization in somatosensory cortex. Proc Natl Acad Sci U S A 93: 5584-5589

Fox SE, Ranck JB, Jr. (1981) Electrophysiological characteristics of hippocampal complex-spike cells and theta cells. Exp Brain Res 41: 399-410

Fox SE, Wolfson S, Ranck JB, Jr. (1986) Hippocampal theta rhythm and the firing of neurons in walking and urethane anesthetized rats. Exp Brain Res 62: 495-508

Freund TF, Buzsaki G (1996) Interneurons of the hippocampus. Hippocampus 6: 347-470

Funahashi M, Stewart M (1998) Properties of gamma-frequency oscillations initiated by propagating population bursts in retrohippocampal regions of rat brain slices. J Physiol (Lond) 510: 191-208

REFERENCES

Gadea-Ciria M, Stadler H, Lloyd KG, Bartholini G (1973) Acetylcholine release within the cat striatum during the sleep-wakefulness cycle. Nature 243: 518-519

Garthwaite J, Beaumont PS (1989) Excitatory amino acid receptors in the parallel fibre pathway in rat cerebellar slices. Neurosci Lett 107: 151-156

Gerber U, Sim JA, Gahwiler BH (1992) Reduction of potassium conductances mediated by metabotropic glutamate receptors in rat CA3 pyramidal cells does not require protein kinase C or protein kinase A. Eur J Neurosci 4: 792-797

Glaum SR, Miller RJ (1993) Activation of metabotropic glutamate receptors produces reciprocal regulation of ionotropic glutamate and GABA responses in the nucleus of the tractus solitarius of the rat. J Neurosci 13: 1636-1641

Godwin DW, Vaughan JW, Sherman SM (1996) Metabotropic glutamate receptors switch visual response mode of lateral geniculate nucleus cells from burst to tonic. J Neurophysiol 76: 1800-1816

Greene JRT, Mason AJR (1996a) Neuronal diversity in the subiculum: Correlations with the effects of somatostatin on intrinsic properties and GABA-mediated IPSPs in vitro. J Neurophysiol 76: 1657-1666

Greene JRT, Mason AJR (1996b) Effects of somatostatin and related peptides on the membrane potential and input resistance of rat ventral subicular neurons in vitro. J Pharmacol Exp Ther 276: 426-432

Greene JRT, Totterdell S (1997) Morphology and distribution of electrophysiologically defined classes of pyramidal and nonpyramidal neurons in rat ventral subiculum in vitro. J Comp Neurol 380: 395-408

Grover LM, Yan C (1999) Evidence for involvement of group II/III metabotropic glutamate receptors in NMDA receptor-independent long-term potentiation in area CA1 of rat hippocampus. J Neurophysiol 82: 2956-2969

Guilbaud G, Peschanski M, Gautron M, Binder D (1980) Neurones responding to noxious stimulation in VB complex and caudal adjacent regions in the thalamus of the rat. Pain 8: 303-318

Hagihara K, Tsumoto T, Sato H, Hata Y (1988) Actions of excitatory amino acid antagonists on geniculo-cortical transmission in the cat's visual cortex. Exp Brain Res 69: 407-416

Haley JE, Sullivan AF, Dickenson AH (1990) Evidence for spinal N-methyl-D-aspartate receptor involvement in prolonged chemical nociception in the rat. Brain Res 518: 218-226

Hall RD, Lindholm EP (1974) Organization of motor and somatosensory neocortex in the albino rat. Brain Res 66: 23-38

REFERENCES

Harris RM, Hendrickson AE (1987) Local circuit neurons in the rat ventrobasal thalamus-GABA immunocytochemical study. Neuroscience 21: 229-236

Hartell NA, Headley PM (1996) NMDA-receptor contribution of spinal nociceptive reflexes: Influence of stimulus parameters and of preparatory surgery. Neuropharmacology 35: 1567-1572

Harvey J, Collingridge GL (1993) Signal transduction pathways involved in the acute potentiation of NMDA responses by 1S,3R-ACPD in rat hippocampal slices. Br J Pharmacol 109: 1085-1090

Herb A, Burnashev N, Werner P, Sakmann B, Wisden W, Seeburg PH (1992) The KA-2 subunit of excitatory amino acid receptors shows widespread expression in brain and forms ion channels with distantly related subunits. Neuron 8: 775-785

Herkenham M (1980) Laminar organization of thalamic projections to the rat neocortex. Science 207: 532-535

Herrling PL, Meier CL, Salt TE, Seno N (1990) Involvement of NMDA receptors and non-NMDA receptors in cortico-cortical and thalamo-cortical excitatory postsynaptic potentials in the anaesthetised cat. J Physiol 425: 89P

Hestrin S (1992) Activation and desensitization of glutamate-activated channels mediating fast excitatory synaptic currents in the visual cortex. Neuron 9: 991-999

Hestrin S, Sah P, Nicoll RA (1990) Mechanisms generating the time course of dual component excitatory synaptic currents recorded in hippocampal slices. Neuron 5: 247-253

Hirano T, Hagiwara S (1988) Synaptic transmission between rat cerebellar granule and Purkinje cells in dissociated cell culture: effects of excitatory-amino acid transmitter antagonists. Proc Natl Acad Sci U S A 85: 934-938

Hochman S, Jordan LM, Schmidt BJ (1994) TTX-resistant NMDA receptor-mediated voltage oscillations in mammalian lumbar motoneurons. J Neurophysiol 72: 2559-2562

Hollmann M, Boulter J, Maron C, Beasley L, Sullivan J, Pecht G, Heinemann S (1993) Zinc potentiates agonist-induced currents at certain splice variants of the NMDA receptor. Neuron 10: 943-954

Hollmann M, Hartley M, Heinemann S (1991) Ca2+ permeability of KA-AMPA--gated glutamate receptor channels depends on subunit composition. Science 252: 851-853

Hollmann M, O'Shea-Greenfield A, Rogers SW, Heinemann S (1989) Cloning by functional expression of a member of the glutamate receptor family. Nature 342: 643-648

Houamed KM, Kuijper JL, Gilbert TL, Haldeman BA, O'Hara PJ, Mulvihill ER, Almers W, Hagen FS (1991) Cloning, expression, and gene structure of a G protein-coupled glutamate receptor from rat brain. Science 252: 1318-1321

REFERENCES

Hu B, Bourque CW (1992) NMDA receptor-mediated rhythmic bursting activity in rat supraoptic nucleus neurones in vitro. J Physiol (Lond) 458: 667-687

Huang L, Rowan MJ, Anwyl R (1999) Induction of long-lasting depression by (+)-alpha-methyl-4- carboxyphenylglycine and other group II mGlu receptor ligands in the dentate gyrus of the hippocampus in vitro. Eur J Pharmacol 366: 151-158

Huerta PT, Lisman JE (1993) Heightened synaptic plasticity of hippocampal CA1 neurons during a cholinergically induced rhythmic state. Nature 364: 723-725

Huerta PT, Lisman JE (1995) Bidirectional synaptic plasticity induced by a single burst during cholinergic theta oscillation in CA1 in vitro. Neuron 15: 1053-1063

Huettner JE (1990) Glutamate receptor channels in rat DRG neurons: activation by kainate and quisqualate and blockade of desensitization by Con A. Neuron 5: 255-266

Hughes SW, Cope DW, Crunelli V (1998) Dynamic clamp study of Ih modulation of burst firing and delta oscillations in thalamocortical neurons in vitro. Neuroscience 87: 541-550

Ikeda K, Nagasawa M, Mori H, Araki K, Sakimura K, Watanabe M, Inoue Y, Mishina M (1992) Cloning and expression of the epsilon 4 subunit of the NMDA receptor channel. FEBS Lett 313: 34-38

Ishizuka N, Weber J, Amaral DG (1990) Organization of intrahippocampal projections originating from CA3 pyramidal cells in the rat. J Comp Neurol 295: 580-623

Iwasato T, Erzurumlu RS, Huerta PT, Chen DF, Sasaoka T, Ulupinar E, Tonegawa S (1997) NMDA receptor-dependent refinement of somatotopic maps. Neuron 19: 1201-1210

Jane DE, Jones PL, Pook PC, Tse HW, Watkins JC (1994) Actions of two new antagonists showing selectivity for different sub- types of metabotropic glutamate receptor in the neonatal rat spinal cord. Br J Pharmacol 112: 809-816

Jefferys JG (1995) Nonsynaptic modulation of neuronal activity in the brain: electric currents and extracellular ions. Physiol Rev 75: 689-723

Jefferys JG, Traub RD, Whittington MA (1996) Neuronal networks for induced '40 Hz' rhythms. Trends Neurosci 19: 202-208

Jensen KF, Killackey HP (1987) Terminal arbors of axons projecting to the somatosensory cortex of the adult rat. I. The normal morphology of specific thalamocortical afferents. J Neurosci 7: 3529-3543

Jensen O, Lisman JE (1996) Theta/gamma networks with slow NMDA channels learn sequences and encode episodic memory: role of NMDA channels in recall. Learn Mem 3: 264-278

REFERENCES

Jensen O, Idiart MA, Lisman JE (1996) Physiologically realistic formation of autoassociative memory in networks with theta/gamma oscillations: role of fast NMDA channels. Learn Mem 3: 243-256

Jones EG, Leavitt RY (1974) Retrograde axonal transport and the demonstration of non-specific projections to the cerebral cortex and striatum from thalamic intralaminar nuclei in the rat, cat and monkey. J Comp Neurol 154: 349-377

Jones MS, Barth DS (1997) Sensory-evoked high-frequency (gamma-band) oscillating potentials in somatosensory cortex of the unanesthetized rat. Brain Res 768: 167-176

Kamondi A, Acsady L, Wang XJ, Buzsaki G (1998) Theta oscillations in somata and dendrites of hippocampal pyramidal cells in vivo: activity-dependent phase-precession of action potentials. Hippocampus 8: 244-261

Kano M, Kato M (1987) Quisqualate receptors are specifically involved in cerebellar synaptic plasticity. Nature 325: 276-279

Katakura N, Chandler SH (1990) An iontophoretic analysis of the pharmacologic mechanisms responsible for trigeminal motoneuronal discharge during masticatory-like activity in the guinea pig. J Neurophysiol 63: 356-369

Katsumaru H, Kosaka T, Heizmann CW, Hama K (1988) Gap junctions on GABAergic neurons containing the calcium-binding protein parvalbumin in the rat hippocampus (CA1 region). Exp Brain Res 72: 363-370

Kawabata S, Tsutsumi R, Kohara A, Yamaguchi T, Nakanishi S, Okada M (1996) Control of calcium oscillations by phosphorylation of metabotropic glutamate receptors. Nature 383: 89-92

Kawaguchi Y (1993) Physiological, morphological, and histochemical characterization of three classes of interneurons in rat neostriatum. J Neurosci 13: 4908-4923

Kawaguchi Y, Hama K (1988) Physiological heterogeneity of nonpyramidal cells in rat hippocampal CA1 region. Exp Brain Res 72: 494-502

Kawaguchi Y, Kubota Y (1993) Correlation of physiological subgroupings of nonpyramidal cells with parvalbumin- and calbindinD28k-immunoreactive neurons in layer V of rat frontal cortex. J Neurophysiol 70: 387-396

Keinanen K, Wisden W, Sommer B, Werner P, Herb A, Verdoorn TA, Sakmann B, Seeburg PH (1990) A family of AMPA-selective glutamate receptors. Science 249: 556-560

Keller BU, Hollmann M, Heinemann S, Konnerth A (1992) Calcium influx through subunits GluR1/GluR3 of kainate/AMPA receptor channels is regulated by cAMP dependent protein kinase. Embo J 11: 891-896

REFERENCES

Kenshalo DR Jr, Chudler EH, Anton F, Dubner R (1988) SI nociceptive neurons participate in the encoding process by which monkeys perceive the intensity of noxious thermal stimulation. Brain Res 454: 378-382

Kenshalo DR Jr, Isensee O (1983). Responses of primate SI cortical neurons to noxious stimuli. J Neurophysiol 50: 1479-1496

Kharazia VN, Weinberg RJ (1999) Immunogold localization of AMPA and NMDA receptors in somatic sensory cortex of albino rat. J Comp Neurol 412: 292-302

Khateb A, Fort P, Serafin M, Jones BE, Muhlethaler M (1995) Rhythmical bursts induced by NMDA in guinea-pig cholinergic nucleus basalis neurones in vitro. J Physiol (Lond) 487: 623-638

Kim YI, Chandler SH (1995) NMDA-induced burst discharge in guinea pig trigeminal motoneurons in vitro. J Neurophysiol 74: 334-346

King AE, Liu XH (1996) Dual action of metabotropic glutamate receptor agonists on neuronal excitability and synaptic transmission in spinal ventral horn neurons in vitro. Neuropharmacology 35: 1673-1680

King AE, Lopez-Garcia JA, Cumberbatch M (1992) Antagonism of synaptic potentials in ventral horn neurones by 6-cyano-7- nitroquinoxaline-2,3-dione: a study in the rat spinal cord in vitro. Br J Pharmacol 107: 375-381

Klink R, Alonso A (1993) Ionic mechanisms for the subthreshold oscillations and differential electroresponsiveness of medial entorhinal cortex layer II neurons. J Neurophysiol 70: 144-157

Knowles WD, Schwartzkroin PA (1981) Local circuit synaptic interactions in hippocampal brain slices. J Neurosci 1: 318-322

Kogo M, Funk GD, Chandler SH (1996) Rhythmical oral-motor activity recorded in an in vitro brainstem preparation. Somatosens Mot Res 13: 39-48

Kolb B, Walkey J (1987) Behavioural and anatomical studies of the posterior parietal cortex in the rat. Behav Brain Res 23: 127-145

Konnerth A, Llano I, Armstrong CM (1990) Synaptic currents in cerebellar Purkinje cells. Proc Natl Acad Sci U S A 87: 2662-2665

Kramis R, Vanderwolf CH, Bland BH (1975) Two types of hippocampal rhythmical slow activity in both the rabbit and the rat: relations to behavior and effects of atropine, diethyl ether, urethane, and pentobarbital. Exp Neurol 49: 58-85

Kutsuwada T, Kashiwabuchi N, Mori H, Sakimura K, Kushiya E, Araki K, Meguro H, Masaki H, Kumanishi T, Arakawa M, et al. (1992) Molecular diversity of the NMDA receptor channel. Nature 358: 36-41

REFERENCES

Lacaille JC, Mueller AL, Kunkel DD, Schwartzkroin PA (1987) Local circuit interactions between oriens/alveus interneurons and CA1 pyramidal cells in hippocampal slices: electrophysiology and morphology. J Neurosci 7: 1979-1993

Lacaille JC, Schwartzkroin PA (1988a) Stratum lacunosum-moleculare interneurons of hippocampal CA1 region. II. Intrasomatic and intradendritic recordings of local circuit synaptic interactions. J Neurosci 8: 1411-1424

Lacaille JC, Schwartzkroin PA (1988b) Stratum lacunosum-moleculare interneurons of hippocampal CA1 region. I. Intracellular response characteristics, synaptic responses, and morphology. J Neurosci 8: 1400-1410

Lamour Y, Willer J-C, Guilbaud G (1982) Neuronal responses to noxious stimulation in rat somatosensory cortex. Neurosci Lett 29: 35-40

Lamour Y, Willer J-C, Guilbaud G (1983) Rat somatosensory (SmI) cortex: I. Characteristics of neuronal responses to noxious stimulation and comparison with responses to non-noxious stimulation. Exp Brain Res 49: 35-45

Lamsa K, Palva JM, Ruusuvuori E, Kaila K, Taira T (2000) Synaptic GABA(A) activation inhibits AMPA-kainate receptor-mediated bursting in the newborn (P0-P2) rat hippocampus. J Neurophysiol 83: 359-366

Lee MG, Chrobak JJ, Sik A, Wiley RG, Buzsaki G (1994) Hippocampal theta activity following selective lesion of the septal cholinergic system. Neuroscience 62: 1033-1047

Leranth C, Carpi D, Buzsaki G, Kiss J (1999) The entorhino-septo-supramammillary nucleus connection in the rat: morphological basis of a feedback mechanism regulating hippocampal theta rhythm. Neuroscience 88: 701-718

Leresche N, Asprodini E, Emri Z, Cope DW, Crunelli V (2000) Somatostatin inhibits GABAergic transmission in the sensory thalamus via presynaptic receptors. Neuroscience 98: 513-522

Leresche N, Lightowler S, Soltesz I, Jassik-Gerschenfeld D, Crunelli V (1991) Low-frequency oscillatory activities intrinsic to rat and cat thalamocortical cells. J Physiol (Lond) 441: 155-174

Lester RA, Jahr CE (1990) Quisqualate receptor-mediated depression of calcium currents in hippocampal neurons. Neuron 4: 741-749

Lewin GR, McKintosh E, McMahon SB (1994) NMDA receptors and activity-dependent tuning of the receptive fields of spinal cord neurons. Nature 369: 482-485

Li X-G, Somogyi P, Ylinen A, Buzsaki G (1994) The hippocampal CA3 network: An in vivo intracellular labeling study. J Comp Neurol 339: 181-208

Liman ER, Knapp AG, Dowling JE (1989) Enhancement of kainate-gated currents in retinal horizontal cells by cyclic AMP-dependent protein kinase. Brain Res 481: 399-402

REFERENCES

Lincoln DW (1969) Correlation of unit activity in the hypothalamus with EEG patterns associated with the sleep cycle. Exp Neurol 24: 1-18

Lipowsky R, Gillessen T, Alzheimer C (1996) Dendritic Na+ channels amplify EPSPs in hippocampal CA1 pyramidal cells. J Neurophysiol 76: 2181-2191

Lisman JE, Idiart MA (1995) Storage of 7 +/- 2 short-term memories in oscillatory subcycles. Science 267: 1512-1515

Lomeli H, Wisden W, Kohler M, Keinanen K, Sommer B, Seeburg PH (1992) High-affinity kainate and domoate receptors in rat brain. FEBS Lett 307: 139-143

Lu S-M, Lin R C-S (1993) Thalamic afferents of the rat barrel cortex: A light- and electron-microscopic study using Phaseolus vulgaris Leucoagglutinin as an anterograde tracer. Somatosens Mot Res 10: 1-16

Lujan R, Nusser Z, Roberts JD, Shigemoto R, Somogyi P (1996) Perisynaptic location of metabotropic glutamate receptors mGluR1 and mGluR5 on dendrites and dendritic spines in the rat hippocampus. Eur J Neurosci 8: 1488-1500

Luscher C, Xia H, Beattie EC, Carroll RC, von-Zastrow M, Malenka RC, Nicoll RA (1999) Role of AMPA receptor cycling in synaptic transmission and plasticity. Neuron 24: 649-658

Luthi A, Chittajallu R, Duprat F, Palmer MJ, Benke TA, Kidd FL, Henley JM, Isaac JT, Collingridge GL (1999) Hippocampal LTD expression involves a pool of AMPARs regulated by the NSF-GluR2 interaction. Neuron 24: 389-399

Lynch G, Larson J, Kelso S, Barrionuevo G, Schottler F (1983) Intracellular injections of EGTA block induction of hippocampal long- term potentiation. Nature 305: 719-721

Lynch GS, Dunwiddie T, Gribkoff V (1977) Heterosynaptic depression: a postsynaptic correlate of long-term potentiation. Nature 266: 737-739

Maccaferri G, McBain CJ (1996) The hyperpolarization-activated current (Ih) and its contribution to pacemaker activity in rat CA1 hippocampal stratum oriens-alveus interneurones. J Physiol (Lond) 497: 119-130

Maccaferri G, Roberts JD, Szucs P, Cottingham CA, Somogyi P (2000) Cell surface domain specific postsynaptic currents evoked by identified GABAergic neurones in rat hippocampus in vitro. J Physiol (Lond) 524 Pt 1: 91-116

MacVicar BA (1985) Depolarizing prepotentials are Na+ dependent in CA1 pyramidal neurons. Brain Res 333: 378-381

MacVicar BA, Tse FW (1989) Local neuronal circuitry underlying cholinergic rhythmical slow activity in CA3 area of rat hippocampal slices. J Physiol (Lond) 417: 197-212

REFERENCES

Martin LJ, Blackstone CD, Huganir RL, Price DL (1992) Cellular localization of a metabotropic glutamate receptor in rat brain. Neuron 9: 259-270

Masu M, Tanabe Y, Tsuchida K, Shigemoto R, Nakanishi S (1991) Sequence and expression of a metabotropic glutamate receptor. Nature 349: 760-765

Mayer ML, Vyklicky L, Jr. (1989) Concanavalin A selectively reduces desensitization of mammalian neuronal quisqualate receptors. Proc Natl Acad Sci U S A 86: 1411-1415

McBain CJ (1994) Hippocampal inhibitory neuron activity in the elevated potassium model of epilepsy [corrected and republished in J Neurophysiol 1995 Feb;73(2):2853-63]. J Neurophysiol 72: 2853-2863

McBain CJ, DiChiara TJ, Kauer JA (1994) Activation of metabotropic glutamate receptors differentially affects two classes of hippocampal interneurons and potentiates excitatory synaptic transmission. J Neurosci 14: 4433-4445

McBain CJ, Mayer ML (1994) *N*-methyl-D-aspartic acid receptor structure and function. Physiol Rev 74: 723-760

McCormick DA, Connors BW, Lighthall JW, Prince DA (1985) Comparative electrophysiology of pyramidal and sparsely spiny stellate neurons of the neocortex. J Neurophysiol 54: 782-806

McCormick DA, Pape HC (1990) Properties of a hyperpolarization-activated cation current and its role in rhythmic oscillation in thalamic relay neurones. J Physiol (Lond) 431: 291-318

Meguro H, Mori H, Araki K, Kushiya E, Kutsuwada T, Yamazaki M, Kumanishi T, Arakawa M, Sakimura K, Mishina M (1992) Functional characterization of a heteromeric NMDA receptor channel expressed from cloned cDNAs. Nature 357: 70-74

Mitchell SJ, Ranck JB, Jr. (1980) Generation of theta rhythm in medial entorhinal cortex of freely moving rats. Brain Res 189: 49-66

Morin F, Beaulieu C, Lacaille JC (1996) Membrane properties and synaptic currents evoked in CA1 interneuron subtypes in rat hippocampal slices. J Neurophysiol 76: 1-16

Morita T, Sakimura K, Kushiya E, Yamazaki M, Meguro H, Araki K, Abe T, Mori KJ, Mishina M (1992) Cloning and functional expression of a cDNA encoding the mouse beta 2 subunit of the kainate-selective glutamate receptor channel. Brain Res Mol Brain Res 14: 143-146

Moriyoshi K, Masu M, Ishii T, Shigemoto R, Mizuno N, Nakanishi S (1991) Molecular cloning and characterization of the rat NMDA receptor. Nature 354: 31-37

Morris SH, Knevett S, Lerner EG, Bindman LJ (1999) Group I mGluR agonist DHPG facilitates the induction of LTP in rat prelimbic cortex in vitro. J Neurophysiol 82: 1927-1933

REFERENCES

Mulkey RM, Malenka RC (1992) Mechanisms underlying induction of homosynaptic long-term depression in area CA1 of the hippocampus. Neuron 9: 967-975

Mullin WJ, Phillis JW (1975) The effect of graded forelimb afferent volleys on acetylcholine release from cat sensorimotor cortex. J Physiol 244: 741-756

Nakanishi N, Axel R, Shneider NA (1992) Alternative splicing generates functionally distinct N-methyl-D- aspartate receptors. Proc Natl Acad Sci U S A 89: 8552-8556

Nakanishi N, Shneider NA, Axel R (1990) A family of glutamate receptor genes: evidence for the formation of heteromultimeric receptors with distinct channel properties. Neuron 5: 569-581

Nawy S, Jahr CE (1990) Suppression by glutamate of cGMP-activated conductance in retinal bipolar cells. Nature 346: 269-271

Nayak A, Zastrow DJ, Lickteig R, Zahniser NR, Browning MD (1998) Maintenance of late-phase LTP is accompanied by PKA-dependent increase in AMPA receptor synthesis. Nature 394: 680-683

Neugebauer V, Chen PS, Willis WD (1999) Role of metabotropic glutamate receptor subtype mGluR1 in brief nociception and central sensitization of primate STT cells. J Neurophysiol 82: 272-282

Neugebauer V, Lucke T, Schaible H-G (1993) N-Methyl-D-Aspartate (NMDA) and non-NMDA receptor antagonists block the hyperexcitability of dorsal horn neurons during development of acute arthritis in rat's knee joint. J Neurophysiol 70: 1365-1377

Newman J, Grace AA (1999) Binding across time: the selective gating of frontal and hippocampal systems modulating working memory and attentional states. Conscious Cogn 8: 196-212

Nicoll RA, Malenka RC (1999) Expression mechanisms underlying NMDA receptor-dependent long-term potentiation. Ann N Y Acad Sci 868: 515-525

Nyakas C, Luiten PG, Spencer DG, Traber J (1987) Detailed projection patterns of septal and diagonal band efferents to the hippocampus in the rat with emphasis on innervation of CA1 and dentate gyrus. Brain Res Bull 18: 533-545

Otani S, Auclair N, Desce JM, Roisin MP, Crepel F (1999) Dopamine receptors and groups I and II mGluRs cooperate for long-term depression induction in rat prefrontal cortex through converging postsynaptic activation of MAP kinases. J Neurosci 19: 9788-9802

Palva JM, Lamsa K, Lauri SE, Rauvala H, Kaila K, Taira T (2000) Fast network oscillations in the newborn rat hippocampus in vitro. J Neurosci 20: 1170-1178

Parra P, Gulyas AI, Miles R (1998) How many subtypes of inhibitory cells in the hippocampus? Neuron 20: 983-993

REFERENCES

Paxinos G, Watson C (1986) The rat brain in stereotaxic coordinates. Academic Press, Australia, pp X.

Petralia RS, Wang YX, Wenthold RJ (1994) The NMDA receptor subunits NR2A and NR2B show histological and ultrastructural localization patterns similar to those of NR1. J Neurosci 14: 6102-6120

Pfurtscheller G, Neuper C (1992) Simultaneous EEG 10 Hz desynchronization and 40 Hz synchronization during finger movements. Neuroreport 3: 1057-1060

Pin JP, Duvoisin R (1995) The metabotropic glutamate receptors: structure and functions. Neuropharmacology 34: 1-26

Pin JP, Waeber C, Prezeau L, Bockaert J, Heinemann SF (1992) Alternative splicing generates metabotropic glutamate receptors inducing different patterns of calcium release in Xenopus oocytes. Proc Natl Acad Sci U S A 89: 10331-10335

Pinco M, Lev-Tov A (1993) Synaptic excitation of alpha-motoneurons by dorsal root afferents in the neonatal rat spinal cord. J Neurophysiol 70: 406-417

Pockett S, Brookes NH, Bindman LJ (1990) Long-term depression at synapses in slices of rat hippocampus can be induced by bursts of postsynaptic activity. Exp Brain Res 80: 196-200

Pollard M (2000) Ionotropic glutamate receptor-mediated responses in the rat primary somatosensory cortex evoked by noxious and innocuous cutaneous stimulation in vivo. Exp Brain Res 131: 282-292

Price DD, Dubner R (1977) Neurons that subserve the sensory-discriminative aspects of pain. Pain 3: 307-338

Purves RD (1979) The physics of iontophoretic pipettes. J Neurosci Methods 1: 165-178

Rall W (1969) Time constants and electrotonic length of membrane cylinders and neurons. Biophys J 9: 1483-1508

Ranck JB, Jr. (1973) Studies on single neurons in dorsal hippocampal formation and septum in unrestrained rats. I. Behavioral correlates and firing repertoires. Exp Neurol 41: 461-531

Rauschecker JP, Singer W (1979) Changes in the circuitry of the kitten visual cortex are gated by postsynaptic activity. Nature 280: 58-60

Rauschecker JP, Singer W (1981) The effects of early visual experience on the cat's visual cortex and their possible explanation by Hebb synapses. J Physiol 310: 215-239

Raymond CR, Thompson VL, Tate WP, Abraham WC (2000) Metabotropic glutamate receptors trigger homosynaptic protein synthesis to prolong long-term potentiation. J Neurosci 20: 969-976

REFERENCES

Raymond LA, Blackstone CD, Huganir RL (1993) Phosphorylation and modulation of recombinant GluR6 glutamate receptors by cAMP-dependent protein kinase. Nature 361: 637-641

Regehr WG, Tank DW (1991) The maintenance of LTP at hippocampal mossy fiber synapses is independent of sustained presynaptic calcium. Neuron 7: 451-459

Rittenhouse CD, Shouval HZ, Paradiso MA, Bear MF (1999) Monocular deprivation induces homosynaptic long-term depression in visual cortex. Nature 397: 347-350

Robinson HP, Kawahara M, Jimbo Y, Torimitsu K, Kuroda Y, Kawana A (1993) Periodic synchronized bursting and intracellular calcium transients elicited by low magnesium in cultured cortical neurons. J Neurophysiol 70: 1606-1616

Sakimura K, Bujo H, Kushiya E, Araki K, Yamazaki M, Meguro H, Warashina A, Numa S, Mishina M (1990) Functional expression from cloned cDNAs of glutamate receptor species responsive to kainate and quisqualate. FEBS Lett 272: 73-80

Sakimura K, Morita T, Kushiya E, Mishina M (1992) Primary structure and expression of the gamma 2 subunit of the glutamate receptor channel selective for kainate. Neuron 8: 267-274

Sakowitz OW, Schurmann M, Basar E (2000) Oscillatory frontal theta responses are increased upon bisensory stimulation. Clin Neurophysiol 111: 884-893

Salt TE (1986) Mediation of thalamic sensory input by both NMDA receptors and non-NMDA receptors. Nature 322: 263-265

Salt TE (1987) Excitatory amino acid receptors and synaptic transmission in the rat ventrobasal thalamus. J Physiol (Lond) 391: 499-510

Salt TE, Eaton SA (1989) Function of non-NMDA receptors and NMDA receptors in synaptic responses to natural somatosensory stimulation in the ventrobasal thalamus. Exp Brain Res 77: 646-652

Salt TE, Eaton SA (1991) Sensory excitatory postsynaptic potentials mediated by NMDA and non-NMDA receptors in the thalamus in vivo. Eur J Neurosci 3: 296-300

Salt TE, Eaton SA (1994) The function of metabotropic excitatory amino acid receptors in synaptic transmission in the thalamus: studies with novel phenylglycine antagonists. Neurochem Int 24: 451-458

Salt TE, Eaton SA (1995) Distinct presynaptic metabotropic receptors for L-AP4 and CCG1 on GABAergic terminals: pharmacological evidence using novel alpha-methyl derivative mGluR antagonists, MAP4 and MCCG, in the rat thalamus in vivo. Neuroscience 65: 5-13

REFERENCES

Salt TE, Herrling PL (1995) Excitatory amino acid transmitter function in mammalian central pathways. In: Wheal H, Thomson A (eds) Excitatory Amino Acids and Synaptic Transmission. Academic Press, London, pp 223-237

Salt TE, Meier CL, Seno N, Krucker T, Herrling PL (1995) Thalamocortical and corticocortical excitatory postsynaptic potentials mediated by excitatory amino acid receptors in the cat motor cortex in vivo. Neuroscience 64: 433-442

Sannita WG (2000) Stimulus-specific oscillatory responses of the brain: a time/frequency-related coding process. Clin Neurophysiol 111: 565-583

Sayer RJ, Schwindt PC, Crill WE (1992) Metabotropic glutamate receptor-mediated suppression of L-type calcium current in acutely isolated neocortical neurons. J Neurophysiol 68: 833-842

Schaffer K (1892) *Beitrag zur histologie der ammonshorn-formation*

Schaible H-G, Grubb BD, Neugebauer V, Oppmann M (1991) The effects of NMDA antagonists on neuronal activity in cat spinal cord evoked by acute inflammation in the knee joint. Eur J Neurosci 3: 981-991

Scharfman HE, Schwartzkroin PA (1988) Further studies of the effects of somatostatin and related peptides in area CA1 of rabbit hippocampus. Cell Mol Neurobiol 8: 411-429

Scharfman HE, Schwartzkroin PA (1989) Selective depression of GABA-mediated IPSPs by somatostatin in area CA1 of rabbit hippocampal slices. Brain Res 493: 205-211

Schwartzkroin PA, Mathers LH (1978) Physiological and morphological identification of a nonpyramidal hippocampal cell type. Brain Res 157: 1-10

Schweitzer P, Madamba SG, Siggins GR (1998) Somatostatin increases a voltage-insensitive K+ conductance in rat CA1 hippocampal neurons. J Neurophysiol 79: 1230-1238

Selmer IS, Schindler M, Humphrey PP, Emson PC (2000) Immunohistochemical localization of the somatostatin sst(4) receptor in rat brain. Neuroscience 98: 523-533

Shiells RA, Falk G (1990) Glutamate receptors of rod bipolar cells are linked to a cyclic GMP cascade via a G-protein. Proc R Soc Lond B Biol Sci 242: 91-94

Shigemoto R, Kulik A, Roberts JDB, Ohishi H, Nusser Z, Kanoko T, Somogyi P (1996) Target-cell-specific concentration of a metabotropic glutamate receptor in the presynaptic active zone. Nature 381: 523-525

Shirokawa T, Nishigori A, Kimura F, Tsumoto T (1989) Actions of excitatory amino acid antagonists on synaptic potentials of layer II/III neurons of the cat's visual cortex. Exp Brain Res 78: 489-500

Siapas AG, Wilson MA (1998) Coordinated interactions between hippocampal ripples and cortical spindles during slow-wave sleep. Neuron 21: 1123-1128

REFERENCES

Sik A, Penttonen M, Ylinen A, Buzsaki G (1995) Hippocampal CA1 interneurons: an in vivo intracellular labeling study. J Neurosci 15: 6651-6665

Sik A, Ylinen A, Penttonen M, Buzsaki G (1994) Inhibitory CA1-CA3-hilar region feedback in the hippocampus. Science 265: 1722-1724

Sillito AM, Murphy PC, Salt TE (1990a) The contribution of the non-N-methyl-D-aspartate group of excitatory amino acid receptors to retinogeniculate transmission in the cat. Neuroscience 34: 273-280

Sillito AM, Murphy PC, Salt TE, Moody CI (1990b) Dependence of retinogeniculate transmission in cat on NMDA receptors. J Neurophysiol 63: 347-355

Simons DJ (1978) Response properties of vibrissa units in rat SI somatosensory neocortex. J Neurophysiol 41: 798-820

Simons DJ, Carvell GE (1989) Thalamocortical response transformation in the rat vibrissa/barrel system. J Neurophysiol 61: 311-330

Sinclair BR, Seto MG, Bland BH (1982) theta-Cells in CA1 and dentate layers of hippocampal formation: relations to slow-wave activity and motor behavior in the freely moving rabbit. J Neurophysiol 48: 1214-1225

Sladeczek F, Momiyama A, Takahashi T (1993) Presynaptic inhibitory action of a metabotropic glutamate receptor agonist on excitatory transmission in visual cortical neurons. Proc R Soc Lond B Biol Sci 253: 297-303

Soltesz I, Deschenes M (1993) Low- and high-frequency membrane potential oscillations during theta activity in CA1 and CA3 pyramidal neurons of the rat hippocampus under ketamine-xylazine anesthesia. J Neurophysiol 70: 97-116

Soltesz I, Lightowler S, Leresche N, Jassik-Gerschenfeld D, Pollard CE, Crunelli V (1991) Two inward currents and the transformation of low-frequency oscillations of rat and cat thalamocortical cells. J Physiol (Lond) 441: 175-197

Sommer B, Burnashev N, Verdoorn TA, Keinanen K, Sakmann B, Seeburg PH (1992) A glutamate receptor channel with high affinity for domoate and kainate. Embo J 11: 1651-1656

Somogyi P, Hodgson AJ, Smith AD, Nunzi MG, Gorio A, Wu JY (1984) Different populations of GABAergic neurons in the visual cortex and hippocampus of cat contain somatostatin- or cholecystokinin- immunoreactive material. J Neurosci 4: 2590-2603

Somogyi P, Tamas G, Lujan R, Buhl EH (1998) Salient features of synaptic organisation in the cerebral cortex. Brain Res Brain Res Rev 26: 113-135

Stanford IM, Traub RD, Jefferys JG (1998) Limbic gamma rhythms. II. Synaptic and intrinsic mechanisms underlying spike doublets in oscillating subicular neurons. J Neurophysiol 80: 162-171

REFERENCES

Stern P, Edwards FA, Sakmann B (1992) Fast and slow components of unitary EPSCs on stellate cells elicited by focal stimulation in slices of rat visual cortex. J Physiol (Lond) 449: 247-278

Steward O (1976) Topographic organization of the projections from the entorhinal area to the hippocampal formation of the rat. J Comp Neurol 167: 285-314

Stewart M, Luo Y, Fox SE (1992) Effects of atropine on hippocampal theta cells and complex-spike cells. Brain Res 591: 122-128

Storm JF (1990) Potassium currents in hippocampal pyramidal cells. Prog Brain Res 83: 161-187

Suzuki SS, Smith GK (1987) Spontaneous EEG spikes in the normal hippocampus. I. Behavioral correlates, laminar profiles and bilateral synchrony. Electroencephalogr Clin Neurophysiol 67: 348-359

Swartz KJ, Bean BP (1992) Inhibition of calcium channels in rat CA3 pyramidal neurons by a metabotropic glutamate receptor. J Neurosci 12: 4358-4371

Swartz KJ, Merrit A, Bean BP, Lovinger DM (1993) Protein kinase C modulates glutamate receptor inhibition of Ca2+ channels and synaptic transmission. Nature 361: 165-168

Tallent MK, Siggins GR (1997) Somatostatin depresses excitatory but not inhibitory neurotransmission in rat CA1 hippocampus. J Neurophysiol 78: 3008-3018

Tamamaki N, Nojyo Y (1995) Preservation of topography in the connections between the subiculum, field CA1, and the entorhinal cortex in rats. J Comp Neurol 353: 379-390

Tamas G, Buhl EH, Lorincz A, Somogyi P (2000) Proximally targeted GABAergic synapses and gap junctions synchronize cortical interneurons. Nat Neurosci 3: 366-371

Tamas G, Buhl EH, Somogyi P (1997) Fast IPSPs elicited via multiple synaptic release sites by different types of GABAergic neurone in the cat visual cortex. J Physiol (Lond) 500: 715-738

Tanabe Y, Masu M, Ishii T, Shigemoto R, Nakanishi S (1992) A family of metabotropic glutamate receptors. Neuron 8: 169-179

Tanabe Y, Nomura A, Masu M, Shigemoto R, Mizuno N, Nakanishi S (1993) Signal transduction, pharmacological properties, and expression patterns of two rat metabotropic glutamate receptors, mGluR3 and mGluR4. J Neurosci 13: 1372-1378

Taylor GW, Merlin LR, Wong RK (1995) Synchronized oscillations in hippocampal CA3 neurons induced by metabotropic glutamate receptor activation. J Neurosci 15: 8039-8052

REFERENCES

Taylor KE, Cahusac MB (1994) The effects of the metabotropic glutamate receptor agonist 1S, 3R-ACPD on neurons in the rat primary somatosensory cortex in vivo. Neuropharm 33: 103-108

Thompson PM, Zebrowski G, Neuman RS (1991) Alteration of neocortical activity in response to noxious stimulation: participation of the dorsal raphe. Neuropharmacology 30: 135-141

Tolbert DL, Pittman T, Alisky JM, Clark BR (1994) Chronic NMDA receptor blockade or muscimol inhibition of cerebellar cortical neuronal activity alters the development of spinocerebellar afferent topography. Brain Res Dev Brain Res 80: 268-274

Toth K, Borhegyi Z, Freund TF (1993) Postsynaptic targets of GABAergic hippocampal neurons in the medial septum-diagonal band of broca complex. J Neurosci 13: 3712-3724

Toth K, Freund TF, Miles R (1997) Disinhibition of rat hippocampal pyramidal cells by GABAergic afferents from the septum. J Physiol (Lond) 500: 463-474

Traub RD, Bibbig A (2000) A model of high-frequency ripples in the hippocampus based on synaptic coupling plus axon-axon gap junctions between pyramidal neurons. J Neurosci 20: 2086-2093

Traub RD, Jefferys JC, Whittington MA (1994) Enhanced NMDA conductance can account for epileptiform activity induced by low Mg2+ in the rat hippocampal slice. J Physiol 478: 379-393

Traub RD, Whittington MA, Buhl EH, Jefferys JG, Faulkner HJ (1999) On the mechanism of the gamma --> beta frequency shift in neuronal oscillations induced in rat hippocampal slices by tetanic stimulation. J Neurosci 19: 1088-1105

Traub RD, Whittington MA, Colling SB, Buzsaki G, Jefferys JG (1996a) Analysis of gamma rhythms in the rat hippocampus in vitro and in vivo. J Physiol (Lond) 493: 471-484

Traub RD, Whittington MA, Stanford IM, Jefferys JG (1996b) A mechanism for generation of long-range synchronous fast oscillations in the cortex. Nature 383: 621-624

Traynelis SF, Hartley M, Heinemann SF (1995) Control of proton sensitivity of the NMDA receptor by RNA splicing and polyamines. Science 268: 873-876

Trepel C, Racine RJ (1998) Long-term potentiation in the neocortex of the adult, freely moving rat. Cereb Cortex 8: 719-729

Tsumoto T, Masui H, Sato H (1986) Excitatory amino acid transmitters in neuronal circuits of the cat visual cortex. J Neurophysiol 55: 469-483

Ugolini A, Corsi M, Bordi F (1997) Potentiation of NMDA and AMPA responses by group I mGluR in spinal cord motoneurons. Neuropharmacology 36: 1047-1055

REFERENCES

Urban NN, Henze DA, Lewis DA, Barrionuevo G (1996) Properties of LTP induction in the CA3 region of the primate hippocampus. Learn Mem 3: 86-95

van Hooft JA, Giuffrida R, Blatow M, Monyer H (2000) Differential expression of group I metabotropic glutamate receptors in functionally distinct hippocampal interneurons. J Neurosci 20: 3544-3551

Vanderwolf CH (1969) Hippocampal electrical activity and voluntary movement in the rat. Electroencephalogr Clin Neurophysiol 26: 407-418

Vanderwolf CH, Leung LS (1982) Effects of entorhinal, cingulate and neocortical lessions on atropine resistant hippocampal RSA. Neurosci Lett, Suppl. 10: S501

Verdoorn TA, Burnashev N, Monyer H, Seeburg PH, Sakmann B (1991) Structural determinants of ion flow through recombinant glutamate receptor channels. Science 252: 1715-1718

Verheugen JA, Fricker D, Miles R (1999) Noninvasive measurements of the membrane potential and GABAergic action in hippocampal interneurons. J Neurosci 19: 2546-2555

Wang X, Gruenstein EI (1997) Mechanism of synchronized Ca2+ oscillations in cortical neurons. Brain Res 767: 239-249

Wang LY, Taverna FA, Huang XP, MacDonald JF, Hampson DR (1993) Phosphorylation and modulation of a kainate receptor (GluR6) by cAMP- dependent protein kinase. Science 259: 1173-1175

Werner P, Voigt M, Keinanen K, Wisden W, Seeburg PH (1991) Cloning of a putative high-affinity kainate receptor expressed predominantly in hippocampal CA3 cells. Nature 351: 742-744

Whittington MA, Stanford IM, Colling SB, Jefferys JG, Traub RD (1997) Spatiotemporal patterns of gamma frequency oscillations tetanically induced in the hippocampal slice. J Physiol 502: 591-607

Whittington MA, Traub RD, Jefferys JG (1995) Synchronized oscillations in interneuron networks driven by metabotropic glutamate receptor activation. Nature 373: 612-615

Willis WD, Jr. (1985) Pain pathways in the primate. Prog Clin Biol Res 176: 117-133

Wise SP, Jones EG (1977) Cells of origin and terminal distribution of descending projections of the rat somatic sensory cortex. J Comp Neurol 175: 129-157

Woodhall G, Gee CE, Robitaille R, Lacaille JC (1999) Membrane potential and intracellular Ca2+ oscillations activated by mGluRs in hippocampal stratum oriens/alveus interneurons. J Neurophysiol 81: 371-382

Yezierski RP, Schwartz RH (1986) Response and receptive-field properties of spinomesencephalic tract cells in the cat. J Neurophysiol 55: 76-96

REFERENCES

Ylinen A, Bragin A, Nadasdy Z, Jando G, Szabo I, Sik A, Buzsaki G (1995a) Sharp wave-associated high-frequency oscillation (200 Hz) in the intact hippocampus: network and intracellular mechanisms. J Neurosci 15: 30-46

Ylinen A, Soltesz I, Bragin A, Penttonen M, Sik A, Buzsaki G (1995b) Intracellular correlates of hippocampal theta rhythm in identified pyramidal cells, granule cells, and basket cells. Hippocampus 5: 78-90

Yoshida A, Dostrovsky JO, Chiang CY (1992) The afferent and efferent connections of the nucleus submedius in the rat. J Comp Neurol 324: 115-133

Young MR, Blackburn-Munro G, Dickinson T, Johnson MJ, Anderson H, Nakalembe I, Fleetwood-Walker SM (1998) Antisense ablation of type I metabotropic glutamate receptor mGluR1 inhibits spinal nociceptive transmission. J Neurosci 18: 10180-10188

Young MR, Fleetwood-Walker SM, Dickinson T, Blackburn-Munro G, Sparrow H, Birch PJ, Bountra C (1997) Behavioural and electrophysiological evidence supporting a role for group I metabotropic glutamate receptors in the mediation of nociceptive inputs to the rat spinal cord. Brain Res 777: 161-169

Zalutsky RA, Nicoll RA (1990) Comparison of two forms of long-term potentiation in single hippocampal neurons [published erratum appears in Science 1991 Feb 22;251(4996):856]. Science 248: 1619-1624

Zhang L, McBain CJ (1995) Potassium conductances underlying repolarization and after-hyperpolarization in rat CA1 hippocampal interneurones. J Physiol (Lond) 488: 661-672

Ziskind-Conhaim L (1990) NMDA receptors mediate poly- and monosynaptic potentials in motoneurons of rat embryos. J Neurosci 10: 125-135

PUBLICATIONS

Pollard M (2000) Ionotropic glutamate receptor-mediated responses in the rat primary somatosensory cortex evoked by noxious and innocuous cutaneous stimulation in vivo. Exp Brain Res 131: 282-292

Pollard M, Eaton SA (1998) NMDA receptor-mediated component of nociceptive sensory synaptic responses in rat primary somatosensory neurones. Eur J Neurosci Abs 10 (Suppl. 10): P77

Pollard M, Kogo N, Roberts JDB, Ferraguti F, Somogyi P (2000) Cell types expressing somatostatin and/or mGluR1α in the rat hippocampal CA1 area. Soc Neurosci Abs 26: P1136